SPATIOTEMPORAL ASSESSMENT OF AXONAL TRANSPORT AND CYTOSKELETAL STRUCTURE IN RETINAL GANGLION CELLS FOLLOWING ACUTE ELEVATED INTRAOCULAR PRESSURE IN THE RAT

by

Andrea Nuschke

Submitted in partial fulfilment of the requirements
for the degree of Doctor of Philosophy

at

Dalhousie University
Halifax, Nova Scotia
January, 2017

© Copyright by Andrea Nuschke, 2017

DEDICATION

For my parents

Their love and support has sustained my psyche

throughout this degree, and life in general.

TABLE OF CONTENTS

LIST OF TABLES ..... **x**

LIST OF FIGURES ..... **xi**

ABSTRACT ..... **xvi**

LIST OF ABBREVIATIONS USED ..... **xvii**

ACKNOWLEDGEMENTS ..... **xx**

CHAPTER 1 – INTRODUCTION **1**

1.1 The Retina and Optic Nerve (ON) **1**

1.1.1 Gross Visual Anatomy 1

1.1.2 Retinal Function and Organization 2

1.1.3 RGC Types 5

1.1.2 Anatomy of the RGC Retinal Projection 8

1.1.3 Glia of the Retina and ON 11

1.2 The Neuronal Cytoskeleton **13**

1.2.1 Microtubules 13

1.2.2 Actin 16

1.2.3 Neurofilaments (NFs) 19

1.2.4 Phosphorylation-Dependent Regulation of Cytoskeletal Proteins 22

1.3 Axonal Transport (AT) **24**

1.3.1 Molecular Motors, their Adapters, and Structural Scaffolds 24

1.3.2 Slow and Fast Transport Components 28

1.4 RGC Injury Related to Elevated Intraocular Pressure (IOP) **30**

1.4.1 Glaucoma 30

1.4.2 Animal Models of RGC Injury with Elevated Intraocular Pressure 30

1.4.3 Relevant Types of Neuronal Insults 35

1.4.4 Experimental Methods of Evaluating AT Function and Axonal Structure in RGCs, and Activation of Surrounding Retinal and ON Glia 42

1.4.5 RGC Response to Elevated IOP 48

1.4.6 Reversibility of RGC Damage 56

1.5 Goals of Thesis 59

CHAPTER 2 – MATERIALS AND METHODS 60

2.1 Animals, Animal Care, and Anesthesia 60

2.2 AT Tracing 61

2.2.1 AT Tracers Used 61

2.2.2 Retrograde AT Tracing 61

2.2.3 Anterograde AT Tracing 63

2.3 Pressure Column 65

2.4 Acute Elevated IOP 68

2.5 Recovery Times and Sample Sizes 69

2.6 Western Blot (WB) 69

2.7 Tissue Processing 71

2.8 IHC 73

2.9 Fluorescence Imaging 75

2.10 Quantitative and Qualitative Retinal Analyses 78

2.10.1 Manual and Automated Cell Counting in Whole-Mounted Retinas 78

2.10.2 Grading of Somal pNF in Whole-Mounted Retinas 79

2.10.3 Qualitative Analysis of Retinal Glia in Retinal Cross-Sections 84

2.11 Fluorescence Analysis of ONH and ON Sections 85

2.12 Statistical Analysis 89

CHAPTER 3 – CHARACTERIZATION OF RITC AND CTB FOR TRACKING AT IN RGCS 90

3.1 Rationale, Objective, and Hypotheses 90

3.2 Experimental Design 91

3.3 Results 92

3.3.1 Time Course and Qualitative Analysis of RITC Retrograde AT 92

3.3.2 Time Course and Qualitative Analysis of CTB Retrograde AT 97

3.3.3 Comparison of RITC and CTB Retrograde AT 102

3.3.6 Estimations of RITC and CTB Transport Rates 102

3.4 Summary and Key Findings 104

CHAPTER 4 – RETROGRADE AT IN RGCS FOLLOWING ELEVATED IOP 105

4.1 Rationale, Objective, and Hypotheses 105

4.2 Experimental Design 106

4.2 Results 108

4.2.1 RGC Degeneration and Loss Following Transient Elevated IOP 108

4.2.2 Retrograde AT in the ONH Following Elevated IOP 122

4.3.3 Retrograde AT in the ON Following Elevated IOP 125

4.4 Summary and Key Findings 135

CHAPTER 5 - ANTEROGRADE AT IN RGCS FOLLOWING TRANSIENT ELEVATED IOP 136

5.1 Rationale, Objective, and Hypotheses 136

5.2 Experimental Design 137

5.3 Results 139

5.3.1 Time Course of Anterograde CTB AT 139

5.3.2 Estimation of the Rate of Anterograde CTB AT 142

5.3.3 Quantification of Brn3a+ Cells in the GCL at 3, 6, and 24 Hours Following Elevated IOP 142

5.3.4 Anterograde AT of CTB in the ONH Following Elevated IOP 146

5.3.5 Anterograde AT of CTB in the ON Following Elevated IOP 153

5.3.6 Anterograde AT of CTB in the ON Following Sham Elevated IOP 163

5.4 Summary and Key Findings 166

CHAPTER 6 – NF REGULATION IN THE RETINA AND ONH FOLLOWING ELEVATED IOP 167

6.1 Rationale, Objective, and Hypotheses 167

6.2 Experimental Design 168

6.3 Results 170

6.3.1 Expression of pNF in the Retina Following 30 Minutes of Elevated IOP 170

6.3.2 Expression of pNF in the Retina Following 90 Minutes of Elevated IOP 170

6.3.3 pNF and nonpNF Expression in the ONH Following Elevated IOP 178

6.4 Summary and Key Findings 197

CHAPTER 7 – GLIAL ACTIVATION IN THE RETINA AND ONH FOLLOWING ELEVATED IOP 198

7.1 Rationale, Objective, and Hypotheses 198

7.2 Experimental Design 199

7.3 Results 201

7.3.1 Qualitative Analysis of Iba1+ Microglia in the Retina Following Elevated IOP 201

7.3.2 Qualitative Analysis of GFAP Expression in the Retina Following Elevated IOP 206

7.3.3 Quantitative Analysis of GFAP Expression in the Retina Following Elevated IOP 206

7.3.4 Quantitative Analysis of Iba1 and GFAP Expression in the ONH Following Elevated IOP 210

7.3.5 Iba1 and GFAP Labelling in the ONH Following Sham Elevated IOP 226

7.4 Summary and Key Findings 230

CHAPTER 8 – DISCUSSION 231

8.1 Overview 231

8.2 RITC and CTB as Tracers of AT in the Rat Visual System 234

8.2.1 Factors Affecting the Speed and Uniformity of RITC and CTB Uptake and Transport in RGCs 234

8.2.2 Rates of RITC and CTB Transport in RGC Axons 237

8.2.3 Advantages and Disadvantages of RITC and CTB Tracers 239

8.2.4 Summary of RITC and CTB Tracer Characterization 240

8.3 Considerations Regarding Variation in Animal Models of Elevated IOP 241

8.3.1 Species Used in Studies of Elevated IOP 242

8.3.2 Species- and Strain-Specific Variation in Retinal Blood Supply and ONH Structure 242

8.3.3 RGC Susceptibility to Damage Varies with Species, Strain, and Age 244

8.3.4 Variation in Techniques to Elevate IOP 244

8.3.5 Variation in Techniques to Measure IOP 245

8.3.6 Variation in Techniques to Assess RGC Loss 247

8.3.7 Summary of Variation in Animal Models of Elevated IOP 249

8.4 AT Dysfunction in Response to Elevated IOP 249

8.4.1 Spatiotemporal Progression of AT Disruption Following Elevated IOP 250

8.4.2 AT Function and RGC Loss in Response to Elevated IOP 254

8.4.3 Mechanisms Underlying AT Disruption in Response to Elevated IOP 257

8.4.5 Summary of AT Following Elevated IOP 259

8.5 Alterations of NFs in the RGC Soma and Axon Following Elevated IOP 261

8.5.1 IOP-Induced Somal Accumulation of pNF and Axonal Degeneration in the Retina 261

8.5.2 NF Phosphorylation in the ONH Following Elevated IOP 263

8.5.3 Mechanisms Underlying Alteration of NFs in Elevated IOP 264

8.5.4 NF Expression and Phosphorylation as an Early Marker of Neuronal Injury 266

8.5.4 Summary of IOP-Induced NF Alterations 267

8.6 Modulation of Glia in the Retina and ONH Following Elevated IOP 268

8.6.1 Changes in Retinal Glia Following Elevated IOP 268

8.6.2 Changes in ONH Glia Following Elevated IOP 272

8.6.3 Mechanisms of IOP-Induced Glial Activation and its Influence on RGC Survival 275

8.6.5 Summary of Glial Responses to Elevated IOP 278

8.7 Time Course of Retinal, ONH, and ON Pathology Following Elevated IOP 280

8.7.1 Early Events During IOP Elevation 281

8.7.2 Progression of Events Following a Sub-Critical IOP-Induced Injury to RGCs 282

8.7.3 Progression of Events Following a Critical IOP-Induced Injury to RGCs 285

8.7.3 Summary of Time Course of IOP-Induced Pathology 292

8.8 Factors Underlying the Vulnerability of RGCs to Injury 294

8.8.1 Critical Threshold 295

8.8.2 Variations in Vulnerability Within the RGC Population 299

8.9 Limitations 305

8.9.1 Sample Size 305

8.9.2 Tracer Uptake Dynamics 306
8.9.3 Sources of Error in Fluorescence Quantification 307
8.9.4 Phospho-Specific Antibodies 308
8.9.5 CTB and Inflammation 308
8.10 Conclusions and Future Directions 309
REFERENCES 315
APPENDIX 1: COPYRIGHT PERMISSIONS 350

LIST OF TABLES

Table 1.1 Components of fast and slow transport. 29

Table 2.1 Primary Antibodies for Immunohistochemistry (IHC) 74

Table 4.1 Average ON Fluorescence and RGC Density at 3, 7, and 14 Days Following Elevated IOP 113

Table 4.2 Qualitative Evaluation of AT Disruption in the ONH and Axonal Degeneration in the Peripapillary Retina, ONH, and ON 115

Table 5.1 Average ON Fluorescence and RGC Density at 3, 6, and 24 Hours Following Elevated IOP 143

Table 6.1 Median pNF Grades at 1, 2, and 3 mm of Retinal Eccentricity Following Elevated IOP 171

Table 8.1 Updated Estimations of RITC and CTB AT Rates in the Rat Visual Pathway 238

Table 8.2 Comparison of Sub-Critical and Critical Elevated IOP-Induced Injury 293

Table 8.3 Extrinsic and Intrinsic Influences on RGC Selective Vulnerability 300

LIST OF FIGURES

Figure 1.1 Gross Anatomy of the Eye. 3

Figure 1.2 Retinal Anatomy and Connectivity. 4

Figure 1.3 Alpha and Beta RGCs. 7

Figure 1.4 Structure of Human and Mouse LC. 10

Figure 1.5 Glia of the Retina. 12

Figure 1.6 The Neuronal Cytoskeleton. 14

Figure 1.7 Microtubule Catastrophe and Rescue. 15

Figure 1.8 Orientation of Microtubules Within the Neuron. 17

Figure 1.9 Assembly and Disassembly of Actin Filaments. 18

Figure 1.10 Neurofilament Subunits. 20

Figure 1.11 Neurofilament Assembly. 21

Figure 1.12 Kinesin and Dynein Motor Proteins. 26

Figure 1.13 Aqueous Humor Dynamics in the Eye. 32

Figure 1.14 Elevated IOP-Induced Mechanical and Ischemic Insults Combine to Cause RGC Axonal Injury in the ONH. 37

Figure 1.15 Mechanosensitive Channels in the RGC Plasma Membrane. 40

Figure 1.16 AT Tracers in the Rat Visual System. 44

Figure 1.17 RGC Loss After Elevated IOP-Induced Transient Retinal Ischemia. 51

Figure 2.1 Stereotaxic Injections of CTB into the Rat SC. 62

Figure 2.2 Intravitreal Injection of CTB. 64

Figure 2.3 Use of Hydraulic Pressure Column to Increase IOP. 66

Figure 2.4 Pressure Column Calibration. 67

Figure 2.5 Summary of Recovery Times and Sample Sizes in Elevated IOP AT Experiments. 70

Figure 2.6 Fluorescent Labelling in Whole-Mounted Retinas and ONH Sections..... 76

Figure 2.7 Image Optimization for Automated Brn3a Counting. 80

Figure 2.8 Comparison of Manual and Automated Brn3a Counting. 82

Figure 2.9 Quantification of CTB transport in the ON. 86

Figure 2.10 Quantification of CTB Transport and IHC of NFs and GFAP in Longitudinal Sections of the ONH..... 87

Figure 3.1 Time Course of Retrograde RITC Arrival to the Retina Following Application to the SC. 93

Figure 3.2 Time Course of Retrograde RITC AT in the Proximal ON. 94

Figure 3.3 AT of RITC in the ONH and Retina at 7 Days Following Application to the SC in Two Rats. 95

Figure 3.4 Time Course of CTB in the Proximal ON and the ONH at 24 hours, 2, 3, and 5 Days Following Application to the SC. 98

Figure 3.5 Time Course of Retrograde CTB Arrival at the Retina 24 hours, 2 days, 3 days, and 5 Days Following Application to the SC. 100

Figure 3.6 Comparison of RITC and CTB in the Retina at 7 Days Following Application to the SC. 103

Figure 4.1 RGC Loss at 7 Days Following Elevated IOP. 109

Figure 4.2 Quantification of Brn3a+ Cells in Retinal Whole-Mounts Following Elevated IOP. 111

Figure 4.3 Structural Degeneration of RGCs Retrogradely Filled with CTB at 3, 7, and 14 Days Following 90 Minutes of Elevated IOP. 116

Figure 4.4 IHC Analysis of Retinal Whole-Mounts at 3 Days Following 90 Minutes of Elevated IOP. 118

Figure 4.5 Degeneration of pNF+ RGCs in the Central and Peripheral Retina at 3 Days Following 90 Minutes of Elevated IOP. 120

Figure 4.6 Retrograde AT of CTB in the ONH After 30 or 90 Minutes of Elevated IOP. 123

Figure 4.7 CTB Retrograde AT in ONs at 3, 7, and 14 Days Following 30 Minutes of Elevated IOP. 126

Figure 4.8 CTB Retrograde AT in ONs at 3, 7, and 14 Days Following 90 Minutes of Elevated IOP. 128

Figure 4.9 Quantification of CTB AT in the ON at 3, 7, and 14 Days Following 30 and 90 Minutes of Elevated IOP. 130

Figure 4.10 Individual Paired Measurements of Average CTB Intensity in the ON at 3, 7, and 14 days Following 30 or 90 Minutes of Elevated IOP. 133

Figure 5.1 Time Course of CTB Anterograde AT. 140

Figure 5.2 Brn3a+ Cell Density at 1, 2, and 3 mm of Retinal Eccentricity Following 30 or 90 Minutes of Elevated IOP. 144

Figure 5.3 AT of CTB in the ONH at 3, 6, and 24 Hours Following Either 30 or 90 Minutes of Elevated IOP. 147

Figure 5.4 Quantification of CTB AT in the ONH at 3, 6, and 24 Hours Following 30 Minutes of Elevated IOP. 149

Figure 5.5 Quantification of CTB AT in the ONH at 3, 6, and 24 Hours Following 90 Minutes of Elevated IOP. 151

Figure 5.6 AT of CTB in Longitudinal Sections of ONs at 3, 6, and 24 Hours Following 30 Minutes of Elevated IOP. 155

Figure 5.7 AT of CTB in the ON at 3, 6, and 24 Hours Following 90 Minutes of Elevated IOP. 157

Figure 5.8 Quantification of CTB AT in the ON at 3, 6, and 24 Hours Following Either 30 or 90 Minutes of Elevated IOP. 159

Figure 5.9 Individual Paired Measurements of Average CTB Intensity in the ON at 3, 6, and 24 Hour Following 30 or 90 Minutes of Elevated IOP. 161

Figure 5.10 CTB Labelling Intensity in the ONH and the Proximal and Distal ON at 24 Hours Following Sham Elevated IOP. 164

Figure 6.1 Example Images of pNF Labelling in Retinal Whole Mounts Following Elevated IOP. 172

Figure 6.2 Somal pNF Grading in Retinal Whole Mounts Following 30 Minutes of Elevated IOP. 174

Figure 6.3 Somal pNF Grading in Retinal Whole Mounts Following 90 Minutes of Elevated IOP. 176

Figure 6.5 Distribution of nonpNF Labelling in Control and Experimental ONHs at 3, 6, and 24 Hours Following 30 and 90 Minutes of Elevated IOP. 180

Figure 6.6 Comparison of nonpNF Labelling Intensity Between Control and Experimental ONHs at 3, 6, and 24 Hours Following 30 Minutes of Elevated IOP. 183

Figure 6.7 Comparison of nonpNF Labelling Intensity Between Control and Experimental ONHs at 3, 6, and 24 Hours Following 90 Minutes of Elevated IOP. 187

Figure 6.8 Distribution of pNF Labelling in Control and Experimental ONHs at 3, 6, and 24 Hours Following 30 and 90 Minutes of Elevated IOP. 189

Figure 6.9 Comparison of pNF Labelling Intensity Between Control and Experimental ONHs at 3, 6, and 24 Hours Following 30 Minutes of Elevated IOP. 191

Figure 6.10 Comparison of pNF Labelling Intensity Between Control and Experimental ONHs at 3, 6, and 24 Hours Following 90 Minutes of Elevated IOP. 194

Figure 6.11 pNF and nonpNF Labelling Intensity in the ONH at 24 Hours Following Sham Elevated IOP. 196

Figure 7.1 Example of Iba1 Labelling in a Cross-Section of the Peripapillary Retina. 202

Figure 7.2 Iba1 Labelling in Cross-Sections of the Peripapillary Retina at 3, 6, and 24 Hours Following 30 and 90 Minutes of Elevated IOP. 204

Figure 7.3 GFAP Labelling in the Peripapillary Retina at 3, 6, and 24 Hours Following 30 and 90 Minutes of Elevated IOP 207

Figure 7.4 Retinal GFAP Quantification Using WB at 24 Hours Following 90 Minutes of Elevated IOP. 209

Figure 7.5 Example Images of GFAP and Iba1 Labelling in Longitudinal Sections of Control ONHs. 211

Figure 7.6 Change in the Percent of Iba1+ Area in the ONH Over 3, 6, and 24 Hours of Recovery Following 30 or 90 Minutes of Elevated IOP. 214

Figure 7.7 Comparison of the Percent of Iba1+ Area in the ONH Between Control and Experimental ONHs at 3, 6, and 24 Hours Following 30 Minutes of Elevated IOP. 216

Figure 7.8 Comparison of the Percent of Iba1+ Area in the ONH Between Control and Experimental ONHs at 3, 6, and 24 Hours Following 90 Minutes of Elevated IOP. 219

Figure 7.9 Change in GFAP Labelling in the ONH Over 3, 6, and 24 Hours of Recovery Following 30 or 90 Minutes of Elevated IOP..... 221

Figure 7.10 Comparison of GFAP Labelling Between Control and Experimental ONHs at 3, 6, and 24 Hours Following 30 Minutes of Elevated IOP..... 224

Figure 7.11 Comparison of GFAP Labelling Between Control and Experimental ONHs at 3, 6, and 24 Hours Following 90 Minutes of Elevated IOP..... 227

Figure 7.12 Comparison of Iba1 and GFAP Labelling Between Control and Sham ONHs at 24 Hours Following 90 Minutes of Elevated IOP. 229

Figure 8.1 Time Course of Degenerative Pathology in the Visual Pathway Following 90 Minutes of Elevated IOP to 120 mmHg..... 286

Figure 8.2 Latency to Reach a Critical Threshold of Injury in RGCs During Different Severities of IOP Elevation..... 297

ABSTRACT

Retinal ganglion cell (RGC) axons relay visual information to the brain via the optic nerves (ONs) and optic tracts of the vertebrate visual pathway. RGC loss leads to irreversible blindness in many optic neuropathies, and is often associated with elevated intraocular pressure (IOP). Studies of experimentally elevated IOP have identified axonal transport (AT) disruption, cytoskeletal modification, and glial activation as contributing factors to RGC death. However, the capacity of these factors to recover following a transient IOP elevation remains unclear. This thesis employed AT tracing and immunological techniques to examine the spatiotemporal progression of RGC and glial responses in rat retina and ON following 30 or 90 minutes of acute elevated IOP, representing a sub-critical or critical insult, respectively. Anterograde AT was examined over 24 hours, and retrograde AT over 14 days, post-injury. Neurofilament (NF) phosphorylation and glial activation were evaluated concurrently with anterograde AT. Thirty minutes of elevated IOP did not cause RGC loss, however, retrograde AT was mildly reduced at all time points. There was a trend towards NF dephosphorylation in the optic nerve head (ONH), and some microglial activation was observed. Conversely, 90 minutes of elevated IOP caused significant RGC loss by 3 hours (40%), followed by a second wave of loss by 7 days (98%). Accumulation of phosphorylated NF was observed in a subset of RGC somas, the proportion of which increased with eccentricity. All AT was significantly disrupted at the ONH, and reduced retrograde AT in the ON suggested dysfunction in the distal axon or terminal. Microglial processes were increased in the inner plexiform layer, and activated microglia became prominent through all retinal layers over 24 hours. Notably, loss of AT function was not recovered following either duration of elevated IOP. These findings suggest that, rather than exhibiting reversible dysfunction following a sub-critical insult, RGCs succumb to high IOP-induced stress in a cell-by-cell manner that is acute and permanent, the degree of which depends on the duration of IOP elevation – short insults (e.g. 30 minutes duration) cause dysfunction and/or loss of a small population of vulnerable RGCs, whereas longer insults affect proportionally more RGCs. Differences in extrinsic and intrinsic risk factors likely contribute to variation in the critical threshold across the RGC population. This work contributes to a timeline of cellular events following acute elevated IOP, and supports the importance of studying critical injury and subtype-specific differences in RGCs.

LIST OF ABBREVIATIONS USED

A/P – anterior/ posterior

AC – amacrine cell

ANOVA – analysis of variance

APP – amyloid precursor protein

ARVO – Association of Research in Vision and Ophthalmology

AU – arbitrary units

ISO - isofluorane

AT – axonal transport

ATP – adenosine triphosphate

BC – bipolar cell

BDNF – brain-derived neurotrophic factor

Brn3a – brain-specific homeobox/ POU domain protein 3a

CDK5 – cyclin-dependent kinase 5

CNS – central nervous system

CTB – cholera toxin beta

D/V – dorsal/ ventral

DMSO - dimethylsulfoxide

EM – electron microscopy

GCL – ganglion cell layer

GDP – guanosine - 5'- diphosphate

GFAP – glial fibrillary acidic protein

GFP – green fluorescent protein

GTP – guanosine - 5'- triphosphate

HC – horizontal cell

Iba1 – ionized calcium-binding adapter molecule 1

IHC - immunohistochemistry

INL – inner nuclear layer

IOP – intraocular pressure

IP3 – inositol triphosphate

IPL – inner plexiform layer

KIFs – kinesin superfamily proteins

LC – lamina cribrosa

LGN – lateral geniculate nucleus

MAP – mean arterial pressure

MAPs – microtubule associated proteins

MBP – myelin basic protein

MT – microtubule

NF – neurofilament

NF-H – neurofilament heavy

NF-L – neurofilament light

NF-M – neurofilament medium

NFL – nerve fibre layer

NMDA – N-methyl-D-aspartate

nonpNF – non-phosphorylated neurofilament

ON – optic nerve

ONH – optic nerve head

ONL – outer nuclear layer

OPL – outer plexiform layer

OPP – ocular perfusion pressure

OS – outer segments

Panx – pannexin

PANX1 – pannexin 1 channel

PBS – phosphate buffered saline

PFA – paraformaldehyde

pNF – phosphorylated neurofilament

PR – photoreceptors

RGC – retinal ganglion cell

RITC – rhodamine isothiocyanate

SC – superior colliculus

SEM – standard error of means

TRP – transient receptor potential

TRPV4 – transient receptor potential vanilloid isoform 4

TTX - tetrodotoxin

WB – western blot

ACKNOWLEDGEMENTS

I have been incredibly fortunate to meet, get to know, and learn from many exceptional people during the course of this degree. I would like express my sincere appreciation to my advisor, Dr. Balwantray Chauhan, for this opportunity, for teaching me many skills essential for research (and life), and for his support and guidance. Many thanks also to Dr. Xu Wang, who, in many ways, was a co-supervisor in the early years of this project, and who conceived many of the ideas behind it - she is a wonderful friend and mentor. One of the greatest advantages of being a part of the retina and optic nerve lab is the shared company of so many bright minds and friendly faces with which to share ideas, successes, and the pangs of science life. Kelly Stevens was my bench Miyagi, softball idol, and personal counselor; Michele Archibald has been a wonderful teacher and friend – thank you for all the help. Thanks to my colleague and office pal, Corey Smith, for his stats consults and work on the mixed effects model, and putting up with my persistent throat clearing. Thanks to Julie Levesque for help with the cell counting analysis. Special mentions also to Elizabeth Cairns, Dr. Spring Farrell, Jeanette Nason, and Ben Smith, and the entirety of the retina lab – I appreciate you all. Thanks to Dr. Neil O'Leary and Dr. Vishva Danthurebandara for their work and input on my statistical analyses, and to my supervisory committee for their hours and input, in particular Dr. Steven Barnes for his guidance. To my physiology colleagues, in particular Borbala Podor and Dylan Quinn, these Tupper years would have been pretty dull without you. Finally, deepest thanks to my friends and family, including my wonderfully supportive partner Jamie, for the never-ending support that made this all possible - love you all!

CHAPTER 1 – INTRODUCTION

In mammalian vision, retinal ganglion cells (RGCs) perform the crucial step of relaying visual information from retina to brain. Without this function, the eye's unique perception of the physical world is lost. RGC axonal injury and RGC loss occur in several optic neuropathies, leading to visual disability and blindness - limitations accompanied by a decline in quality of life and considerable psychosocial impact [1] - in millions of people worldwide [2]. Among other processes, modification of RGC axonal structure, disruption of axonal transport (AT), and changes in glial function have been linked to the pathophysiology of RGC death [3-5]. Studies of RGC dysfunction and death are often pursued through the use of animal models exhibiting elevated intraocular pressure (IOP), which causes mechanical and ischemic insults to RGC axons as they leave the eye. The purpose of this thesis was to elucidate the timeline of key cellular events following elevated IOP that are associated with either RGC survival or RGC degeneration. The following sections describe the structural and functional components of RGC axonal degeneration in response to elevated IOP.

1.1 The Retina and Optic Nerve (ON)

1.1.1 Gross Visual Anatomy

Vertebrates have evolved remarkable systems for collecting and processing visual input from the environment. At the core of the visual system is the retina: a multilayered and extensively organized sheet of neural tissue that transmits visual information to

higher visual centres in the brain via RGC axons. When light enters the cornea and passes through the pupil (Figure 1.1), it is focused on the retina by the lens, the convexity of which can be adjusted by the ciliary muscles [6]. This light must then cross the layers of the retina to arrive at the outer segments of the photoreceptors, embedded in the pigment epithelium of the choroid, where phototransduction takes place.

1.1.2 Retinal Function and Organization

The cascade of visual information in the retina begins with the photoreceptors (Figure 1.2). In a process called phototransduction, photoreceptors transduce photonic energy into an electrical signal via light sensitive molecules called opsins [6]. Rod-photoreceptor (important for low-light vision) and cone-photoreceptor (used in colour vision and day vision) somas are located in the outer nuclear layer (ONL) of the retina, with their pedicles extending into the outer plexiform layer (OPL) [6].

The OPL is the first retinal neuropil in the visual cascade. Here photoreceptor pedicles form a synaptic plexus with the dendritic processes of bipolar cells (BCs) and horizontal cells (HCs). The inner nuclear layer (INL) contains the somas of BCs, HCs, amacrine cells (ACs), as well as Müller cells, which are radial glial cells that form the outer and inner limiting retinal membranes, and displaced RGCs. BCs, HCs and ACs then send their processes into the innermost neuropil, the inner plexiform layer (IPL) [7].

The IPL is functionally and morphologically divided into two laminae according to the type of BC input being received: OFF-BCs, which are excited in darkness, terminate in sublamina a (deeper in the retina), whereas ON-BCs, which are inhibited in

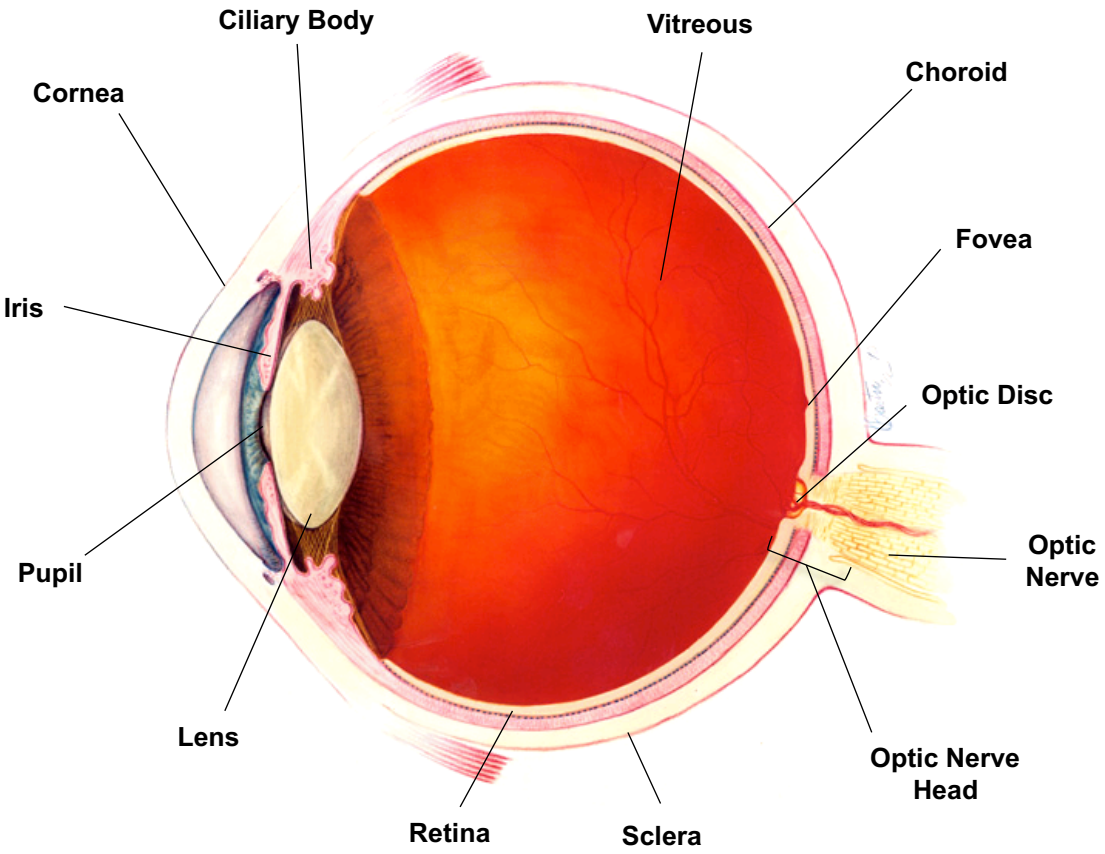

Figure 1.1 Gross Anatomy of the Eye. From the National Eye Institute, National Institutes of Health, Bethesda, MD.

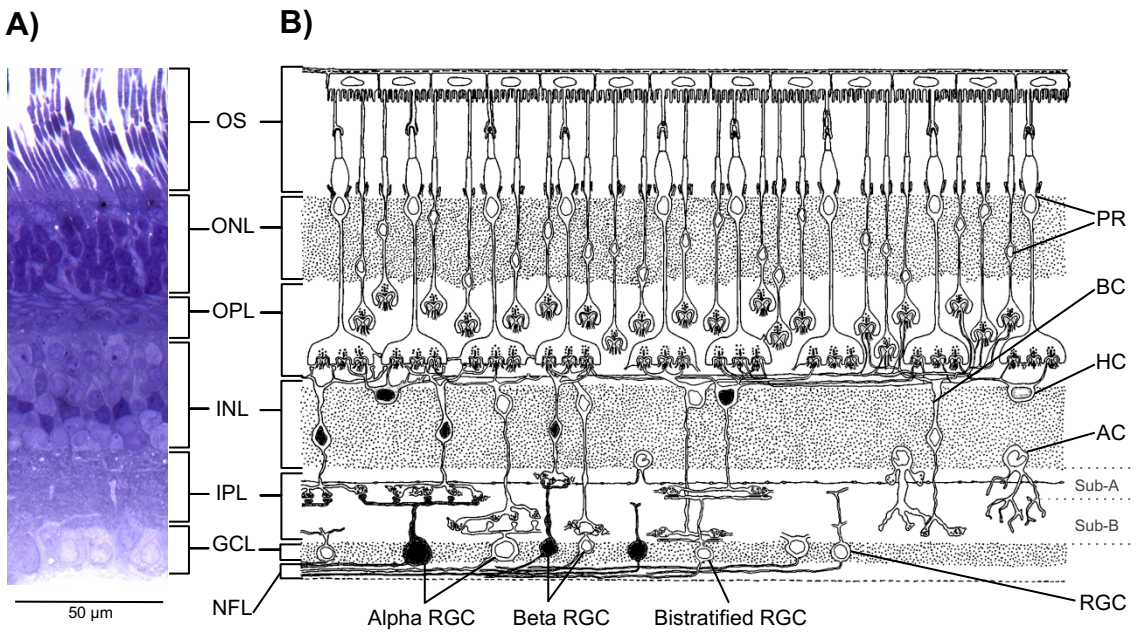

Figure 1.2 Retinal Anatomy and Connectivity. **A)** Nissl stained retinal cross-section showing: photoreceptor outer segments (OS); the outer nuclear layer (ONL); the outer plexiform layer (OPL); the inner nuclear layer (INL); the inner plexiform layer (IPL); and the ganglion cell layer (GCL). **B)** Schematic of retinal neurons and their connections. Photoreceptors (PRs) synapse upon bipolar cells (BCs) in the OPL, and BCs upon retinal ganglion cells (RGCs) in the IPL. Lateral integration is performed by horizontal cells (HCs) in the OPL, and amacrine cells (ACs) in the IPL. ON (dendrites in sublamina A) and OFF (dendrites in sublamina B) alpha and beta RGCs, as well as an ON-OFF bistratified RGC, are depicted. RGC axons extending along the inner surface of the retina form the nerve fibre layer (NFL). Panel **(A)** adapted from Lee and colleagues [8], with permission. Panel **(B)** adapted from Field and Chichilnisky [9], with permission.

darkness, terminate in sublamina b (closer to the vitreous) [7]. These BCs in turn contact the dendritic arbors of OFF- and ON- RGCs, which are similarly named for ramifying in either sublamina a or b, respectively. There is also a subset of RGCs with arborisations in both sublaminae, called ON-OFF RGCs, that are capable of detecting the onset and offset of light [10].

RGC somas are located in the ganglion cell layer (GCL) along with displaced ACs. Visual signals then travel along RGC axons, which form the nerve fibre layer (NFL), and converge at the optic nerve head (ONH) to exit the eye [7]. While the GCL is so named for the presence of RGC somas, it should be noted that displaced ACs, which have a similar soma size to small RGCs, make up a significant portion of the GCL, representing anywhere from 3 to 50% of the resident cell population, depending on species and eccentricity from the ONH [11-14].

1.1.3 RGC Types

Many types of RGCs exist, characterized by unique morphology, anatomy and function, and the diversity of mammalian RGCs is large and variable among species. Morphological classification of RGCs originated with the seminal work of Santiago Ramón y Cajal in 1892 [15]. Ramón y Cajal's detailed drawings revealed how RGCs differ in many physical qualities, including size and shape of dendritic arbor, and depth of ramification in the IPL. Early physiological recordings also revealed a dichotomy in RGC responses to stimuli: some exhibited a sustained response to a prolonged stimulus, whereas others responded transiently [16]. Variability in structure and function has lead to numerous lines of classification and varying estimates of the number of RGC types.

As many as 22 morphologically distinct RGCs have been described in the mouse retina [17], and 23 in humans [18]. Despite their complexity, RGCs are commonly divided into three main morphological classes: alpha cells (Figure 1.3 A), beta cells (Figure 1.3 B), and gamma cells [19, 20]. These classes have been identified across multiple species, including humans [21], non-human primates [22-25] , cats [20, 26], ferrets [27], and rodents [17, 28-30].

Alpha cells, otherwise known as parasol and magnocellular cells, have large dendritic arbors and make up between 5 and 10% of the total RGC population in primates [25]. They are described to be the morphological correlate to the physiologically classified Y cells, which display a brisk-transient response [20, 31, 32]. Alpha cells are found in greater proportion in the peripheral retina and often receive convergent input from tens of thousands of rods. Such input results in poor spatial resolution, but high sensitivity to small transient changes in illumination and movement in the visual field, in addition to vision in scotopic conditions [7, 33].

Beta cells, otherwise known as midget and parvocellular cells, have smaller diameter somas and dendritic arbors, and make up approximately 70% of the total RGC population in primates [34] and 45% in cats [35]. Like alpha cells, beta cells have a physiological correlate, X cells, which have a brisk-sustained response [20, 31, 32]. Beta cells are found primarily in the central retina and participate in a 1:1:1 relationship of cone-BC-RGC at the fovea [36]. Because of this, midget cells are specialized in chromatic vision, and are important for central acuity and vision in photopic conditions.

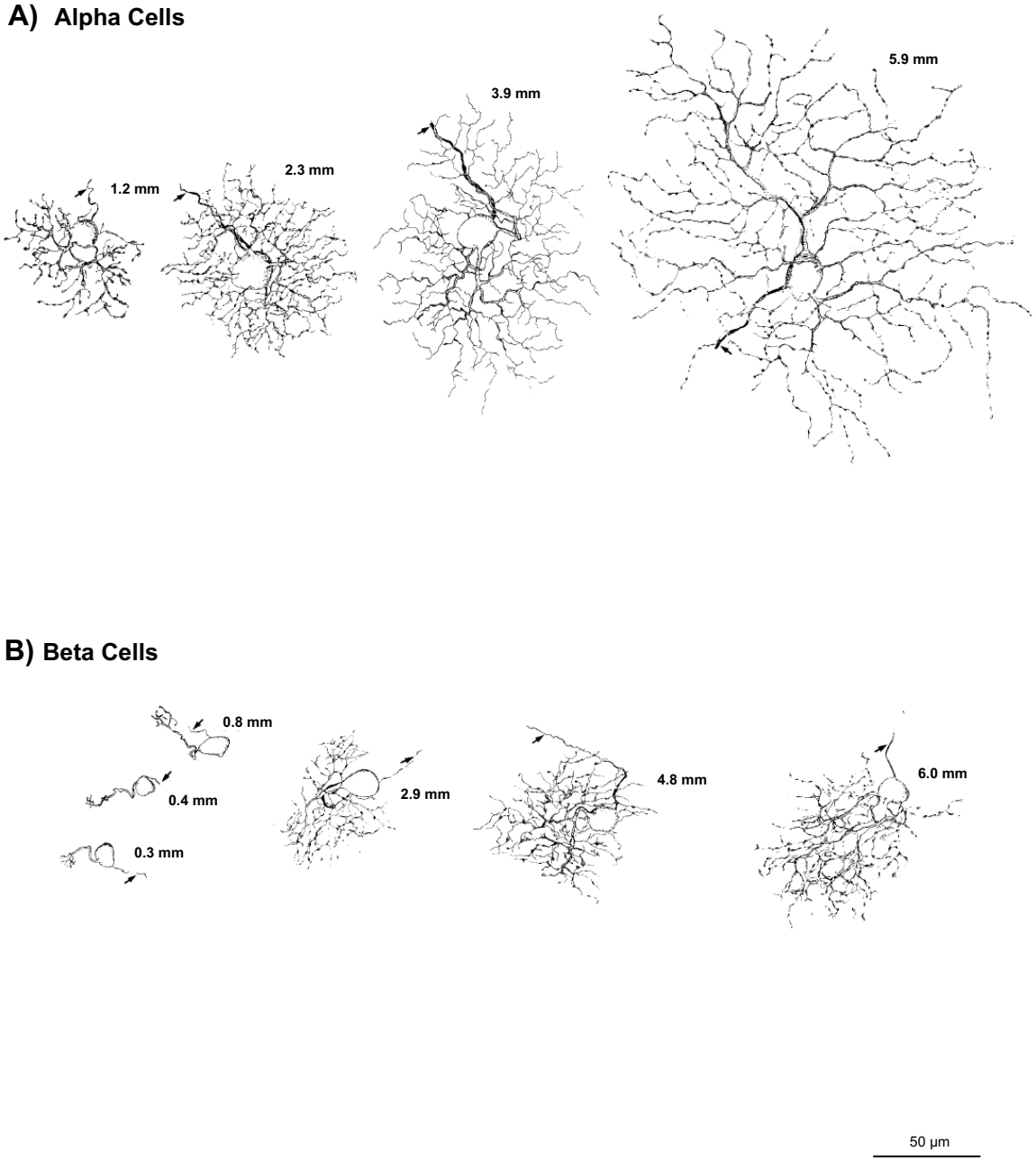

Figure 1.3 Alpha and Beta RGCs. A) Schematic representation of alpha RGCs at increasing eccentricities from the optic disc (distances in mm indicated next to each cell). **B)** Representation of beta RGCs at varying retinal eccentricities. Figure adapted from Ghosh and colleagues [25], with permission.

Gamma cells have been estimated to represent between 50% and 60% of the total RGC population in the cat [37], while the proportion in other species is unclear. However, gamma cells comprise a heterogeneous population, often referred to as "non-alpha, non-beta" cells, encompassing many RGC subtypes [19, 20, 23, 38], including delta and epsilon cells [15].

Finally, non image-forming visual functions, such as the regulation of circadian rhythms, the pupillary light reflex, masking behaviour, and light-induced melatonin suppression, are regulated by a specialized subset of RGCs, referred to as intrinsically photosensitive RGCs (ipRGCs). ipRGCs are able to intrinsically perform phototransduction due to their expression of the photopigment melanopsin [39, 40]. To date, ipRGCs have been divided into as many as 6 subtypes (M1-M6) [41], and are relatively rare, representing approximately 1-3% of the RGC population in rodents [41, 42]) and 0.2-0.8% in humans [43].

1.1.2 Anatomy of the RGC Retinal Projection

In all mammalian visual systems, RGCs are the projection neurons that form the pathway for information transfer from retina to brain. RGCs serve this role via their long axons, which travel along the NFL from peripheral to central retina, where they come together as nerve bundles at the ONH to form the ON. In the human retina, the axons of around 1.5 million RGCs relay signals regarding the spatial, temporal, and spectral properties of the surrounding environment [44].

Upon leaving the eye, axons remain bundled and exit through structural tubes formed by collagen fibres and interspersed astrocytes [6]. These tubes form the

'honeycomb' structure of the lamina cribrosa (LC), which acts as a permeable elastic barrier between the inside and outside of the globe (Figure 1.4 A). In humans, the LC bridges the scleral opening [45]. The LC is similarly located in rats and mice, however, is less structurally defined compared to primates and has a relatively higher glial content (Figure 1.4 B) [46]. Change to LC geometry is thought to play a role in the damage of RGCs associated with glaucoma [47], a phenomenon discussed further in section 1.4.3.1.

While retinotopic organization of nerve bundles is conserved throughout the length of the ON in humans [48], the bundled organization of axons is lost shortly after the posterior boundary of the LC in mice [46]. In humans, approximately half of RGC axons decussate at the chiasm to form the optic tracts [49], whereas this number is between 85% and 97% in rats and mice with some variation between strains [42, 50, 51].

In primates, RGC axons project primarily to the lateral geniculate nucleus (LGN) of the thalamus [25, 52]. Rat and mouse RGCs project almost exclusively to the superior colliculus (SC) [28, 53]; however, a small number of RGCs project to other areas including the LGN, the intergeniculate leaflet, the olivary pretectal nucleus, the suprachiasmatic nucleus and the pretectal area [54, 55]. Retinotectal projections in all species terminate in the superficial layers of the SC - the stratum griseum superficiale and the stratum opticum - where the organization of inputs varies according to retinotopic origin, cell type, and lateralization [56].

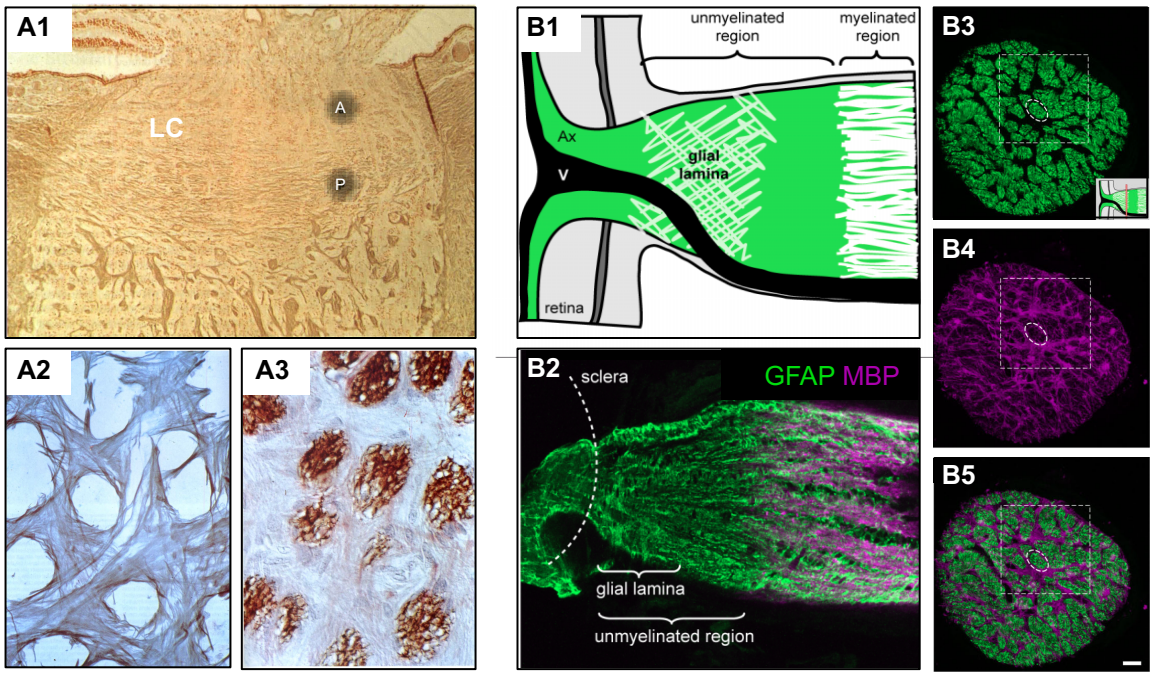

Figure 1.4 Structure of Human and Mouse LC. A) A1: Longitudinal cross-section of a human ONH stained for collagen fibres. The LC is positioned just posterior the retina at the opening of the sclera. LC limits are indicated by A – anterior, and P – posterior. **A2:** Cross-section of the ONH and staining for collagen fibres reveals the porous structure of the LC. **A3:** Staining for astrocytes (pink) and axons (brown) shows astrocytes ensheathing axon bundles as they pass through the pores of the LC. **B) B1**: The location of the LC in mouse is similar to human, beginning just posterior the retina, however, is primarily composed of glia (astrocytes). **B2:** Staining for GFAP (astrocytes) and myelin basic protein (MBP) in the mouse ONH. **B3:** RGC axon bundles in mouse ONH cross-section, inset shows depth of cross-section. **B4:** GFAP (astrocytes) in a cross-section of the mouse ONH. **B5:** Overlay of **B3** and **B4** showing bundles passing through pores provided by the astrocytes. Panels **A1-3**: Adapted from Elkington and colleagues [57], with permission. Panels **B1-5**: Adapted from Sun and colleagues [46], with permission.

1.1.3 Glia of the Retina and ON

There are four main types of resident glia in the visual pathway: Müller cells, which are exclusive to the retina; astrocytes and microglia, which are present in the retina, ONH and ON; and oligodendrocytes, which are present in the myelinated regions of the visual pathway (anatomy and function reviewed by Vecino and colleagues [58]; Figure 1.5). From their soma in the INL, Müller cells extend radial processes through all layers of the neural retina [59]. At the inner border of the retina, Müller cell end feet form the inner limiting membrane bordering the vitreous, while processes at the outer border terminate in the photoreceptor layer [59]. Secondary processes extending from the main trunk of the Müller cell tightly surround neighbouring neurons and vasculature. This configuration allows Müller cells to perform many homeostatic functions, such as the spatial buffering of neurotransmitters and other ions throughout the retinal extracellular environment [58, 59]. Astrocytes are found in the NFL and GCL, and are involved in the maintenance of retinal homeostasis and the blood-retina barrier [58]. Astrocytes are also an essential structural element of the ONH (previously described in section 1.1.2), and are present throughout the ON and higher visual pathway [58, 60]. Microglia, one of the primary immune cells of the visual pathway, are present in the retina, ONH and ON [58, 61]. Finally, oligodendrocytes form the myelin sheath insulating RGC axons as they exit the eye and extend to the brain, the spatial onset of which varies between species [62-64].

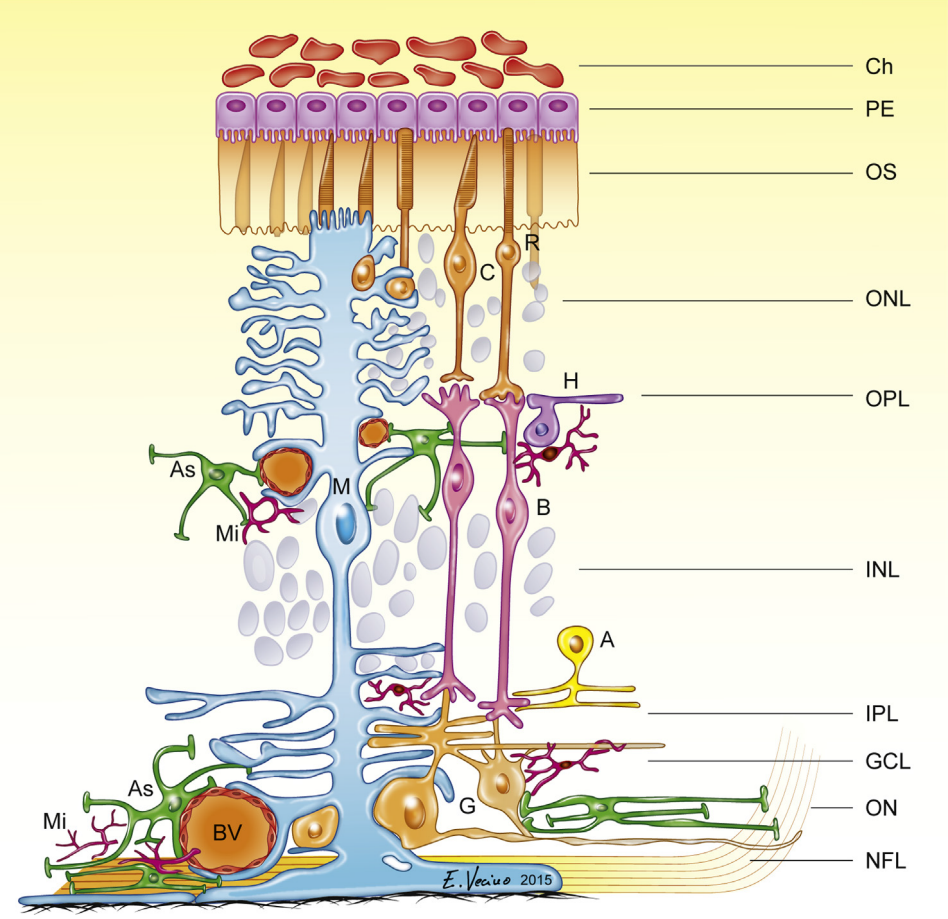

Figure 1.5 Glia of the Retina. Three types of glia are present in the retina. Müller cells (M) extend throughout the thickness of the retina and extend secondary processes ensheathing surrounding neurons and blood vessels (BV). Astrocytes (As), which also interact with neurons and blood vessels, are present in the NFL, GCL and OPL. Resting microglia (Mi) are present in the NFL, GCL, IPL and OPL. A - amacrine cell, As – astrocyte, B – bipolar cell, BV – blood vessel, C – cone, Ch – choroid, G – ganglion cell, GCL – ganglion cell layer, H – horizontal cell, INL – inner nuclear layer, IPL – inner plexiform layer, M – Müller cell, Mi – microglia, NFL – nerve fibre layer, ON – optic nerve, ONL – outer nuclear layer, OPL – outer plexiform layer, OS – outer segments, PE – pigment epithelium, R – rod. From Vecino and colleagues [58], with permission.

1.2 The Neuronal Cytoskeleton

All neurons of the central nervous system (CNS), including RGCs, are equipped with a specialized set of proteins that provide guiding forces during development, as well as structural and functional support in maturity. Collectively, these proteins are known as the neuronal cytoskeleton. Cytoskeletal proteins often exist in a polymerized form as microtubules, actin microfilaments, and neurofilaments (NFs) (Figure 1.6). They are involved in transporting materials from one site of the neuron to another and providing the neuron with its shape, thereby directly affecting the strength of neuronal output, as well as the morphology and function the neuron in general [65-67].

1.2.1 Microtubules

Microtubules contain α- and β-tubulin monomers and are interconnected via microtubule-associated proteins (MAPs) [67]. An α- and β-tubulin together form a heterodimer. Heterodimers polymerize together to form protofilaments. The final structure of a microtubule includes 13 protofilaments arranged to form a hollow cylinder approximately 25 nm in diameter. Tubulins express a binding site for guanosine-5'-triphosphate (GTP) that is important in microtubule polymerization and depolymerization - respectively known as rescue and catastrophe. During assembly, tubulin monomers are bound to GTP. Shortly after assembly, GTP may be hydrolysed to guanosine-5'-diphosphate (GDP) [68]. If hydrolysis occurs at a faster rate than the new GTP-bound tubulin is added, microtubule catastrophe will occur (Figure 1.7).

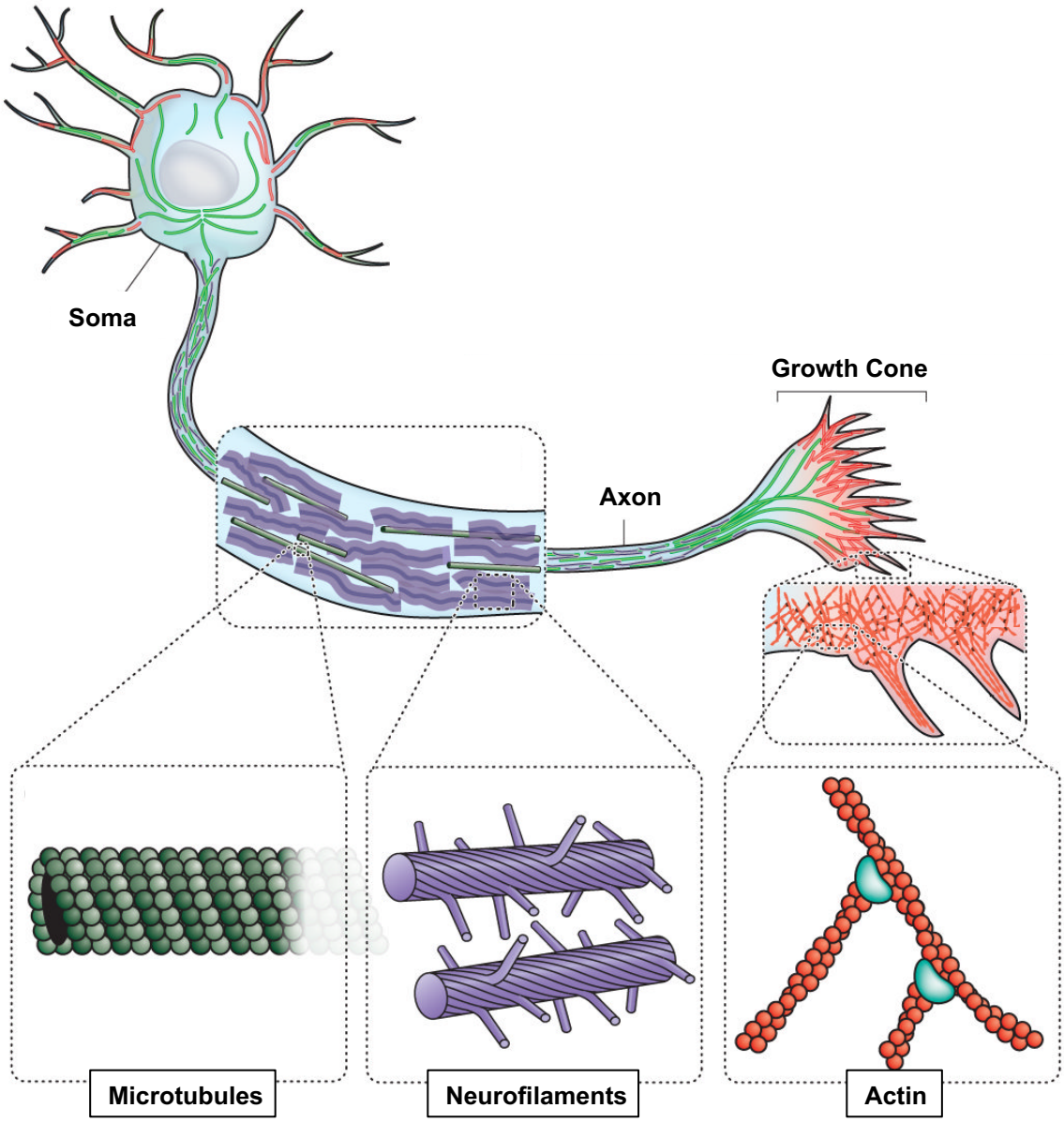

Figure 1.6 The Neuronal Cytoskeleton. Components of the neuronal cytoskeleton are differentially expressed within the neuron: Microtubules (green) provide structural stability throughout the cell; neurofilaments (purple) are solely located in the axon; and actin filaments (orange) concentrate near the plasma membrane and in areas requiring a high degree of motility. Adapted from Fletcher and Mullins [69], with permission.

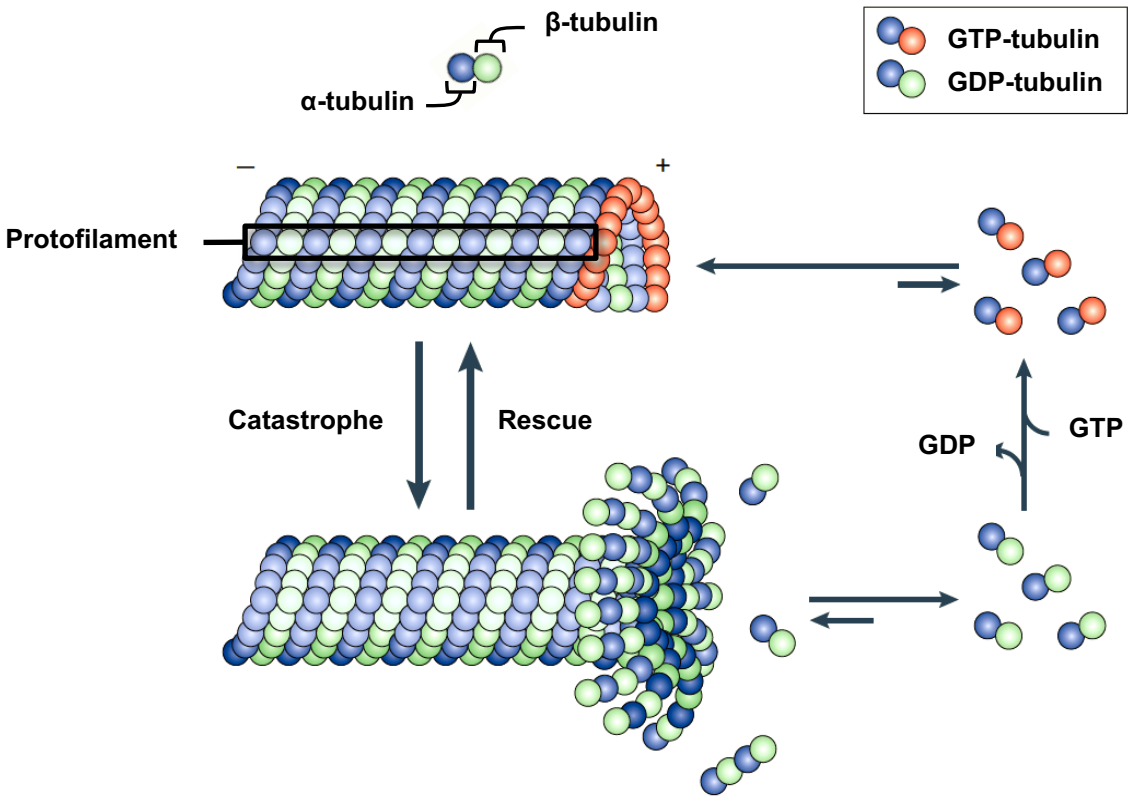

Figure 1.7 Microtubule Catastrophe and Rescue. Protofilaments of tubulin heterodimers connect to form a cylindrical microtubule. Hydrolysis of GTP-tubulin to GDP-tubulin promotes depolymerization, while addition of GTP-tubulin promotes stability. Reproduced from Cheeseman and Desai [70], with permission.

Beyond their functional disparity, axons and dendrites also differ in their organization of microtubules. Microtubules are polarized, with a fast-growing 'plus' end and a slow-growing 'minus' end [71]. While microtubules in the axon are unipolar, with 'plus' ends always pointing away from the cell body, microtubules in dendrites can be oriented in either direction [72] (Figure 1.8). Orientation of microtubules is important in the AT of cellular materials, as will be discussed in section 1.3.1. Microtubules of the dendrite and axon also associate with different MAPs. MAPs are thought to control the spacing of microtubules, which is known to be much tighter in axons than dendrites [73].

1.2.2 Actin

Actin filaments have a different structure from microtubules, and play very different roles in the neuron. They are formed by the polymerization of globular actin (G-actin) into filamentous actin (F-actin), forming a single-stranded, left-handed helix approximately 5 nm in diameter [67]. Assembly of actin is an adenosine-5'-triphosphate (ATP)–dependent process where the addition of ATP-actin (G-actin bound to ATP) occurs at the 'plus' end [74] (Figure 1.9). The growth and cellular location of actin is mediated by several different actin binding proteins [67].

Due to their dynamic nature, actin filaments are localized to compartments of the neuron requiring a high degree of motility. Dendritic spines, the dynamic post-synaptic appendages located on dendrites, are rich in actin and devoid of tubulin [75]. The motile ends of axonal growth cones take advantage of actin dynamics to make quick directional changes in response to environmental cues [76].

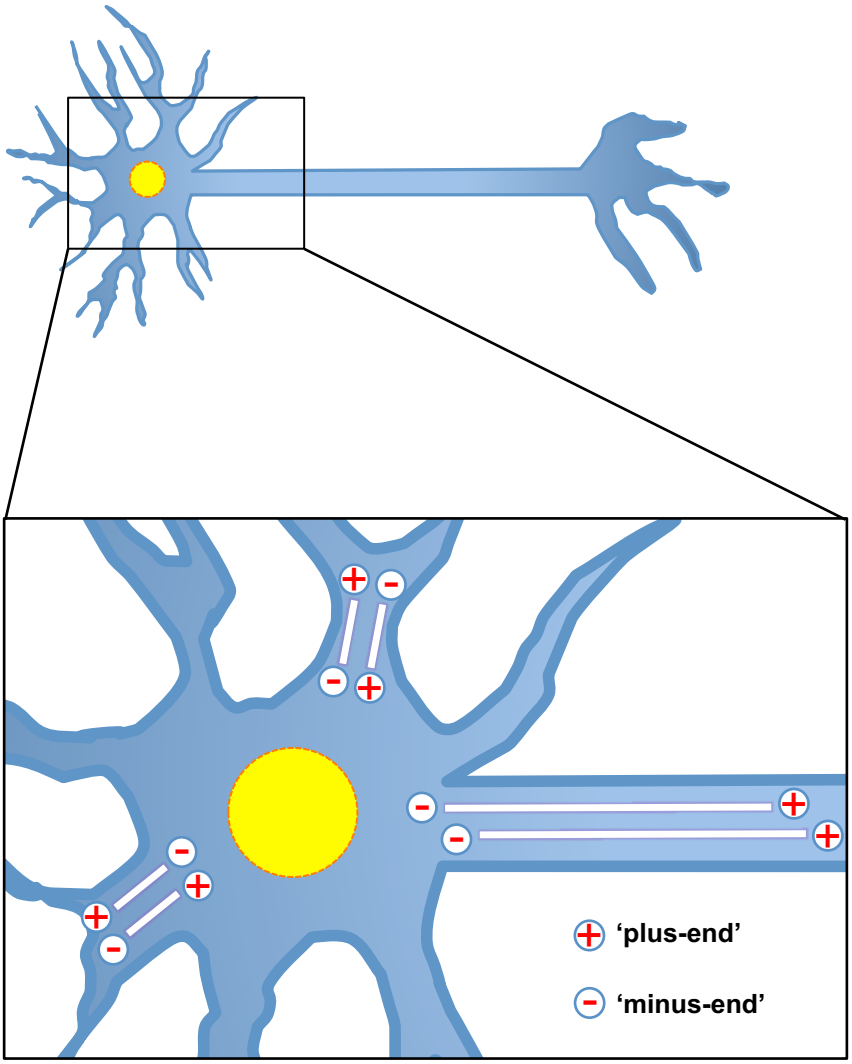

<u>Figure 1.8</u> Orientation of Microtubules Within the Neuron. Microtubules are polarized structural filaments, with a fast-growing '+' end and a slow-growing '-' end, that differ in their orientation depending on their location within the neuron. Microtubules in the axon are unipolar, with 'plus' ends always pointing away from the cell body, while microtubules in dendrites can be oriented in either direction.

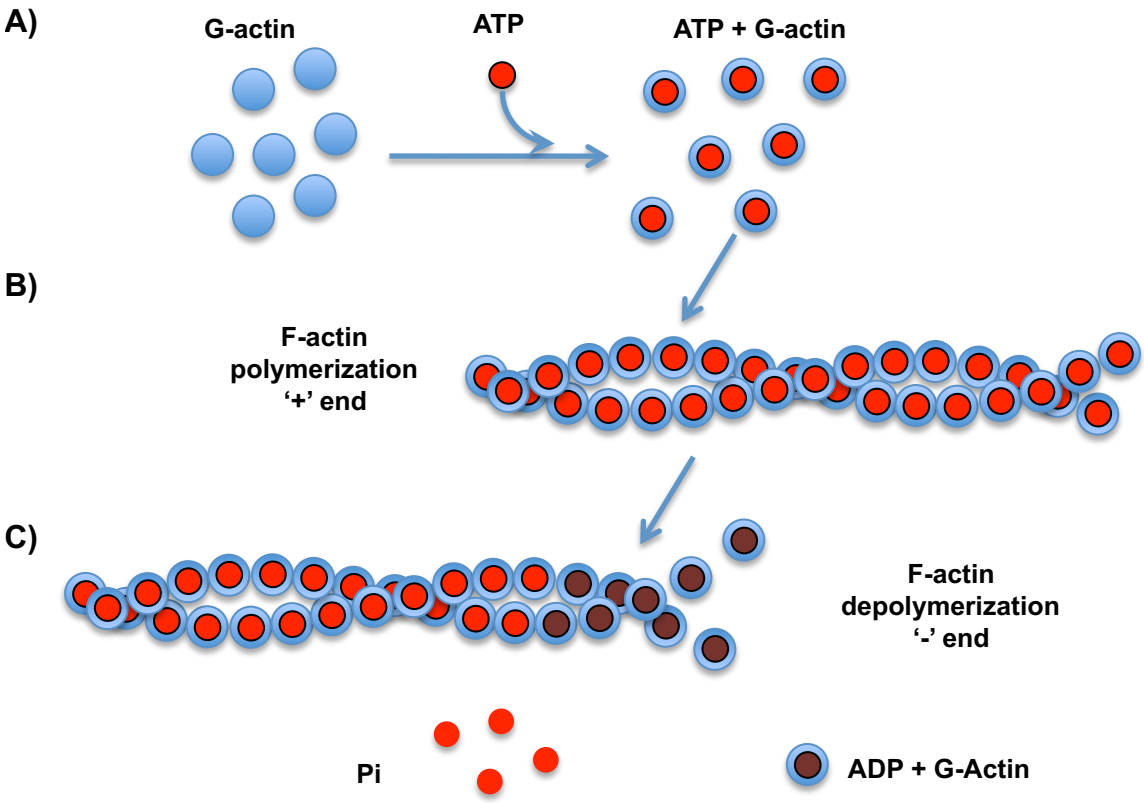

Figure 1.9 Assembly and Disassembly of Actin Filaments. **A)** G-actin becomes bound to ATP. **B)** Activation with ATP causes polymerization of G-actin to form F-actin. **C)** Hydrolysis of ATP to ADP + Pi causes depolymerization of F-actin at the '-' end.

1.2.3 Neurofilaments (NFs)

NFs are a type of intermediate filament specific to neurons. They are approximately 10 nm in diameter and are the most abundant cytoskeletal protein, outnumbering microtubules 5- to 10-fold [77]. There are three NF subunit isoforms: light (NF-L), medium (NF-M), and heavy (NF-H), named for their respective molecular weights (Figure 1.10). Additional accessory subunits, α-internexin and peripherin, have been proposed to also co-polymerize with NFs.

Each subunit consists of a homologous head and rod domain, and a tail domain that varies between subunits. The rod domain is important for dimerization of subunits, while the head and tail domains aid in protein-protein interactions [78]. NF assembly begins with the dimerization of two subunits to form a coiled-coil (Figure 1.11). These dimers consist of a NF-L/NF-L pair (a homodimer), or NF-L paired with either NF-M or NF-H (heterodimers). This type of pairing occurs because the two larger subunits have been shown to be incapable of self- or co-polymerization [79]. The NF dimers arrange head-to-tail to form a tetramer. The tetramers arrange end-to-end to form protofilaments, which come together to form a hollow cylinder, as in microtubule assembly [80].

The intermediate filament-binding proteins α-internexin and peripherin have been proposed to co-polymerize with NF triplet proteins. While early investigations hypothesized that α-internexin and peripherin formed their own independent filament system, it has since been shown that both of these proteins are present in stoichiometric amounts correlated to NF triplet proteins [81, 82]. α-internexin has been shown to associate with NF-M, is crucial to NF-M transport in the absence of NF-L and NF-H [82], and also may play important roles in NF association with the membrane-bound

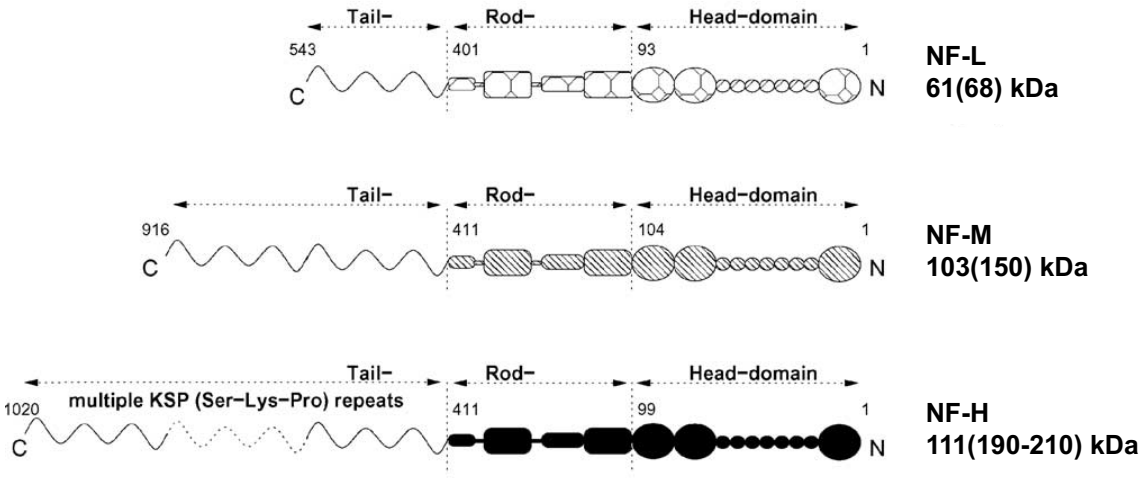

Figure 1.10 Neurofilament Subunits. Neurofilament subunits are amino acid chains, each with a homologous head and rod domain and variable tail domain. NF-L – neurofilament light, NF-M – neurofilament medium, NF-H – neurofilament heavy. Molecular weights are listed for each isoform, and molecular weights of phosphorylated forms are in parentheses. C – carboxy terminal, N – amino terminal. Reproduced from Petzold [80], with permission.

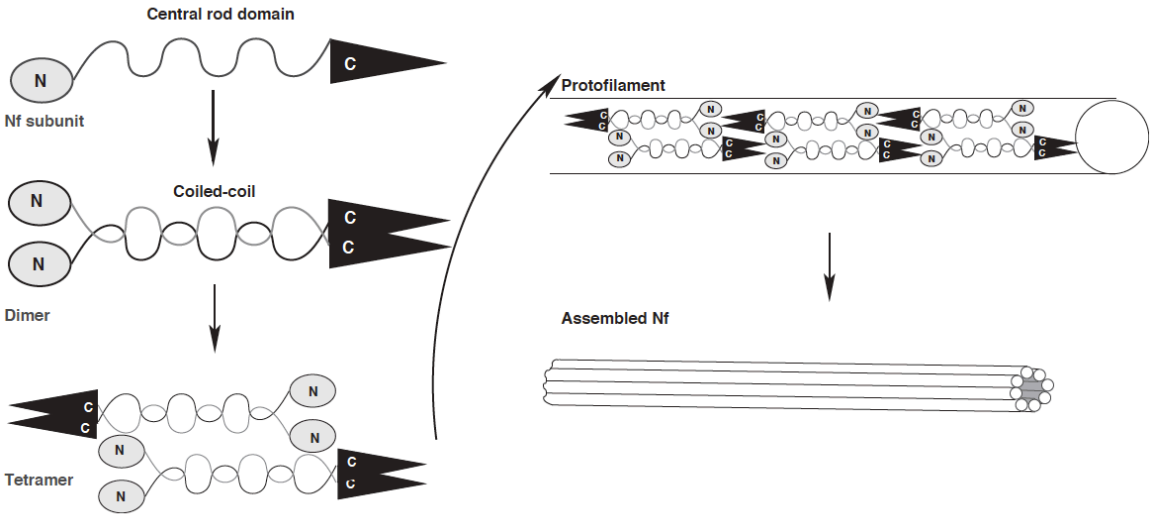

Figure 1.11 Neurofilament Assembly. Neurofilament subunits dimerize to form a coiled-coil. Coiled-coils tetramerize head-to tail and tetramers arrange end-to-end to form protofilaments. These protofilaments come together to form a complete neurofilament. C – carboxy terminal, N – amino terminal. Reproduced from Petzold [80], with permission.

cytoskeleton and promotion of neuronal plasticity [83]. Expression of α-internexin declines in peripheral neurons in early development, however, peripherin expression increases shortly thereafter, functioning similar to α-internexin in peripheral neurons [81, 83].

In the healthy neuron, NF proteins are located primarily in the axon, less in the cell body and dendrites, and absent from dendritic spines and nerve terminals [84, 85]. NFs modulate neuronal structure by maintaining axon calibre [83, 86] and confer normal dendritic arbourization in developing neurons [87]. Unsurprisingly, NF dysfunction is linked to many pathological conditions [67, 88].

1.2.4 Phosphorylation-Dependent Regulation of Cytoskeletal Proteins

Phosphorylation (the addition of a phosphate group) and dephosphorylation (its removal) are ubiquitously employed as a means to regulate various intracellular processes and are executed by kinases and phosphatases, respectively [89]. Modification of phosphorylation state can lead to activation or deactivation of proteins [90-92], including other enzymes, and affect protein conformation [89], structural stability [93, 94] and mobility [92, 95-97]. A key process effecting change in neuronal structure is phosphorylation of the cytoskeleton. While microtubules and actin filaments are mostly regulated by their respective binding proteins, phosphorylation is central to NF regulation, with many phosphorylation sites present directly on the head and tail domains [88, 98]. The main purpose of the phosphorylation-dephosphorylation balance in NFs is to regulate structural stability within the neuron [88].

MAPs bind and stabilize microtubules and promote tubulin polymerization [99]. Microtubule-associated regulating kinase is capable of phosphorylating MAPs, causing them to dissociate from microtubules [100]. This dissociation inhibits tubulin-polymerization and destabilizes the microtubule. The same relationship is true for the Tau family of MAPs, which are phosphorylated by numerous kinases including protein kinase N [101].

The actin depolymerizing factor/ Cofilin family of binding proteins, which are essential for regulation of actin dynamics, are themselves regulated by phosphorylation. Phosphorylation of actin depolymerizing factor/cofilin by LIM kinase inhibits its depolymerizing activity, tipping the actin equilibrium towards the filamentous form [102].

NFs, produced in the soma, express numerous lysine-serine-proline motifs on their head and tail where phosphorylation can occur [83]. A multitude of enzymes are capable of phosphorylating and dephosphorylating NFs. Glycogen synthetase kinase-3, protein kinases A and C and cyclin-dependent kinase-5 (CDK5) are all involved in phosphorylating the head domain [103-105]. Phosphorylation of the tail domain involves a range of protein kinases, including protein kinase A and CDK5 [78, 106, 107]. Interestingly, phosphorylation of NFs, a phenomenon likely involved in RGC degeneration after injury [108-111], confers resistance to degradation by proteases such as calpain [93]. Neurofilament dephosphorylation is primarily achieved by protein phosphatase 1 and 2A [107], and possibly calcineurin [112].

While NFs are only lightly phosphorylated in the soma and dendrites, their tail domains become heavily phosphorylated after transport into the axonal compartment [80,

107]. Phosphorylation of the head domains is known to inhibit NF assembly, whereas phosphorylation of the tail domains causes an extension of charged NF-H side-arms leading to greater NF-to-NF spacing. NF-H is the most commonly phosphorylated NF subunit, and likely the most heavily phosphorylated protein in the human brain [80]. Phosphorylation of NFs also regulates NF transport throughout the cell, by either decreasing NF binding affinity for anterograde motors, or by increasing NF-NF interactions that compete with AT motor binding [113].

1.3 Axonal Transport (AT)

Mammalian neurons typically have multiple dendritic processes close to the cell body and an axon, whose length can vary from hundreds of microns in interneurons to a metre or longer in primary motor and sensory neurons [114]. The axonal compartment of motor and sensory neurons, including that of RGCs, can comprise greater than 90% of the internal cell volume and, with limited or no mechanisms to transcribe proteins, relies heavily on the transport of essential materials from the cell body [115]. Like other neurons, RGCs are able to transport a variety of cargo via the interplay of motor, adapter, and structural proteins.

1.3.1 Molecular Motors, their Adapters, and Structural Scaffolds

Microtubules and actin form a network of structural ‘highways’ by which molecular motors move cargo from one end of the cell to the other. This section reviews the various motor proteins that associate with microtubules and actin.

1.3.1.1 Kinesin and Dynein

Microtubules have a polarized organization in the axon: 'plus' ends face towards the nerve terminal while 'minus' ends are closer to the cell body. There are two main families of molecular motors that use the microtubule highway: Kinesins and dyneins (Figure 1.12). Kinesins are primarily 'plus end'-directed motors (with a few exceptions e.g. C-Kinesins) moving towards the nerve terminal, i.e. anterograde AT, whereas dynein motors are directed towards the 'minus ends' and participate in retrograde AT towards the cell body [116].

The kinesin superfamily proteins (KIFs) are part of a large gene family of 45 motor proteins [117]. KIFs are heterotetramers of two light and two heavy amino acid chains. The two heavy chains come together to form a coiled-coil and two amino (N)-terminal globular heads. These globular heads form the KIF motor domains, which contain both a microtubule-binding sequence and an ATP-binding sequence. To begin the transport process, one motor domain associates with a β-tubulin binding site on the microtubule. The catalytic core of the motor domain hydrolyzes ATP and begins an attachment-detachment cycle between the two motor heads. While the precise transfer mechanism remains uncertain, it is known that motor heads take 8 nm 'steps' down the microtubule at a rate between 0.2-1.5 μm/s, depending on ATP availability and the presence and size of transport cargo [118-120]. This rate, known as 'processivity', is consistent with fast AT, to be discussed in section 1.3.2.

On the carboxy (C)-terminal ends of KIF heavy chains, there are two light chains that can bind directly, or indirectly via adapter/scaffolding proteins, to cargo. While KIF motor domains are highly homologous, the light chains express a high degree of sequence

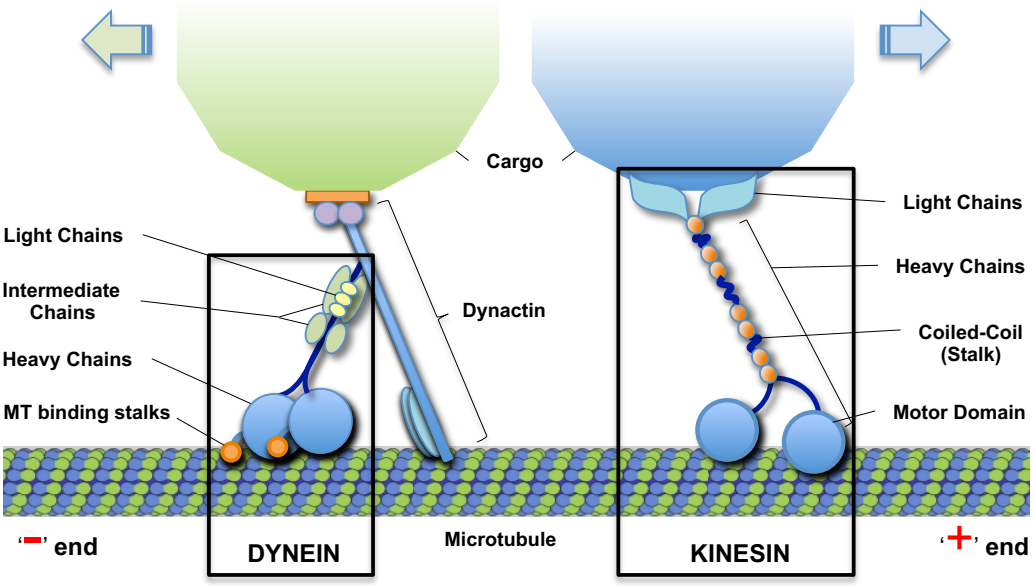

Figure 1.12 Kinesin and Dynein Motor Proteins. Long-distance transport of materials throughout the neuron is achieved via the actions of kinesin and dynein motor proteins. The motor abilities of kinesin, a 'plus' end-directed motor, are conferred by its two heavy chains, each consisting of a coiled-coil stalk region and ATP-hydrolyzing motor domain. Kinesin light chains bind various cellular cargoes. Dynein, a 'minus' end-directed motor, has motor domains with specialized microtubule (MT) binding stalks that perform similar ATP-driven 'steps'. Unlike kinesin, dynein requires an additional scaffolding protein (dynactin) to bind its cargo.

variability. There is also a wide array of adapter/scaffolding proteins capable of mediating the link between cargo and KIF. Consequently, there is a high degree of selectivity in binding cargo - each KIF is unique in the cargo it carries [120]. Finally, different KIFs are active in different areas of the cell (dendrite, axon, cell body), and at different points in development, leading to targeted protein transport depending on the needs of any particular cell compartment [121].

The dynein family of motor proteins is relatively small compared to the KIF superfamily, and only one type, cytoplasmic dynein -1, is associated with AT. Cytoplasmic dynein -1, like kinesin, is a microtubule-associated ATPase. While slightly different in substructure, it is also formed by two heavy chains containing motor domains and microtubule binding domains, and two light chains that are capable of binding cargo. Although dynein can bind directly to its cargo, it is believed that the majority of these associations are mediated by the protein complex dynactin (Figure 1.12) [122, 123].

1.3.1.2 Myosin

Myosin is another motor protein family involved in transport, and expresses both similarities and differences with kinesin and dynein. Myosins, like kinesin and dynein, are driven by ATP-hydrolysis, and use multiple adapter proteins to bind a variety of cargo. However, while kinesin and dynein perform long-range transport along microtubules, myosin travels by the actin cytoskeleton and performs short-range transport of vesicles, small organelles, and endoplasmic reticulum [124]. Myosin is frequently involved in shuttling cargo back and forth between microtubule transport and its final destination at the plasma membrane [125].

1.3.2 Slow and Fast Transport Components

Molecular cargo is most specifically classified according to its rate of transport. In fast anterograde or retrograde AT, mitochondria and membranous organelles, including those involved in secretory and endocytotic pathways, are translocated in the order of hundreds of millimeters per day. In slow AT, cargo that is primarily comprised of cytoskeletal protein polymers, and associated proteins and protein complexes, is moved only millimeters per day (Table 1.1). Both kinesin and dynein contribute to both classes of transport, and, to some degree, are both capable of travelling short distances in their non-preferred direction [67, 97].

Some factors are known to affect the processivity of molecular motors, including local ATP concentration, binding of tau to microtubules, and load of cargo [67, 126]. Also, it has been shown that both NFs and microtubules move bidirectionally and in short bursts followed by prolonged pauses [127, 128]. In addition to intermittent transport, there has also been evidence that multiple kinesins and dyneins may associate with the same cargo, leading to the hypothesis that it is the balance between bound and actively transporting motors that determines the direction and velocity of transport [63, 125, 129-131].

Table 1.1 Components of fast and slow transport.

Rate Class	Rate	Moving Structures	Composition
Fast Components			
Fast Anterograde	200-400 mm/day	Golgi-derived vesicles and tubules (secretory pathway)	Synaptic vesicle proteins, kinesin, enzymes for neurotransmitter metabolism
Bi-Directional	50-100 mm/day	Mitochondria	Cytochromes, enzymes of oxidative phosphorylation
Fast Retrograde	200-400 mm/day	Endosomes, lysosomes (endocytotic pathway)	Internalized membrane receptors, neurotrophins, active lysosomal hydrolases
Slow Components			
Slow Component 'a'	0.3-3 mm/day	Neurofilaments, Microtubules	Neurofilament proteins, tubulin, spectrin, tau
Slow Component 'b'	2-8 mm/day	Microfilaments, cytosolic protein complexes	Actin, clathrin, dynein, dynactin, glycolytic enzymes

Data from Brown [132], with permission

1.4 RGC Injury Related to Elevated Intraocular Pressure (IOP)

RGC loss is a hallmark of IOP-related eye diseases, such as glaucoma. Various animal models of retinal and ON injury that are used to study RGC degeneration employ elevations of IOP. Sources of damage to RGCs caused by elevated IOP include mechanical stress and ischemia, leading to an array of effects on retinal and ON physiology that affect RGC survival, including remodeling of the cytoskeleton, disruption of AT and changes in neighboring glia [4, 133, 134].

1.4.1 Glaucoma

Glaucoma comprises a group of optic neuropathies, including primary open-angle, angle-closure, and secondary glaucoma [135, 136], that together are the leading cause of irreversible blindness worldwide [137]. While a complete understanding of the factors contributing to glaucoma development is lacking, elevated IOP is a common symptom. In glaucoma, elevated IOP may contribute to mechanical stress, as well as vascular and biochemical events, in the retina and ONH leading to structural damage and functional impairment of RGCs axons, and eventually loss of RGC somas (discussed further in section 1.4.3) [2].

1.4.2 Animal Models of RGC Injury with Elevated Intraocular Pressure

Many animal models have been designed for the purpose of studying the pathophysiology of RGC loss. Chronic elevated IOP models are typically designed to disrupt the dynamics of endogenous pressure regulation in the eye by interfering with

aqueous outflow through the angle, and are frequently used to investigate glaucoma-like disease progression. Acute, experimentally elevated IOP is capable of producing a range of IOPs, including those high enough to cause ischemic insult to the retina, and is therefore a useful technique for the study of critical injury and acute death of RGCs. This section will discuss common techniques used to experimentally elevate IOP.

1.4.2.1 Chronic IOP Elevation Models

There have been numerous rodent models developed to create chronic elevations of IOP to mimic glaucoma by blocking aqueous humor outflow [138, 139]. The aqueous humor is secreted by the ciliary body in the posterior chamber of the eye (Figure 1.13 A). The aqueous then moves into the anterior chamber and is mostly drained via the trabecular meshwork into Schlemm's canal. Many aqueous veins directly connect the lumen of Schlemm's canal to the episcleral veins (Figure 1.13 B), returning the aqueous to the venous system [140].

Episcleral vein occlusion interferes with the outflow of aqueous either by sclerosing the veins with an injection of hypertonic saline, or by cauterization. These approaches lead to moderate long-term IOP elevation (+10-25 mmHg for extended periods) [141-143]; however, the cauterization model differs in that the length and degree of IOP elevation directly correlates with the number of veins cauterized [138]. Other techniques that obstruct aqueous outflow include laser photocoagulation of the trabecular meshwork and injection of microbeads into the anterior chamber. Laser photocoagulation produces significant and progressive RGC loss and a relatively transient increase of IOP (2-6 weeks), the degree of which depends on the intensity and duration of the laser

Figure 1.13 Aqueous Humor Dynamics in the Eye. A) Aqueous humor is produced by the ciliary body, enters the anterior chamber though the pupil and is drained through the trabecular meshwork into Schlemm's canal. **B)** From Schlemm's canal, the aqueous returns to the vasculature via many aqueous veins directly connected to the episcleral veins. Red arrows indicate flow of aqueous. Panel **A** reproduced from Goel and colleagues [144], with permission. Panel **B** adapted from Langham [140], with permission.

A)

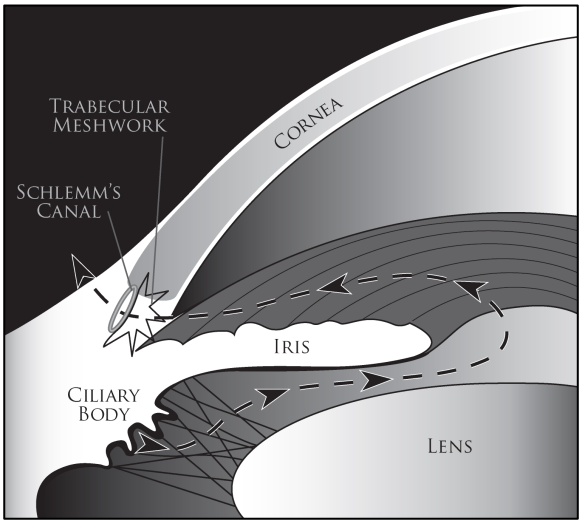
Trabecular Meshwork
Cornea
Schlemm's Canal
Iris
Ciliary Body
Lens

B)

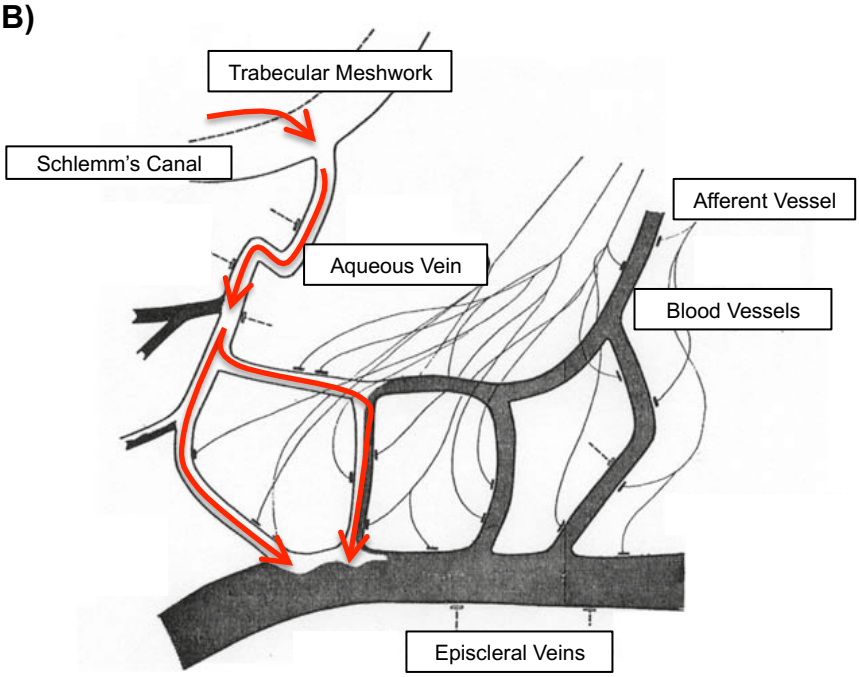
Trabecular Meshwork
Schlemm's Canal
Afferent Vessel
Aqueous Vein
Blood Vessels
Episcleral Veins

application, as well as the number of laser spots [138]. Microbeads injected into the anterior chamber build up in the angle of the eye and block aqueous flow through the trabecular meshwork. A variety of microbead models have been developed, which cause a variety of IOP elevations - less than 5 mmHg, to greater than 50 mmHg [145-148] - and RGC loss from 20-40% over 3-5 weeks [146, 149, 150].

1.4.2.2 Acute IOP Elevation Models

Due to its procedural reversibility, acute elevated IOP is often used either to investigate critical points of ischemic- and pressure- induced injury, or to study the effects of a transient disruption of blood flow, e.g. an ischemia/reperfusion injury. Some models of IOP-induced acute ischemia/reperfusion may emulate damage incurred in angle-closure glaucoma or other conditions of retinal ischemia [151]. Acute elevated IOP offers many advantages over chronic models, including, but not limited to, having a duration and severity that can be finely regulated, and providing reproducible data [138].

Acutely elevating IOP above the level of mean arterial blood pressure (MAP) interferes with retinal perfusion, causing ischemia. First described by Smith and Baird [152] and Büchi and colleagues [153], this technique is most often executed by cannulating the anterior chamber with a hypodermic needle attached via tubing to a reservoir of sterile saline, its' height being modifiable to control pressure. Acute IOP elevations in the literature range in duration from approximately 10 minutes to 12 hours, and in magnitude from approximately 10 mmHg to 150 mmHg [154-159]. Acute IOP elevation of 90-110 mmHg causes global ischemia, obstructing both the retinal and uveal circulation [160]. Global ischemia affects all retinal layers [161]. Due to its technical

simplicity and easily modified insult, IOP-induced ischemia is frequently used as a model for studying the impact of RGC damage.

1.4.3 Relevant Types of Neuronal Insults

1.4.3.2 Mechanical Injury

Elevated IOP is a highly recognized risk factor for the development and progression of glaucoma [136]. Mechanical stress on RGC axons in the retina and ONH caused by elevated IOP induces damaging biochemical cascades that contribute to RGC loss [162, 163].

Mechanical deformation of structural tissues in the ONH has been examined in acute experimental elevation of IOP in human, non-human primate, and rodent eyes [47, 164-166]. Posterior displacement of the LC in response to short-term increases of IOP ranges from 26 μm in non-human primates, to 79 μm in humans, with the majority of movement occurring within the first 15 mmHg of pressure increase [47, 164, 167]. In rats, deformation of the ONH and peripapillary structures (i.e. adjacent to the ONH) is visible within seconds of IOP increase to 50 mmHg, and reversible decreases in retinal thickness were observed as early as 10 minutes after onset of elevated IOP. These studies support the concept that significant mechanical trauma is likely inflicted upon RGC axons at the level of the LC in response to elevated IOP.

Many cell types in the retina and ON are capable of responding to mechanical distortion in their surrounding environment. Glia of the retina and ON – namely astrocytes, Müller cells, and microglia – all express mechanosensitive pannexin channels in their plasma membrane [168-171]. Pannexin channels are unopposed membrane-

spanning hemichannels that can release ATP in response to mechanical stimulation [172]. Isolated rat ONH astrocytes have been shown to release ATP via pannexin channels in response to mechanical stimulation, and both pannexin 1 and 2 are upregulated in response to prolonged stretching [170]. Newman [171] demonstrated that ATP release from pannexin channels on Müller cells induces delayed inhibition of RGC spiking via activation of K^+ permeable adenosine receptors after ATP had been dephosphorylated by ectoATPases and ectonucleotidases in the extracellular space. Release of ATP by retinal and ON glia may be beneficial and/or detrimental to RGC survival [170], depending on the type of purinergic receptor being stimulated: activation of P2X7 receptors on the RGC plasma membrane (preferentially activated by ATP) causes influx of Ca^{2+}, which can lead to activation of apoptotic and inflammatory cascades [173, 174], while activation of P1 receptors (preferentially activated by adenosine) causes inhibition of RGCs [171, 175], which may be protective in pathophysiological conditions associated with excitotoxicity, such as glaucoma [176]. An increase in retinal ATP has been documented in isolated retinas exposed to hydrostatic pressure [177, 178], and elevated levels of ATP have been measured in the aqueous humor of individuals with glaucoma [179]. Thus, via mechanosensitive cation channels, glia of the retina and ONH are capable of transducing mechanical stimuli by releasing ATP into the extracellular space, affecting RGC survival (Figure 1.14 A).

In addition to glial responses to mechanical stimuli, RGCs may be capable of sensing changes in pressure directly. It has been proposed that release of ATP from pannexin channels expressed on the RGC plasma membrane initiates damaging autocrine signaling whereby ATP feeds back onto P2X7 receptors on the RGC membrane, causing

Figure 1.14 Elevated IOP-Induced Mechanical and Ischemic Insults Combine to Cause RGC Axonal Injury in the ONH. A) Cascade of cellular events resulting from mechanical compression at the ONH. **B)** Cascade of cellular events resulting from ischemia at the ONH. Panx – pannexin. Adapted from He and colleagues [180], with permission.

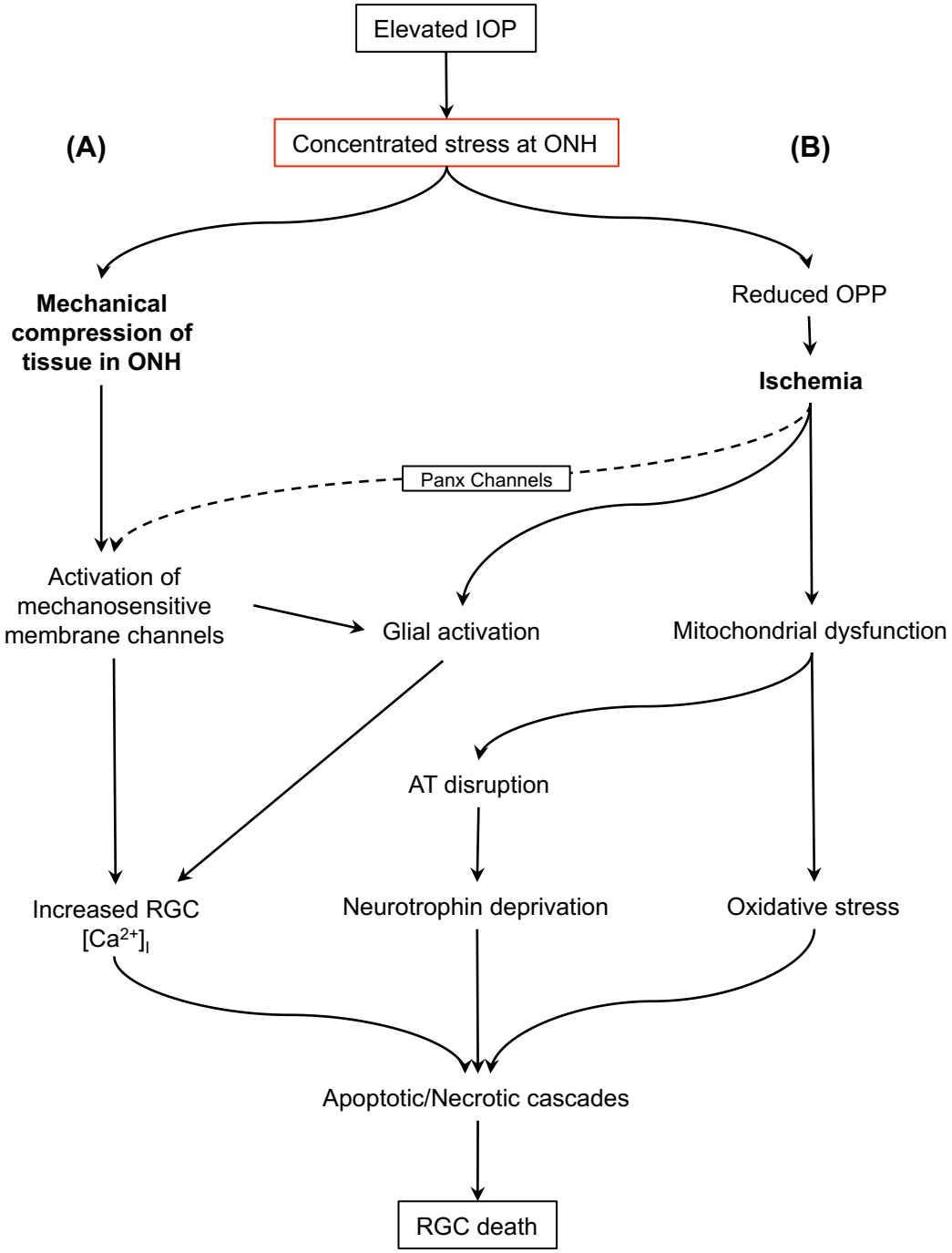
Elevated IOP
Concentrated stress at ONH
(A)
(B)
Mechanical compression of tissue in ONH
Reduced OPP
Ischemia
Panx Channels
Activation of mechanosensitive membrane channels
Glial activation
Mitochondrial dysfunction
AT disruption
Increased RGC [Ca2+]I
Neurotrophin deprivation
Oxidative stress
Apoptotic/Necrotic cascades
RGC death

influx of cytotoxic Ca^{2+} (Figure 1.15), a pathway which is blocked by removal of extracellular ATP and P2X7 antagonists [173]. Indeed, pharmacological blockade of pannexin channels inhibits retinal ATP release [177], while blockade of P2X7 receptors prevents ATP-associated damage in RGCs following exposure to increased hydrostatic pressure [178]. The differential effects that ATP release from Müller cells (paracrine) versus from RGCs (autocrine) has on RGC survival may arise because paracrine release exposes ATP to dephosphorylation in the extracellular space, increasing the likelihood of adenosine receptor stimulation, whereas autocrine release may stimulate adjacent P2X7 receptors on the RGC membrane before ATP can be dephosphorylated [171, 173].

RGCs themselves express mechanosensitive transient receptor potential vanilloid isoform 4 (TRPV4) channels [162]. TRPV4 channels, from the TRP superfamily of membrane-spanning cation-permeable channels, are known to open in response to mechanical stimulation. Interestingly, neuronal expression of TRPV4 in the retina is specific to RGCs [181], potentially contributing to the high susceptibility of RGCs to IOP-related injury, relative to other retinal cell types. Mechanical stimulation of the retina leads to influx in Ca^{2+} through TRPV4 channels, further contributing to elevated intracellular Ca^{2+} and RGC death [162].

1.4.3.1 Ischemia

Elevating IOP to levels above ocular perfusion pressure (OPP), defined as the MAP minus the IOP, interferes with ocular blood flow [160, 182], thereby causing ischemic insult to the retina. Using optical microangiography to measure ocular blood flow in rats in response to increasing steps of elevated IOP, Zhi and colleagues [183]

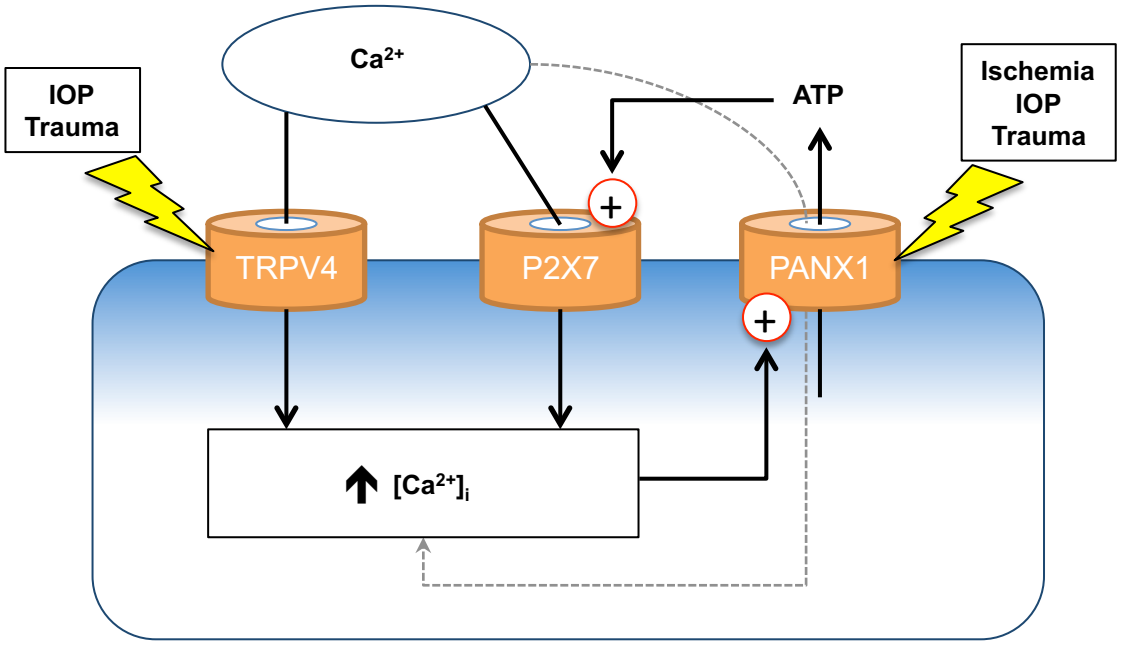

Figure 1.15 Mechanosensitive Channels in the RGC Plasma Membrane. RGCs can respond to mechanical stimulation themselves via the mechanosensitive channels TRPV4 and pannexin 1 (PANX1). TRPV4 cation channels open in response to elevated IOP and/or mechanical trauma to the RGC membrane and allow influx of Ca^{2+}, leading to elevated intracellular Ca^{2+}. PANX1 channels also respond to mechanical deformation of the membrane by elevated IOP and trauma, as well as ischemia, releasing ATP into the extracellular space. ATP released by PANX1 channels stimulates adjacent P2X7 receptors leading to further influx of Ca^{2+}. Elevated intracellular Ca^{2+} feeds back onto PANX1 channels, potentiating channel activity. Adapted from Krizaj and colleagues [162], with permission.

determined that inner retinal blood flow begins to be reduced at an IOP of 30 mmHg, and is nearly extinguished at an IOP of 100 mmHg. Alternately, choroidal and ONH blood flows began to be affected at an IOP of 60 mmHg, and were reduced by 80% and 100%, respectively, by 100 mmHg.

Ischemia caused by reduced ocular perfusion induces complex biochemical cascades in retinal neurons and glia that are known to damage RGCs (Figure 1.14 B) [160]. Decreased supply of glucose and oxygen to mitochondria disrupts both glycolysis and oxidative phosphorylation, reducing available intracellular ATP stores. Additionally, ischemia can activate pannexin channels [184], leading to further loss of intracellular ATP and increased extracellular ATP. This resulting lack of intracellular ATP can interfere with AT function, leading to somal deprivation of neurotrophins. In support of this, ATP production-enhancing compounds appear to increase RGC survival following an elevated IOP-induced ischemia/reperfusion injury [185]. Reduced intracellular ATP may also cause glutamate transporters on neurons and glia that normally take-up glutamate from the extracellular environment to work in reverse, increasing extracellular glutamate. Adding to glutamate dysfunction, glia appear to develop a reduced ability to buffer extracellular glutamate, leaving neurons at risk of excitotoxicity [186]. Buildup of ATP and glutamate in the extracellular space can over-stimulate P2X7 and N-methyl-D-aspartate (NMDA) receptors, respectively, causing a similar rise in intracellular Ca^{2+} as that observed in mechanical injury. Mitochondrial dysfunction in ischemia also leads to the over-production of free radicals, causing oxidative stress [187]. Together, high intracellular Ca^{2+}, depleted neurotrophic support and oxidative stress, among other

signaling pathways activated in ischemia, work to promote apoptotic and necrotic cascades, leading to RGC death.

1.4.4 Experimental Methods of Evaluating AT Function and Axonal Structure in RGCs, and Activation of Surrounding Retinal and ON Glia

The function of AT and the structure of the axonal cytoskeleton in RGCs, as well as the activities of neighbouring glia in the retina and ON, are all intimately linked to RGC survival in response to elevated IOP [4, 188]. Many experimental methods have been developed to evaluate AT, the axonal cytoskeleton, and glia, in efforts to better understand RGC injury, degeneration, and loss. The following sections provide an overview of popular approaches to these evaluations.

1.4.4.1 Experimental Evaluation of AT

Two frequently used methods for AT assessment include: 1) tracking the intra-axonal movement of actively transported fluorescent tracers, and 2) evaluating the intra-axonal distribution of endogenous AT-associated proteins.

1.4.4.1.1 Actively Transported Tracers

Various dyes and tracers are capable of labelling RGC axons in the retinofugal projection [189-196]. However, only those tracers whose intracellular dispersion depends on active transport are suited to studies examining functional AT disruption [197]. Additionally, tracers that are inherently fluorescent offer many advantages over techniques requiring secondary detection (e.g. immunolabelling, horseradish peroxidase

(HRP), etc.): 1) they save time by eliminating the need of one or more incubation periods, as is necessary in secondary labelling procedures; 2) they are not subject to artifacts caused by variations in exposure to secondary labels; and 3) the lack of secondary processing avoids interference with subsequent immunological investigation. Two inherently fluorescent, actively transported tracers that are commonly used in RGCs are rhodamine isothiocyanate (RITC) and fluorescently conjugated cholera toxin B (CTB; Figure 1.16).

RITC is a red-fluorescing molecule (emission 573 nm) that, when applied to live tissue, is endocytosed and transported in vesicles throughout all cellular compartments [195, 198]. Although RITC is transported both anterogradely and retrogradely [195], description of its appearance in the ON following retrograde AT is lacking. The rate of anterograde and retrograde AT of RITC in rat RGCs is estimated to be approximately 10 and 5 mm/day, respectively [195].

Cholera toxin is produced by the bacterium *Vibrio Cholerae*, and enters cells by endocytosis after binding to GM1 ganglioside receptors in the membrane [199, 200]. The recombinant form of cholera toxin, containing only the non-toxic beta subunit (i.e. CTB), can be used as a tracer of fibre tracts within the CNS [190, 201-204], and can be pre-conjugated to fluorescent dyes (emissions from 488 to 647 nm) [205]. Recently, CTB conjugated to the Alexa 488 fluorophore has been shown to label somas, dendrites and axons of RGCs following either anterograde or retrograde application [206]. Reported rates of CTB transport in rat RGCs are 80-102 mm/day anterogradely [206, 207] and 136-191 mm/day retrogradely [206].

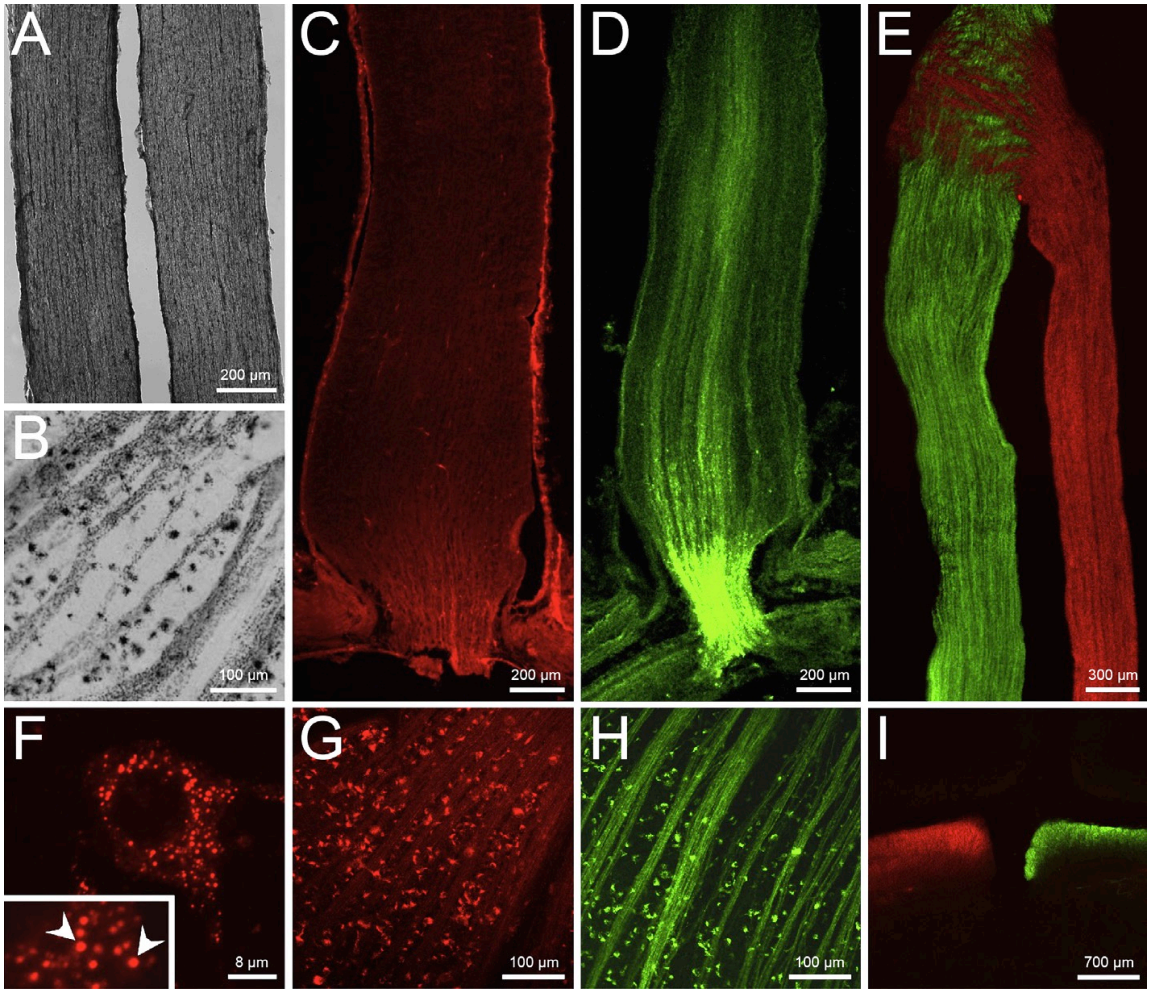

Figure 1.16 AT Tracers in the Rat Visual System. A and B) Retrograde AT of HRP in the rat ON **(A)** and retina **(B)**. **C)** Retrograde AT of RITC in the retrobulbar ON and ONH. **D)** Retrograde AT of CTB in the retrobulbar ON and ONH. **E)** Anterograde AT of CTB conjugated (green) and RITC (red) in the ON and chiasm. **F)** High magnification image of RITC-filled vesicles in the RGC cytoplasm. **G)** Retrograde RITC labelling in the retina. **H)** Retrograde labelling in the retina with CTB. **I)** Anterograde labelling of RGC terminals in the SC with RITC (red) and CTB (green). Reproduced from Nuschke and colleagues [197], with permission.

1.4.4.1.2 Endogenous AT-Associated Proteins

Evaluating the expression of endogenous AT-associated proteins, frequently achieved by immunohistochemistry (IHC), may also provide information regarding the state of AT function. Dynein, amyloid precursor protein (APP) and brain-derived neurotrophic factor (BDNF), among other proteins, are associated with AT in neurons, and have previously been used as a measure of AT function in RGCs [63, 129-131].

Dynein is the primary motor protein associated with retrograde AT, making it a useful target for IHC evaluation of AT function. Martin and colleagues [129] demonstrated that both acute and chronic elevations of IOP caused focal accumulations of dynein protein in peripheral RGC axon bundles within the ONH, suggesting of a localized disruption in AT function.

APP, a synaptic protein that is produced in large quantities in the neuronal soma [208-210], is a frequent cargo of fast anterograde AT [211, 212] and IHC for APP has been previously used to assess AT function in RGCs [130]. Acute elevation of IOP leads to rapid accumulation of APP in the ONH [130].

Finally, BDNF is well known as a neurotrophic factor that is retrogradely transported from RGC terminals to the soma to promote RGC survival [213, 214]. Measurement of uptake and AT of radioactive BDNF and IHC for endogenous BDNF protein have been used to evaluate retrograde AT function in RGCs [63, 131], and, like IHC for dynein and APP, have also demonstrated a localized disruption of AT in the ONH in response to elevated IOP.

1.4.4.2 Evaluating Axonal Structure

RGC axonal degeneration is central to glaucomatous damage [4, 188, 215, 216], and a key point of investigation in experimental studies of RGC damage and survival [163, 188, 216, 217]. Many methods can be used to assess RGC axonal integrity, including: 1) tracking diffusion of carbocyanine dyes within the axonal membrane; 2) evaluation of axonal ultrastructure using electron microscopy (EM); 3) IHC to measure expression of axonal structural proteins, such as NF, microtubules, and MAPs; and 4) IHC or enzyme assays to measure expression and activity of enzymes important to axonal structure, such as the ubiquitin-proteosome pathway, CDK5, calcineurin, and calpain.

Because carbocyanine dyes are lipid soluble substances that diffuse passively throughout the cell membrane [218], they are useful for identifying sites of structural obstruction in the axon. Carbocyanine dyes have been used in conjunction with actively transported tracers in studies of RGC damage to differentiate between functional and structural blockades of AT [188].

RGC axonal ultrastructure can be examined via EM to reveal detailed characteristics of degeneration in studies of RGC damage. Indeed, this method has been used to identify the subcellular composition of AT blockades in RGC axons within the ONH in response to elevated IOP [219].

NFs are primarily non-phosphorylated in the soma and phosphorylated in the axon. This distribution of NF phosphorylation is altered in axonal injury ([220, 221]; discussed further in section 1.4.5.2). Moreover, expression of MAPs, which are important in microtubule stabilization [100], is also altered in axonal injury [157, 222]. Changes in NF, microtubules, and MAP proteins can be evaluated by IHC or western blot

(WB) [130, 157, 223, 224]. WB reliably quantifies the amount of protein, however, contrary to IHC, does not provide detail of the spatial distribution of protein expression within the tissue. Investigation of phospho-specific epitopes of NF has been accomplished by IHC of fixed tissue sections with antibodies specific to phosphorylated (pNF) and non-phosphorylated (nonpNF) epitopes of NF [130, 157, 221, 225]. It should be noted that endogenous protein phosphorylation states can be inadvertently modified during sample preparation in both WB and IHC; however, with special precautions, such as rapid fixation and/ or freezing, the risk of this limitation can be minimized [226, 227]

Finally, IHC and various enzymatic assays can be used to assess changes in the expression and activity of key enzymes relevant to the maintenance of axonal structure in RGCs [108, 228, 229]. These enzymes include those associated with the ubiquitin proteasome pathway, a process highly involved in proteolytic degeneration within the axon [230, 231], as well as CDK5, calcineurin, and calpain [108, 110, 228, 232-235], which are intimately linked to NF phosphorylation and degredation [92, 93, 112, 236]. The effects of elevated IOP on CDK5, calcineurin, and calpain activity in RGCs are discussed further in sections 1.4.5.2 and 1.4.5.3.

1.4.4.3 Evaluating Glial Activation

In their quiescent form, Müller cells, astrocytes, and microglia perform functions important for RGC survival [237-239]. Stressful stimuli in the retina and ON environment can lead to an activated glial phenotype, a process referred to as reactive gliosis, which can have detrimental effects on RGC survival [4, 186, 237, 240-242]. Reactive gliosis, in general, is characterized by changes in glial protein expression, glial

proliferation, hypertrophy and other morphological changes, and the secretion of various cytokines [243, 244]. Reactive gliosis in the retina and ON in response to elevated IOP is discussed further in section 1.4.5.4.

Immunological investigation of glial fibrillary acidic protein (GFAP), a structural protein that is expressed in activated Müller glia and upregulated in reactive astrocytes [203, 245, 246], with either IHC or WB is a common approach to evaluating glial activation, both in terms of protein expression [247] and morphology [243]. Indeed, examination of GFAP expression has been used extensively in studies of RGC damage [203, 243, 245, 246, 248]. Furthermore, retinal and ON microglial activation can be both morphologically and transcriptionally evaluated using antibodies to proteins such as ionized calcium-binding adapter molecule 1 (Iba1), cluster of differentiation 68, and major histocompatibility complex II, among others [245, 249-252]. Various techniques, such as cDNA microarray and qPCR, have been used to study alterations in retinal glia-related gene expression [247]. Finally, there have been many transgenic mice developed that label retinal glia, including mice that express green fluorescent protein (GFP) in Müller cells under the control of either a GFAP [253, 254] or retinaldehyde binding protein 1 [255] promoter, mice that express either lacZ [256] or GFP [257] in astrocytes under the control of a GFAP promoter[256], and also mice that express GFP in microglia under the control of the promoter CX3C chemokine receptor 1 [258].

1.4.5 RGC Response to Elevated IOP

RGCs and neighbouring glia in the retina and ONH exhibit many cues of functional and structural damage well before significant RGC death has occurred. This

section reviews current knowledge of RGC loss in response to elevated IOP, as well as possible early indicators of damage, including changes in RGC cytoskeletal proteins, AT disruption, and reactive gliosis.

1.4.5.1 Overview of RGC Loss in Experimental Elevation of IOP

Loss of RGCs in response to chronic elevated IOP is highly variable between models, species, strains, and individual animals [146, 149, 259, 260]. Injection of polystyrene microbeads into the anterior chamber in mice has been reported to produce IOP elevations of approximately +5-8 mmHg and RGC losses of between 20% and 43% after approximately 4 weeks post injection [146, 261], while microbead application in rats leads to RGC loss ranging from 10-20% at 4 weeks, to 18-27% by 8 weeks post injection [146, 147]. Injection of hypertonic saline into the episcleral vein in rats produces highly variable increases of IOP (+1-40 mmHg) [259, 262] and damage to RGCs is also highly variable between individual rats [259]. Levkovitch-Verbin and colleagues [260] used laser photocoagulation of both the trabecular meshwork and episcleral veins in rats to produce IOP elevations that peaked at +30 mmHg and decreased to +5 mmHg by 6 weeks [260]. Concomitant RGC loss was approximately 16% at 1 week, 60% at 6 weeks and 70% at 9 weeks following injury onset. Together, these results indicate that RGC loss in response to chronic elevated IOP is highly dependent on the type of injury, and even on the individual animal, making comparison between studies a challenge (the impact of variation in studies of elevated IOP is discussed further in section 8.3).

Acute elevation of IOP causing retinal ischemia is a well-characterized injury, and the associated RGC loss is consistent and well documented [263-265]. Selles-Navarro

and colleagues [264] examined the relationship between duration of elevated IOP-induced ischemia and RGC survival over 5, 7, and 14 days of recovery (Figure 1.17). While there was little observable change in RGC survival following 30 and 45 minutes of ischemia, a pattern of progressive and significant RGC loss – 33% at 5 days, 37% at 7 days and 49% at 14 days - became evident after 60 minutes of ischemia. By 120 minutes of ischemia, RGC loss was 73% at 5 days, 78% at 7 days and 82% at 14 days. These results are similar to the progression of RGC damage and soma loss in other studies using acute elevated IOP causing retinal ischemia [266].

1.4.5.2 Alteration of Cytoskeletal Proteins

Restructuring of NFs is a well-documented response to neuronal injury [267, 268]. Out of 113 genes found to be downregulated in rat retinas two weeks following axotomy, the NF family of proteins demonstrated the greatest cumulative decrease, with NF-L decreasing by 5-fold, and NF-H and NF-M decreasing by 2.5-fold [269]. Changes in RGC axonal NF expression in the ONH have also been reported within hours of elevating IOP to 45 mmHg in the pig [157, 225] – at 3 hours of elevated IOP, expression of phosphorylated NF-H, and phosphorylation-independent NF-H and NF-M was downregulated within the LC regions of the ONH. It was postulated that dephosphorylation of axonal NFs may have predisposed them to proteolysis, leading to the overall loss of NF expression. Additionally, dephosphorylation of NF-H in the ONH has been observed in a non-human primate model of chronic glaucoma [221]. It is well established that dephosphorylation of NF within neurons, by phosphatases such as calcineurin [270], increases the likelihood of NF degredation by proteolytic enzymes such

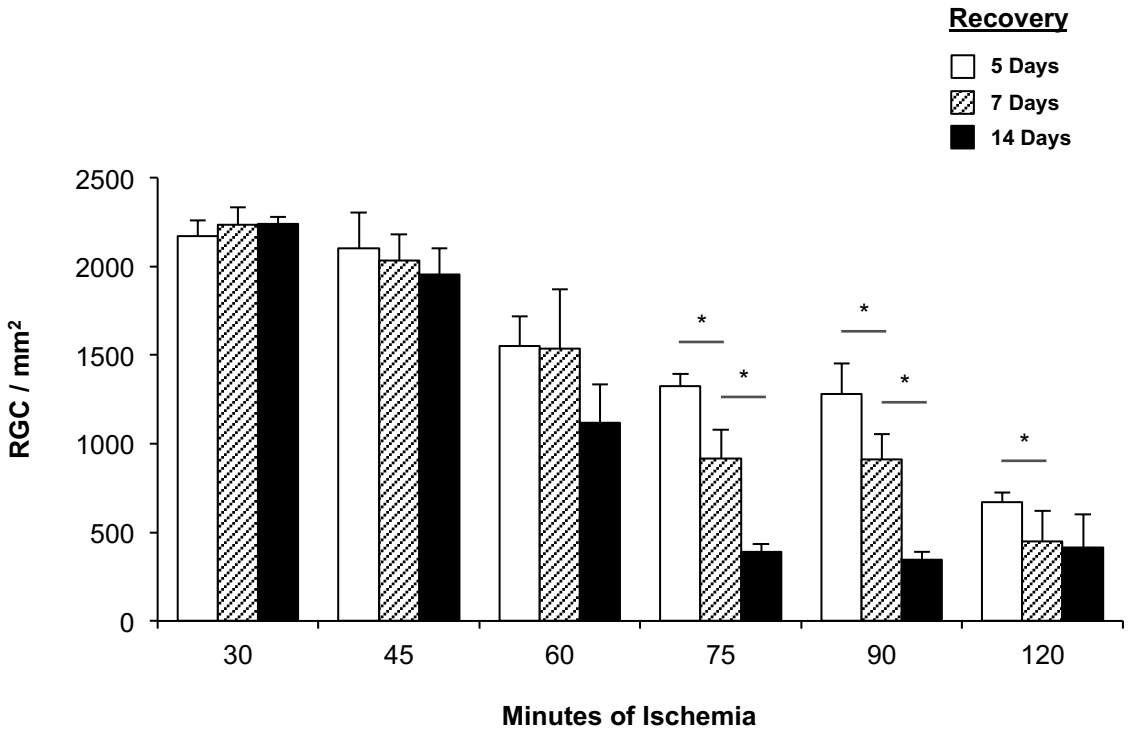

Figure 1.17 RGC Loss After Elevated IOP-Induced Transient Retinal Ischemia.

Mean densities (per mm^2) of RGCs at 5, 7, and 14 days after induction of various periods of ocular ischemia in rat. (* = $p < 0.05$) Data from Selles-Navarro and colleagues [264].

as calpain [93, 94]. Indeed, both calcineurin and calpain activity is increased in response to elevated IOP [108, 228, 271] and their blockade is shown to be protective in RGCs [229, 234, 272, 273]. It is likely that elevation in intra-axonal Ca^{2+} in response to mechanical and ischemic stress at the ONH contributes to the increased activity of calcineurin and calpain that can lead to breakdown of NFs and localized axonal degeneration.

Compartmental redistribution of phosphorylated and non-phosphorylated NFs occurs shortly after axonal injury in RGCs, and could be useful as an indicator of damage to RGCs. Typically, very little phosphorylated NF is present in the neuronal soma [80]. However, it has been well documented that neurons with transected axons accumulate phosphorylated NFs in their cell bodies as early as 3 days following injury [267, 274]. This phenomenon has also been observed at 10 days following photocoagulation of the trabecular meshwork in rats [275]. Somal accumulation of phosphorylated NF may be caused by the upregulation of NF-phosphorylating enzymes in the soma. Indeed, CDK5 and its activator, p35, have been shown to be upregulated in the experimental eye of a rat model of glaucoma [232]. Phosphorylation of NF side-arms would likely lead to dissociation of neurofilaments from molecular motors, and an increase in NF-NF association, leading to intra-somal buildup [276]. Additionally, CDK5 inhibitors have been shown to protect against RGC death in the rat retina following ischemia/reperfusion injury [233]. It is possible that monitoring accumulation of pNF in the soma presents a viable method of evaluating axonal damage in experimental glaucoma and other conditions of RGC and ON damage.

Other components of the RGC cytoskeleton are also rapidly modified in response to injury. Balaratnasingam and colleagues [157] found a decrease in tubulin staining in the ONH within 12 hours of raising IOP. Changes in dendritic structure have also been observed in non-human primate and murine models of experimental glaucoma [277, 278]. Interestingly, RGCs appear to experience a transitional period following injury during which they exhibit some reactionary alterations in morphology, such as the reduction in size of their dendritic arbours, but have not yet committed to death [279]. Such rearrangement of dendritic morphology would implicate changes in the regulation of actin and microtubule polymerization and/or activation of structurally destructive signaling pathways [279].

1.4.5.3 AT Disruption

Because of long axons separating their soma and axon terminals, RGCs are particularly reliant on AT. Therefore, it is not surprising that AT disruption is associated with loss of RGCs in models of ON trauma [280] and acute and chronic elevations of IOP [129, 163, 225].

Many studies have examined the spatiotemporal patterns of AT blockade in response to RGC injury. Multiple experiments using models of elevated IOP have reported accumulation of AT tracers in the LC region of the ONH [219, 281-283]. This has also been reported in more recent studies where, following intravitreal injection of RITC, transport blockade in the ONH was observed as early as 6 hours after onset of elevated IOP [225]. Similarly, Chidlow and colleagues [130] found an accumulation of APP, a protein often transported along RGC axons, in the ONH as early as 8 hours after

onset of elevated IOP, and Martin and colleagues [129] found an accumulation of the dynein motor protein in the ONH in as early as 4 hours. Thus, AT in RGCs appears highly sensitive to elevated IOP, particularly within the axons of the ONH.

The mechanisms behind AT blockade in response to elevated IOP remain not fully understood. Osborne [284] suggested that lack of local ATP production in response to ischemia in the ONH has a direct effect on the ATP-dependent motility of kinesin and dynein. However, AT blockade has also been observed at IOPs below systemic arterial pressure, indicating that there are more factors at play than ischemia alone [285]. Interestingly, the same enzymes responsible for phosphorylation of NFs have also been implicated in the regulation of kinesin motility. Glycogen synthase kinase 3 phosphorylates sites on kinesin light chains, inhibiting fast anterograde AT while having no effect on retrograde AT [286], and, while a direct association of CDK5 to kinesin has not been observed, inhibition of CDK5 activity inhibits fast anterograde AT, also with no effect on retrograde transport [286]. Therefore, AT blockade is an early response (within hours) to elevated IOP that arises from many signaling pathways in response to mechanical and ischemic insult at the ONH.

1.4.5.4 Reactive Gliosis

Under resting conditions, the function of retinal and ON glia is primarily supportive: astrocytes assist in the clearing of substances from the synaptic cleft and conduct metabolic factors between capillaries and axons; Müller cells perform spatial buffering of glutamate and other substances, among other functions; microglia are important in immune response; and oligodendrocytes provide electrical insulation for

RGC axons [287]. Stress in the retina and ONH can induce reactive gliosis, often having adverse effects on RGC survival. Studies of many models of RGC injury, both chronic and acute, have demonstrated changes in retinal and ON glia with RGC damage and loss [60, 288-291].

Several studies employing acute models of elevated IOP have reported glial responses shortly after the insult [60, 248, 292, 293]. Signs of microglial activation, including proliferation and a shift from a ramified to ameboid morphology, have been observed in models of acute elevated IOP [251]. Interestingly, such signs of microglial activation can be observed through all retinal layers in both elevated IOP and contralateral control eyes [251]; however, the mechanism responsible for contralateral microglial activation is not fully understood. Müller cells and astrocytes have also been shown to respond to acute elevated IOP [60, 248, 294, 295]. Müller cells often respond to stress by upregulating GFAP expression throughout the cell. Indeed, many studies of acute elevated IOP have reported increased Müller cell GFAP expression [248, 296]. Müller cell hypertrophy and impaired glutamate uptake have also been reported [294, 297]. Alternately, changes in GFAP expression in the ONH in response to elevated IOP, attributed to the local network of astrocytes, are less predictable – while some studies report upregulated GFAP expression [241], others report no changes [248] or even a decrease [292, 298].

Glial activation has also been well studied in models of chronic IOP elevation. Similar to the microglial responses observed following acute elevated IOP, microglia in both the experimental and contralateral control eye become activated, increasing in number and size, during chronic elevated IOP [245, 299]. Microglial activation also

occurs in the ONH and ON in chronic elevated IOP models [300], with some studies demonstrating that blockade of microglial activation can ameliorate RGC survival [300, 301]. Upregulation of GFAP in Müller cells has also been frequently reported in response to chronically elevated IOP [242, 246, 302], and has also been observed bilaterally in a model chronic elevated IOP [245].

1.4.6 Reversibility of RGC Damage

Understanding the reversibility of RGC damage is of value for developing treatments in diseases of RGC loss, such as glaucoma. While some degree of RGC loss often already exists upon detection of glaucoma, there are likely also populations of RGCs that are functionally impaired but have yet to progress to structural damage and death [303]. This is also true in experimental glaucoma, where functional impairment of RGCs manifests prior to histological signs of structural damage [304]. This type of functional-before-structural progression highlights the importance of investigating reversible damage in RGCs.

Limited studies have evaluated the reversibility of changes in axonal structure and function attributed to elevated IOP. Early work examining AT function in the ONH of non-human primates suggested the possibility of reversible AT disruption following various severities and durations of elevated IOP. Quigley and Anderson [283] used autoradiography to measure anterograde AT of tritiated leucine in monkeys following 4-hours of elevated IOP not exceeding MAP (i.e. retinal perfusion is intact). It was observed that accumulated leucine had cleared from the LC between 1 and 5 hours following elevated IOP injury and that the ability of RGCs to transport new material

recovered by 1 hour. Furthermore, RGC axons exposed to 4 hours of elevated IOP followed by a recovery period structurally resembled axons that had undergone only 1 hour of elevated IOP, rather than those observed immediately following 4 hours of elevated IOP, indicating RGC axons have the ability to both functionally and structurally recover from moderate levels of elevated IOP [283]. Radius and Anderson [305] also examined reversibility of AT and structural changes following IOP elevations both above MAP, where perfusion of the anterior ONH and retina was blocked, and at lower IOP elevations. Directly following 30 minutes of IOP above MAP, axons in the retina and ON exhibited swollen morphology and transported organelles had accumulated at the LC. However, following 24 hours of recovery the axons in the retina and ONH exhibited only mild swelling and were otherwise normal. Longer durations of elevated IOP produced progressively less axonal recovery, and the most severe insult (OPP of -10 mmHg) caused complete axonal atrophy in the retina and ON by 2 weeks post-insult. Conversely, 4 hours of lower IOP (OPP of 30 mmHg) followed by 24 hours of recovery did not reveal abnormalities in axon structure or accumulation of organelles. Similarly, Johansson [306] described a reversible AT blockade produced by 2 hours of 50 mmHg of IOP. Potential for RGC functional recovery in chronic injury has been demonstrated in human glaucoma [307-310] and a mouse model of experimental glaucoma [311], however recovery of structural damage from chronic injury to RGC axons has yet to be achieved. Together, the results from these studies suggest that RGCs can withstand certain amounts of damage, and that the magnitude of IOP increase (ischemic or not), as well as injury duration, are both key contributors to the severity and reversibility of elevated IOP-related RGC damage.

Select studies have also examined the reversibility of glial responses following elevated IOP. Sun and colleagues [243] investigated changes in the morphology of ONH astrocytes following a mild and transient elevation of IOP to 30 mmHg, the pressure necessary to cause the first observable reduction in RGC function [312]. Three days following elevated IOP the honeycomb organization of astrocyte processes in the ONH was disrupted: their processes became noticeably thicker, and GFAP expression was increased to greater than two-fold of normal. This was not accompanied by any change in RGC axon bundle morphology, or disruption of AT. Thickness of primary processes returned to normal by seven days following elevated IOP, and the organization of astrocytic processes in the ONH was largely recovered by 6 weeks.

1.5 Goals of Thesis

Disruption of AT, modification of the RGC cytoskeleton, and glial activation in the retina, ONH, and ON have all been observed in models of elevated IOP [129, 157, 221, 243, 274, 285, 313, 314]. While these effects have been shown to progress together over time during prolonged insults, their progression, or recovery, following a transient elevation of IOP is not well understood.

The goals of this thesis were to:

1) Characterize RITC and fluorescently-conjugated CTB as AT tracers in the rat visual system;

2) Examine and compare changes in AT function in RGC axons at various times following two magnitudes of elevated IOP, varied by duration, constituting either a mild and recoverable 'sub-critical' insult, or a severe and progressive 'critical' insult;

3) Examine concurrent changes in NF phosphorylation, an indicator of axon structural damage, in the retina and ONH;

4) Examine concurrent changes in retinal and ONH glia; and

5) Integrate these observations to construct timelines of structural and functional changes in the retina, ONH, and ON following both magnitudes of elevated IOP insult.

CHAPTER 2 – MATERIALS AND METHODS

2.1 Animals, Animal Care, and Anesthesia

Rats were chosen because of their wide availability and applicability. Furthermore, among small laboratory animals, their ocular blood supply bears meaningful resemblance to humans [160, 315]. Male and female Brown Norway rats (270-390 g; Charles River Laboratories, QC) were used in all experiments. They were housed in a 12-hour light–dark cycle environment and given food and water *ad libitum*. All procedures complied with the Association for Research in Vision and Ophthalmology (ARVO) Statement for the Use of Animals in Ophthalmic and Vision Research and ethics board approval was obtained from the Dalhousie University Committee on Laboratory Animals. For surgery, rats were anesthetized with inhalant isofluorane (ISO, Aerrane, Baxter Corporation, Mississauga, ON) via a portable ISO inhalation system (Summit Medical Equipment Company, Band, OR) using 2-3.5% ISO in oxygen (flow of 1 L/min). Post-operative care included a subcutaneous injection of buprenorphine hydrochloride (0.02 mg/kg; Buprenex, Animal Resource Centre, McGill University, Montreal, QC) administered approximately 15 minutes before cessation of anesthesia. Following all surgeries, rats recovered in their cage, which was placed on a heating pad, and were given mash. Rats were sacrificed with an intraperitoneal injection of pentobarbital sodium (340 mg/mL).

2.2 AT Tracing

2.2.1 AT Tracers Used

Both CTB conjugated to the fluorophore Alexa 488 (Invitrogen, Carlsbad, CA) and RITC (Sigma Aldrich, St. Louis, MO) were used in experiments characterizing AT tracers. CTB was chosen for subsequent experiments to track retrograde and anterograde AT in response to transient elevated IOP.

2.2.2 Retrograde AT Tracing

In preparation for retrograde application of CTB, the animal was placed in a stereotaxic frame and ISO/O_2 flow was adjusted to maintain a surgical plane of anesthesia. Fur was trimmed from the top of the head and the surgical area cleaned with 70% ethanol, followed by disinfection with iodine antiseptic. Using a scalpel, an incision was made medially from between the ears to just behind the eyes, and the lambda and bregma landmarks of the skull were exposed and the overlying membrane removed. A drill was used to create 3 mm diameter holes on either side of bregma (Figure 2.1 A). With fine forceps and Vannas scissors, the dura was removed from the overlying injection sites. A 10 uL Hamilton syringe with a blunt-tip 33-gauge needle mounted on the stereotaxic arm was used to inject 1 - 2 µl of 1% CTB in phosphate buffered saline (PBS) into each of 3 coordinates (in mm) from bregma, corresponding to the stereotaxic location of the SC: Anterior/posterior (A/P) -5.5, lateral +/- 1.5, dorsal/ventral (D/V) -5.0 then up to -4.2 (1 µl total); A/P -6.4, lateral +/- 1.5, D/V -5.0 then up to -3.6 (2 µl total) and A/P

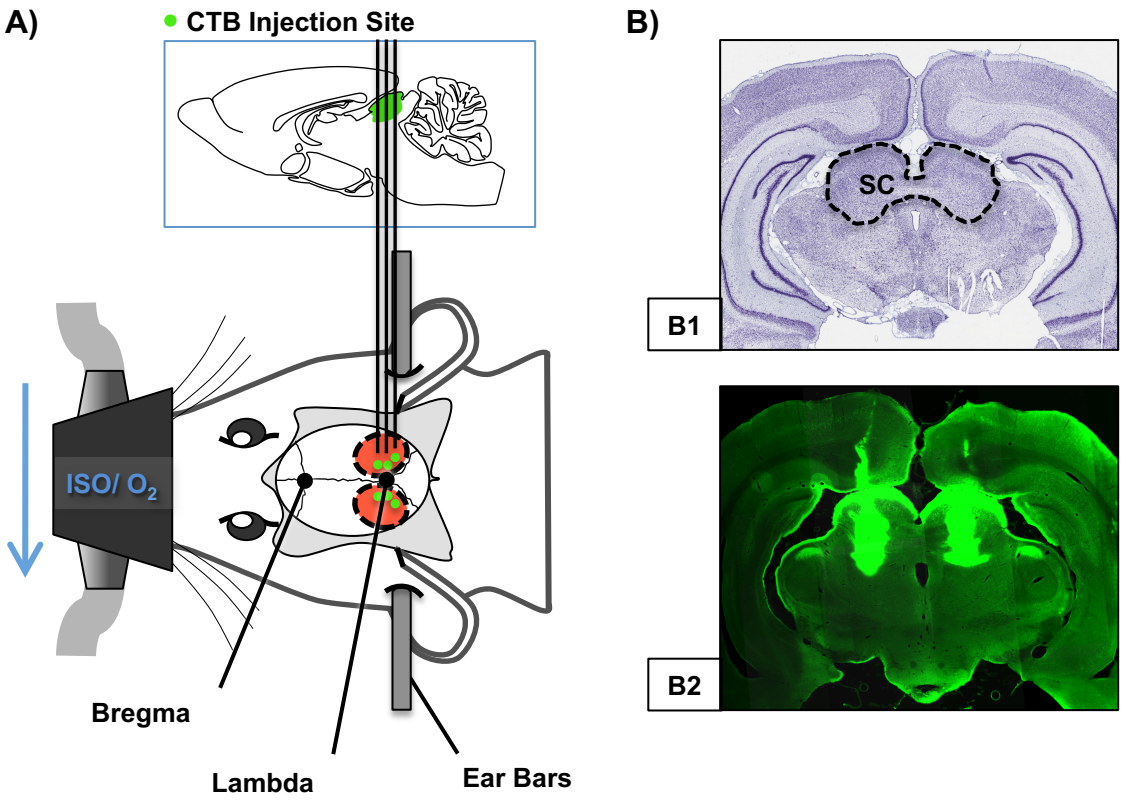

Figure 2.1 Stereotaxic Injections of CTB into the Rat SC. A) Two holes through the skull were drilled on either side of Lambda (red circles) and CTB (green) was injected into 3 coordinates bilaterally, corresponding to stereotaxic coordinates of the SC. **B) B1:** Nissl stained coronal section of rat brain -5.88 mm from bregma (from brainmaps.org [316]), with the SC demarcated (dotted line). **B2:** Bilateral injections of CTB into all layers of the SC in a similar stereotaxic location to **B1**. ISO: isofluorane, SC: superior colliculus.

6.9, lateral +/- 2.0, D/V -4.0 (2 μl). The 2 most anterior injections were varied in depth (D/V), with half of the injection volume ejected at each depth, to ensure thorough labelling of the SC. After ejecting CTB from the syringe, the needle was left in place for 2 min and then slowly removed. After injections were completed bilaterally, the incision was closed with 3 wound clips. Accuracy of SC coordinates following bilateral injections was assessed by coronal cryostat sectioning (30 μm) of a subset of brains post-mortem and imaging of the SC with confocal microscopy (N = 4; Figure 2.1 B).

Retrograde application of RITC to the SC was similar in procedure to retrograde application of CTB, with few exceptions. Following removal of the dura, the superficial cortex was carefully removed using a surgical suction pump attached to a blunted 25-gauge hypodermic needle until the surface of the SC was in view. Small pieces of surgical foam soaked in 2.5% RITC with 2% dimethyl sulfoxide (DMSO; Sigma Aldrich, St. Louis, MO) in sterile water were placed on the surface of the SC and the incision was closed as previously described.

2.2.3 Anterograde AT Tracing

To track anterograde AT in RGCs, CTB was injected directly into the vitreous of both eyes. During injections, anesthesia was maintained with a nose cone to allow manipulation of the head position. A suture line through the upper eyelid was used to retract the lid and visualize the dorsotemporal limbus (Figure 2.2 A). The experimental (right) eye was injected first to allow absorption prior to IOP increase. Forceps and Vannas scissors were used to remove a small patch of conjunctiva approximately 1 mm

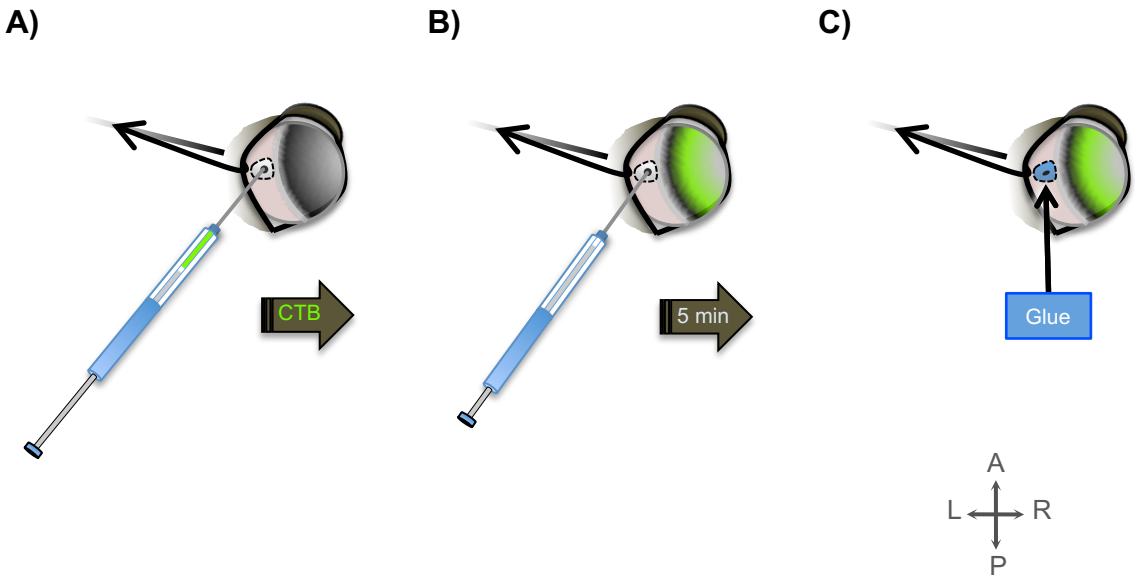

Figure 2.2 Intravitreal Injection of CTB. A) A Hamilton needle, containing CTB, is placed 1 mm posterior the limbus at 2 mm depth through the sclera. **B)** CTB is injected into the dorsal-temporal vitreous cavity and the needle is left in place for 5 minutes. **C)** Tissue glue is used to prevent CTB backflow upon removal of the needle. A, P: anterior, posterior; L, R: left, right.

posterior the limbus. The tip of a 30-gauge needle was used to penetrate the sclera to facilitate insertion of the blunt injection needle. Following this, the 33-gauge blunt-tip needle of a 10 uL Hamilton syringe containing CTB was inserted caudally, to a depth of approximately 2 mm and at an angle of 30° from the sclera to avoid injury to the lens. While holding the needle steady, 4.5 μL of 0.5% CTB was rapidly injected (to encourage dispersion) into the eye and the needle left in place for 5 minutes to avoid backflow through the injection hole (Figure 2.2 B). After slowly removing the needle, the hole was sealed with Histoacryl (B.Braun, Melsungen, Germany) tissue adhesive (Figure 2.2 C). The same procedure was repeated in the fellow eye.

2.3 Pressure Column

A wall-mounted pressure column was used to elevated IOP (Figure 2.3). The pressure column consisted of a 60 mL saline-filled reservoir that could be raised and lowered along a wall-mounted track via a pulley system to create hydraulic pressure. The reservoir was connected via plastic tubing to a three-way stopcock, followed by further tubing connected to a 1 mL syringe and 30-gauge hypodermic needle placed in the anterior chamber. The stopcock allowed saline to also flow to a sphygmomanometer, placed at eye height, for simultaneous monitoring of system pressure. The accuracy of sphygmomanometer measurements was examined by increasing IOP in 10 cmH_2O steps (N = 1), and comparing the measured value with the theoretical pressure created by the height of the saline reservoir (Figure 2.4), as well as with simultaneous readings from a TonoLab rebound tonometer (Colonial Medical Supply, Franconia, NH) that were obtained from 80-170 cmH_2O of column pressure.

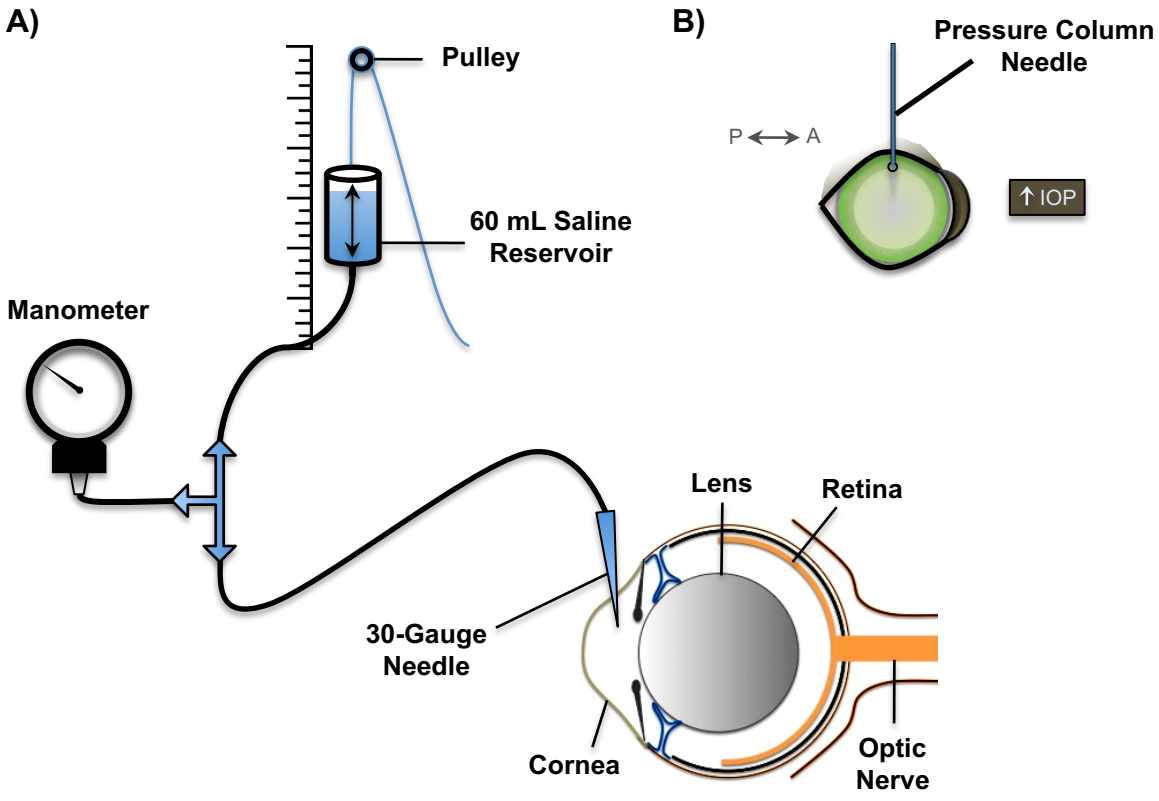

Figure 2.3 Use of Hydraulic Pressure Column to Increase IOP. A) A needle, connected via tubing to a saline reservoir that can be raised or lowered to control pressure, was placed in the anterior chamber of the eye. A sphygmomanometer was used to monitor system pressure. **B)** The pressure column needle was placed in the anterior chamber of the eye following application of CTB either to the SC or the vitreous (pictured). P: posterior, A: anterior.

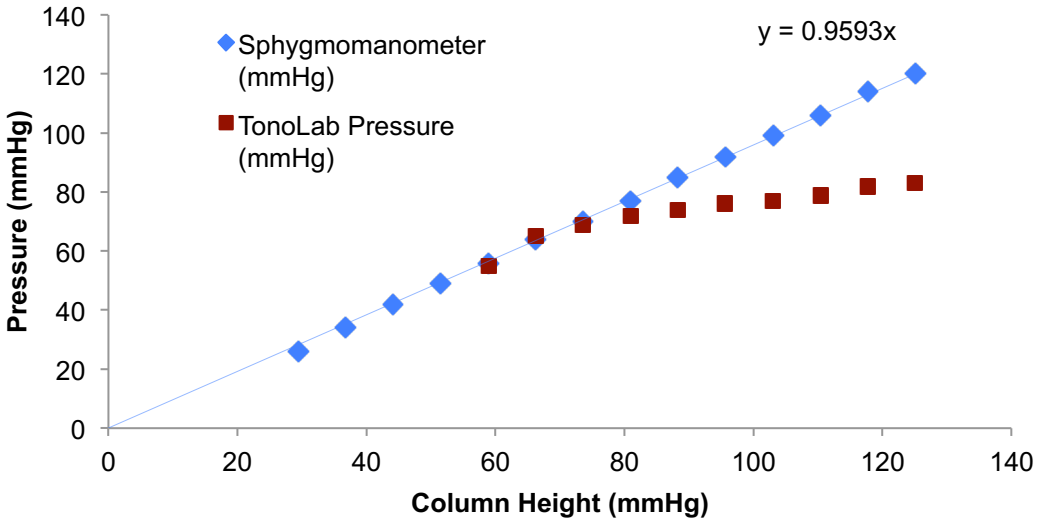

Figure 2.4 Pressure Column Calibration. Sphygmomanometer measurements, beginning after 20 mmHg of pressure, showed good correlation (slope = 0.9593) with the theoretical pressure produced by column height (converted from cmH_2O to mmHg). TonoLab measurements showed good correlation both with sphygmomanometer measurements and theoretical column height pressure until IOPs of approximately 80 mmHg, after which TonoLab measurements were no longer representative of IOP.

2.4 Acute Elevated IOP

Immediately following either anterograde or retrograde application of tracer, mydriasis (dilation) was induced in the experimental eye with 1-2 drops of 1% tropicamide to facilitate placement of the 30-gauge needle into the anterior chamber for IOP increase. In all experiments of elevated IOP, the right eye (OD) was the experimental eye, while the left eye (OS) served as a paired control for each animal. Rats used in anterograde tracer experiments were transferred to the stereotaxic device following intravitreal injections. The 1 mL pressure-column syringe with a 30-gauge needle, connected to the pressure column, was mounted on the stereotaxic arm. The needle was positioned at the periphery of the cornea and was pushed through the cornea and into the anterior chamber with curved forceps to stabilize the eye. Care was taken to avoid contact with the iris or lens. Prior to raising the saline reservoir, the stopcock was rotated to open the flow of saline to both the eye and the sphygmomanometer. Then, with the pulley, the reservoir was slowly raised to a pressure of 120 mmHg, causing complete ischemia of the retina. Cessation of blood flow was immediately visible by observation of the optic disc through the pupil with a surgical dissecting microscope. After the pressure had been raised for the allocated duration (see below), the column was slowly lowered back to baseline and the flow of saline stopped. Thereafter, the needle was carefully removed from the eye. Reperfusion was confirmed by visualization of the return of blood flow at the optic disc. A 0.3-0.5 mL subcutaneous bolus of saline was given to the animal for hydration prior to lowering the pressure, along with the injection of the analgesic buprenorphine hydrochloride.

Complete blockade of retinal blood flow has been reported in IOP elevations from 100-120 mmHg in rats [317]. Furthermore, the effects of various durations of retinal ischemia due to elevated IOP have been well studied [264]. While 30 minutes of ischemia constitutes a mild insult that does not result in RGC loss (i.e. sub-critical), 90 minutes of ischemia constitutes a severe insult that results in significant and progressive RGC loss (i.e. critical) [264]. Therefore, in order to compare RGC axon structure and function between situations of potentially reversible damage, and severe and progressive damage, contrasting insults of 30 and 90 minutes of elevated IOP were used in all elevated IOP experiments.

2.5 Recovery Times and Sample Sizes

Nineteen rats were used in studies characterizing RITC and CTB, and 76 rats were used in studies of recovery following elevated IOP (for a summary of sample sizes and recovery times, see Figure 2.5). Sample sizes of each study (Chapter 3 - tracer characterization; Chapter 4 - retrograde AT following elevated IOP; Chapter 5 - anterograde AT following elevated IOP; Chapter 6 – NF phosphorylation following elevated IOP; and Chapter 7 – glial activation following elevated IOP) are described under the 'experimental design' subheading in their respective results chapters.

2.6 Western Blot (WB)

WB analysis was used to quantify GFAP expression in isolated retinas, ONHs and proximal ONs 24 hours after 90 minutes of elevated IOP. Proteins from control and experimental retinas were isolated individually in 200 μL of radioimmunoprecipitation

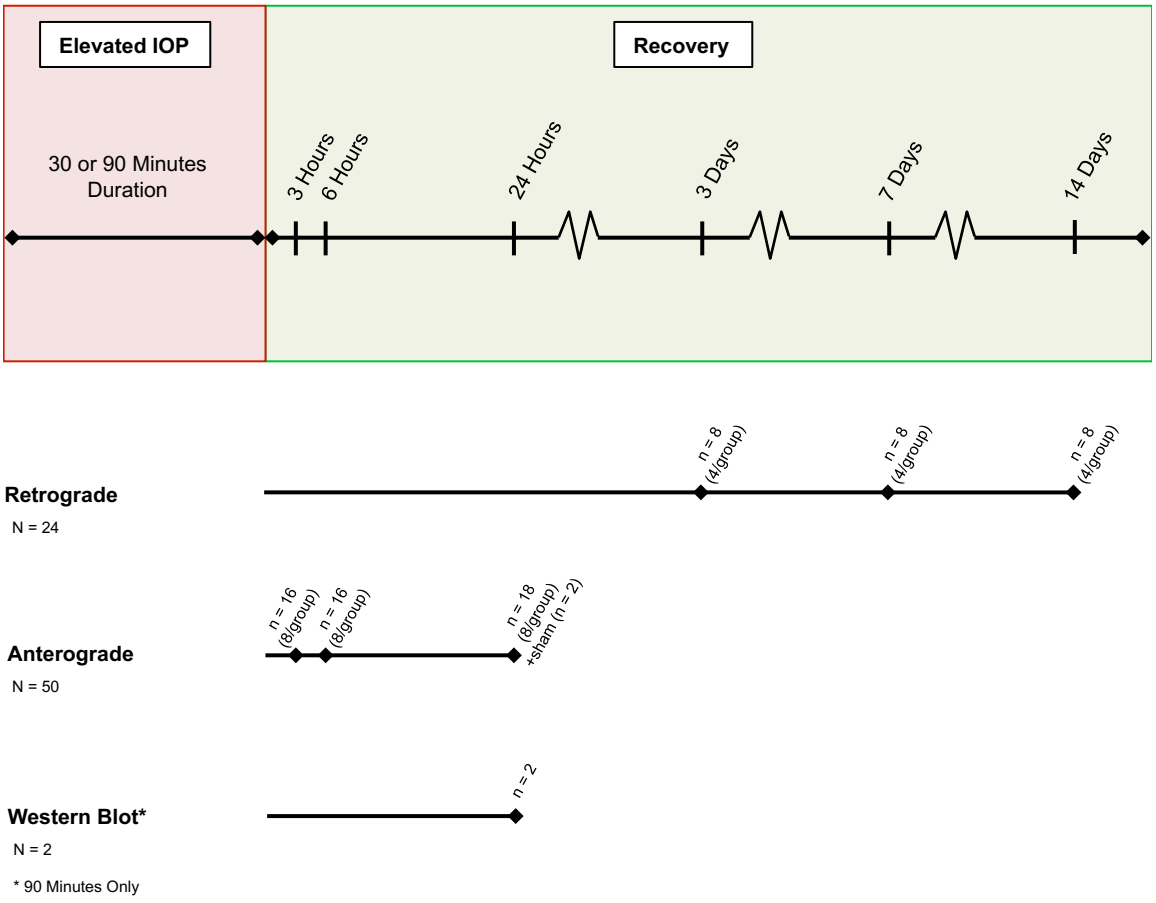

<u>Figure 2.5</u> Summary of Recovery Times and Sample Sizes in Elevated IOP AT Experiments. The study of retrograde AT was completed at 3, 7, and 14 days following elevated IOP, while experiments examining anterograde AT were completed at 3, 6, and 24 hours following elevated IOP. Western blot analysis for GFAP expression in the retina, ONH, and ON was examined at 24 hours following elevated IOP.

assay buffer containing protease inhibitors (Sigma Aldrich, St. Louis, MO), while ONHs and proximal ONs were isolated in volumes of 50 and 100 μL, respectively. Protein extracts (2 μg for ONH and ON; 20 μg for retinas) were run on 7.5% SDS-polyacrylamide gels for 20 minutes at 90 V followed by 90 minutes at 113V. Gels were transferred to immobilon P transfer membranes (Millipore Corporation, Bedford, MA) for 60 minutes at 93 V. Membranes were blocked in 5% fat free dry milk and 0.1% Tween 20 in Tris-buffered saline and were subsequently trimmed into two pieces to incubate for either two hours in mouse anti-GFAP (1:40,000; Vector Labs, Burlingame, CA), or overnight in mouse anti-actin (Sigma Aldrich, St. Louis, MO), at 4°C. Membranes were washed in 0.1% Tween 20 in Tris-buffered saline and immunoreactive bands were detected using horseradish peroxidase conjugated anti-mouse antibody (1:1000; Vector Labs, Burlingame, CA) and the ECL detection solution (Amersham Biosciences, Piscataway, NJ). Films were exposed from 10 seconds up to 2 minutes, depending on the experiment, and optical density of the bands was measured with image analysis software (ImageJ, National Institutes of Health, Bethesda, MD). Actin bands were used to normalize protein levels, and ratios of control to experimental optical density were calculated.

2.7 Tissue Processing

Rats used in retrograde AT experiments were perfused with saline followed by 4% paraformaldehyde (PFA). Approximately 2 mm of the retrobulbar ON, as well as a portion of the pigmented nasal conjunctiva for orientation, were kept attached when the eye was enucleated. The cornea was perforated with a hypodermic needle to allow

penetration of fixative and the eye was post-fixed in 4% PFA for two hours at 4°C. Bone cutters were used to access the brain, from which the ONs were dissected with the chiasm and right optic tract intact for orientation. In some cases the brain was kept for analysis of SC injections. Both the ONs and brain were also post-fixed in 4% PFA at 4°C, for 2 hours and 24 hours, respectively. Rats in anterograde AT experiments were not perfused as the brain was not kept for analysis, however eyes and ONs were isolated and post-fixed similarly.

Following fixation, all eyes were washed in PBS and dissected in the same manner. After removing the cornea, a small notch was cut into the temporal eyecup, deep enough to mark the retina, to maintain retinal orientation during dissection. A 360° incision was made approximately 1 mm behind the limbus, and the retina was loosened with forceps and removed from the eyecup by cutting around the optic disc. Dura and connective tissue surrounding the ONH stump and all sclera, except for some remaining around the ONH, was removed. Vitreous was carefully cleaned from the inner surface of isolated retinas. Those retinas that were not intended for IHC were immediately flat-mounted in Vectashield (Vector Labs, Burlingame, CA). Some retinas from tracer characterization studies were hemisected, with half whole-mounted for *en face* imaging of the GCL, and half cross-sectioned to examine the depth of labelling in the inner retina.

All ONHs, ONs, and retinas intended for cryostat sectioning were placed in 30% sucrose at 4°C overnight. ONHs and ONs were sectioned longitudinally, and retinas cross-sectioned at 20 μm thickness.

2.8 IHC

A variety of primary antibodies, listed in Table 2.1, were used to examine RGC survival, changes in RGC axon structure, and activation of glia in the retina and ONH. RGCs were labeled with goat anti-brain-specific homeobox/ POU domain protein 3A (Brn3a; 1:100; Santa Cruz Biotechnology Inc., Santa Cruz, CA). Whole-mounted retinas were first permeabilised by placement in 0.5% Triton-X 100 in PBS (PBS-Tx) (Sigma Aldrich, St. Louis, MO) and freezing at -80°C for 15 minutes. Retinas were then rinsed in fresh 0.5% PBS-Tx for 10 minutes at 23°C and incubated overnight with Brn3a in blocking buffer (2% bovine serum albumin in 2% PBS-Tx). They were subsequently washed in PBS and incubated for two hours in CY3 anti-goat (1:200; Jackson ImmunoResearch Laboratories, West Grove, PA) in blocking buffer. Finally, retinas were washed in PBS and then mounted in Vectashield.

The retinas of one animal in the anterograde CTB characterization studies were sectioned longitudinally and co-labeled with Brn3a. The sections were first blocked in 2% normal donkey serum in 0.1% PBS-Tx for one hour at 23°C, followed by incubation in goat anti-Brn3a (1:200) overnight at 4°C in blocking buffer. Following washes in PBS, the sections were incubated in CY3 anti-goat for one hour at 23°C, washed again in PBS and mounted in Vectashield.

In addition to Brn3a labelling, all whole-mounted retinas from animals used in anterograde AT experiments were also co-labeled with a monoclonal antibody specific for phosphorylated forms of NF-L and NF-H (mouse anti-2F11 clone; Dako, Glostrup, Denmark; Figure 2.6 A). Following Brn3a labelling, these retinas were blocked again for 1 hour in 10% normal goat serum and 5% bovine serum albumin in 0.3% PBS-Tx,

Table 2.1 Primary Antibodies for Immunohistochemistry (IHC)

Antibody	Specificity	Supplier	Labels	Experiment	Concentration
Brn3a	Brn3a (Mouse)	Santa Cruz Biotechnology	RGCs	Quantifying surviving RGCs	Whole-mounted retinas: 1:100
2F11	pNF-L and pNF-H (Human)	Dako	RGC axons, somas of damaged RGCs	Evaluating NF phosphorylation in retina and ONH	Whole-mounted retinas: 1:1000 ONH section: 1:200
SMI-32	nonpNF-H (Mammalian)	Covance	RGC somas and axons		ONH section: 1:200
GFAP	Glial fibrillary acidic protein (Human)	Dako	Astrocytes	Evaluating glial activation in the retina and ONH	ONH section: 1:200
Iba1	Ionized calcium binding adaptor molecule 1 (Human, mouse and rat)	Wako	Microglia		ONH section: 1:60

followed by mouse anti-2F11 (1:1000) in blocking buffer for 5 days at 4°C. After 5 days, the retinas were washed in PBS, followed by CY5 anti-mouse (1:200; Jackson ImmunoResearch Laboratories, West Grove, PA) in PBS for 2 hours. They were then washed and mounted in Vectashield.

Sequential ONH sections already containing anterogradely transported CTB were labeled with a combination of either mouse anti-2F11 for phosphorylated NF (1:200, Dako, Glostrup, Denmark) and rabbit anti-GFAP (1:200; Dako, Glostrup, Denmark) for astrocytes, or mouse anti-SMI-32 (1:200; BioLegend, San Diego, California) for non-phosphorylated NF-H and rabbit-Iba-1 for microglia (1:60; Wako, Osaka, Japan, Figure 2.6 B). Briefly, slides were re-hydrated in PBS for 10 minutes and blocked in 3% normal goat serum with 1% bovine serum albumin in 0.3% PBS-Tx for one hour at 23°C. They were washed in PBS and then incubated in primary antibodies for two days at 4°C. Following re-washing in PBS, slides were then incubated in secondary antibodies: CY3 anti-mouse (1:200; Jackson ImmunoResearch, West Grove, Pennsylvania) and CY5 anti-rabbit (1:200; Jackson ImmunoResearch, West Grove, Pennsylvania) for one hour at 23°C. Following a final wash in PBS, slides were mounted in Vectashield.

2.9 Fluorescence Imaging

All images were acquired with confocal microscopy (E800; Nikon Canada Inc., Mississauga, Ontario). Filter sets included DAPI, GFP and HYQ Cy5. To allow comparison between control and experimental eyes, imaging parameters (size, gain, offset, scan speed) were kept constant between paired control and experimental ONH sections.

Figure 2.6 Fluorescent Labelling in Whole-Mounted Retinas and ONH Sections. A) Whole-mounted retinas of rats in anterograde AT experiments already containing CTB (green) were additionally labeled with Brn3a (red) and pNF (blue). **B)** Longitudinal sections of ONHs also from rats in anterograde AT experiments were additionally labeled with pNF (red) and GFAP (blue). Scales 100 μm.

A) Retina IHC

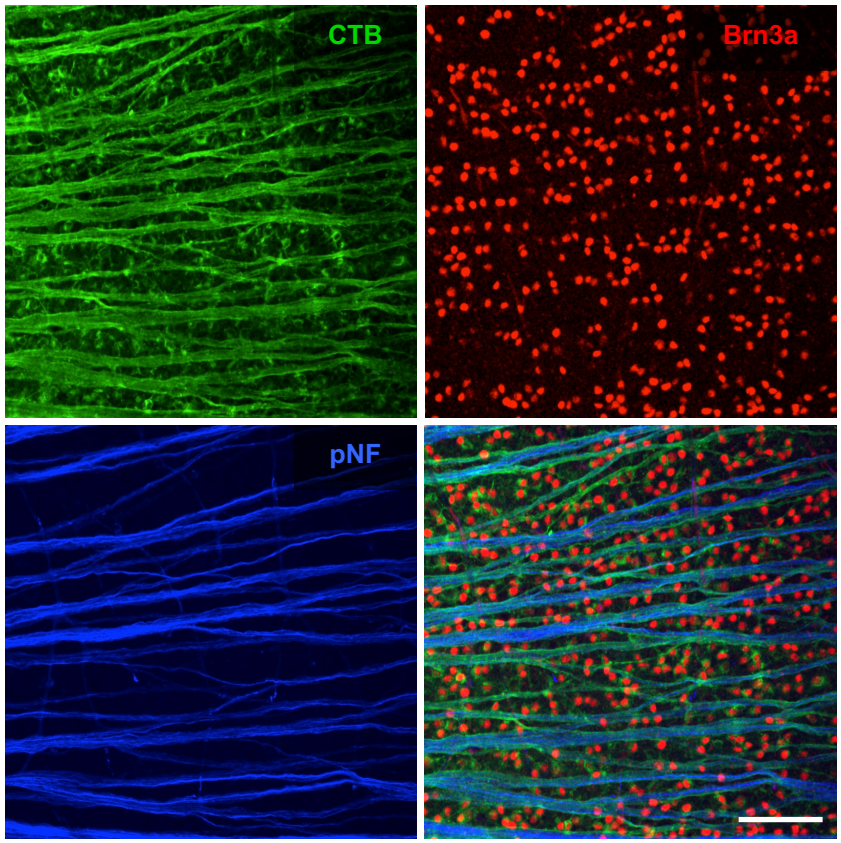

B) ONH IHC

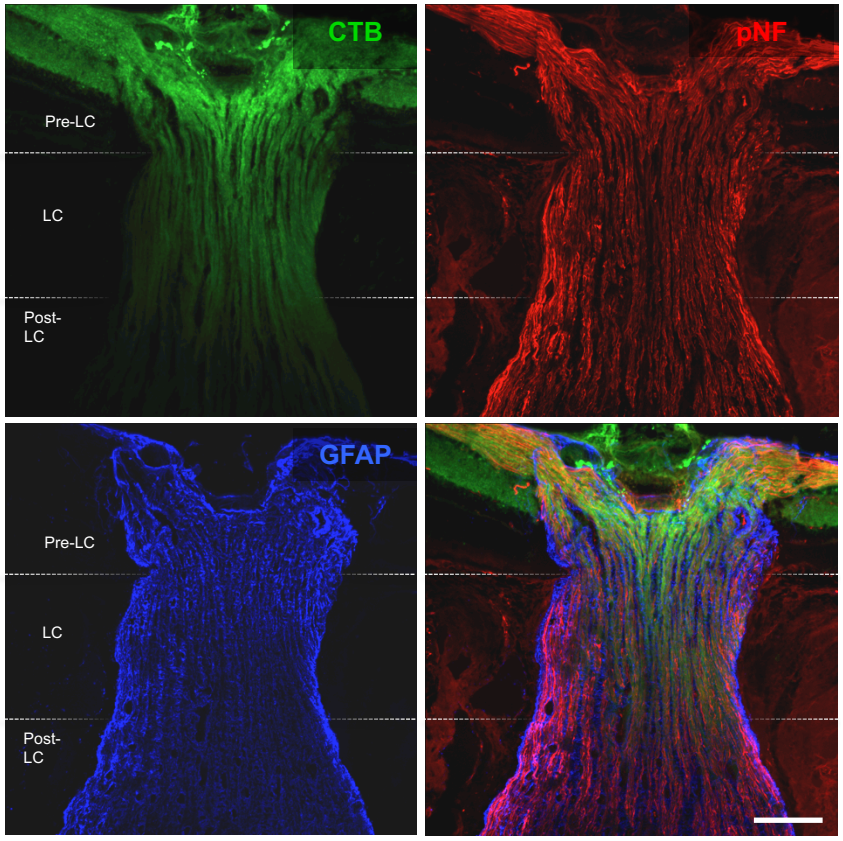

Similarly, control and experimental ONs from the same animal were imaged in the same image frame.

ONHs were imaged with both 10x (Nikon Plan Fluor, numerical aperture 0.3; Nikon Canada Inc., Mississauga, Ontario) and 20x (Nikon Plan Fluor, numerical aperture 0.75; Nikon Canada Inc., Mississauga, Ontario) objectives. Images with the 20x objective were digitally stitched with ImageJ ("2D stitching" plugin; ImageJ, National Institutes of Health, Bethesda, MD). To obtain a complete image of each pair of ONs, a series of 5-7 low-power (4x objective; Nikon Plan Fluor, numerical aperture 0.13; Nikon Canada Inc., Mississauga, Ontario) images were acquired along the length of each pair of ONs, beginning at the chiasm and extending to the transected ends of the ONs. These images were then digitally stitched with ImageJ 2D stitching.

In whole-mounted retinas, Z-stacks of the GCL, whose volume varied to accommodate the unevenness of the tissue, were obtained to ensure all labeled RGCs in a given frame were represented for counting. Images (500 x 500 μm) were obtained at eccentricities of 1, 2, and 3 mm from the optic disc in each retinal quadrant (temporal, nasal, superior, inferior).

2.10 Quantitative and Qualitative Retinal Analyses

2.10.1 Manual and Automated Cell Counting in Whole-Mounted Retinas

In experiments characterizing RGC loss over time following 30- or 90-minutes of elevated IOP, images of Brn3a+ cells in whole-mounted retinas were given a file name by

an independent experimenter to the experimenter who quantified Brn3a+ cells to avoid potential bias. Cells were quantified with the cell counter plugin in ImageJ.

Brn3a has been reported to label greater than 90% of the RGC population in rats [318] and, as a nuclear marker, offers reasonable spatial separation between adjacent RGCs, making it suitable for automated quantification. Images were pre-processed in ImageJ for background reduction and exclusion of fluorescent particles less than 4 pixels (2.5 μm) in diameter, to optimize image clarity (Figure 2.7 A). Following image binarization, particles greater than 20 pixels (12.5 μm) in diameter were then quantified with ImageJ (Figure 2.7 B).

To validate automated quantification, 20 random Brn3a control images were quantified with both manual and automated counting techniques, and compared (Figure 2.8 A). Comparison of Brn3a+ RGC counts between the two methods demonstrated a high degree of concordance (Pearson's correlation coefficient (r) = 0.89), with 89.2 % (mean Brn3a+ cells/ 500 μm^2 ± 1 SD = 473 ± 121) of all counted cells identified by both manual and automatic methods, while 2.8 % (mean = 15 ± 10) and 7.9 % (mean = 42 ± 45) were identified by only manual or automatic counting methods, respectively (Figure 2.8 B). In all cases of automated quantification, retinas with high background noise and/or poor quality of retinal Brn3a labelling were excluded from analysis. Animals that did not exhibit any quantifiable images in either the control or experimental retina were excluded from analysis.

2.10.2 Grading of Somal pNF in Whole-Mounted Retinas

In retinas from animals in the anterograde AT studies (also labeled with

Figure 2.7 Image Optimization for Automated Brn3a Counting. A) Schematic of image processing steps used to improve clarity in images of Brn3a-labeled whole-mounted retinas intended for automated counting. **B)** Overlay of original image and mask of auto-counted cells.

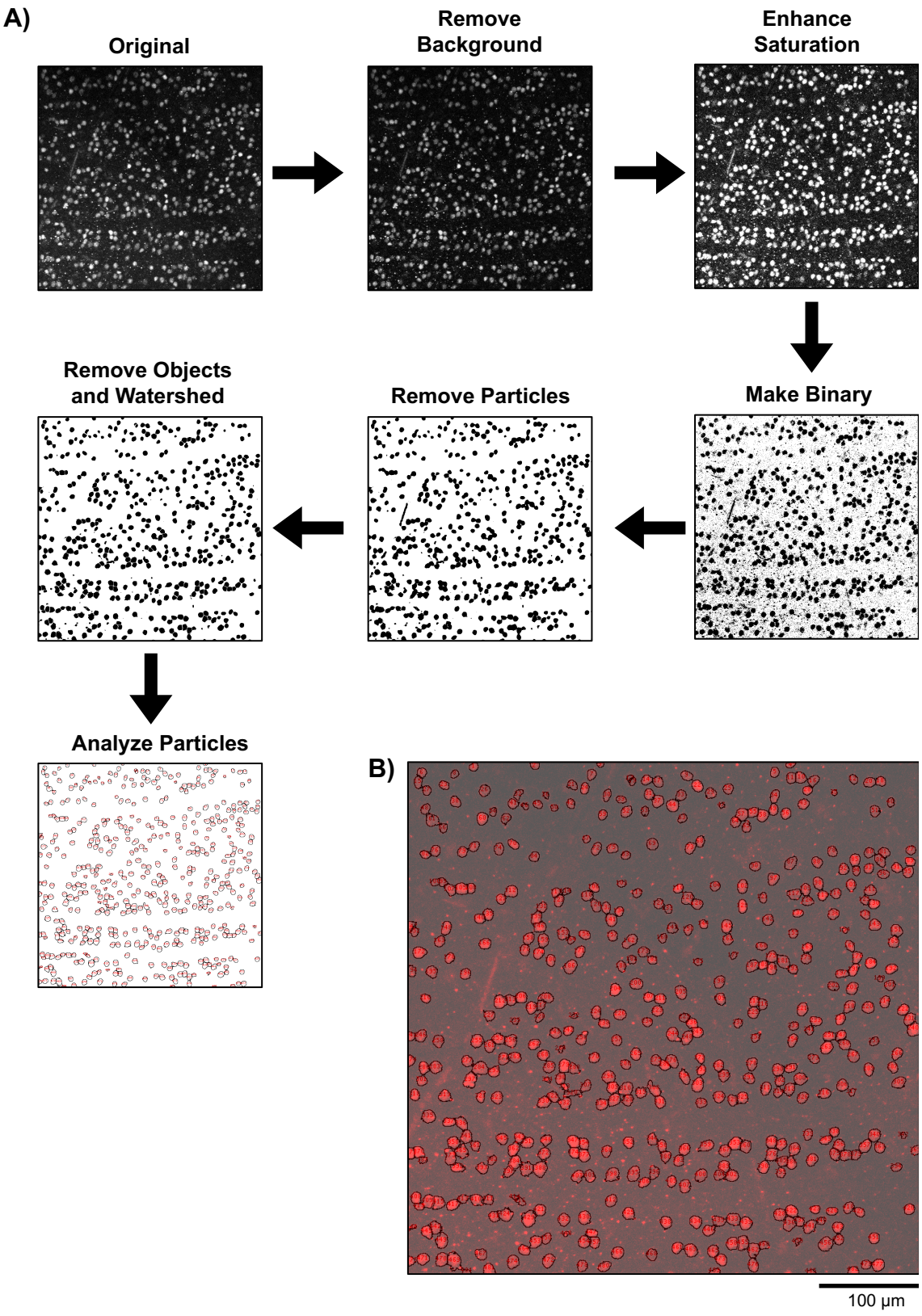
A)
Original
Remove Background
Enhance Saturation
Make Binary
Remove Particles
Remove Objects and Watershed
Analyze Particles
B)
100 µm

Figure 2.8 Comparison of Manual and Automated Brn3a Counting. A) Manual and automated counts of Brn3a+ cells were compared across 20 rats. **B)** Average Brn3a+ counts showed good concordance between manual and automated counting methods. 'Manual only' and 'automated only' cells accounted for 2.8% and 7.9% of all Brn3a+ cells that were counted, respectively. Data in **B** represented as mean ± 2SEM.

A)

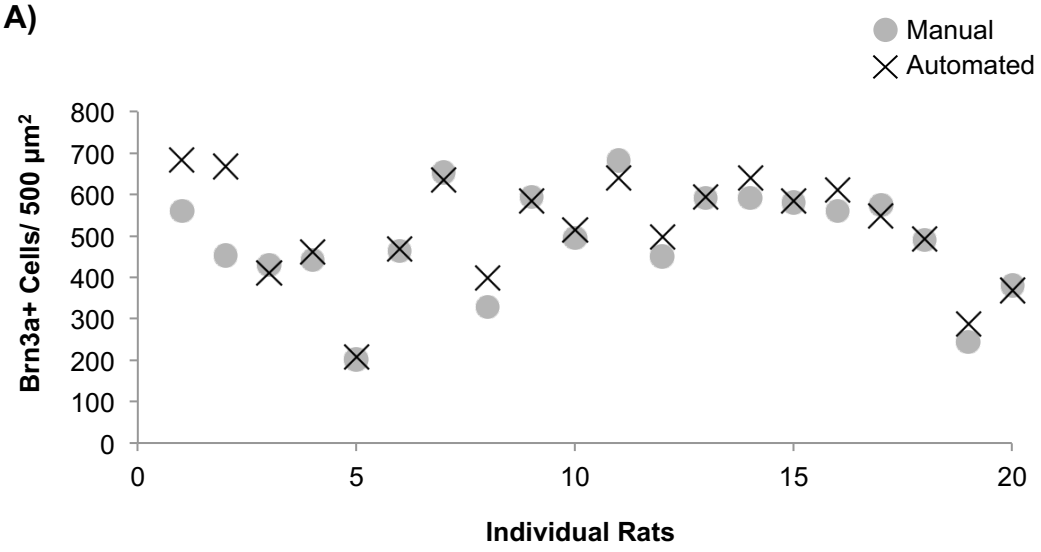
Manual
Automated
Brn3a+ Cells/ 500 µm²
800
700
600
500
400
300
200
100
0
0
5
10
15
20
Individual Rats

B)

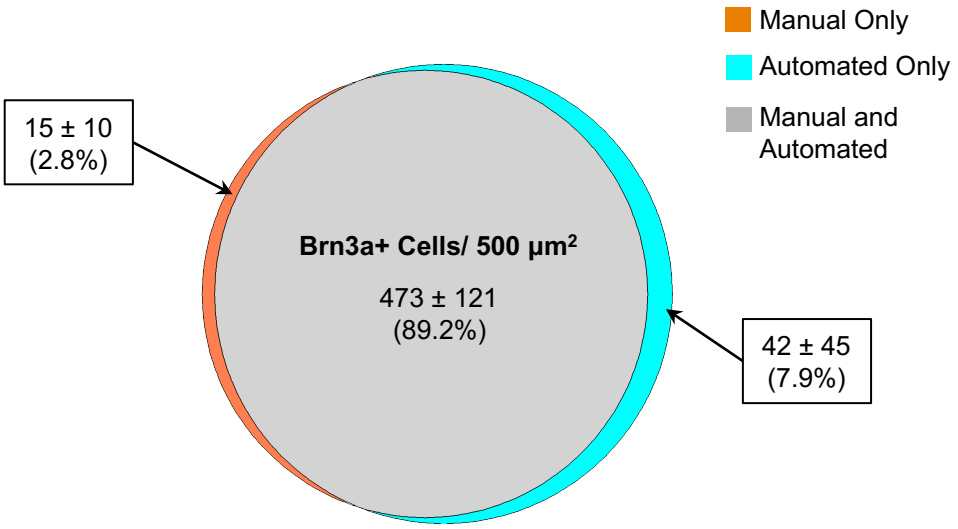
Manual Only
Automated Only
Manual and Automated
15 ± 10
(2.8%)
Brn3a+ Cells/ 500 µm²
473 ± 121
(89.2%)
42 ± 45
(7.9%)

Brn3a), the proportion of RGCs expressing phosphorylated NF in their somas, a marker of axonal damage [267] was analysed. Somal expression of phosphorylated NF following 30 or 90 minutes of elevated IOP was assessed at 1, 2, and 3 mm of eccentricity from the optic disc and converted to a 4-point grading system: 0 = no phosphorylated NF+ cells; 1 = phosphorylated NF+ cells in less than 25% of image area (500 x 500 μm); 2 = phosphorylated NF+ cells in approximately 50% of image area; and 3 = phosphorylated NF+ cells in greater than 80% of the image area. As before, grading was performed in a masked fashion to avoid potential bias.

2.10.3 Qualitative Analysis of Retinal Glia in Retinal Cross-Sections

Retinal glia labeled with either GFAP (astrocytes and Müller glia) or Iba1 (microglia) antibodies were analysed in cross-sections of the peripapillary retina in animals included in the anterograde AT study. Natural background fluorescence in retinal sections allowed for demarcation of the anatomical layers of the retina, from the NFL to the RPE, for consideration in the qualitative analysis of GFAP and Iba1 labelling. Qualitative observations were made regarding the distribution of GFAP and Iba1 labelling throughout the thickness of the retina, as well as regarding the morphology of Iba1+ microglia – either ramified (i.e. quiescent microglia), or ameboid (i.e. activated and mobilized microglia) [244, 252].

2.11 Fluorescence Analysis of ONH and ON Sections

To evaluate changes in CTB transport along the ONs, average fluorescence was plotted along the length of the nerve. A line was fitted through the centre of each of nerve for reference (Figure 2.9 A), and the average fluorescence across the width of the nerve was then determined at each pixel of length perpendicular to the centerline. The values for control and experimental ONs were plotted together (Figure 2.9 B).

Fluorescence in ONH sections from pNF, nonpNF, and GFAP labelling, in addition to transported CTB, was quantified within anatomical ONH regions. These regions included the pre-lamina cribrosa (pre-LC1 and pre-LC2), the lamina cribrosa (LC1 and LC2), and every 100 μm posterior of the LC (post-100 μm to post-600 μm; Figure 2.10 A). A measurement area of 200 x 1000 μm was drawn in the centre of each ONH section, oriented by defining the inner border of the LC1 region as the anterior limit of the scleral opening (Figure 2.10 A). Ten sampling boxes of 30 x 30 μm were first randomly derived in each anatomical region ("RandomSamplePerimeter Method" macro, ImageJ; Figure 2.10 B). The average fluorescence intensity for each box was then quantified and averaged for each anatomical region (Figure 2.10 C).

As an exception to fluorescence quantification of CTB, NF, and GFAP, labelling of microglial cells in the ONH with Iba1 was quantified as the percent Iba1+ area in each ONH region (100 x 200 μm) using a similar process as Brn3a automated counting. Briefly, ONH images were pre-processed in Image J to improve signal to noise ratio, as described above for automated cell counting. After the image was binarized, the 'analyze particles' function was used to calculate the percent area of Iba1 label in each ONH region.

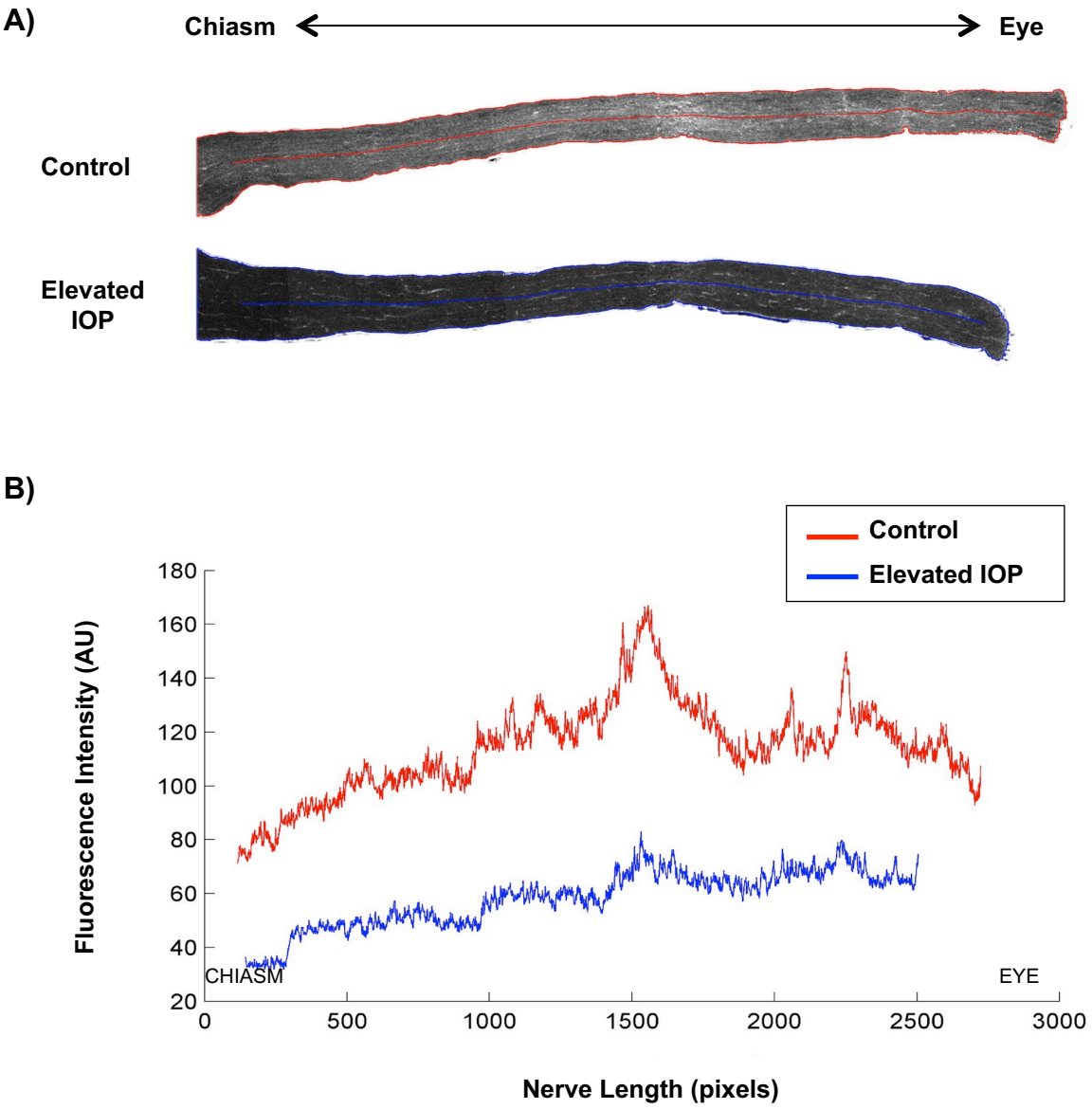

Figure 2.9 Quantification of CTB transport in the ON. A) Retrograde AT of CTB moves from chiasm to eye, and anterogradely from the eye to the chiasm. Average fluorescence measurements across the width of control (red) and experimental (i.e. elevated IOP; blue) ONs were made at every pixel of ON length perpendicular to a centreline. **B)** Fluorescence intensity of control (red) and experimental (blue) ONs plotted along ON length. AU: arbitrary units.

Figure 2.10 Quantification of CTB Transport and IHC of NFs and GFAP in Longitudinal Sections of the ONH. A) ONH anatomical regions were demarcated on longitudinal sections of ONHs. **B)** Random sampling of fluorescence across various ONH regions (10 samples per region) for various ONH labels. **C)** Average fluorescent intensity plotted as a function of ONH region.

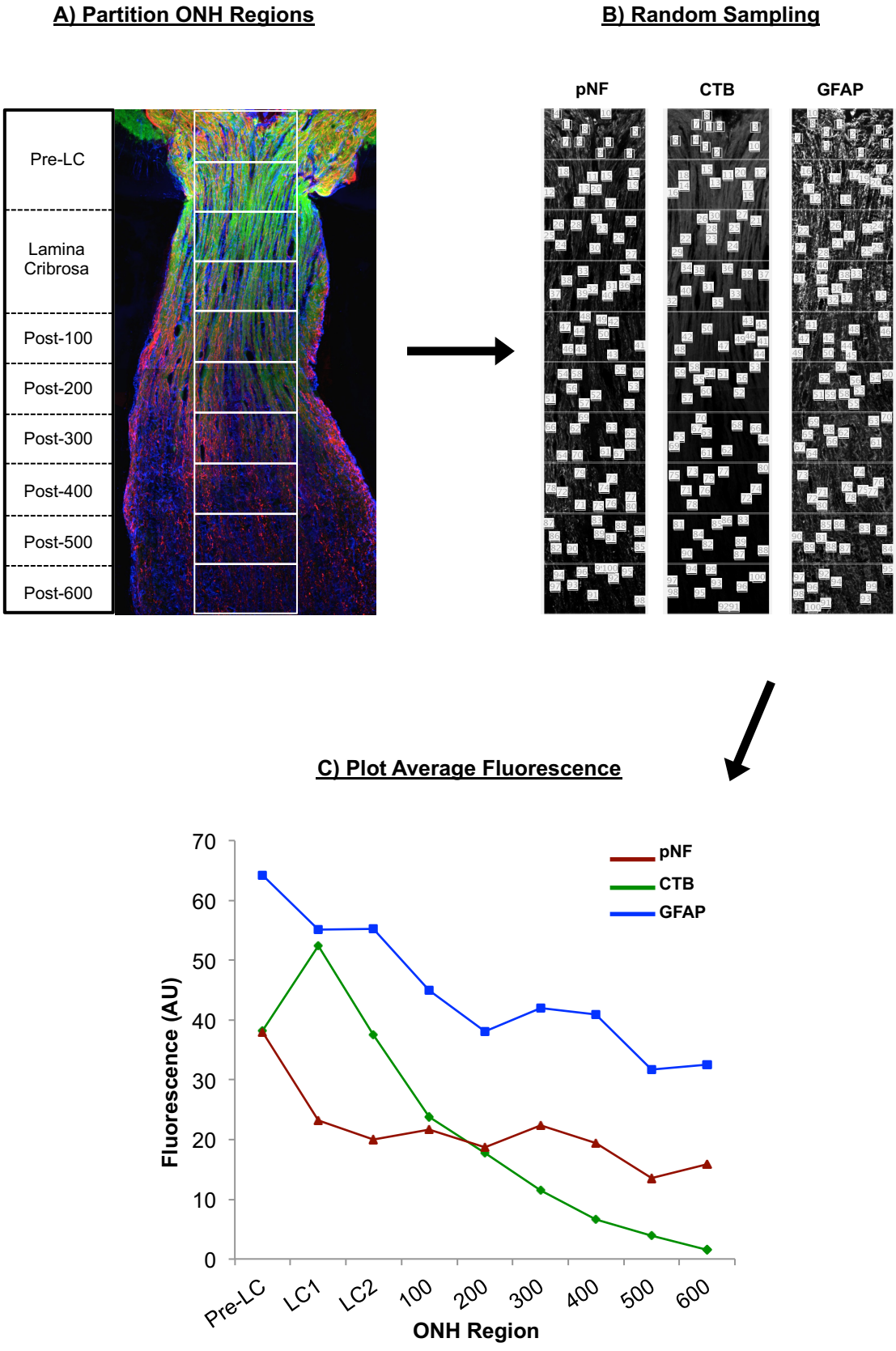
A) Partition ONH Regions
B) Random Sampling
Pre-LC
Lamina Cribrosa
Post-100
Post-200
Post-300
Post-400
Post-500
Post-600
pNF
CTB
GFAP
C) Plot Average Fluorescence
Fluorescence (AU)
70
60
50
40
30
20
10
0
pNF
CTB
GFAP
Pre-LC
LC1
LC2
100
200
300
400
500
600
ONH Region

For all labels - CTB, phosphorylated and non-phosphorylated NF, GFAP, and Iba1 – the pre-LC1 and pre-LC2 regions in each image were averaged to obtain one 'pre-LC' value, as variations in tissue shape in the innermost pre-LC region (pre-LC1) occasionally prevented measurement in that region. Fluorescent intensity of CTB and the other labels, as well as microglial area, were plotted as a function of ONH region.

2.12 Statistical Analysis

In ON transport analysis, main effects of elevated IOP (2 levels = control and experimental) and recovery time (3 levels = 3, 7, and 14 days for retrograde; 3, 6, and 24 hours for anterograde), and their interactions, were assessed using a mixed effects regression model separately for each duration of elevated IOP (30 or 90 minutes). In ONH fluorescence analysis from anterograde AT, elevated IOP experiments, main effects of elevated IOP (2 levels = control and experimental), recovery time (3 levels = 3, 6, and 24 hours), and ONH region (9 levels = pre-LC, LC1, LC2, post-100 to post-600 μm) were assessed with a two-way repeated measures ANOVA with contrasts (SPSS version 21, IBM corp., Armonk, NY), separately for each injury condition (30 or 90 minutes). Data were expressed as the mean ± 2 SEM. Differences in means were assessed by paired and independent sample t-tests.

CHAPTER 3 – CHARACTERIZATION OF RITC AND CTB FOR TRACKING AT IN RGCS

3.1 Rationale, Objective, and Hypotheses

Both RITC and fluorescently conjugated CTB have been used successfully as anterograde and retrograde tracers in the rodent visual system [130, 158, 195, 197, 198, 319, 320]. However, the majority of studies employing RITC or CTB to study AT function isolate their observations to the 'end-point' tissue - in the retina for retrograde studies [195, 198], or to the SC for anterograde studies [321, 322]. This approach provides meaningful data regarding AT function, however, lacks the resolution to identify specific locations of AT disruption along the ON. Comparatively fewer studies of RITC and CTB have demonstrated the quality of labelling in the ON. Anterograde AT of RITC has been described in the ONH [157, 225], and ON [198, 280], retrograde AT of RITC has not been shown in the ON. Similarly, CTB has been used anterogradely in the ONH [130, 320] and the ON [206, 321], but has been only marginally described in the ON following retrograde application [319]. A comprehensive description of AT of both RITC and CTB in the ONH and ON is needed to provide a baseline for experimental studies examining AT function in RGCs.

The objective of these experiments was to characterize and compare retrograde AT of RITC and fluorescently conjugated CTB in RGCs, including the quality of labelling (particularly in the axon) and the rate of transport. The findings were subsequently used to select a tracer for later use in experiments examining the effects of transient elevated IOP on retrograde AT. It was hypothesized that both RITC and CTB

would allow visualization of AT, however, CTB would provide a superior signal in the axon. Parts of this work were included in a recent publication [197].

3.2 Experimental Design

RITC Retrograde AT Time Course

To study the rate of RITC retrograde transport to the ONH and retina, as well as the quality of labelling within RGC axons in the ON, a time course experiment was conducted. Rats underwent bilateral application of RITC to the SC (for detailed procedure, see section 2.2.2) and were sacrificed at 8 hours, 24 hours, 3 days, 7 days and 14 days. Images of whole-mounted retinas were examined for the timing of RITC AT from the SC to the retina. Longitudinal sections of the proximal ON (approximately 2 mm behind the globe) were examined for RITC labelling, particularly regarding the ability of RITC to label individual axon fibres and other fine neuronal morphology. Additionally, retrograde RITC labelling in all RGC cellular compartments within the retina ONH and ON was examined in two rats at 7 days following RITC application.

CTB Retrograde AT Time Course

Similar time course experiments investigating the retrograde transport of CTB in rat RGCs were completed. AT of CTB in the retina, ONH and ON was examined at 24 hours, 2 days, 3 days and 5 days following bilateral application of CTB to the SC (for detailed procedure, see section 2.2.2). CTB labelling within the axon was examined in longitudinal sections of both the proximal portion of the ON, and the ONH. The time

point of earliest detection of CTB in the retina was examined by obtaining stitched images of entire whole-mounted retinas from both eyes at each of the time points.

RITC and CTB - Estimation of Transport Rate, Comparison of Tracers

Rates of RITC and CTB retrograde AT were estimated by comparing the length of the furthest anatomical point from the application site where labelling was observable with the time elapsed since the application of the tracer. The quality of labelling was compared between tracers in order to select the one best suited for future investigation of the effects of transient elevated IOP on retrograde AT.

Sample Sizes

A total of 15 rats were used in experiments characterizing RITC and CTB tracers. Rats used for RITC retrograde AT experiments were survived for 8 hours, (n = 2), 24 hours (n = 3), 3 days (n = 2), 7 days (n = 2), 14 days (n = 1) and 21 days (n = 1) following tracer application. Rats used for CTB retrograde AT experiments were survived for 24 hours (n = 1), 2 days (n = 1), 3 days (n = 1) and 5 days (n = 1) following tracer application.

3.3 Results

3.3.1 Time Course and Qualitative Analysis of RITC Retrograde AT

Retrograde AT of RITC labels RGC somas, dendrites, and, to a lesser degree, intraretinal axons, but not RGC axons in the ONH and ON (Figure 3.1, 3.2 and 3.3).

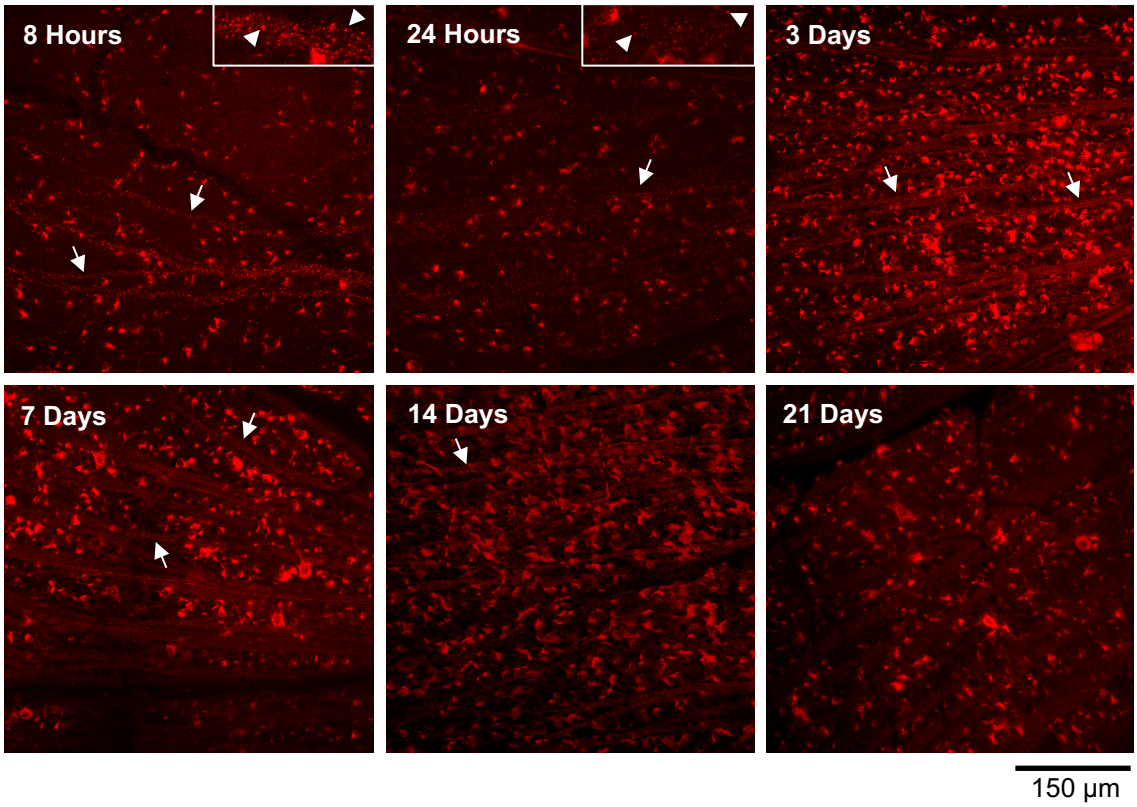

Figure 3.1 Time Course of Retrograde RITC Arrival to the Retina Following Application to the SC. Faint labelling of RGC cell bodies and axons (arrows) was observable 8 hours following application to the SC. RITC labelling in axon bundles appeared vesicularized at 8 and 24 hours following application (inset and arrow heads). RITC labelling of RGC somas increased in density and uniformity across the retina at 3 days, and RITC-labeled axon fibre bundles in the retina continued to be visible at 7 and 14 days (arrows). RITC labelling persisted in RGC somas as late as 21 days following application. All images were acquired within 2 mm of the optic disc.

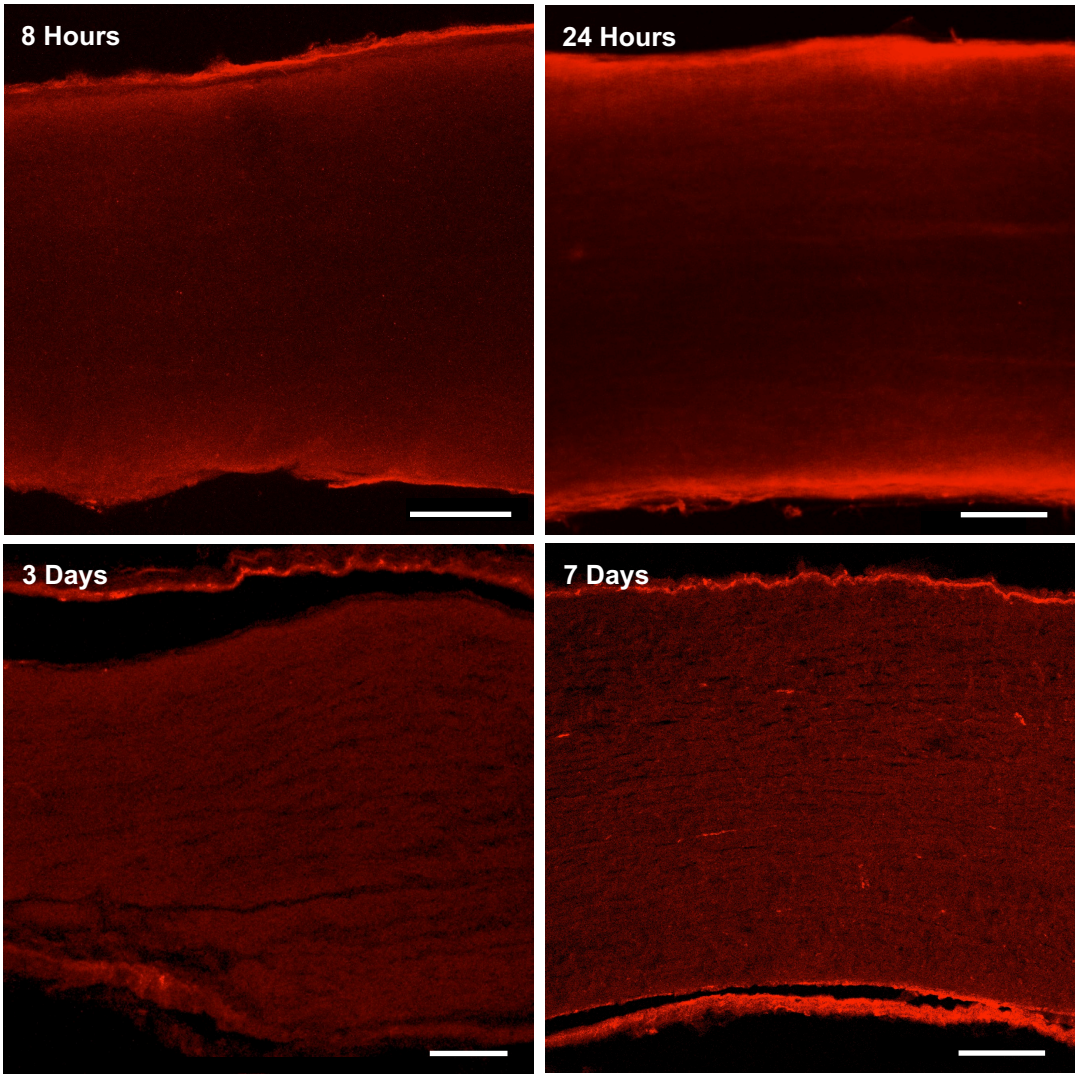

<u>Figure 3.2</u> Time Course of Retrograde RITC AT in the Proximal ON.

Axon fibre bundles were not perceptible at 8 or 24 hours following application of RITC to the SC. Labelling of axon fibre bundles was faint but discernable at 3 and 7 days following RITC application to the SC. Scale 150 μm.

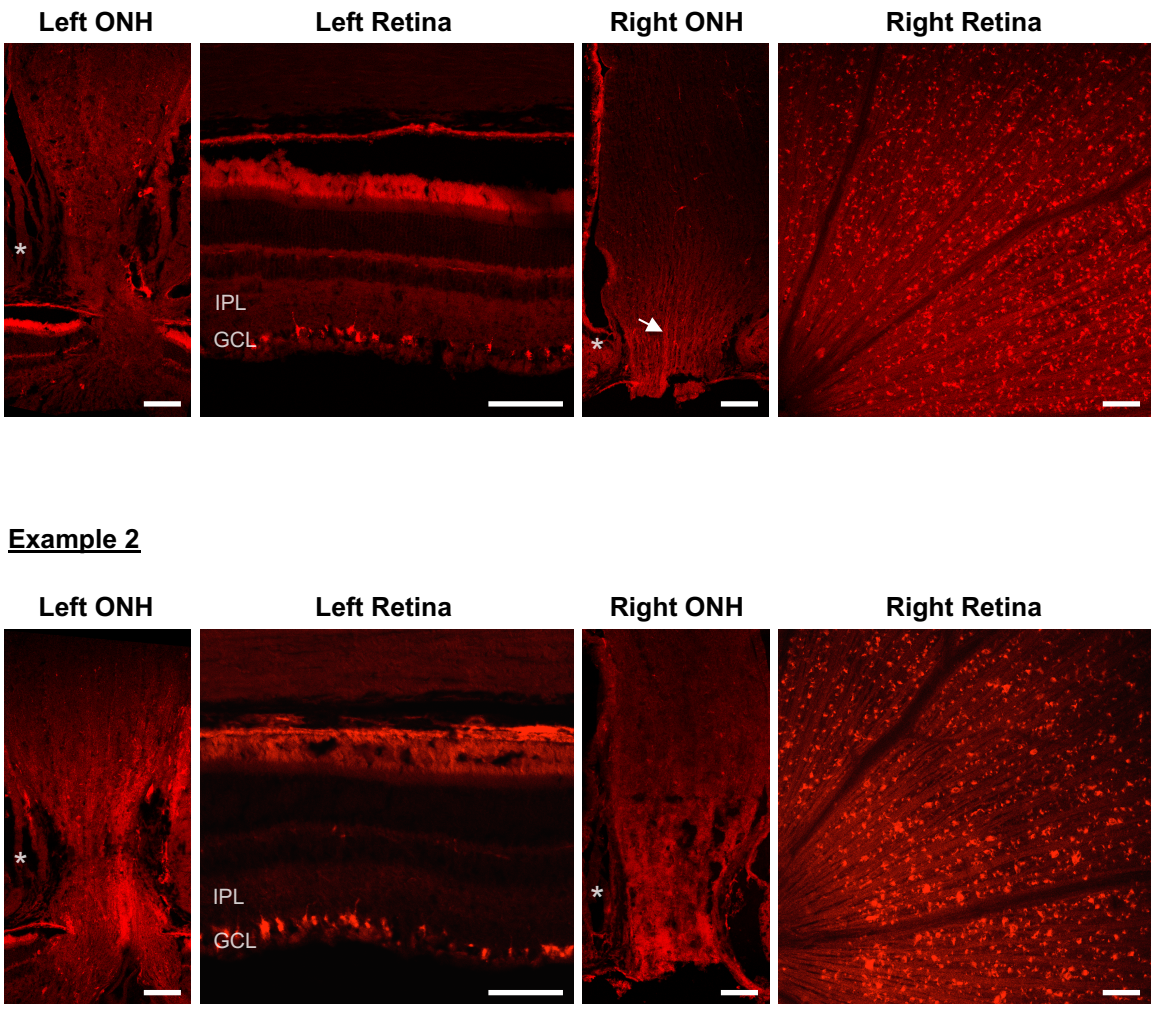

Figure 3.3 AT of RITC in the ONH and Retina at 7 Days Following Application to the SC in Two Rats. Example 1 shows faint RITC labelling in both ONHs, with morphology of RGC axon fibre bundles only visible in the OD ONH (arrow). Example 2 shows more intense labelling in the ONH, however morphology of axon fibre bundles was not visible. RGC somas and proximal dendrites were brightly labeled in retinal cross-sections of both rats, with axon fibre bundles also visible. Asterisk (*) denotes level of sclera. IPL – inner plexiform layer, GCL – ganglion cell layer. All scales 100 μm.

RITC detection in the retina via retrograde AT was examined at various time points following application of the tracer to the SC (Figure 3.1). RITC had a vesicularized appearance in axon fibre bundles in all quadrants of the central retina at the 8-hour time point. RITC-filled RGC somas were most apparent at 2 mm of eccentricity and in the superior quadrant of the retina. Sparse RITC-filled RGC somas were also visible in the periphery of the nasal, superior, and inferior quadrants, while the temporal quadrant was devoid of labelling. By 24 hours, RITC+ RGC somas were visible in all quadrants and appeared to increase in density over time until 3 days after tracer application, remaining stable thereafter. RGC dendritic labelling was apparent from 7 to 21 days. Intra-retinal axonal labelling remained vesicularized at 24 hours, peaked in brightness and uniformity by 3 days, and was predominantly absent by 21 days. RITC+ axon bundles in the proximal ON were absent at 8 and 24 hours, and were barely visible at 3 and 7 days, despite intra-retinal axonal labelling at those time points (Figure 3.2). Together, these results indicate that RITC is capable of being transported from SC to retina in under 8 hours and that AT of RITC does not occur in synchrony across the entire RGC population; rather, the proportion of RGCs transporting RITC continued to increase from 8 hours to 3 days following SC application. Furthermore, RITC transport in axons appears reduced at 14 days and has ceased by 21 days. Interestingly, despite evidence for active retrograde AT of RITC from 8 hours to 7 days following application, RITC fluorescence is not readily observed in axons within the ON during those time periods.

These findings were reiterated upon further qualitative investigation at the 7-day time point. In addition to RITC filling RGC somas throughout all retinal quadrants (Figure 3.3), labelling also extended into primary dendrites, which were visible in the IPL

in retinal sections (Figure 3.4). Some increased fluorescence was visible in 3 of 4 ONHs examined, however, only one ONH demonstrated a labelling pattern reflective of typical axon bundle morphology (Figure 3.4). These results suggest, again, that RITC, when applied retrogradely, provides a signal in the soma and dendrites that is superior to that observed in the ONH and ON.

3.3.2 Time Course and Qualitative Analysis of CTB Retrograde AT

A similar time course study was performed for CTB conjugated to Alexa 488. Filling of RGC axons and somas by retrograde CTB AT was examined at 24 hours and 2, 3, and 5 days following CTB injections into the SC. Labelling indicative of CTB-filled axons was visible within the proximal ON (Figure 3.4) at all time points and appeared to increase in intensity from 24 hours to 5 days. Retrograde AT of CTB was also visible in axon bundles within the ONH at all time points. Filling of RGC axon bundles was uniform across the entire ONH by 2 days following SC injections, and maintained at later time points. Additionally, detection of CTB in the retina was examined by obtaining composite images (tiled z-projections that were stitched together) of entire retinal whole-mounts from both eyes at each time point (Figure 3.5). Twenty-four hours following CTB application, the filling of RGC somas was not uniform, however CTB+ somas could be observed in all quadrants. CTB+ soma density appeared to increase in all quadrants after 2 days (Figure 3.5). The distribution of CTB+ labelling remained non-uniform at all time points, with the central retina and temporal and nasal quadrants often displaying the highest amount of labelling, while the dorsal and ventral quadrants displayed the least.

Figure 3.4 Time Course of CTB in the Proximal ON and the ONH at 24 hours, 2, 3, and 5 Days Following Application to the SC. A) Retrograde CTB in the proximal (nearer the eye) ON. CTB filled axon fibre bundles were visible 24 hours after CTB application. CTB labelling became more intense by 3 and 5 days. **B)** Retrograde CTB in the ONH. CTB-filled axon fibre bundles were visible in the ONH at 24 hours following CTB application. Intensity of CTB in the ONH was increased by 2 days, and remained so at 3 and 5 days. Asterisk (*) denotes level of sclera.

A)

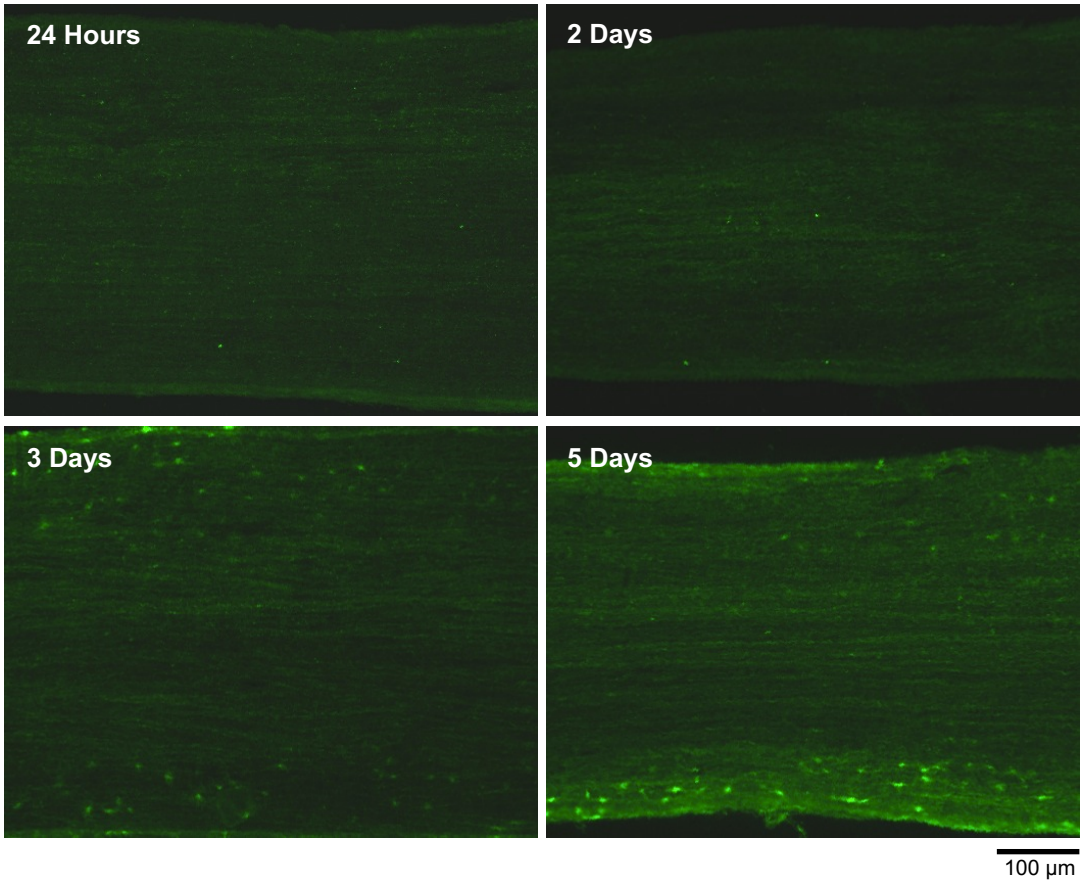
24 Hours
2 Days
3 Days
5 Days
100 µm

B)

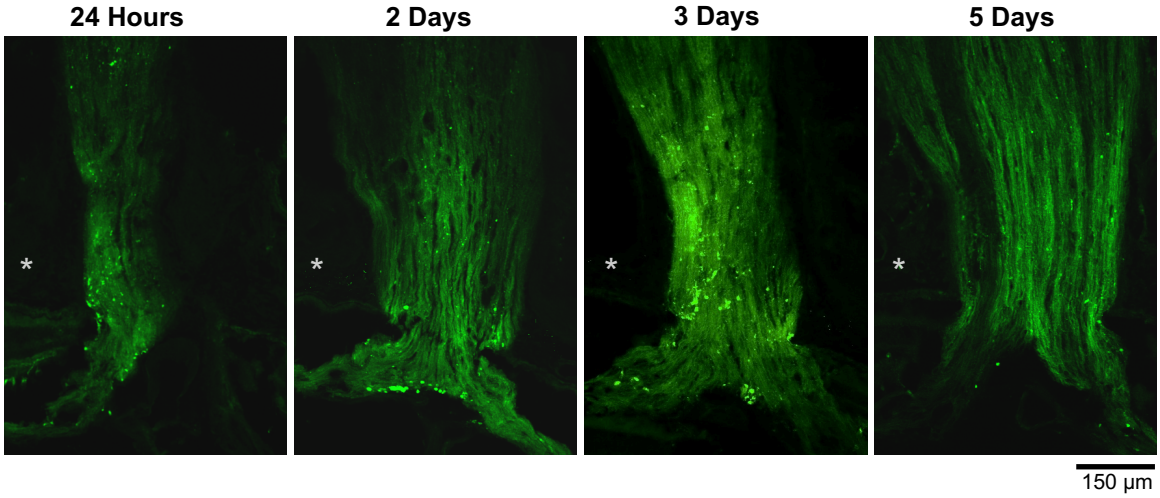
24 Hours
2 Days
3 Days
5 Days
*
*
*
*
150 µm

Figure 3.5 Time Course of Retrograde CTB Arrival at the Retina 24 hours, 2 days, 3 days, and 5 Days Following Application to the SC. CTB labelling was present in all retinal quadrants 24 hours following CTB injection in the SC. Labelling intensified at 2 and 3 days, however, was less intense at 5 days following CTB injection. Labelling was non-uniform across the retinal quadrants at all time points, and was most intense towards the central retina. T = temporal, N = Nasal, D = Dorsal, V = Ventral.

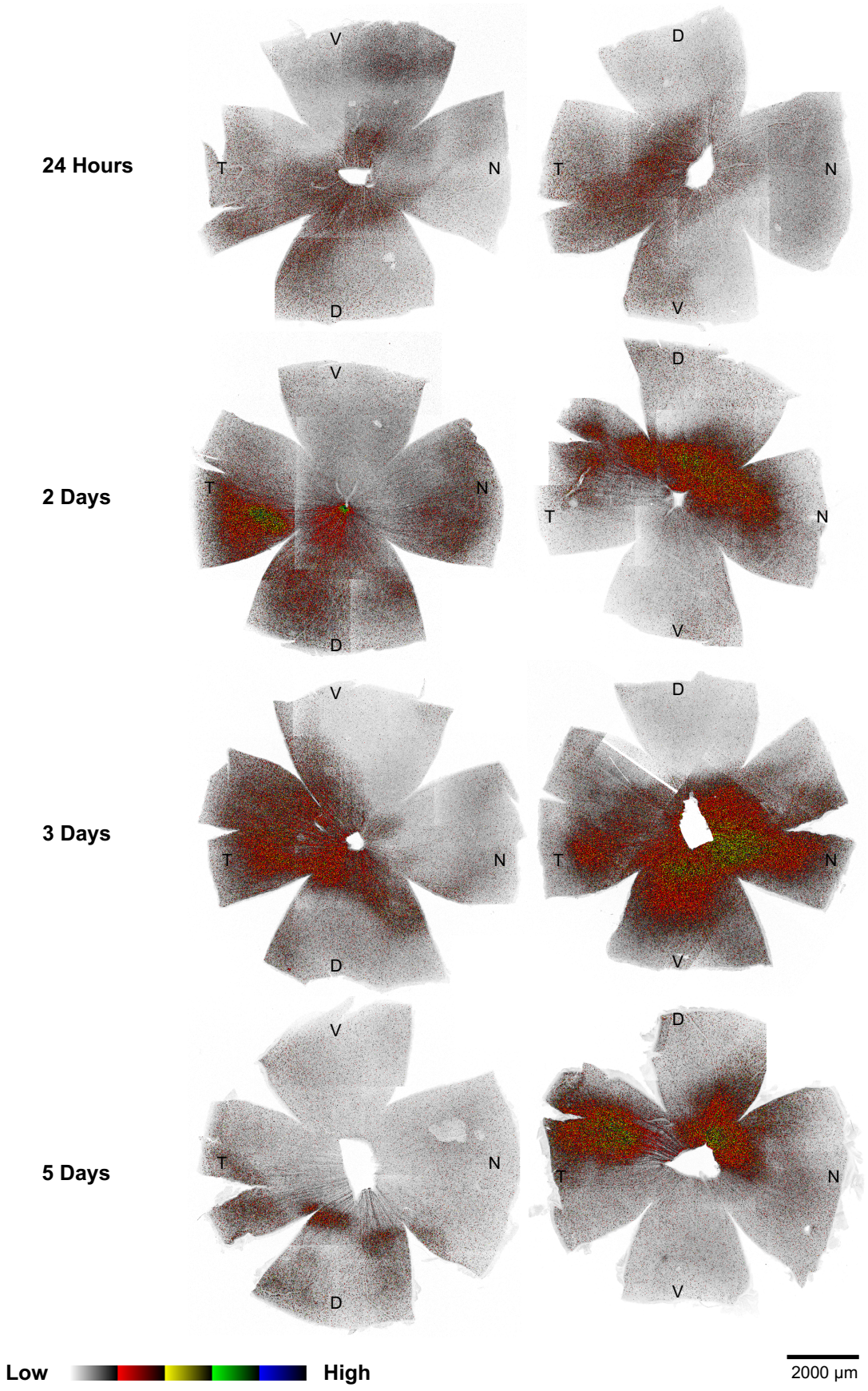
24 Hours
2 Days
3 Days
5 Days
V
D
T
N
Low
High
2000 µm

Overall, CTB retrograde AT was rapid and easily visualized in all cellular compartments (Figures 3.4, 3.5, and 3.6 B and D).

3.3.3 Comparison of RITC and CTB Retrograde AT

Retrogradely transported CTB was consistently visualized in more cellular compartments than RITC (Figure 3.6 A-D). The results of time course analyses suggest that, as with RITC retrograde AT, the number of RGCs retrogradely transporting CTB increases over time (Figures 3.1, 3.5); however, CTB retrograde AT is faster than that of RITC, filling the majority of axons within 24 hours, while the number of RITC-transporting RGCs continues to increase between 24 hours and 3 days following tracer application at the SC (Figures 3.1, 3.2 and 3.4).

3.3.6 Estimations of RITC and CTB Transport Rates

RITC was present in RGC axon fibres and somas in some retinal quadrants as early as 8 hours following application to the SC. Given the length of the entire projection from retina to SC in adult Brown Norway rats is approximately 20 mm (Abbott et al., 2013), retrograde RITC can be estimated to proceed at a rate of at least 60 mm/day. However, given that some RGC somas in the peripheral retina exhibited retrograde filling with RITC, this is likely an underestimate. The rate of RITC anterograde AT was not calculated.

Retrograde filling of RGC axons and somas was clearly visible in all retinal quadrants as early as 24 hours following SC injections, making estimation of the rate of

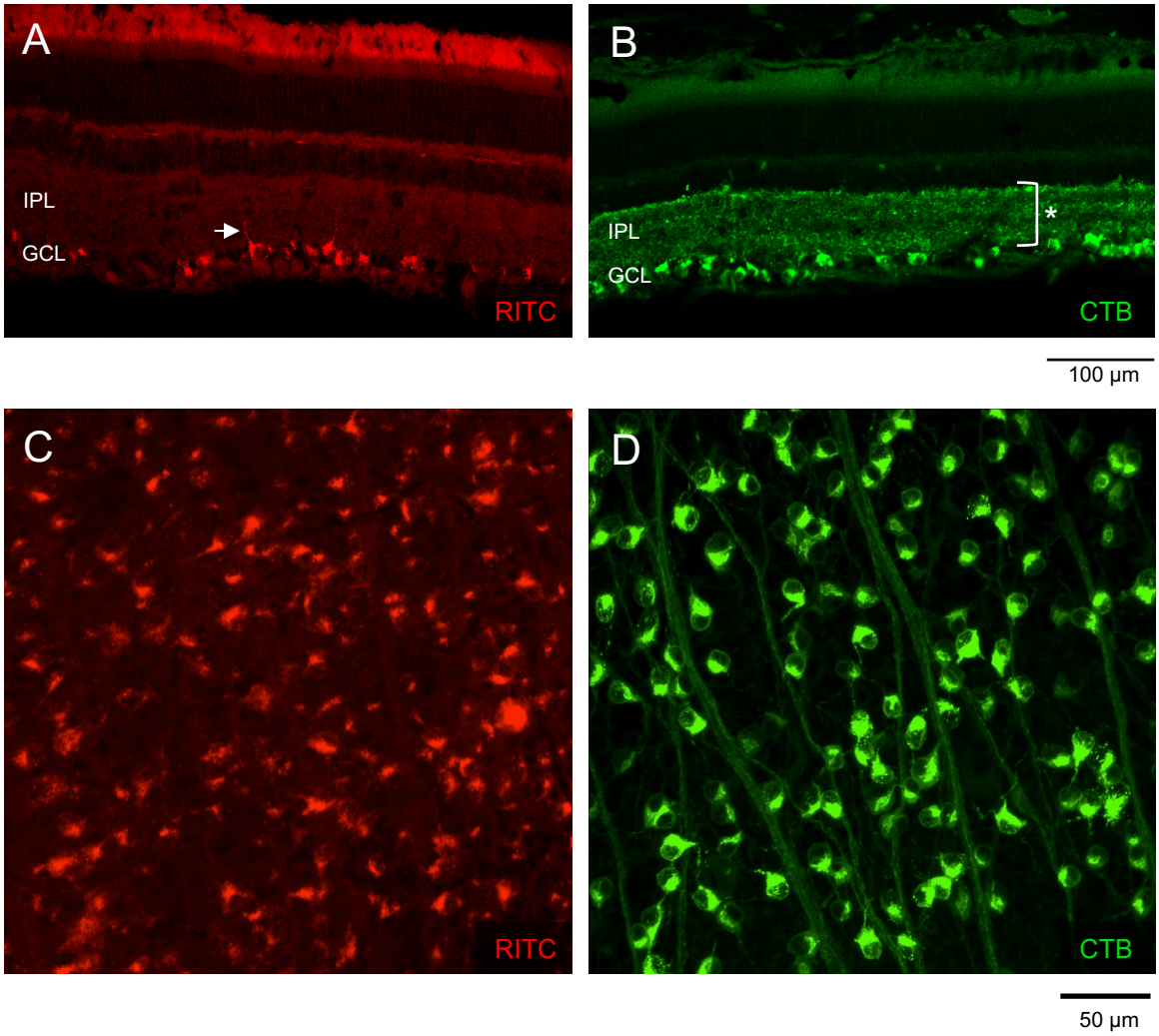

Figure 3.6 Comparison of RITC and CTB in the Retina at 7 Days Following Application to the SC. A) Retrograde RITC in retinal cross-section. Retrogradely transported RITC labels RGC somas and some proximal dendrites (arrow). **B)** Retrograde CTB in retinal cross-section. In addition to labelling RGC somas, retrogradely transported CTB filled RGC dendritic arbours extensively. IPL – inner plexiform layer, GCL – ganglion cell layer. **C)** Profiles of RITC-filled RGCs in a whole-mounted retina. RITC filled many RGCs, however the pattern of labelling often did not allow visualization of the entire soma. **D)** CTB labeled RGC somas clearly and brightly.

retrograde CTB difficult – a rate of 20 mm/day is likely an underestimate. Interestingly, faint CTB-filled axon profiles were visible in the chiasm of two rats that died only 1 and 1.5 hours following SC injections, suggesting that retrograde AT of CTB may proceed at a rate exceeding 200 mm/day.

3.4 Summary and Key Findings

These experiments demonstrated important qualities of the dynamics and appearance of two commonly used fluorescent retrograde AT tracers - RITC and fluorescently conjugated CTB – in the axon, soma, and dendrites of RGCs in the rat visual system.

Key findings included:

1) Both RITC and CTB were gradually taken up by RGCs and transported throughout all cellular compartments.
2) Uptake of both tracers was not uniform across the RGC population.
3) RITC and CTB were transported at different rates.
4) Compared to RITC, retrogradely transported CTB provides a superior visual signal in all neuronal compartments.

Further discussion of RITC and CTB tracers is included in section 8.2

CHAPTER 4 – RETROGRADE AT IN RGCS FOLLOWING ELEVATED IOP

4.1 Rationale, Objective, and Hypotheses

The experiments characterizing RITC and CTB retrograde AT (Chapter 3) found fluorescently conjugated CTB to be a superior indicator of AT in the ON. The experiments described in this chapter used CTB to evaluate retrograde AT in RGC axons within the ONH and ON of rats. Retrograde AT disruption has been observed in animals and humans with glaucoma [323, 324], and also in animal models of IOP-induced RGC injury [63, 129]. For example, acute elevated IOP causing either partial or complete retinal ischemia in rats decreased retrograde AT of radiolabeled BDNF [63]. BDNF, as well as its receptor, tyrosine receptor kinase B, is also elevated in the ONH of monkeys with chronically elevated IOP [131], and retrograde AT disruption in other chronic models of elevated IOP has been demonstrated with various fluorescent tracers, as well as IHC for dynein [129, 157, 225, 325].

Few studies have reported a reversible blockade of retrograde AT following a transient injury to RGCs [158, 285, 326, 327]. Understanding the reversibility of injury responses in RGCs, such as AT disruption, is important in the study of RGC degeneration, and essential to the development of therapies for optic neuropathies involving RGCs.

The objective of these experiments was to examine retrograde AT function at 3, 7, and 14 days of recovery following a transient elevation of IOP. Two severities of elevated IOP, varied by duration, were used to identify differences in retrograde AT function between a situation of known RGC survival (30 minutes of elevated IOP), and one of severe and progressive RGC degeneration (90 minutes of elevated IOP). It was

hypothesized that RGCs exposed to the sub-critical insult would show a transient retrograde AT disruption, which would recover over time, while the critical insult would cause a progressively worsening disruption of retrograde AT.

This work was published in abstract form [328].

4.2 Experimental Design

Evaluation of Retrograde AT

Immediately following bilateral CTB injections into the SC, the site of the majority of RGC terminals in the rat ([42]; injection procedure described in section 2.2.2), IOP was elevated to 120 mmHg in the experimental eye (procedure in section 2.4). This timing was chosen to reflect the state of AT as closely in time as possible to the insult. Given that the rate of CTB retrograde AT is approximately 200 mm/day (8.3 mm an hour), it would take approximately 2.4 hours for CTB to transport retrogradely through the entire retinofugal projection of the adult rat – an approximate distance of 20 mm from brain to eye. Taking into consideration the duration of IOP elevation (30 or 90 minutes), the amount of CTB in RGC axons would reliably reflect the state of retrograde AT from 1-2 hours post-insult and onwards.

After IOP was normalized, rats were sacrificed at 3, 7, or 14 days. These time points were chosen according to previously described time courses of RGC loss following acute, elevated IOP-induced ischemia [264, 329]. Contrary to that of RGC survival, the time course of retrograde AT disruption following elevated IOP is less understood; therefore, 3, 7, and 14-day time points were chosen to encompass periods of early injury, while also allowing sufficient time for injury progression and/or recovery.

After sacrifice, the ON, from the ONH to the chiasm, was dissected, fixed, and sectioned longitudinally. The sections were imaged with confocal microscopy for analysis of CTB transport. Fluorescence intensity, measured in arbitrary units (AU; range 0-255), was averaged across nerve width at every point along nerve length, from chiasm to ONH, for paired longitudinal ONs (control and experimental).

Measurement of RGC Survival

To measure the effect of elevated IOP on RGC survival, RGCs in all retinal quadrants (nasal, temporal, superior, inferior) and at 1, 2, and 3 mm of eccentricity were quantified at 7 and 14 days post-insult (n = 2/group, total n = 8) using the RGC-specific marker Brn3a [318] (for detailed procedure, see section 2.10.1), and qualitative observations for signs of degeneration in CTB+ RGC profiles were made. As an additional measure of degeneration, IHC for pNF was included in retinal whole mount analysis in some animals.

Statistics

The effects of elevated IOP and recovery time on both RGC survival (quantification of Brn3a+ cells) and retrograde AT in the ONH (quantification of CTB intensity) were analyzed using paired and independent sample t-tests. The effects of elevated IOP on CTB intensity in the ON was analyzed with a mixed effects model that examined effects and interactions of injury group (control or experimental), recovery time (3, 7, and 14 days), as well as nerve length and width. Analyses for 30- and 90-minute groups were performed separately.

Sample Sizes

In total, 24 rats were used in experiments evaluating retrograde AT following elevated IOP. Experiments were a 2 x 3 factorial design, with 6 experimental groups separated by 2 levels of insult duration (30 or 90 minutes) and 3 levels of recovery time (3, 7, and 14 days; n = 4/group, N = 24). In the following sections, groups are referred to by their insult duration and recovery time (ex. 30 minutes of elevated IOP and 3 days of recovery = '30min/3d'). Quantification of retrogradely transported CTB in the ONH was completed in all rats (n = 4/group, N = 24). One rat was excluded from CTB intensity analysis in the ON in the 30-minute group due to poor tissue quality (30min/14d: n = 3, N = 23). Quantification of RGC survival using the Brn3a antibody was completed in 2/4 rats for both the 30- and 90-minute insults at 7 and 14 days of recovery (n = 2/group; N = 8).

4.2 Results

4.2.1 RGC Degeneration and Loss Following Transient Elevated IOP

Brn3a labeled a high density of cells in the GCL in all control eyes (Figure 4.1 A and B). Thirty minutes of elevated IOP did not cause significant loss of Brn3a+ cells at either 7 or 14 days following insult, although there was a trend of Brn3a+ cell loss after 14 days (Figure 4.1 A and 4.2 A; Table 4.1). This trend of loss was homogenous across quadrants, but more pronounced towards the optic disc (1 mm: 26% loss; 2 mm: 11% loss; 3 mm: no loss). Conversely, 90 minutes of elevated IOP caused near complete loss of Brn3a+ cells at both 7- and 14-day time points, the severity of which was consistently

Figure 4.1 RGC Loss at 7 Days Following Elevated IOP. A) Brn3a and CTB labelling in retinal whole-mounts at 7 days following 30 minutes of elevated IOP. Brn3a and CTB labelling of RGCs showed a high level of correspondence. There was no visible reduction in the density of Brn3a labelling or CTB back filling following 30 minutes of elevated IOP. **B)** Brn3a and CTB labelling in retinal whole-mounts at 7 days following 90 minutes of elevated IOP. Ninety minutes of elevated IOP caused a pronounced decrease in Brn3a density. CTB labelling was also less dense and had morphology indicative of widespread degeneration.

A) **30 Minutes Elevated IOP**

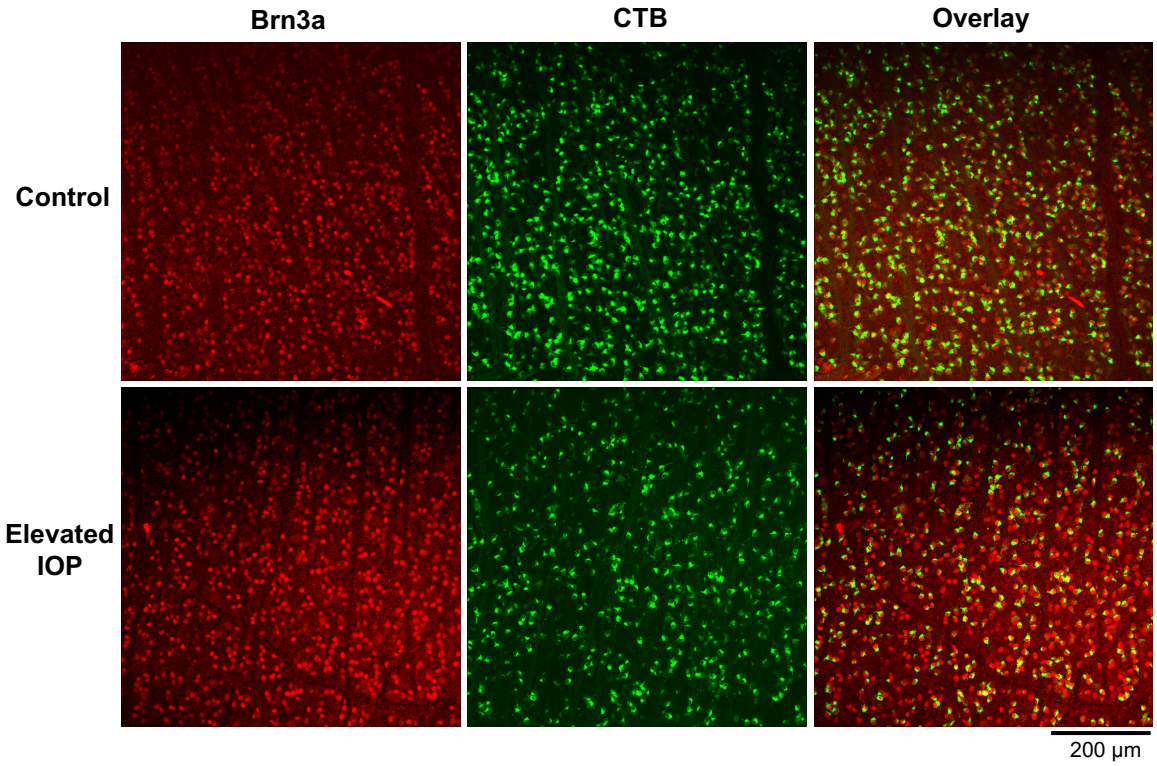

B) **90 Minutes Elevated IOP**

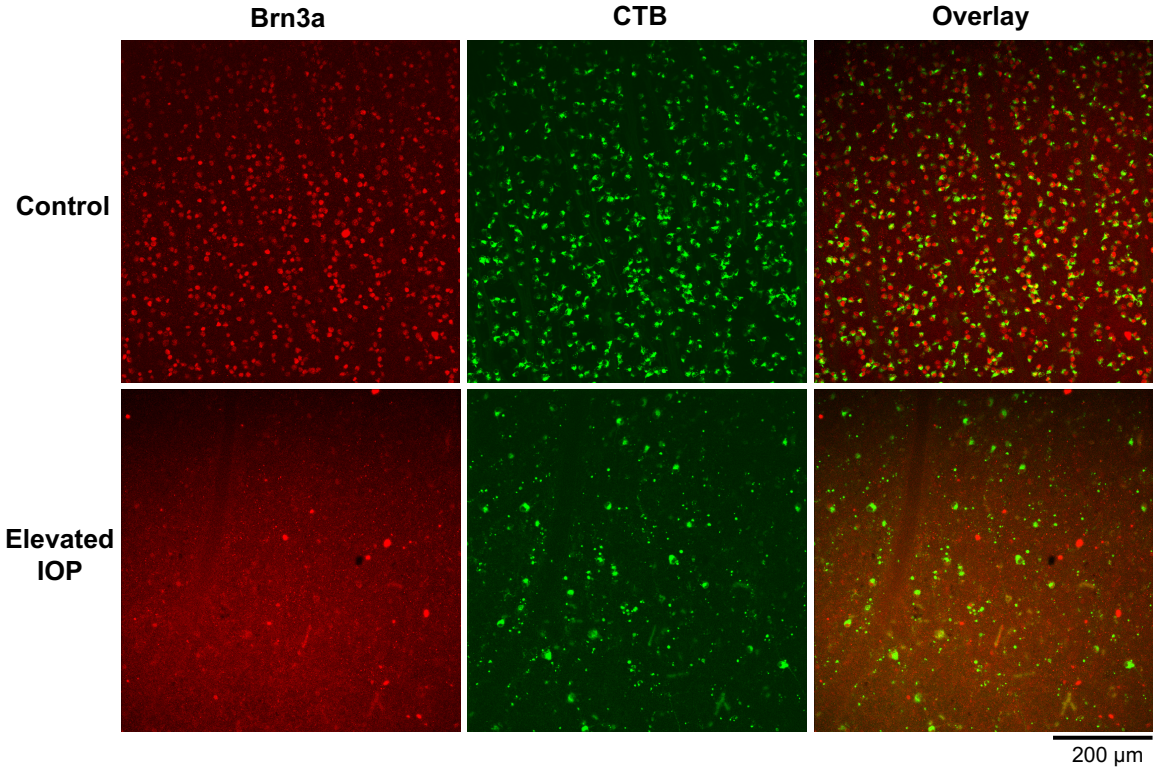

Figure 4.2 Quantification of Brn3a+ Cells in Retinal Whole-Mounts Following Elevated IOP. A) Brn3a+ cell density in control and experimental retinas following 30 minutes of elevated IOP. Brn3a+ cell density was not significantly reduced following either the 7 or 14 days of recovery. **B)** Brn3a+ cell density in control and experimental retinas following 30 minutes of elevated IOP. Ninety minutes of elevated IOP caused significant and severe loss of Brn3a+ cells at 7 and 14 days of recovery. * = $p < 0.05$; ** = $p < 0.01$; *** = $p < 0.001$.

A) 30 Minutes Elevated IOP

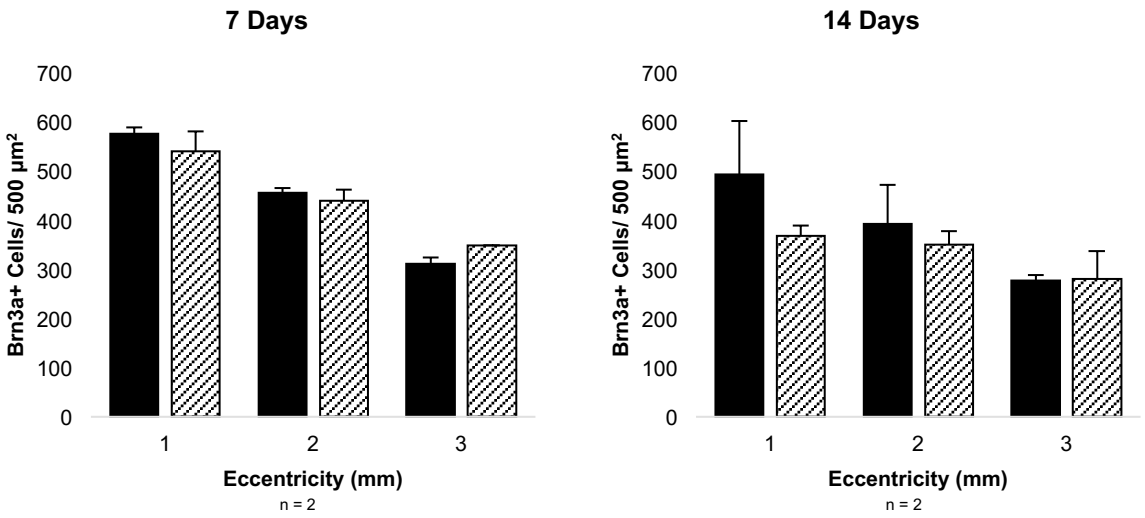

B) 90 Minutes Elevated IOP

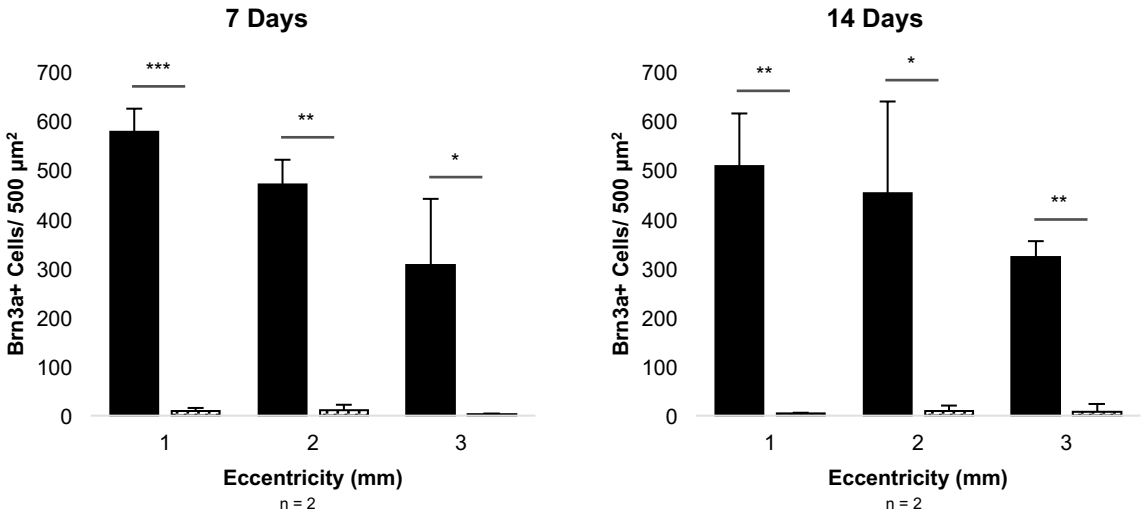

Table 4.1 Average ON Fluorescence and RGC Density at 3, 7, and 14 Days Following Elevated IOP

		Average Brn3a+ Cells/ 500 µm^2 at 1, 2, and 3 mm of Eccentricity						Average ON Fluorescence (AU)		
	Recovery	1 mm		2 mm		3 mm		Control	Elevated IOP	Difference
		Control	Elevated IOP	Control	Elevated IOP	Control	Elevated IOP			
30 Minutes Elevated IOP	3 Days	-	-	-	-	-	-	67.05 ± 11.09	53.30 ± 6.81	-13.75 ± 14.31
	7 Days	575.75 ± 17.50	540.13 ± 57.25	456.00 ± 13.00	438.38 ± 32.75	311.25 ± 18.50	348.75 ± 0.50	84.59 ± 14.51	81.70 ± 8.64	-2.89 ± 17.81
	14 Days	492.63 ± 154.25	367.00 ± 29.75	391.75 ± 112.50	349.75 ± 39.00	276.75 ± 16.00	280.25 ± 79.50	77.77 ± 3.43*	66.38 ± 21.35*	-11.39 ± 24.11*
	Recovery	1 mm		2 mm		3 mm		Control	Elevated IOP	Difference
		Control	Elevated IOP	Control	Elevated IOP	Control	Elevated IOP			
90 Minutes Elevated IOP	3 Days	-	-	-	-	-	-	73.01 ± 15.87	57.68 ± 12.63	-15.33 ± 6.39
	7 Days	507.88 ± 75.25	4.00 ± 1.50	452.13 ± 132.25	8.63 ± 8.75	323.00 ± 22.50	7.00 ± 12.00	63.38 ± 6.51	42.70 ± 6.07	-20.68 ± 6.02
	14 Days	577.50 ± 33.50	8.38 ± 4.75	469.63 ± 35.75	10.88 ± 7.75	306.63 ± 94.75	3.00 ± 0.50	64.50 ± 12.36	46.13 ± 13.09	-19.85 ± 10.91

Fluorescence intensity data expressed in AU, RGC density in Brn3a+ cells/500 µm^2.

Sample sizes: Brn3a quantification, n = 2/group; ON intensity analysis, n = 4/group except for those indicated with * n = 3.

All data presented as mean ± 2SEM.

less pronounced in the temporal quadrant (not shown), but did not vary with eccentricity (Figure 4.1 B and 4.2 B; Table 4.1). Correspondence between Brn3a labelling and CTB back-filling was high in injured and non-injured eyes (Figure 4.1 A, B), supporting the specificity of Brn3a for RGCs, as previously described by Nadal-Nicolas and colleagues [318]. Despite extensive cell loss following 90 minutes of elevated IOP, surviving RGCs that continued to display healthy morphology, such as the 'cupped' appearance of intact somas with unfragmented CTB labelling in the cytoplasm, were also Brn3a+ (Figure 4.1 B; Figure 4.4 D).

RGC morphology was unaffected in whole-mounted retinas from eyes exposed to 30 minutes of elevated IOP, and the density of CTB-labeled RGC somas appeared comparable between experimental and control eyes. There were also very few fragmented or varicose axon profiles observed in retinas, ONHs, and ONs of 30min/3d and 30min/7d groups, suggesting a lack of axonal degeneration (Table 4.2). Signs of axonal degeneration were observed in experimental ONHs and ONs in the 30min/14d group; however, this was interpreted with caution as similar histology was observed in control tissue.

Ninety minutes of elevated IOP resulted in marked structural degeneration of RGC somas and axons (Figure 4.3). Signs of degenerative pathology, such as abundant punctate, spheroidal, CTB+ particles, often connected to an axon that was disorganized and fragmented in appearance, were frequently observed in experimental retinas from the 90min/3d group (Figure 4.4 A, asterisk). This pathology was more prevalent in the peripheral retina (Figure 4.5). Few signs of any RGCs, healthy or degenerating, were observed in experimental retinas from the 90min/14d group (Figure 4.3). Further IHC

Table 4.2 Qualitative Evaluation of AT Disruption in the ONH and Axonal Degeneration in the Peripapillary Retina, ONH, and ON

Injury Group	Recovery Time	Animal ID	Control		Elevated IOP	
			AT Block?	Axonal Damage?	AT Block?	Axonal Damage?
30 Minutes Elevated IOP	3 Days	R1031011	No	No	No	No
		R2031011	No	No	No	No
		R1060111	No	No	No	No
		R2060111	No	No	No	No
	7 Days	R2022211	No	No	No	No
		R1030611	No	No	No	No
		R2120310	No	No	Yes	ONH+, ON+
		R1120610	No	No	No	No
	14 Days	R1022011	No	ONH+	No	Ret+, ONH+, ON+
		R2022011	No	Ret+, ONH+, ON+	No	ONH+, ON+
		R1120310	No	Ret+, ONH+, ON+	No	Ret++, ONH+, ON++
		R1120110	No	Ret+, ONH+, ON++	No	Ret+, ONH+, ON++
90 Minutes Elevated IOP	3 Days	R1040711	No	No	Yes	Ret++, ONH+, ON+
		R2040711	No	No	Yes	Ret++, ONH+, ON+
		R1050311	No	No	Yes	Ret++, ONH+, ON+
		R1060611	No	No	Yes	Ret+, ONH+, ON+
	7 Days	R2030611	No	No	Yes	Ret+++, ONH+++, ON++
		R3030611	No	No	Yes	Ret+++, ONH+++, ON+++
		R1102110	No	No	Yes	Ret+++, ONH+++, ON++
		R2102110	No	No	Yes	Ret+++, ONH+++, ON++
	14 Days	R1101310	No	No	Yes	Ret+++, ONH+++, ON+++
		R1101410	No	No	Yes	Ret+++, ONH+++, ON+++
		R1022511	No	No	Yes	Ret+++, ONH+++, ON++
		R2022511	No	ON+	Yes	Ret+++, ONH+++, ON+++

Figure 4.3 Structural Degeneration of RGCs Retrogradely Filled with CTB at 3, 7, and 14 Days Following 90 Minutes of Elevated IOP. Retrograde filling of healthy RGCs (control retinas) with CTB revealed a typical 'cupped' morphology of the soma - the cytosol was filled with tracer while the nucleus was not. This morphology was disturbed following 90 minutes of elevated IOP. Degenerative morphology, such as punctate CTB+ particles and fragmented axons, was abundant at the 3 and 7-day time points. By 14 days most CTB+ RGCs had degenerated and CTB+ cellular debris was no longer present.

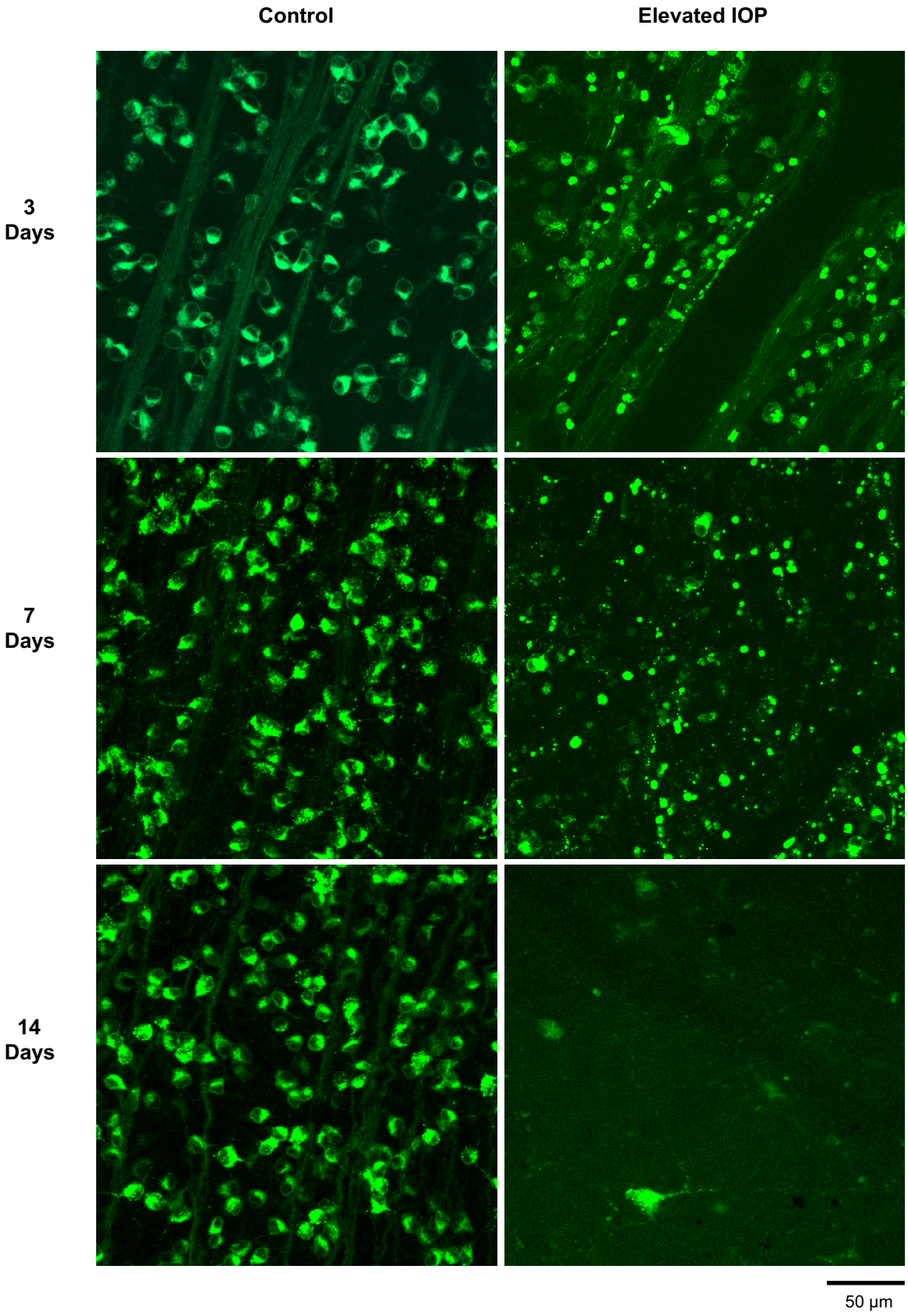
Control
Elevated IOP
3 Days
7 Days
14 Days
50 µm

Figure 4.4 IHC Analysis of Retinal Whole-Mounts at 3 Days Following 90 Minutes of Elevated IOP. A) CTB labelling of RGCs. Degenerative signs included punctate CTB+ spheroidal particles (arrows), which were sometimes connected to a fragmented axon (asterisk). Remaining RGCs with healthy CTB+ morphology are circled. **B)** pNF labelling. Some CTB+ spheroids were also pNF+ (arrowheads). The locations of CTB+ RGC somas did not co-localize with pNF labelling. **C)** Brn3a labelling. The locations of most CTB+ RGC somas co-localized with Brn3a labelling (solid circles). Dashed circles denote Brn3a- CTB+ RGC somas. **D)** Overlay.

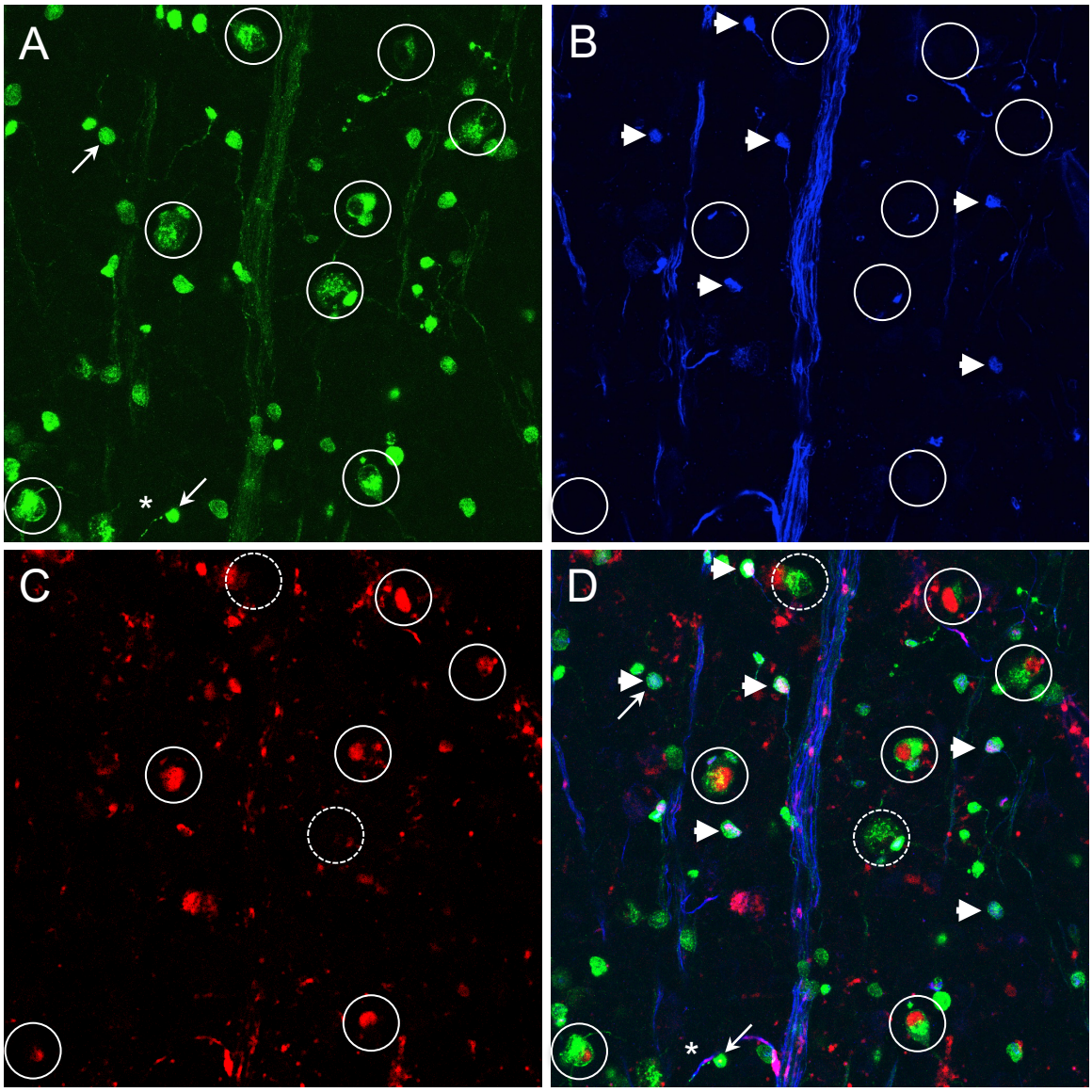
A
B
C
D
*
*
50 µm

Figure 4.5 Degeneration of pNF+ RGCs in the Central and Peripheral Retina at 3 Days Following 90 Minutes of Elevated IOP. pNF labelling revealed signs of RGC degeneration following elevated IOP, such as axonal varicosities and the swollen ends of severed axons. These axonal pathologies were present in both the central and peripheral retina, although were more prominent in the latter.

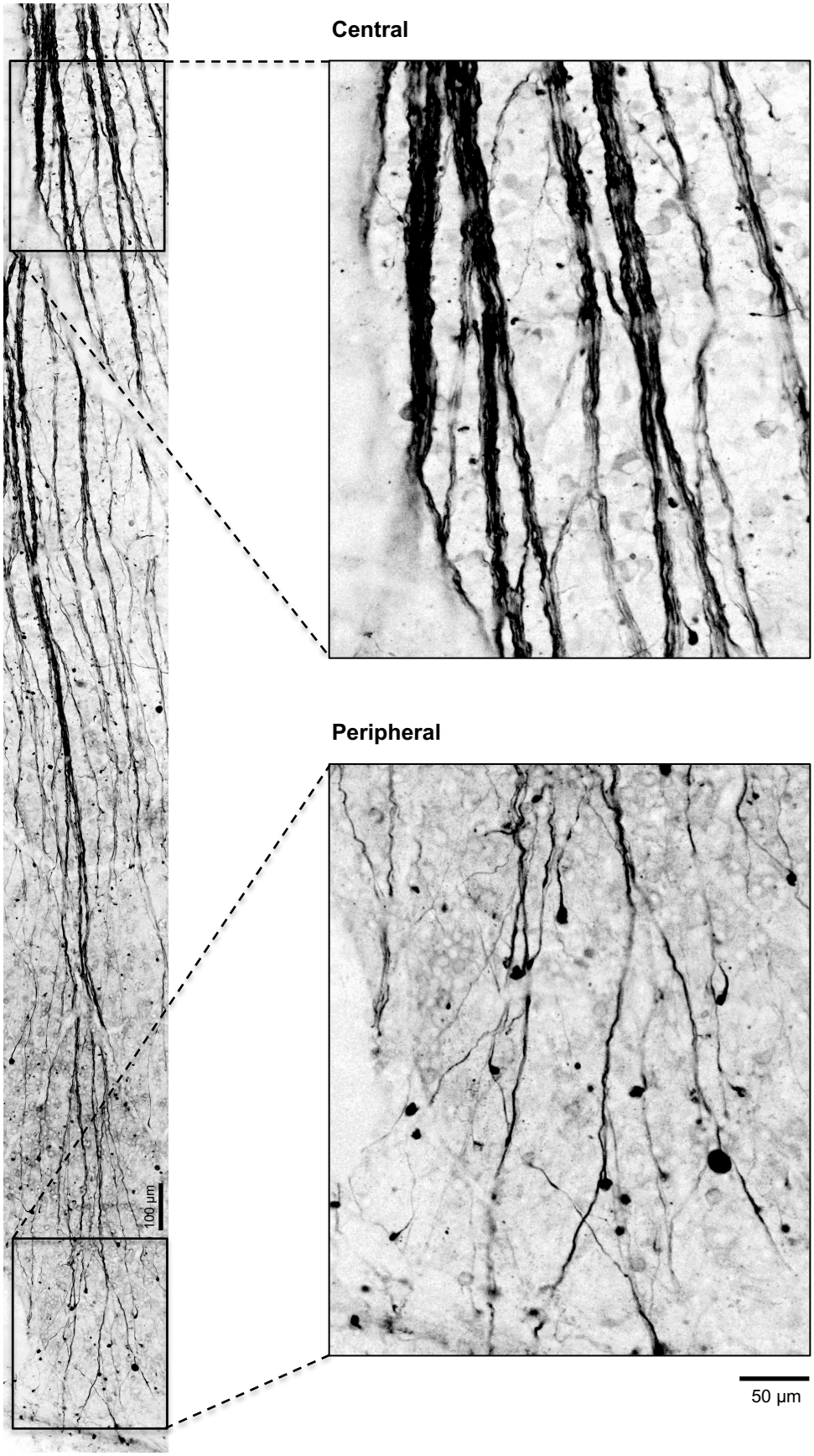
Central
Peripheral
100 µm
50 µm

analysis of whole-mounted experimental retinas from the 90min/3d group revealed that approximately half of the punctate CTB+ structures were also pNF+ (Figure 4.4 B and D, arrowheads). Remaining CTB+ RGC somas were primarily pNF- and Brn3a+ (Figure 4.4 B, C and D, solid circles). Axonal degeneration in experimental ONHs and ONs from the 90-minute group was pronounced and consistent at all time points (Table 4.2).

4.2.2 Retrograde AT in the ONH Following Elevated IOP

Retrograde AT of CTB in RGC axons within the ONH was examined at 3, 7, and 14 days following CTB application at the SC and elevated IOP. Thirty minutes of elevated IOP did not result in obvious disruption of retrograde AT in the ONH at any of the recovery times examined (Figure 4.6 A). Indeed, filling of intraocular RGC axons and their somas suggested that retrograde AT through the ONH was primarily uninhibited (Figure 4.6 A).

Conversely, localized AT disruption, as evidenced by accumulation of CTB in the ONH, was evident at all recovery times following the 90-minute insult (Figure 4.6 B, arrowheads). These observations were remarkably consistent across all animals examined. Labelling intensity of accumulated CTB in the ONH was greatest in the 90min/3d group, and progressively decreased in 90min/7d and 90min/14d groups (Figure 4.6 B). The peripapillary region of experimental retinas from the 90min/3d group predominantly lacked the layered cellular organisation typically observed in retinal cross-sections (Figure 4.6 B), and the thickness of experimental retinas was visibly reduced in 90min/7d and 90min/14d groups (Figure 4.6 B, asterisks). Subjective evaluation of

Figure 4.6 Retrograde AT of CTB in the ONH After 30 or 90 Minutes of Elevated IOP. A) CTB in the ONH at 3, 7, and 14 days following 30 minutes of elevated IOP. **B)** CTB in the ONH at 3, 7, and 14 days following 90 minutes of elevated IOP. Accumulation of CTB was prominent in the ONH (arrowheads) by 3 days following elevated IOP, and persisted at the 7-day time point. Retinal thickness (*) was greatly decreased at the 7- and 14-day time points.

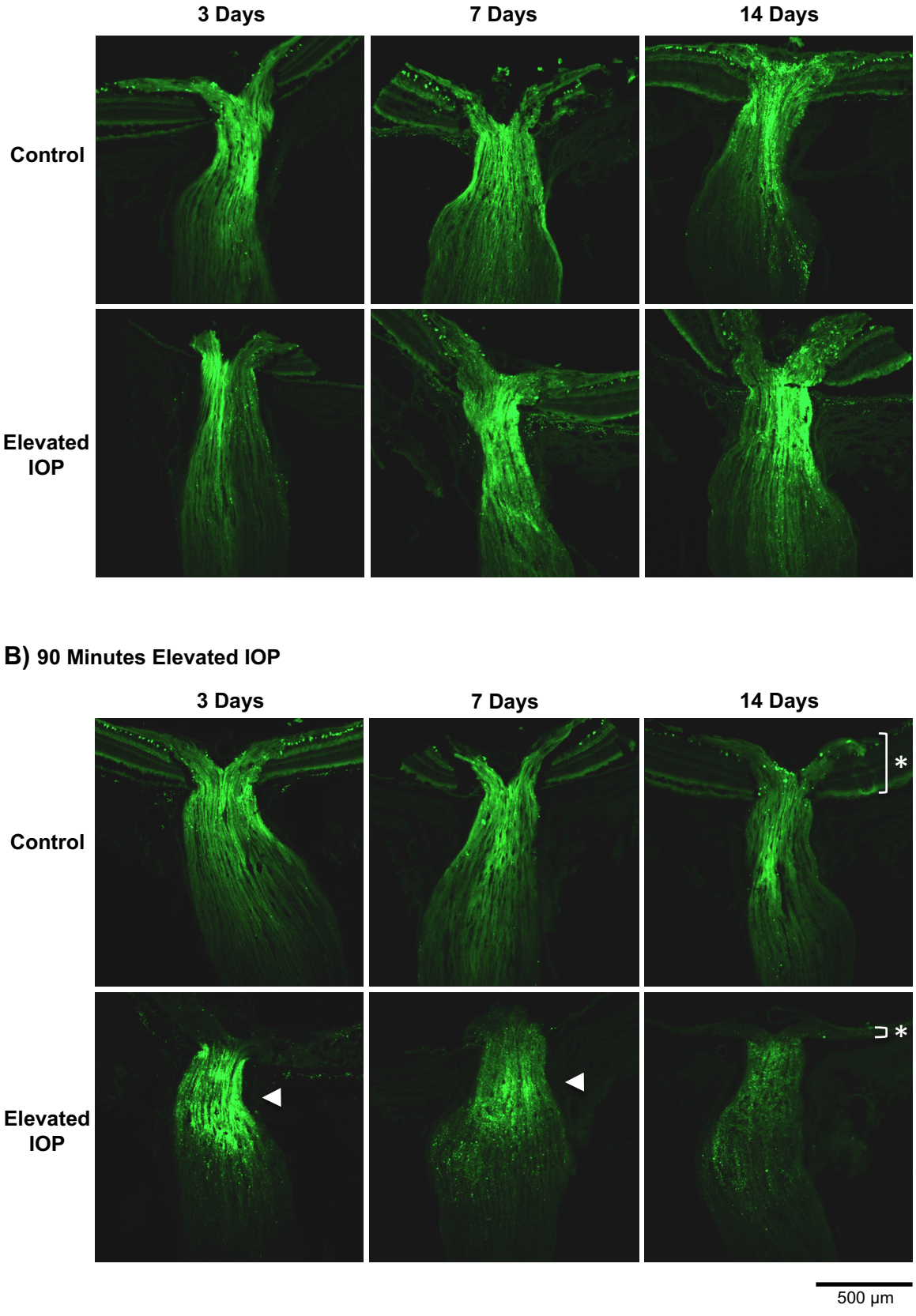
A) 30 Minutes Elevated IOP
3 Days
7 Days
14 Days
Control
Elevated IOP
B) 90 Minutes Elevated IOP
3 Days
7 Days
14 Days
Control
Elevated IOP
*
*
500 µm

experimental ONHs in the 90min/14d group suggested a reduction in width compared to control ONHs (Figure 4.6 B). Notably, sparse, CTB-filled RGC somas were observed in the peripapillary GCL of some experimental retinas, indicating that AT blockade in some RGCs was either incomplete or delayed following elevated IOP.

4.3.3 Retrograde AT in the ON Following Elevated IOP

Figures 4.7 and 4.8 show examples of CTB retrograde AT in ONs (control and experimental) following either 30 or 90 minutes of elevated IOP, respectively. Figures 4.10 A and B show the average differences in fluorescence between control and experimental ONs expressed along nerve length. Both insult durations reduced CTB intensity in the ON (Figure 4.9 A and B). Compared to 30-minute groups, reduction of CTB intensity in experimental ONs was greater in 90-minute groups (Figure 4.9 A and B). There was no trend of recovery of ON CTB intensity over time following either insult duration (Figure 4.9 A and B). These observations were confirmed by the results of the mixed effects analysis, which are discussed in the following paragraphs.

Thirty minutes of elevated IOP caused a significant reduction in the average fluorescence intensity of CTB in experimental ONs compared to control ONs (average intensity difference = -12 ± 9.44 AU; $p < 0.05$). However, no interaction was found between the main effects of elevated IOP and recovery time (average intensity per time point is depicted in Figure 4.9 C and summarized in Table 4.2).

Ninety minutes of elevated IOP caused a significant reduction in the average fluorescence intensity of CTB in experimental ONs compared to control ONs (average intensity difference = -19 ± 4.36 AU; $p < 0.01$; Figure 4.9 C; Table 4.2). As observed in

Figure 4.7 CTB Retrograde AT in ONs at 3, 7, and 14 Days Following 30 Minutes of Elevated IOP. Retrogradely transported CTB in longitudinal sections of ONs is depicted. ONs are oriented so that the chiasm is to the left, and the control nerve is the upper nerve in each pair, while the experimental nerve is below.

3 Days
Control
Elevated IOP
7 Days
Control
Elevated IOP
14 Days
Control
Elevated IOP
1000 µm

Figure 4.8 CTB Retrograde AT in ONs at 3, 7, and 14 Days Following 90 Minutes of Elevated IOP. Retrogradely transported CTB in longitudinal sections of ONs is depicted. ONs are oriented so that the chiasm is to the left, and the control nerve is the upper nerve in each pair, while the experimental nerve is below.

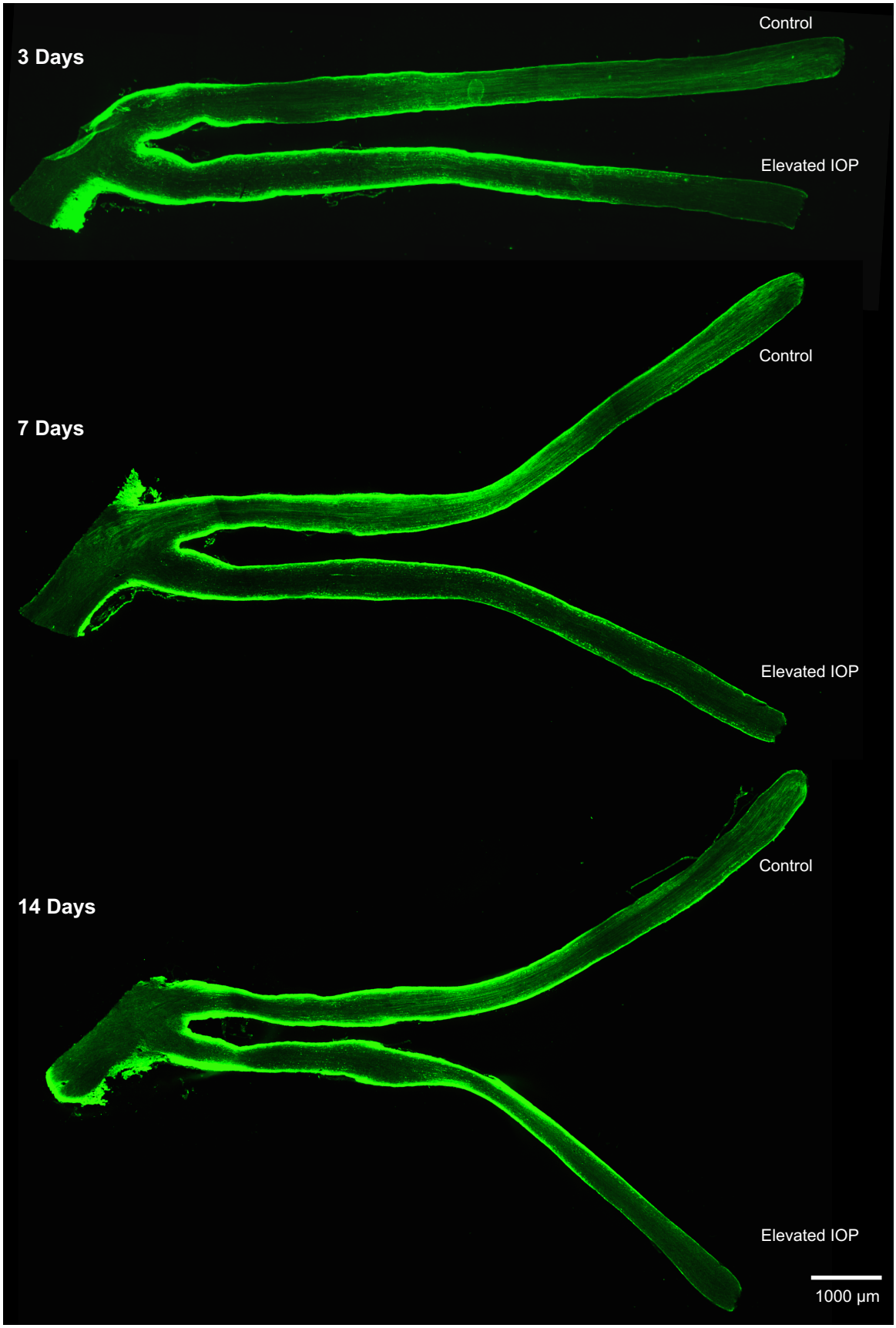
3 Days
Control
Elevated IOP
7 Days
Control
Elevated IOP
14 Days
Control
Elevated IOP
1000 µm

Figure 4.9 Quantification of CTB AT in the ON at 3, 7, and 14 Days Following 30 and 90 Minutes of Elevated IOP. A) Difference in fluorescence intensity between control and elevated IOP ONs along the length of the nerve for all recovery times following 30 minutes of elevated IOP. A decrease in transported CTB was evident as early as 3 hours following elevated IOP and did not preferentially affect either the proximal or distal ON. **B)** Difference in fluorescence intensity between control and elevated IOP ONs following 90 minutes of elevated IOP. A pronounced decrease in CTB transport was present at 3 days of recovery, which persisted at later time points. Data are represented as a moving average (period = 100). **C)** Average difference in fluorescence following 30 and 90 minutes of elevated IOP.

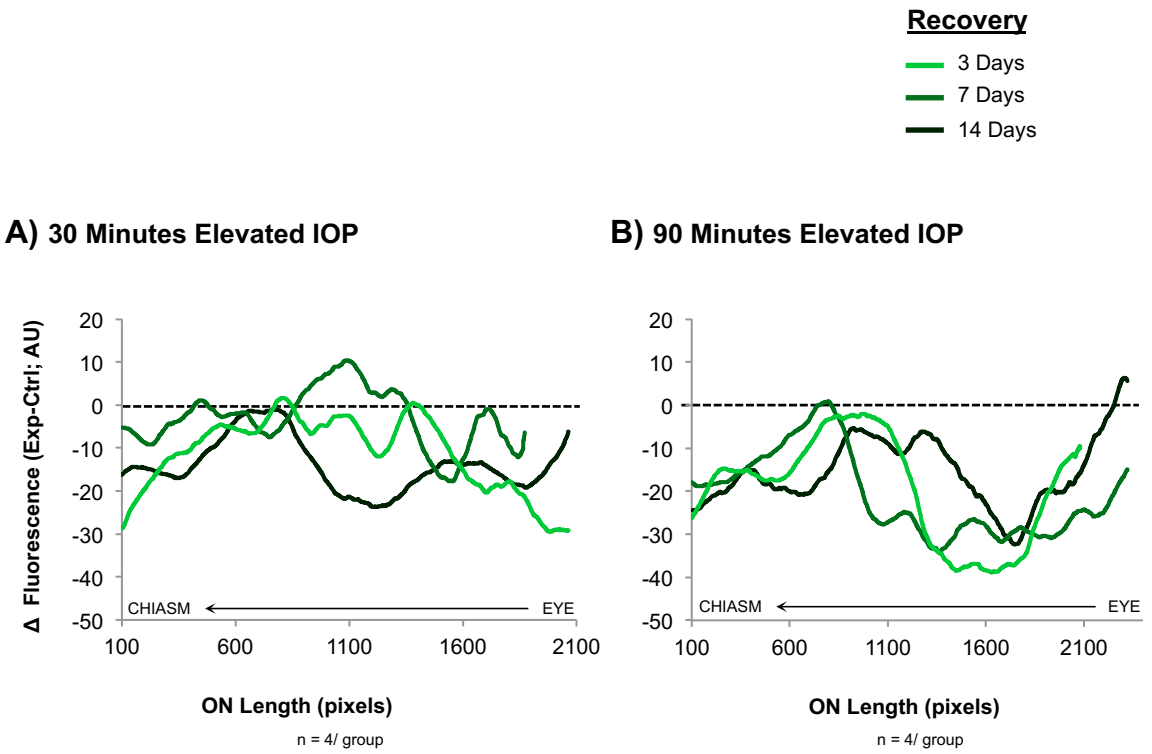
Recovery
3 Days
7 Days
14 Days
A) 30 Minutes Elevated IOP
B) 90 Minutes Elevated IOP
Δ Fluorescence (Exp-Ctrl; AU)
20
10
0
-10
-20
-30
-40
-50
CHIASM
EYE
100
600
1100
1600
2100
ON Length (pixels)
n = 4/ group

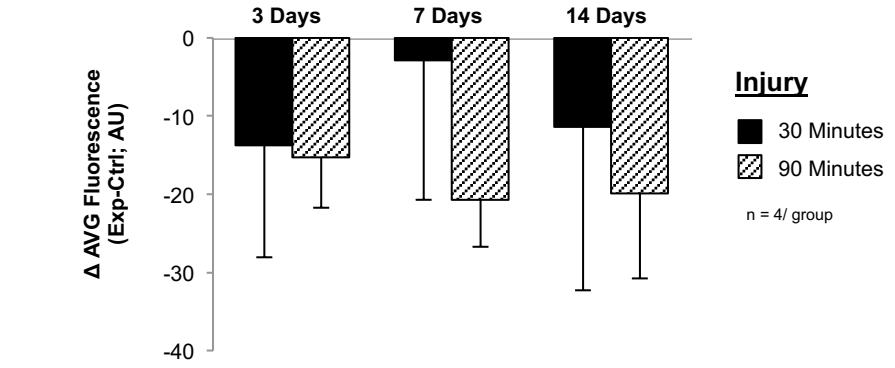
C) Average Differences
3 Days
7 Days
14 Days
Δ AVG Fluorescence (Exp-Ctrl; AU)
0
-10
-20
-30
-40
Injury
30 Minutes
90 Minutes
n = 4/ group

the 30-minute group, there was no interaction between the main effects of elevated IOP or recovery time in the 90-minute group.

The mixed effects model also examined the effect of location of measurement along the nerve on fluorescence intensity. This was a method of determining if retrograde AT blockade occurred at a particular point along the nerve - perhaps closer to the chiasm or closer to the eye. While both insult durations demonstrated a significant effect of nerve length ($p < 0.001$), the actual average difference in fluorescence intensity from the chiasm to the eye in both cases was very small (less than 7 AU). Furthermore, visual inspection of longitudinal transport graphs (Figure 4.9 A and B) did not indicate any trend with respect to nerve length.

Finally, 30 minutes of elevated IOP caused variable changes in ON fluorescence – some animals exhibited reduced fluorescence, some showed no change, and some showed slightly higher fluorescence in the injured nerve (Figure 4.10 A). Contrary to this, 90 minutes of elevated IOP consistently decreased the average ON fluorescence in all animals at all time points (Figure 4.10 B).

Figure 4.10 Individual Paired Measurements of Average CTB Intensity in the ON at 3, 7, and 14 days Following 30 or 90 Minutes of Elevated IOP. A) Average ON intensity values following 30 minutes of elevated IOP. Thirty minutes of elevated IOP did not have a consistent effect on the average fluorescence intensity of CTB in the ON at any time point of recovery. **B)** Average ON intensity values following 90 minutes of elevated IOP. Ninety minutes of elevated IOP caused a reproducible decrease in average CTB fluorescence at all time points, with no recovery over time, indicating a persisting disruption of AT over time.

A) **30 Minutes Elevated IOP**

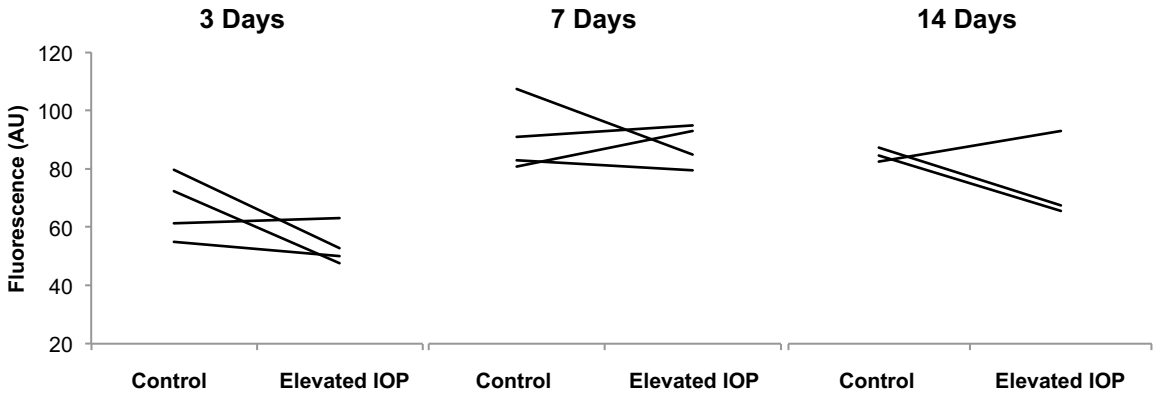

B) **90 Minutes Elevated IOP**

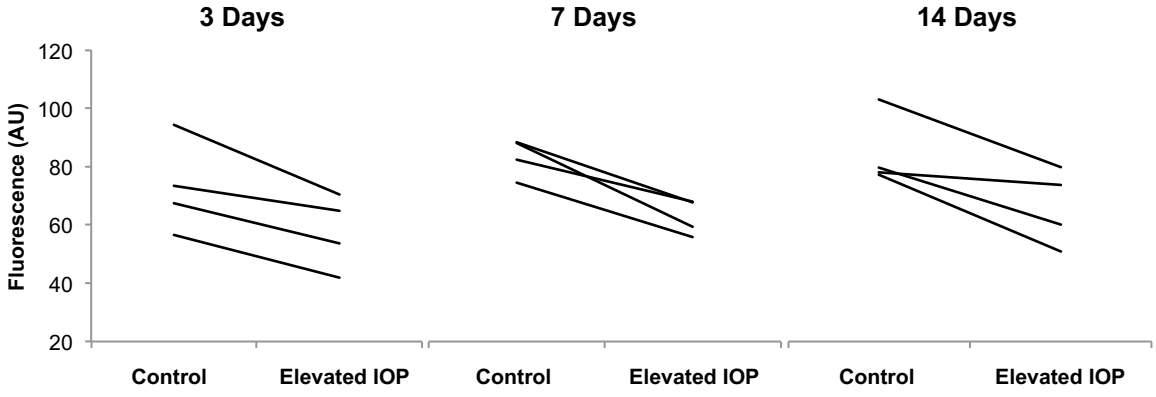

4.4 Summary and Key Findings

The results of the present study, which examined the effects of transient elevated IOP on retrograde AT, demonstrate important qualities of retrograde AT function in RGCs. These qualities include the variable sensitivity of retrograde AT to various durations of elevated IOP, as well as the spatiotemporal relationship between the retrograde AT impairment and the structural degeneration of RGCs at 3, 7, and 14 days following elevated IOP. Furthermore, these experiments further confirm fluorescently conjugated CTB as a capable indicator of AT function in studies of RGC damage.

Key findings include:

1) Retrograde AT impairment in RGCs following elevated IOP can manifest in more than one intracellular location.

2) Two different durations of elevated IOP - 30 and 90 minutes - resulted in significant disruptions of retrograde AT of different magnitudes that do not recover over time.

3) The temporal progression of degenerative events in the retina, ONH, and ON following elevated IOP varied depending on the severity of IOP insult.

Further discussion regarding fluorescently conjugated CTB and the effect of transiently elevated IOP on retrograde AT is included in sections 8.2 and 8.4, respectively.

CHAPTER 5 - ANTEROGRADE AT IN RGCS FOLLOWING TRANSIENT ELEVATED IOP

5.1 Rationale, Objective, and Hypotheses

The experiments described in Chapter 4 examined retrograde AT function in RGCs between 3 and 14 days following elevated IOP. However, many studies report impairments of AT in RGCs less than 12 hours following onset of IOP elevation [157, 225, 283, 285, 305, 306, 330, 331], and some report recovery of AT function following IOP normalization within a similar time frame [158, 283, 285, 306]. However, few studies have examined AT function following an elevation of IOP exceeding MAP [305], and none at times earlier than 24 hours, or through the length of the ON[305]. For the present study, it was proposed that anterograde AT tracing, which offers a method of application that is easy to temporally coordinate with IOP elevation, would provide a useful approach for evaluating AT function at early time points (i.e. hours) of injury.

The objective of these experiments was to evaluate anterograde AT function at early time points – 3, 6, and 24 hours – following transient elevated IOP. Again, two durations of elevated IOP, 30 and 90 minutes, were used to compare the time course of AT function following both sub-critical (30 minutes) and critical (90 minutes) injury to RGCs. It was hypothesized that 30 minutes of elevated IOP would cause a transient disruption in anterograde AT function that would recover over time after the insult, while 90 minutes of elevated IOP would cause a progressively worsening disruption of anterograde AT.

Parts of this work were included in a recent publication [197] and in abstract form [328] [332].

5.2 Experimental Design

Time Course of Anterograde AT of CTB

To gain a better understanding of the rate of anterograde AT of CTB in the rat visual system, a time course study was first conducted in 2 animals. Intravitreal injections of CTB in both eyes (for detailed procedure, see section 2.2.3) were temporally staggered to assess anterograde AT at time points of 3 and 6 hours (n = 1), and 3 and 7 days (n = 1). Additionally, 2 rats that were intended for the anterograde CTB study, but had died at 1 and 1.5 hours following CTB application, were kept for analysis of CTB anterograde AT at earlier time points. A qualitative analysis of RGC anterograde AT labelling in the retina, ONH, and ON was conducted at all time points.

Assessment of Anterograde AT of CTB Following Elevated IOP

To investigate early changes in AT function following elevated IOP, anterograde AT labelling in RGCs was assessed at 3, 6, and 24 hours following elevated IOP. IOP in the experimental eye was raised to 120 mmHg for either 30 or 90 minutes duration (for detailed procedure, see section 2.4) immediately following intravitreal injections of CTB in both eyes. There were 6 experimental groups, named according to the duration of elevated IOP and the recovery time point – e.g. a rat exposed to 30 minutes of elevated IOP and sacrificed at 3 hours post-insult was in the "30min/3h" group. Rats were sacrificed at 3, 6, and 24 hours following cessation of IOP elevation and tissues were harvested for histological processing and imaging. ONHs and ONs were longitudinally sectioned and imaged, and whole-mounted retinas were labeled with Brn3a and pNF antibodies and imaged according to the procedures described in section 2.8 and 2.9.

Measurement of RGC Survival

RGC survival was assessed at 3, 6, and 24 hours following elevated IOP by quantification of Brn3a+ cells in the GCL at 1, 2, and 3 mm of eccentricity from the ONH in all four retinal quadrants. Refer to sections 2.8 and 2.10.1 for detailed procedures.

Sham Controls

Two rats underwent a sham procedure for IOP elevation to isolate any effects that cannulation of the anterior chamber may have had on AT or RGC survival. Briefly, rats that underwent the sham procedure received identical bilateral intravitreal injections of CTB to those animals in the experimental condition. However, following anterior chamber cannulation with the needle attached to the pressure column, IOP was not elevated. The needle was kept in place for 90 minutes duration and then removed, and rats were sacrificed after a period of 24 hours. Retinal, ON, and ONH tissue was processed for examination of CTB anterograde AT and Brn3a+ cell quantification in a manner identical to that described for experimental rats.

Statistics

Evaluation of RGC survival by quantification of Brn3a+ cells in the GCL was analyzed with paired and independent sample t-tests. The effects of elevated IOP and recovery time on CTB intensity in ONHs were analyzed with ANOVA with post-hoc tests, and t-tests. The effects of elevated IOP and recovery time on CTB intensity in the ON were analyzed with mixed effects analysis.

Sample Sizes

Fifty-four rats were used in experiments evaluating anterograde AT following transient elevated IOP (N = 4 for the tracer characterization study, N = 50 for the elevated IOP study). In the elevated IOP study, 8 rats were examined at each of 3 time points - 3, 6, and 24 hours - following either 30 or 90 minutes of elevated IOP (n = 8/group, total N = 48). Two additional rats, sacrificed at 24 hours of recovery, were used in sham experiments (N = 2). Quantification of anterogradely transported CTB in the ONH and ON was completed in all rats (N = 50). Quantification of RGC survival using the Brn3a antibody was completed in the majority of rats used in elevated IOP experiments, with some exclusions due to poor IHC or tissue quality. The sample sizes (n) for Brn3a quantification in each experimental group are as follows: 30min/3h = 4; 30min/6h = 6; 30min/24h = 4; 90min/3h = 4; 90min/6h = 6; 90min/6h = 4 (total N = 28).

5.3 Results

5.3.1 Time Course of Anterograde CTB AT

AT of CTB was examined at 3 and 6 hours, and 3 and 7 days following intravitreal injection. At 3 hours following CTB injection, uptake of CTB by cells in the GCL was primarily isolated to one retinal quadrant, while CTB had spread to all quadrants by 6 hours (Figure 5.1 A). Distribution of CTB across the retina appeared uniform at 3 and 7 days following injection (Figure 5.1 B). Brightly labeled CTB+ axons could be seen in the proximal ON only 3 hours following CTB injection, and faint labelling was observed at the chiasm (Figure 5.1 C). At 6 hours, labelling was bright and

Figure 5.1 Time Course of CTB Anterograde AT. A) An intensity map of CTB diffusion across the retina from the injection site at 3 and 6 hours following intravitreal injection. At 3 hours, CTB was primarily isolated to the same quadrant as the site of injection (*), with faint labelling in adjacent quadrants. At 6 hours, CTB labelling was observed in all quadrants. **B)** CTB labelling in retinal whole-mounts at 3 and 7 days following intravitreal injection. Labelling persisted in all quadrants at both time points. Scale 100 μm. **C)** Anterograde CTB in the ON at 3 and 6 hours, and 3 and 7 days following intravitreal injection. At 3 hours, CTB extended beyond the halfway point between the eye and the chiasm (dye front indicated by the arrow), with very little CTB visible at the chiasm. CTB+ fibres in the chiasm were seen at the 6-hour time point, and increased in intensity at the 3-day time point. CTB intensity in the chiasm remained high at the 7-day time point. **D)** Anterograde CTB in the ONH. CTB labelling of RGC axon fibre bundles in the ONH was incomplete at the 3-hour time point. CTB labelling of axon bundles was bright and uniform at 6 hours, and persisted at the 3 and 7-day time points. Asterisk in **D** (*) denotes level of sclera.

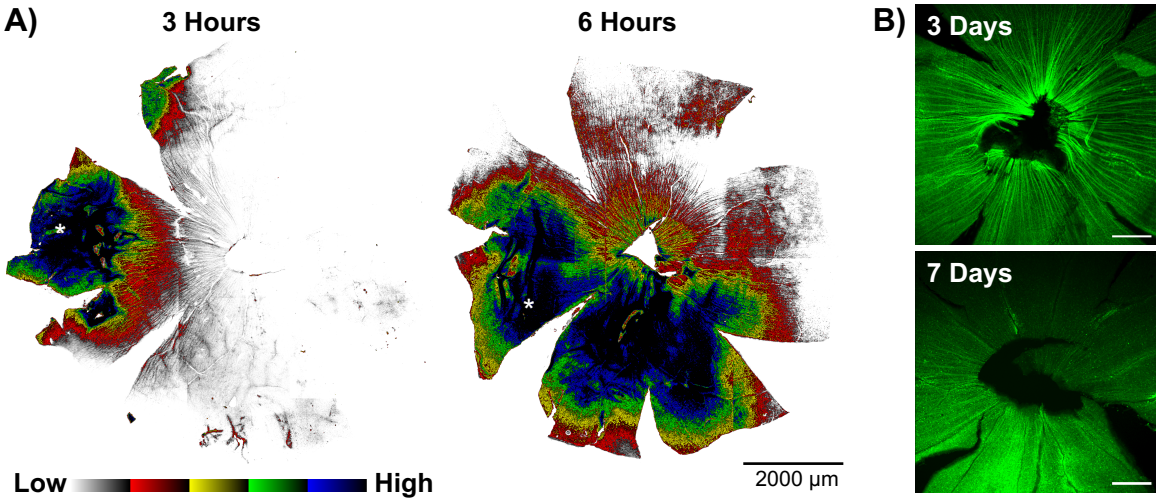
A)
3 Hours
6 Hours
B)
3 Days
7 Days
Low
High
2000 µm

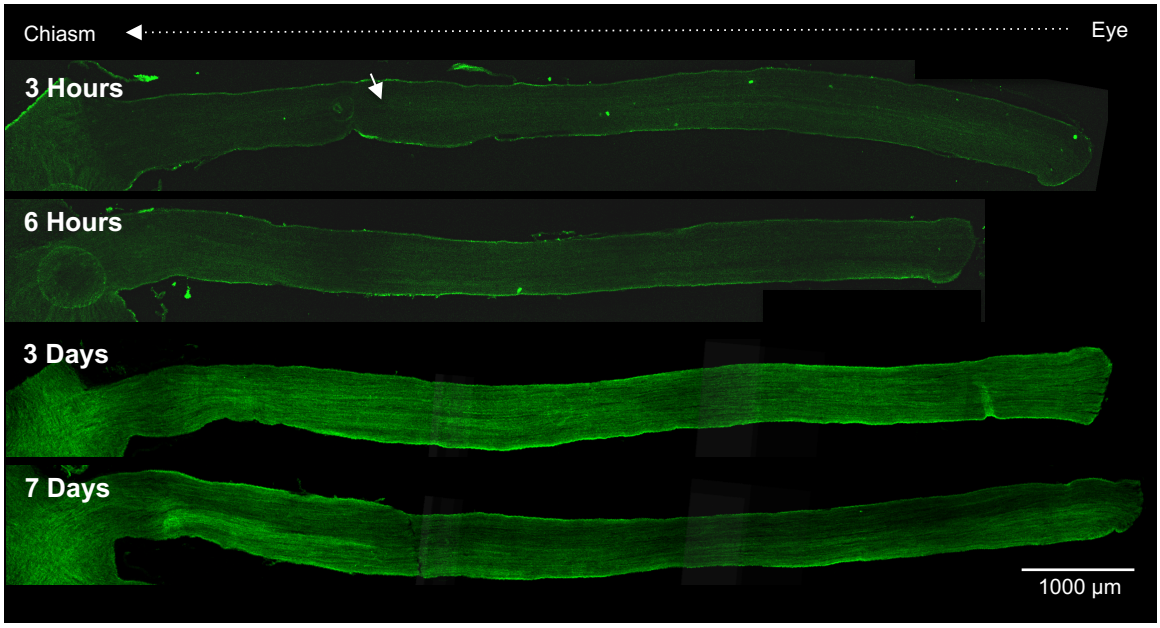
C)
Chiasm
Eye
3 Hours
6 Hours
3 Days
7 Days
1000 µm

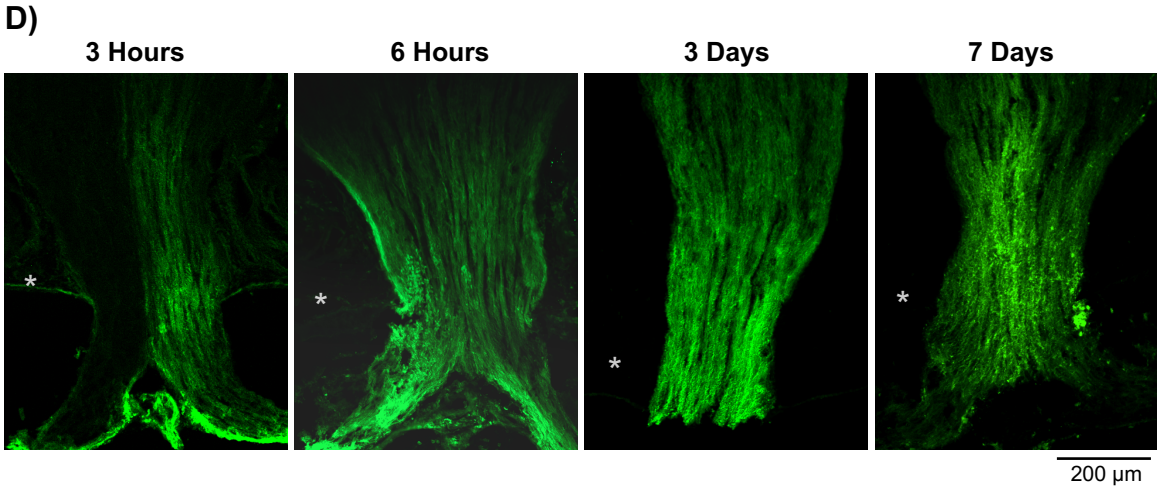
D)
3 Hours
6 Hours
3 Days
7 Days
200 µm

uniform from the proximal ON to the chiasm, with labelling intensity peaking at 3 days and remaining high at 7 days (Figure 5.1 C). Anterograde AT of CTB in the ONH demonstrated a similar pattern, with CTB fluorescence becoming uniform across the width of the ONH by 6 hours, peaking in intensity at 3 days (Figure 5.1 D), and remaining high at 7 days.

5.3.2 Estimation of the Rate of Anterograde CTB AT

A noticeable dye front was visible in the ON at the 3-hour time point (Figure 5.1 C, arrow), however, faint axon fibre profiles were visible as far as the chiasm. The distance from the inner limiting membrane of the retina to the dye front in this animal was approximately 8 mm, while the distance to the chiasm was approximately 11 mm. From these measurements, the rate of CTB anterograde transport was estimated to be between 64-88 mm/day; however, given that tissue beyond the chiasm was not examined, it is possible that this is an underestimate.

5.3.3 Quantification of Brn3a+ Cells in the GCL at 3, 6, and 24 Hours Following Elevated IOP

Thirty minutes of elevated IOP had no significant effect on the number of Brn3a+ cells in the GCL at any of the time points examined (Table 5.1; Figure 5.2 A). In 30min/3h rats, the average densities of Brn3a+ cells measured at eccentricities of 1, 2, and 3 mm from the ONH were 571 ± 34.75, 507 ± 50.65, and 391.32 ± 46.53 cells/500

Table 5.1 Average ON Fluorescence and RGC Density at 3, 6, and 24 Hours Following Elevated IOP

		Average Brn3a+ Cells/ 500 µm^2 at 1, 2, and 3 mm of Eccentricity						Average ON Fluorescence		
	Recovery	1 mm		2 mm		3 mm		Control	Elevated IOP	Difference
		Control	Elevated IOP	Control	Elevated IOP	Control	Elevated IOP			
30 Minutes Elevated IOP	3 Hours	562.13 ± 48.50	565.81 ± 38.70	498.00 ± 29.04	499.06 ± 78.39	373.38 ± 39.94	402.00 ± 78.46	42.28 ± 7.94	41.24 ± 8.59	-1.04 ± 5.85
	6 Hours	571.71 ± 53.64	569.63 ± 48.85	493.50 ± 49.83	501.81 ± 22.50	377.85 ± 72.78	406.44 ± 19.67	61.79 ± 7.53	60.62 ± 12.31	-1.17 ± 7.38
	24 Hours	579.00 ± 22.00	587.33 ± 61.33	475.13 ± 63.25	487.13 ± 35.75	386.88 ± 52.25	397.63 ± 162.75	72.20 ± 8.55	74.21 ± 11.43	-2.01 ± 9.41
90 Minutes Elevated IOP	Recovery	1 mm		2 mm		3 mm		Control	Elevated IOP	Difference
		Control	Elevated IOP	Control	Elevated IOP	Control	Elevated IOP			
	3 Hours	640.67 ± 64.54	281.03 ± 37.82	476.11 ± 29.07	249.25 ± 46.92	420.03 ± 54.09	260.56 ± 95.17	64.59 ± 23.28	36.50 ± 9.41	-28.09 ± 15.60
	6 Hours	569.03 ± 52.44	342.54 ± 65.18	478.24 ± 39.17	275.75 ± 71.15	338.78 ± 28.42	215.67 ± 80.31	71.72 ± 9.89	40.44 ± 6.24	-31.28 ± 8.49
	24 Hours	608.92 ± 86.51	465.44 ± 134.41	494.58 ± 88.52	397.17 ± 74.67	334.67 ± 62.59	280.03 ± 72.04	85.96 ± 19.37	43.59 ± 9.27	-42.37 ± 13.50

Fluorescence data expressed in AU, all data presented as mean ± 2SEM.

Figure 5.2 Brn3a+ Cell Density at 1, 2, and 3 mm of Retinal Eccentricity Following 30 or 90 Minutes of Elevated IOP. A) Quantification of Brn3a+ cells in control and experimental retinal whole-mounts following 30 minutes of elevated IOP. The density of Brn3a+ cells declined with retinal eccentricity similarly in both control and experimental eyes at all time points examined. **B)** Quantification of Brn3a+ cells in control and experimental retinal whole-mounts following 90 minutes of elevated IOP. Brn3a+ cell density was significantly decreased at all retinal eccentricities at 3, 6, and 24 hours following 90 minutes of elevated IOP. * = $p < 0.05$, ** = $p < 0.01$, *** = $p < 0.001$

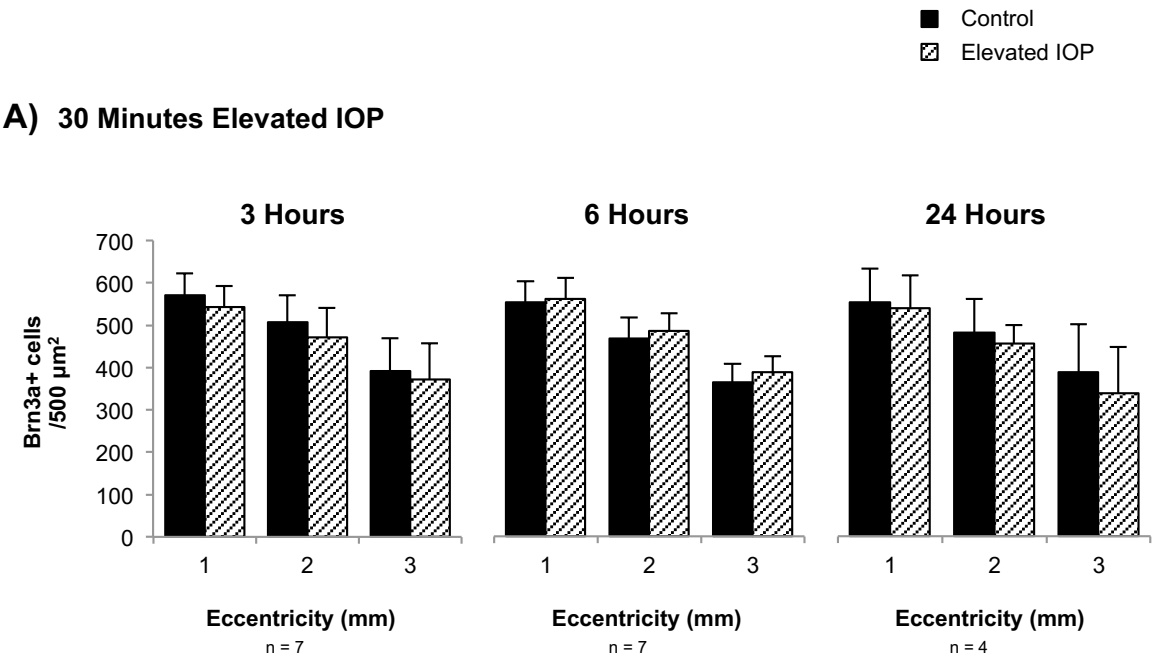
Control
Elevated IOP
A) 30 Minutes Elevated IOP
3 Hours
6 Hours
24 Hours
Brn3a+ cells /500 µm²
700
600
500
400
300
200
100
0
1
2
3
Eccentricity (mm)
n = 7
n = 7
n = 4

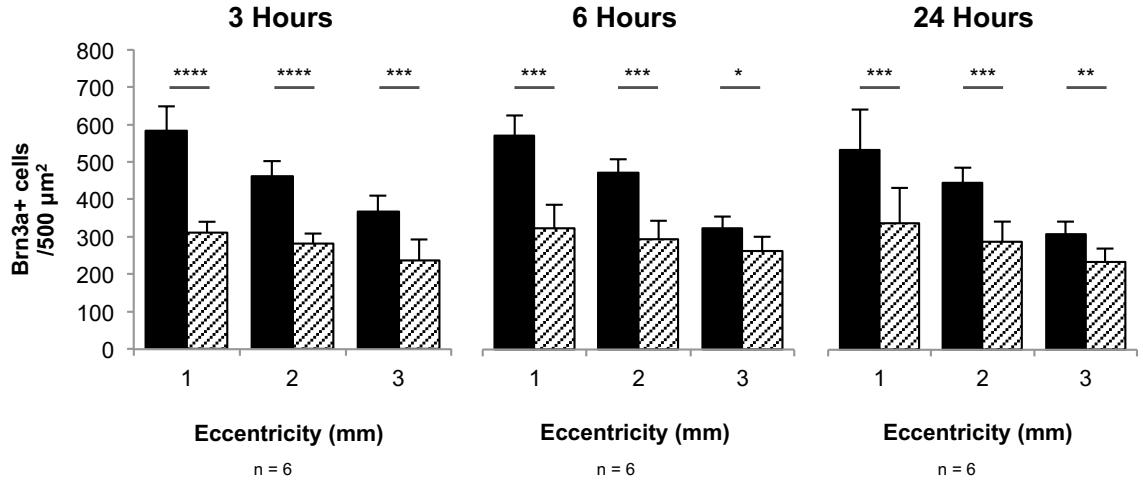
B) 90 Minutes Elevated IOP
3 Hours
6 Hours
24 Hours
Brn3a+ cells /500 µm²
800
700
600
500
400
300
200
100
0
****
****
***
***
***
*
***
***
**
1
2
3
Eccentricity (mm)
n = 6
n = 6
n = 6

μm^2, respectively. These averages did not change significantly with experimental group or recovery time ($p > 0.3$).

Ninety minutes of elevated IOP significantly decreased the density of Brn3a+ cells in the GCL at all time points following insult (Table 5.1; Figure 5.2 B). Brn3a+ cell density at eccentricities of 1, 2, and 3 mm were decreased relative to control densities by 46% ($p < 0.001$), 40% ($p < 0.001$) and 35% ($p < 0.01$) in the 90min/3h group; 43% ($p < 0.001$), 38% ($p < 0.001$), and 22% ($p < 0.05$) in the 90min/6h group; and 34% ($p < 0.01$), 31% ($p < 0.01$), and 25% ($p = 0.01$) in the 90min/24h group.

5.3.4 Anterograde AT of CTB in the ONH Following Elevated IOP

Thirty minutes of elevated IOP had no significant effect on the anterograde AT of CTB at any of the ONH regions or time points examined (Figures 5.3 A, 5.4). No significant effect of the 30-minute insult was found ($p = 0.06$, ANOVA), and there was no interaction between elevated IOP and recovery time ($p = 0.79$, ANOVA). However, there was an overall effect of recovery time on anterograde AT ($p < 0.01$, ANOVA). Indeed, the topographical distribution of CTB labelling in the ONH, regardless of experimental treatment, changed over time in a predictable trend (Figure 5.4 A, B, and C), demonstrating a gradual increase in CTB transport over time. For example, while CTB intensity in the 30min/3h group dropped steeply from the pre-LC region to LC1 and LC2 regions, approaching 0 AU in the post-200 and -300 ONH regions (Figure 5.4 A), the drop in CTB intensity from Pre-LC to post-200 regions in the 30min/6h group was more gradual (Figure 5.4 B), and even more so in the 30min/24h group (Figure 5.4 C). Post-hoc analysis confirmed these results, finding a significant difference in CTB

Figure 5.3 AT of CTB in the ONH at 3, 6, and 24 Hours Following Either 30 or 90 Minutes of Elevated IOP. A) CTB fluorescence in the ONH at 3, 6, and 24 hours following 30 minutes of elevated IOP. There was no meaningful delay of CTB AT through the ONH at any of the recovery times examined. **B)** CTB fluorescence in the ONH at 3, 6, and 24 hours following 90 minutes of elevated IOP. CTB AT was slowed through the ONH beginning at the 3-hour time point, and progressed at the 6- and 24-hour time points. Arrows indicate the advancement of CTB through the ONH.

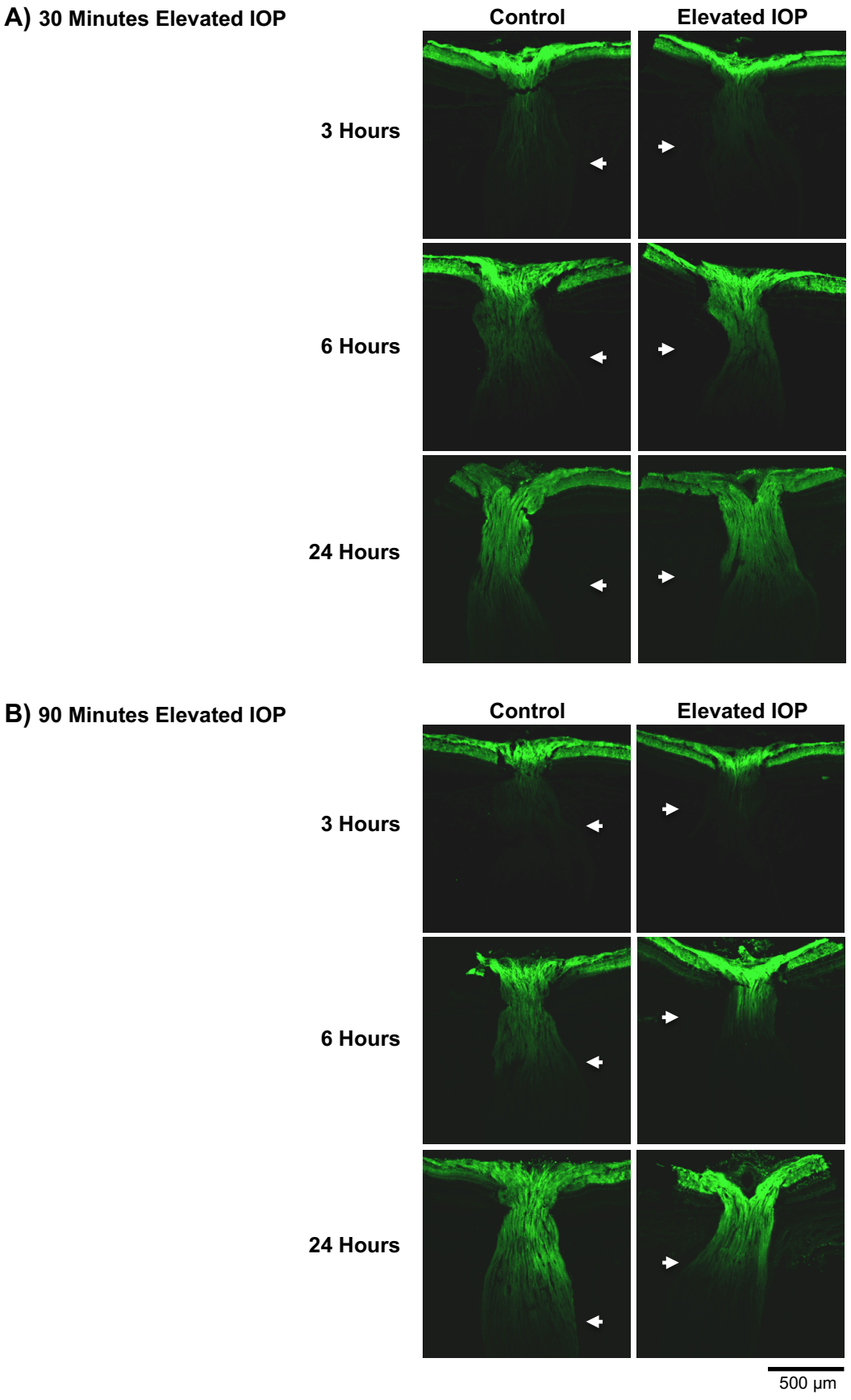
A) 30 Minutes Elevated IOP
Control
Elevated IOP
3 Hours
6 Hours
24 Hours
B) 90 Minutes Elevated IOP
Control
Elevated IOP
3 Hours
6 Hours
24 Hours
500 µm

Figure 5.4 Quantification of CTB AT in the ONH at 3, 6, and 24 Hours Following 30 Minutes of Elevated IOP. A) CTB intensity in the ONH at 3 hours of recovery. CTB intensity was higher in the pre-LC region, dropping significantly by the LC1 region and continuing to decline thereafter. CTB intensity in the experimental eye was not significantly different from that of the control eye. **B)** CTB intensity in the ONH at 6 hours of recovery. Both control and experimental eyes exhibited noticeably increased intensity through the LC1-post 300 regions compared to the same regions at the 3-hour time point. CTB intensity in the experimental eye was not significantly different from that of the control eye. **C)** CTB intensity in the ONH at 24 hours of recovery. CTB intensity approximated a linear decline from the pre-LC to post-600 regions in both control and experimental eyes. CTB intensity in the experimental eye was not significantly different from that of the control eye.

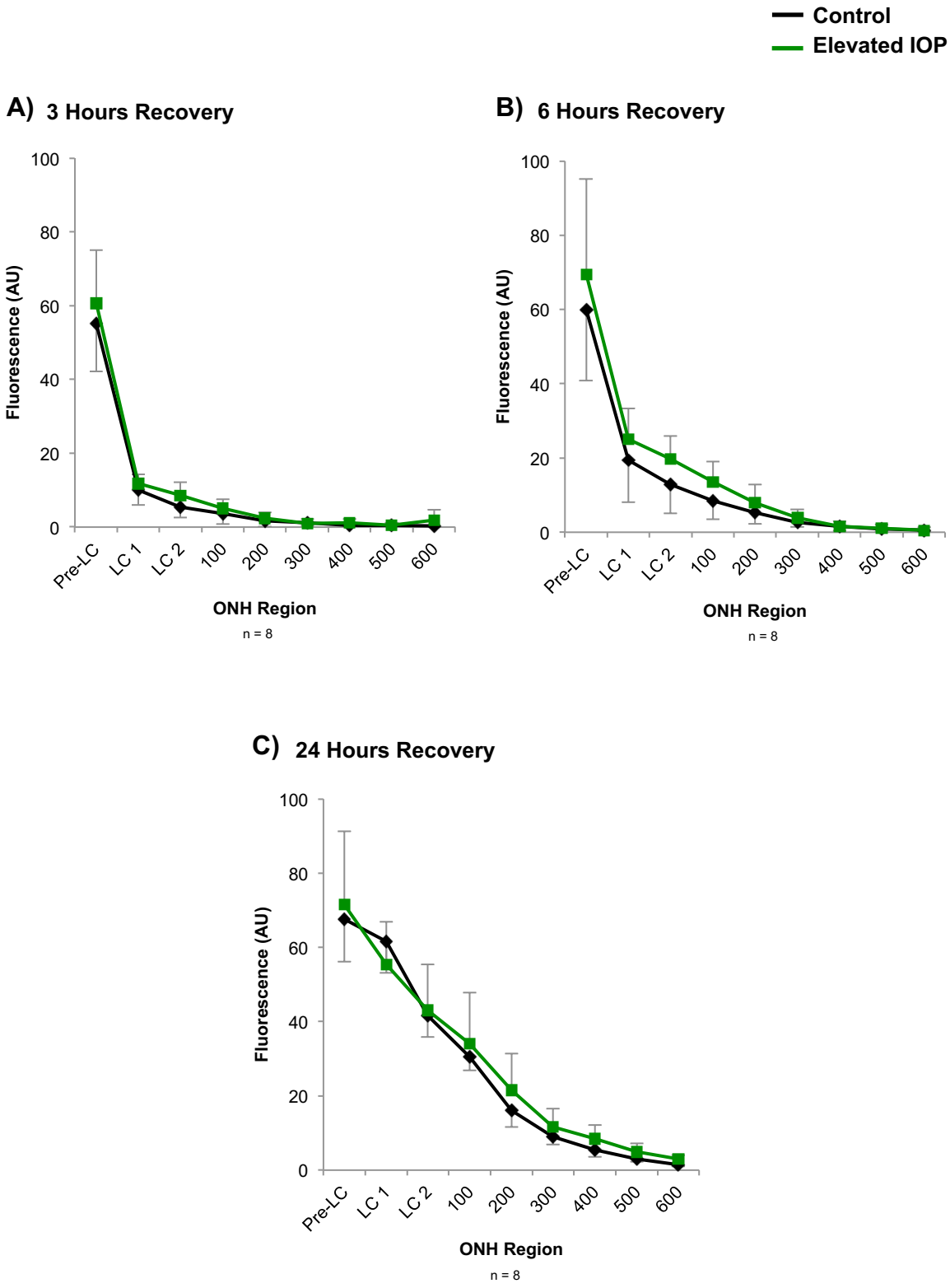
Control
Elevated IOP
A) 3 Hours Recovery
B) 6 Hours Recovery
C) 24 Hours Recovery
Fluorescence (AU)
100
80
60
40
20
0
Pre-LC
LC 1
LC 2
100
200
300
400
500
600
ONH Region
n = 8

Figure 5.5 Quantification of CTB AT in the ONH at 3, 6, and 24 Hours Following 90 Minutes of Elevated IOP. A) CTB intensity in the ONH at 3 hours of recovery. CTB intensity was high in the pre-LC region, but dropped significantly by the LC1 region and continuing to decline thereafter. Intensity in the experimental eye following 3 hours of recovery was significantly decreased in the post-100, 200, and 300 regions compared to control. **B)** CTB intensity in the ONH at 6 hours of recovery. A significant increase in CTB intensity in the pre-LC region of experimental ONHs was observed, suggesting a buildup of CTB as it enters the ONH. CTB intensity continued to be elevated in the first 100 μm of the LC region, but dropped below control levels in subsequent regions. **C)** CTB intensity in the ONH at 24 hours of recovery. CTB intensity approximated a linear decline from the pre-LC to post-600 regions in both control and experimental eyes. CTB intensity in the experimental eyes was greatly reduced in the majority of ONH regions (LC1-Post-400). * = $p < 0.05$, ** = $p < 0.01$

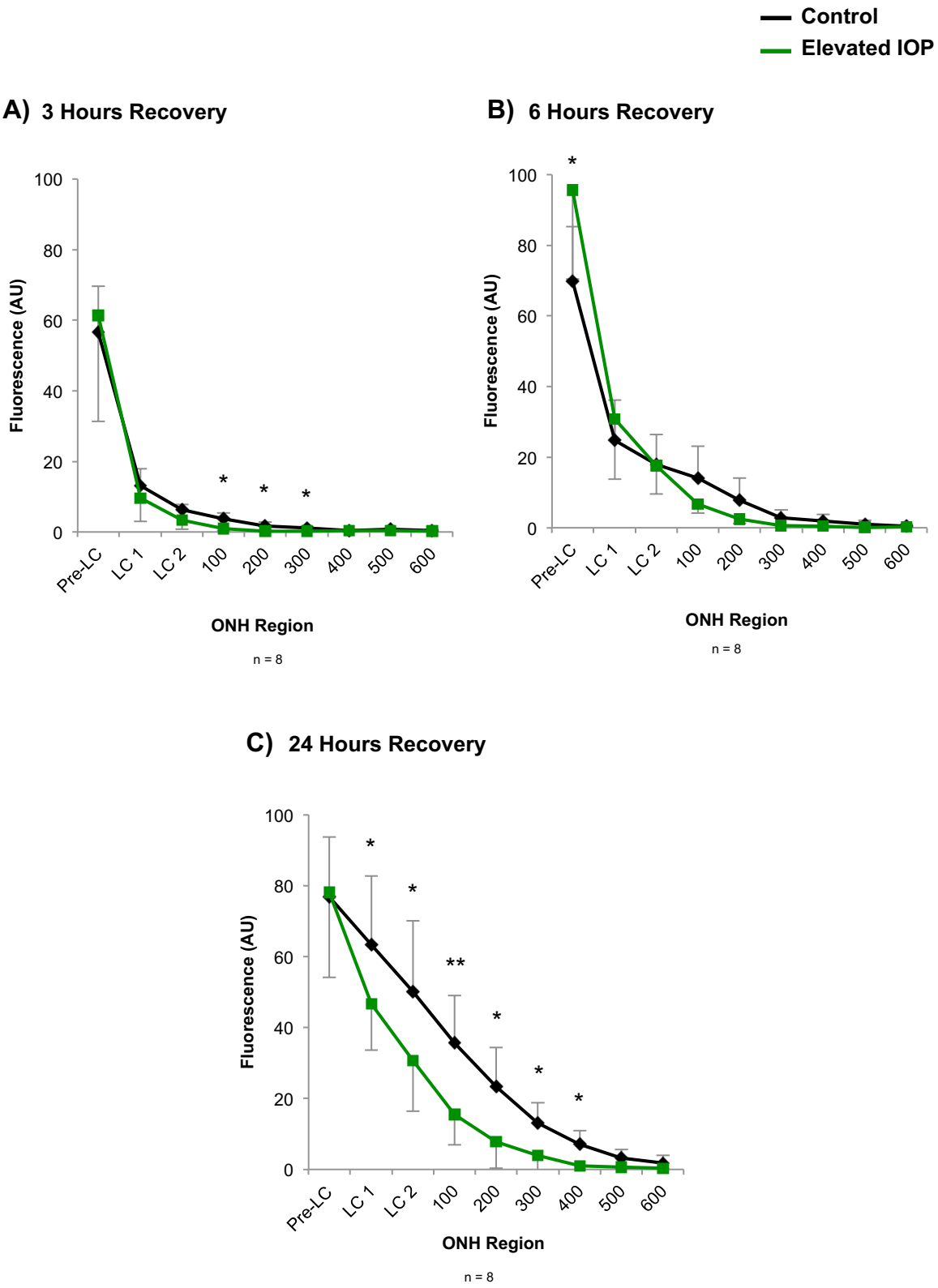
Control
Elevated IOP
A) 3 Hours Recovery
B) 6 Hours Recovery
C) 24 Hours Recovery
Fluorescence (AU)
ONH Region
Pre-LC
LC 1
LC 2
100
200
300
400
500
600
n = 8

intensity between 30min/3h and 30min/24h groups ($p < 0.01$), and 30min/6h and 30min/24h groups ($p < 0.01$).

Ninety minutes of elevated IOP significantly inhibited anterograde AT of CTB through the ONH at all time points examined (Figure 5.3 B, 5.5). There was a significant overall effect of the 90-minute insult on CTB intensity in the ONH ($p < 0.01$, ANOVA). In the 90min/3h group, CTB intensity in experimental ONHs was significantly decreased in the post-100, -200, and -300 regions (all $p < 0.05$; Figure 5.5 A). In the 90min/6h group, elevated IOP resulted in a significant increase in CTB intensity in the pre-LC region compared to control levels ($p < 0.05$) that was accompanied by a decrease in CTB labelling in post-100 to -300 regions (ns; Figure 5.5 B). However, the greatest effect on CTB AT in the ONH was visible in the 90min/24h group, where CTB intensity from the LC1 to post-400 regions of experimental ONHs was significantly reduced with respect to control levels (all $p < 0.05$; Figure 5.5 C). Similar to the results of the 30-minute group results, CTB intensity in general, regardless of experimental treatment, changed significantly across ONH regions ($p < 0.01$, ANOVA), dropping in intensity from pre-LC to post-600 regions, and this distribution of CTB intensity through the ONH changed significantly over time ($p < 0.01$).

5.3.5 Anterograde AT of CTB in the ON Following Elevated IOP

Thirty minutes of elevated IOP had no significant effect on CTB intensity throughout the ON, from the post-laminar region to the chiasm, at all time points examined (Table 5.1; Figure 5.6, 5.8 A and C, and 5.9 A). There was no visible difference between the level of CTB intensity in experimental ONs and that of control

ONs at any time point examined (Figure 5.6). Although CTB intensity in experimental ONs was reduced compared to control at all points along nerve length (Figure 5.8 A), the average intensity of experimental ONs was not significantly different from that of control ONs. These findings were true across all time points examined. However, similar to the ONH results, CTB intensity in the ON in general, regardless of experimental treatment, showed an overall increase over time, with average intensity values from 30min/6h and 30min/24h groups both being significantly different from the average CTB intensity measured from the 30min/3h group ($p < 0.01$ and 0.001, respectively). Examining individual pairs of ONs separately further demonstrates the overall increase in intensity across time points (Figure 5.9 A, top panel), and the lack of a reproducible effect of 30 minutes of elevated IOP on CTB intensity in the ON (Figure 5.9 A, bottom panel).

Ninety minutes of elevated IOP significantly decreased the amount of CTB transported into the ON at all time points examined (Table 5.2; Figure 5.7, 5.8 B and C, and 5.9 B). In all pairs of ONs examined, CTB intensity in experimental ONs was visibly decreased with respect to control levels (Figure 5.7). Quantification demonstrated a decrease in CTB intensity that was consistent at all points of the ON from the post-laminar region to the chiasm (Figure 5.8 B and C). Indeed, the overall effect of 90 minutes of elevated IOP on CTB intensity in the ON was significant ($p < 0.001$), and there was no significant effect of location along the length of the ON, indicating that the decrease in CTB intensity was neither greater nearer the eye, nor towards the chiasm. Although there was no significant interaction between elevated IOP and recovery time, the difference between experimental and control intensity levels increased over time,

Figure 5.6 AT of CTB in Longitudinal Sections of ONs at 3, 6, and 24 Hours Following 30 Minutes of Elevated IOP. At 3 hours of recovery, CTB fluorescence was faintly visible across the entire length of the ON, including in the chiasm, and increased in intensity at 6 and 24 hours following elevated IOP. There was no perceptible difference in CTB AT between control and experimental nerves at any time point following insult.

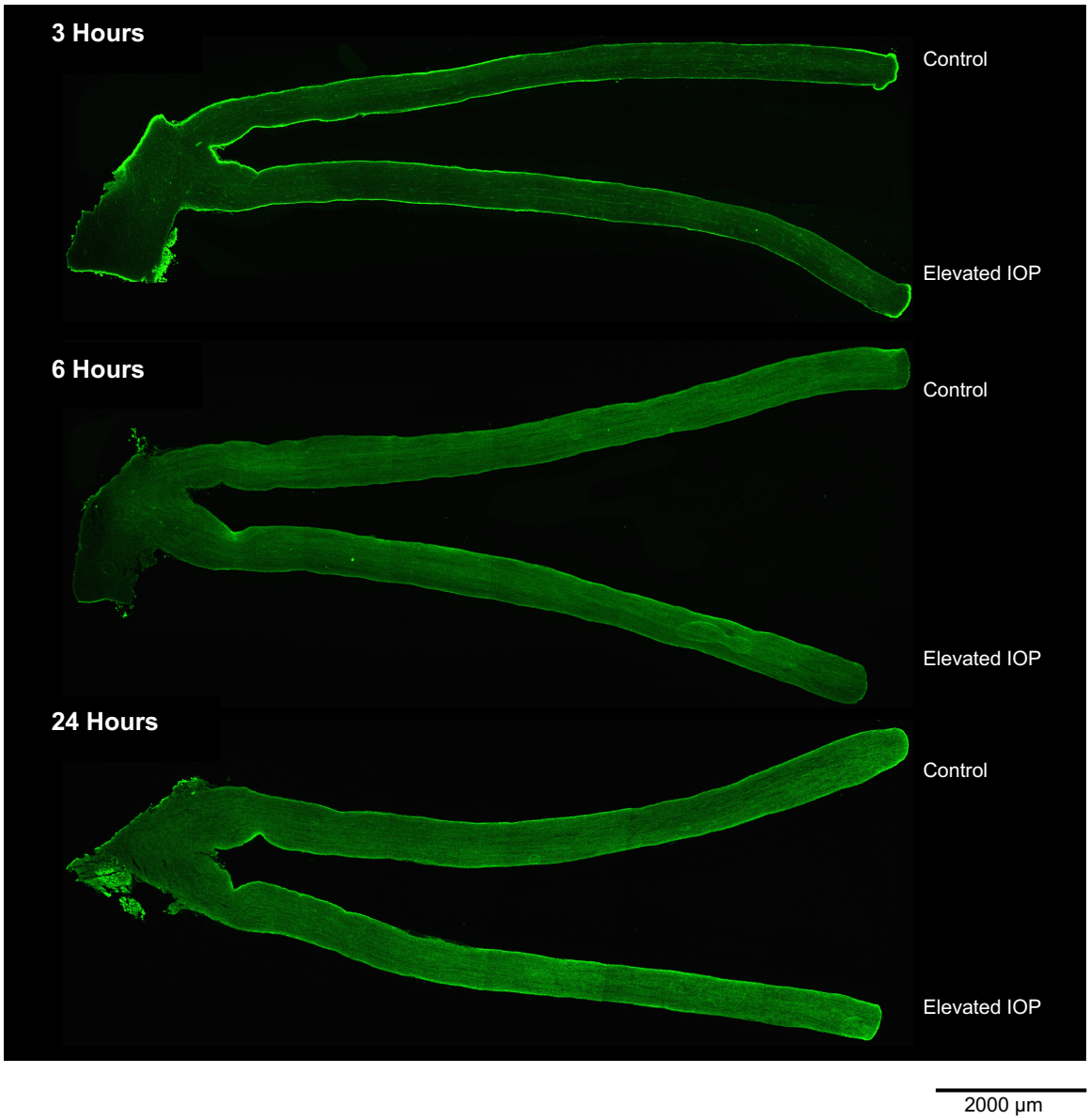
3 Hours
Control
Elevated IOP
6 Hours
Control
Elevated IOP
24 Hours
Control
Elevated IOP
2000 µm

Figure 5.7 AT of CTB in the ON at 3, 6, and 24 Hours Following 90 Minutes of Elevated IOP. CTB fluorescence was noticeably decreased in intensity in the experimental nerve at the 3-hour time point, and continued to be markedly lower than the control nerve at 6 and 24 hours following elevated IOP.

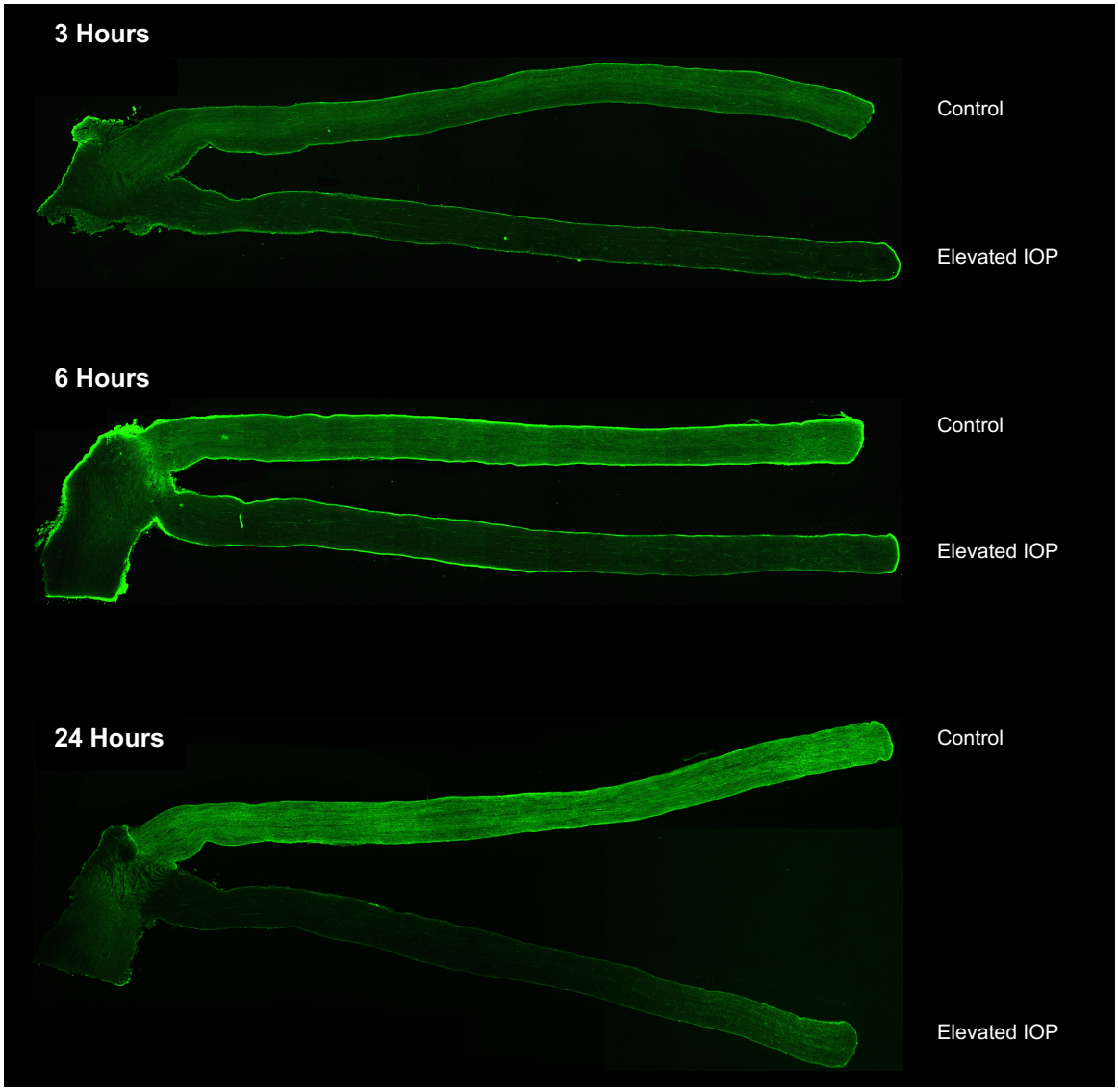
3 Hours
Control
Elevated IOP
6 Hours
Control
Elevated IOP
24 Hours
Control
Elevated IOP
2000 µm

Figure 5.8 Quantification of CTB AT in the ON at 3, 6, and 24 Hours Following Either 30 or 90 Minutes of Elevated IOP. A) CTB intensity throughout the control and experimental ONs following 30 minutes of elevated IOP. Intensity was decreased in the experimental nerve compared to control nerve at all time points following elevated IOP along the entire length of the ON. There was no recovery of CTB AT over time. ON segments closest to the eye demonstrated a progressive worsening of CTB AT dysfunction. **B)** CTB intensity was markedly decreased in the experimental nerve compared to the control nerve at all time points following 90 minutes of elevated IOP. This disruption worsened over time, most noticeably in the proximal ON. **C)** Ninety minutes of elevated IOP produced a greater decline in average CTB intensity compared to 30 minutes of elevated IOP at all time points. ** = $p < 0.01$, *** = $p < 0.001$, **** = $p < 0.0001$

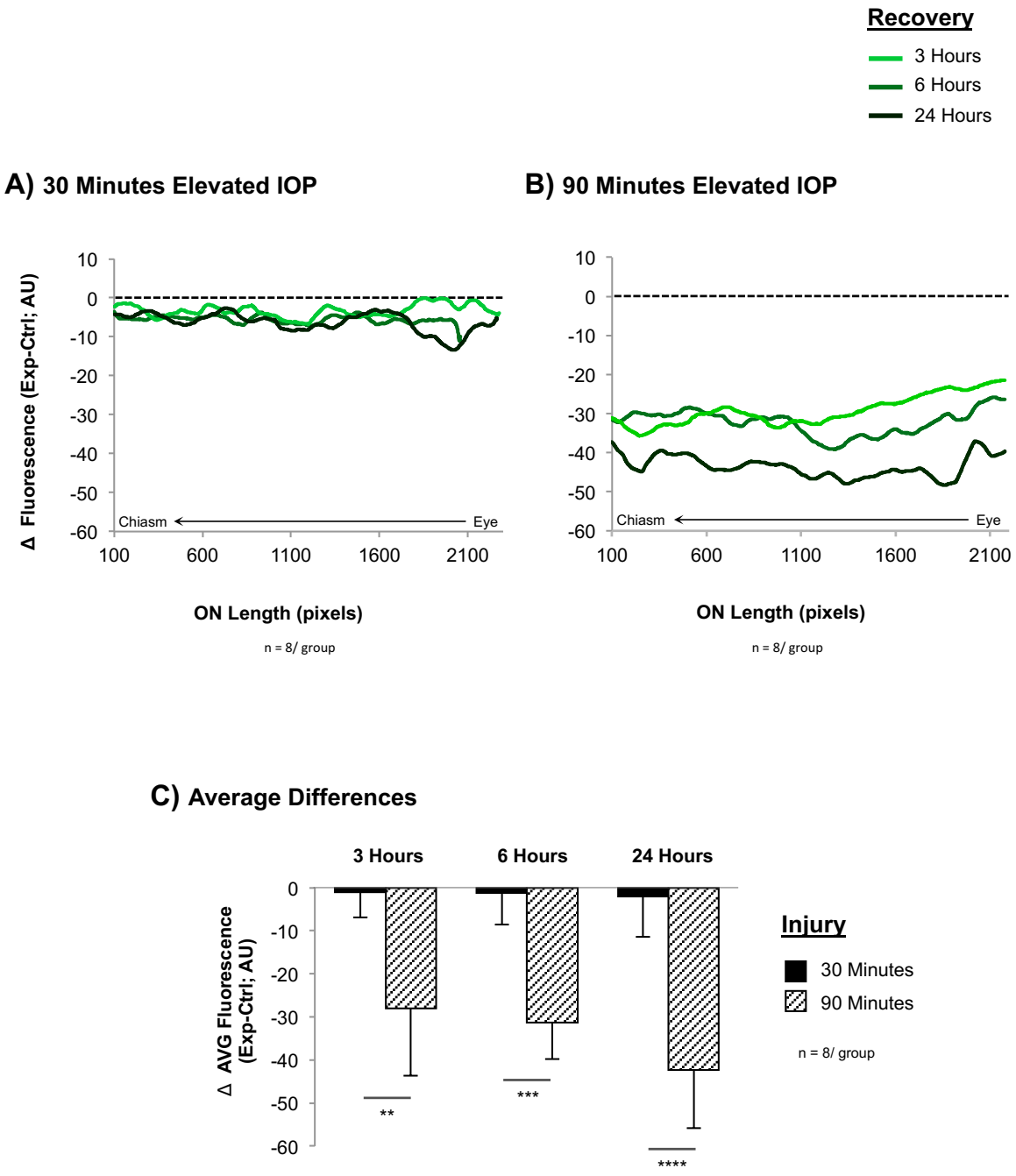
Recovery
3 Hours
6 Hours
24 Hours
A) 30 Minutes Elevated IOP
B) 90 Minutes Elevated IOP
Δ Fluorescence (Exp-Ctrl; AU)
10
0
-10
-20
-30
-40
-50
-60
Chiasm
Eye
100
600
1100
1600
2100
ON Length (pixels)
n = 8/ group
C) Average Differences
3 Hours
6 Hours
24 Hours
Δ AVG Fluorescence (Exp-Ctrl; AU)
**
***
****
Injury
30 Minutes
90 Minutes
n = 8/ group

Figure 5.9 Individual Paired Measurements of Average CTB Intensity in the ON at 3, 6, and 24 Hour Following 30 or 90 Minutes of Elevated IOP. A) Average ON intensity values following 30 minutes of elevated IOP. **B)** Average ON intensity values following 90 minutes of elevated IOP. Top panels: paired measurements of average ON intensity. Each line represents the relationship between control and experimental intensity values in an individual rat. Bottom panels: the same relationships presented as a proportion of their control value.

A) 30 Minutes Elevated IOP

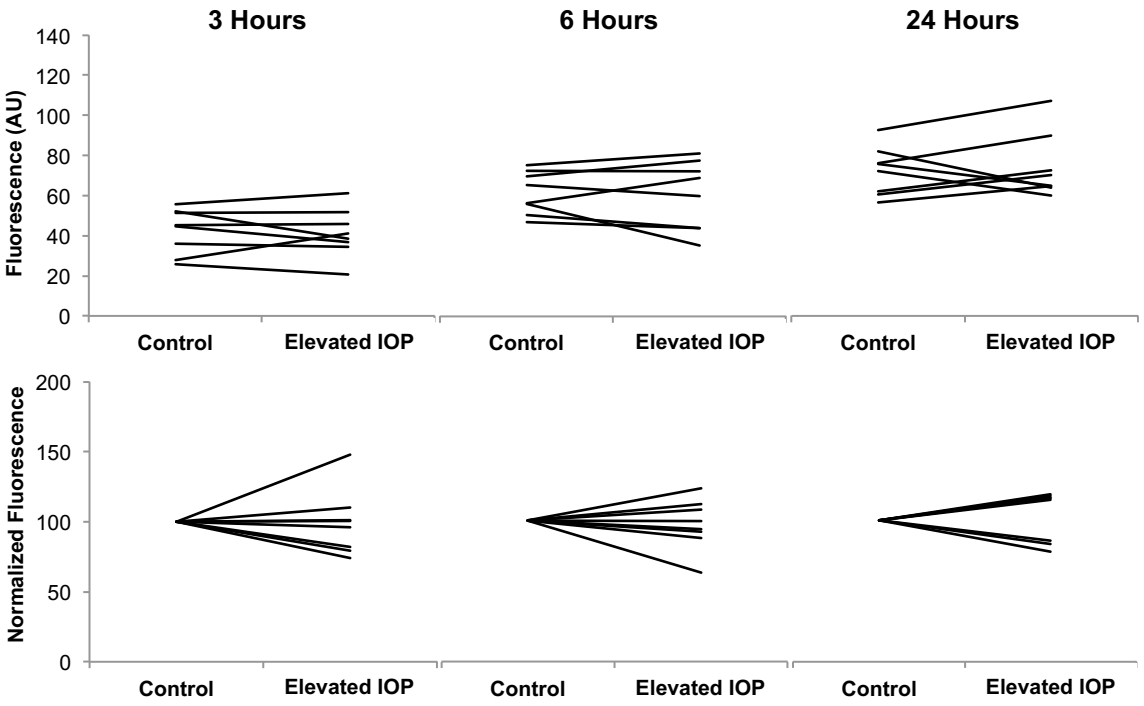

B) 90 Minutes Elevated IOP

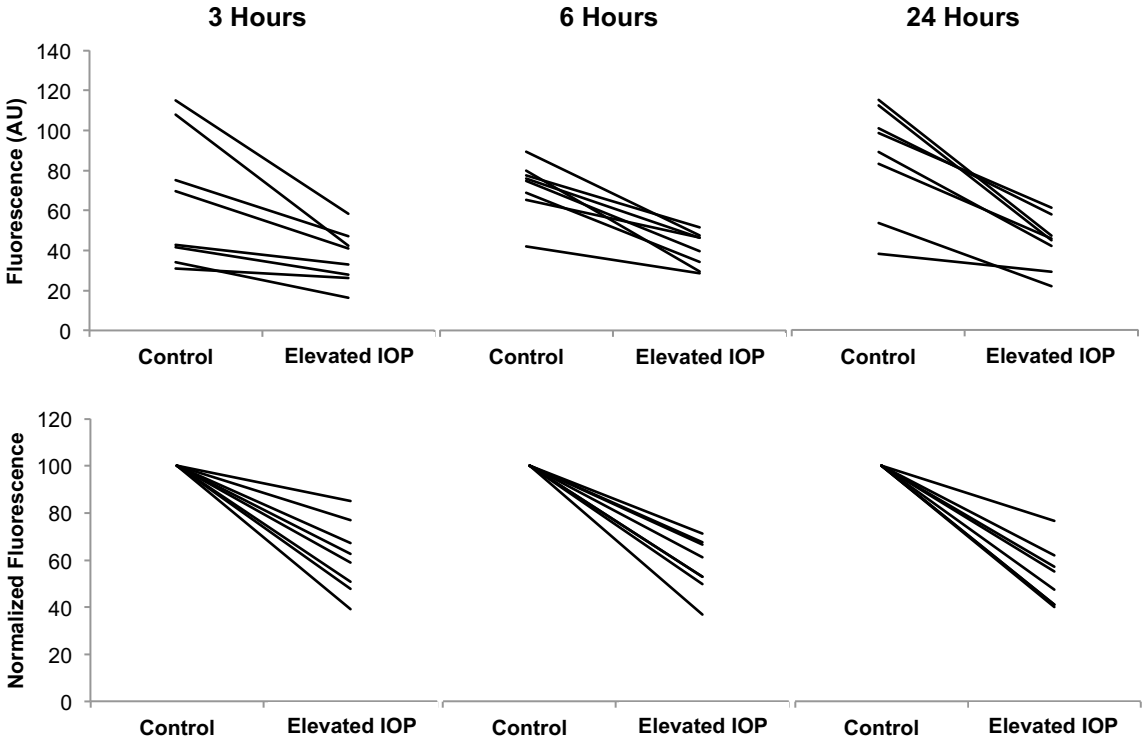

from a difference of -28.09 ± 15.60 AU in the 90min/3h group, to a difference of -42.37 ± 13.50 AU in the 90min/24h group (Table 5.2; Figure 5.8 B and C). Figure 5.9 B, which compares average ON CTB intensities between individual pairs of ONs (top panel) and their proportional change in intensity to control levels (bottom panel), further demonstrates that, contrary to 30 minutes of elevated IOP, 90 minutes of elevated IOP caused a reproducible effect on CTB intensity in the ON.

5.3.6 Anterograde AT of CTB in the ON Following Sham Elevated IOP

The sham procedure did not cause a significant effect on CTB intensity in either proximal or distal regions of the ON at 24 hours of recovery (Figure 5.10 A, B, and C), whereas CTB intensity in experimental ONs following 90 minutes of elevated IOP was significantly lower than both paired control and sham values ($p < 0.01$; Figure 5.10 B and C).

Figure 5.10 CTB Labelling Intensity in the ONH and the Proximal and Distal ON at 24 Hours Following Sham Elevated IOP. **A)** Sampling of CTB fluorescence in proximal and distal segments of control and experimental nerves. **B)** Cannulation of the anterior chamber without elevation of IOP (sham procedure) did not have any effect of CTB fluorescence in the proximal or distal ON, whereas 90 minutes of elevated IOP caused a marked decrease in intensity in the experimental nerve. **C)** Comparison of average fluorescence intensity between proximal and distal segments of sham and elevated IOP nerves (** = $p < 0.01$). **D)** CTB fluorescence intensity through sequential ONH regions in control and sham eyes. Greyed area indicates the LC region.

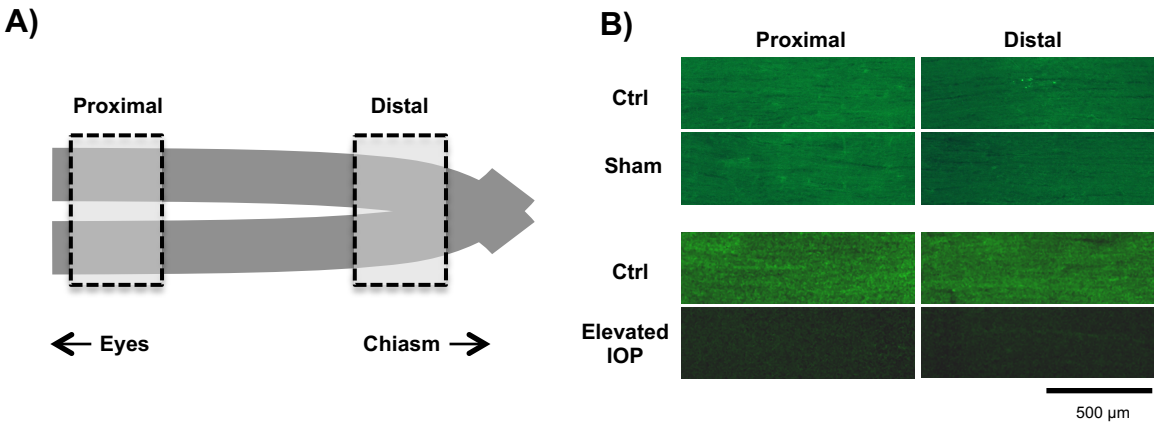
A)
Proximal
Distal
Eyes
Chiasm
B)
Proximal
Distal
Ctrl
Sham
Ctrl
Elevated IOP
500 µm

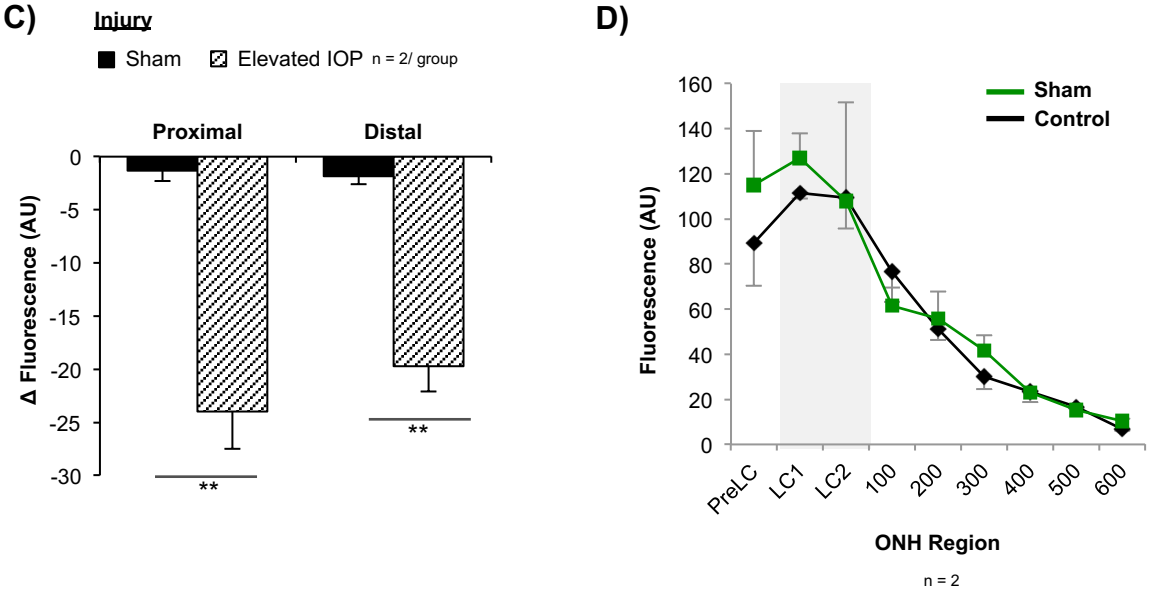
C)
Injury
Sham
Elevated IOP
n = 2/ group
Proximal
Distal
Δ Fluorescence (AU)
0
-5
-10
-15
-20
-25
-30
**
**
D)
Sham
Control
Fluorescence (AU)
160
140
120
100
80
60
40
20
0
PreLC
LC1
LC2
100
200
300
400
500
600
ONH Region
n = 2

5.4 Summary and Key Findings

The results of this study demonstrate the usefulness of CTB as a tracer of AT function in RGCs, and also reveal important details regarding the time course of AT impairment in the ONH and ON in the hours immediately following transient elevated IOP.

Key findings include:

1) Fluorescently conjugated CTB is a fast and capable tracer of anterograde AT in RGCs.

2) Thirty minutes of elevated IOP did not significantly affect either RGC survival or anterograde AT function within 24 hours following insult.

3) Ninety minutes of elevated IOP had an immediate and significant effect on RGC survival and anterograde AT function that progressively worsened over time.

4) The primary site of anterograde AT impairment in RGCs following elevated IOP was at, or before, the ONH.

These findings demonstrate that AT function is resilient to mild enough IOP insult; however, once AT is disrupted, it does not exhibit reversibility following a more severe insult. These findings are discussed further in section 8.4, 8.7, and 8.8. Further discussion regarding fluorescently conjugated CTB is included in section 8.2.

CHAPTER 6 – NF REGULATION IN THE RETINA AND ONH FOLLOWING ELEVATED IOP

6.1 Rationale, Objective, and Hypotheses

The experiments described in Chapters 4 (retrograde AT) and 5 (anterograde AT) demonstrate the effects of transient elevated IOP on retrograde and anterograde AT over various recovery times following the insult. Specifically, such experiments established that 90 minutes of elevated IOP results in a progressively worsening disruption of AT over time, accompanied by marked structural degeneration in the retina and ONH at later time points, whereas 30 minutes of elevated IOP has little effect on AT function and axonal structure. Alterations of key axonal cytoskeletal proteins, have been shown to occur within hours of elevating IOP, prior to gross neuronal degeneration [157], and, in addition to changes in AT, may also be an early indicator of RGC damage. While there are studies examining the effects of elevated IOP on cytoskeletal proteins [147, 157, 221, 225, 245, 274, 275, 333], cytoskeletal changes over time following a transient elevation of IOP have yet to be investigated.

The objective of the following experiments and analyses was to examine changes in the expression and phosphorylation of NFs in the retina and ONH following acute elevated IOP. It was hypothesized that 30 minutes of elevated IOP would have no effect on pNF or nonpNF expression in RGCs, whereas 90 minutes of elevated IOP would cause progressively increasing expression of pNF in RGC somas and alterations of the balance of pNF and nonpNF in RGCs within the ONH.

This work was published in abstract form [328, 332].

6.2 Experimental Design

Animals

Tissue for the following experiments was obtained from animals used in the anterograde AT study (Chapter 5).

pNF Expression in the Retina

Somal expression of pNF in RGCs, an indicator of axonal damage, was investigated at various recovery times following elevated IOP by applying pNF and Brn3a antibodies to retinal whole-mounts and then grading sample images (500 x 500 μm) obtained at 1, 2, and 3 mm of eccentricity according to the percent of the image area exhibiting pNF+ somas: 0 = no pNF+ somas; 1 = pNF+ somas in less than 25% of image area; 2 = pNF+ somas in approximately 50% of image area; 3 = pNF+ somas in greater than 80% of the image area (detailed procedures in sections 2.8, 2.9, and 2.10.2).

Expression of pNF and nonpNF in the ONH

NF expression and phosphorylation in RGC axons was investigated in ONH longitudinal sections. Briefly, two serial ONH sections from each ONH underwent fluorescent IHC labelling for either pNF or nonpNF. These sections were then imaged and fluorescence intensity was quantified in nine sequential 100 x 200 μm ONH regions: pre-LC, LC1, LC2, and post-100, -200, -300, -400, -500, and -600 (detailed procedures in sections 2.8, 2.9, and 2.11).

Statistical Analysis

Main effects of elevated IOP, recovery time and ONH region on pNF and nonpNF labelling intensity in the ONH were analyzed with two-way within-subjects ANOVA with post-hoc testing. Data from 30- and 90-minute animals were included in separate models. Point-by-point differences within and between control and experimental groups were assessed by t-test.

Sample Sizes

Tissue used in the present experiments was obtained from a total of 50 animals (elevated IOP animals: N = 48; sham animals: N = 2).

In experiments examining the somal expression of pNF in RGCs, animals with poor pNF labelling in retinal whole-mounts, in either the control or experimental eye, were excluded from analysis (total excluded = 25). Sample sizes for pNF analysis in retinal whole-mounts ranged from 2 to 6 animals per experimental group (N = 23; n per group: 30min/3h = 4, 30min/6h = 6, 30min/24 = 2, 90min/3h = 3, 90min/6h = 5, 90min/24h = 3).

pNF and nonpNF expression in the ONH was measured and analysed in all animals (N = 48; n per group = 8). ONHs from control and experimental eyes were obtained from all animals.

6.3 Results

6.3.1 Expression of pNF in the Retina Following 30 Minutes of Elevated IOP

Thirty minutes of elevated IOP did not cause any notable accumulation of pNF in RGC somas at any of the recovery times examined (Figure 6.1 A, upper panel). Figure 6.2 A, B, and C shows the percent of images that exhibited pNF grades from 0-3 at 1, 2, and 3 mm of eccentricity in both control and experimental retinas. Median pNF grades for images obtained at 1, 2, and 3 mm of eccentricity in control and experimental retinas at each recovery time are shown in Table 6.1. Images from retinas in the 30-minute group were primarily graded as 0, regardless of experimental treatment (control versus experimental eye; 3, 6, or 24 hours recovery), although the 30min/3h group and experimental retinas of the 30min/24h group demonstrated some grading greater than 0.

6.3.2 Expression of pNF in the Retina Following 90 Minutes of Elevated IOP

Ninety minutes of elevated IOP caused marked accumulation of pNF in RGC somas at all of the recovery time points examined (Figure 6.1 A, lower panel). Figure 6.3 A, B, and C shows the percent of images examined which exhibited pNF grades from 0-3 at 1, 2, and 3 mm of eccentricity in both control and experimental retinas. The median pNF grades for images obtained at 1, 2, and 3 mm of eccentricity in control and experimental retinas at each recovery time are shown in Table 6.1.

Table 6.1 Median pNF Grades at 1, 2, and 3 mm of Retinal Eccentricity Following Elevated IOP

		Control			Elevated IOP		
Injury Group	**Recovery**	**1 mm**	**2 mm**	**3 mm**	**1 mm**	**2 mm**	**3 mm**
30 Minutes Elevated IOP	**3 Hours**	0	0	0	0	0	0.5
	6 Hours	0	0	0	0	0	0
	24 Hours	0	0	0	0	0	0
90 Minutes Elevated IOP	**3 Hours**	0	0	0	0	2.0	3.0
	6 Hours	0	0	0	0	3.0	3.0
	24 Hours	0	0	0	1.5	2.0	2.0

Figure 6.1 Example Images of pNF Labelling in Retinal Whole Mounts Following Elevated IOP. A) Expression of pNF and Brn3a in the retina at 3, 6, and 24 hours following either 30 or 90 minutes of elevated IOP, obtained at approximately 2 mm of eccentricity from the ONH. Thirty minutes of elevated IOP did not induce somal pNF labelling at any of the time points examined. Ninety minutes of elevated IOP induced somal pNF labelling in Brn3a+ cells in the GCL at all time points (arrows). **B)** Somal pNF labelling (B1, arrow) in retinas at 24 hours following 90 minutes of elevated IOP was accompanied by signs of axonal degeneration in the NFL, including axonal varicosities and spheroidal retraction bulbs (B2, arrowheads).

A)

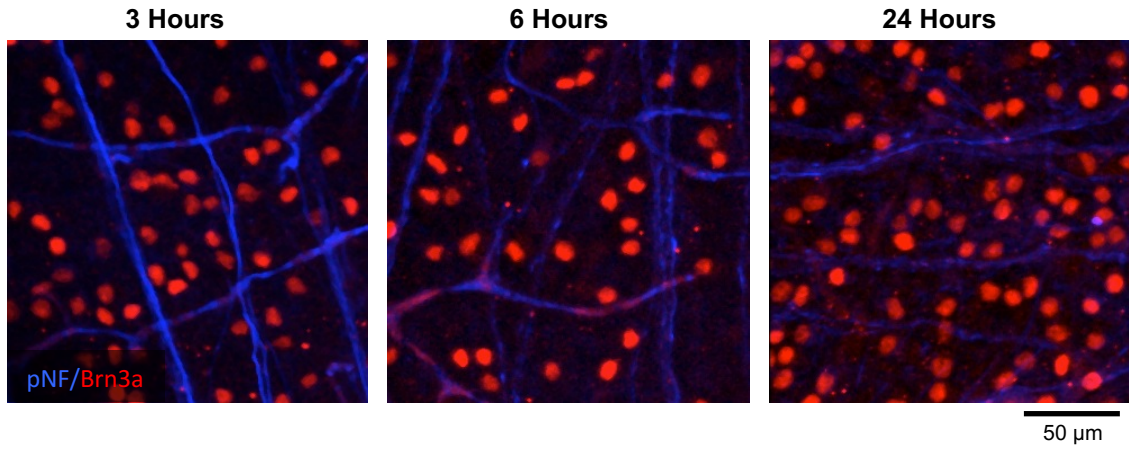
30 Minutes Elevated IOP
3 Hours
6 Hours
24 Hours
pNF/Brn3a
50 µm

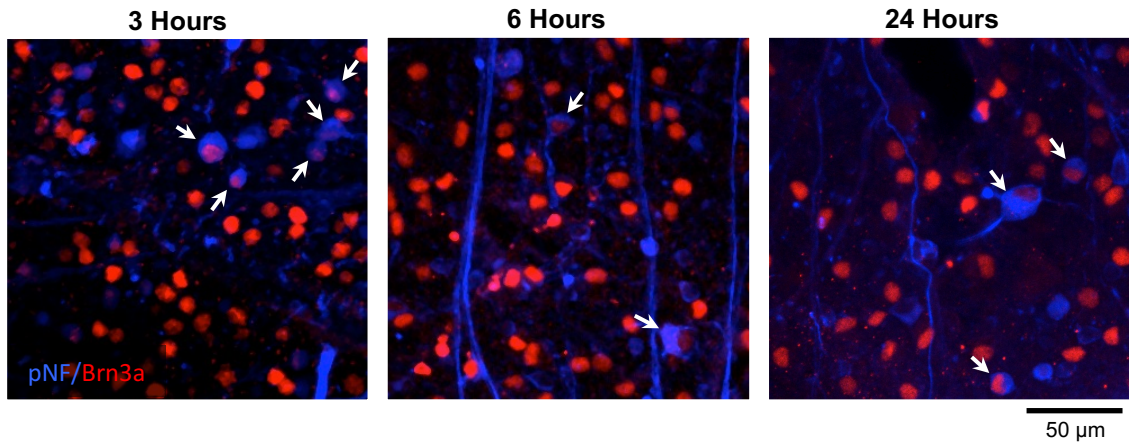
90 Minutes Elevated IOP
3 Hours
6 Hours
24 Hours
pNF/Brn3a
50 µm

B)

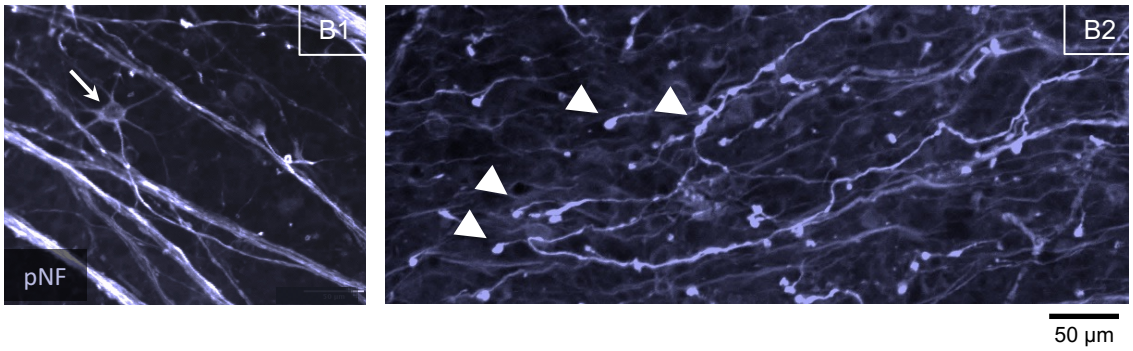
B1
B2
pNF
50 µm

Figure 6.2 Somal pNF Grading in Retinal Whole Mounts Following 30 Minutes of Elevated IOP. Grading of somal pNF labelling at 3 hours **(A)**, 6 hours **(B)**, and 24 hours **(C)** following elevated IOP is shown. Thirty minutes of elevated IOP had mild effects on the grade of somal pNF labelling. Increases in grade, correlating to increased retinal area exhibiting somal pNF labelling, were primarily associated with elevated IOP damage and larger eccentricities.

A) 3 Hours Recovery

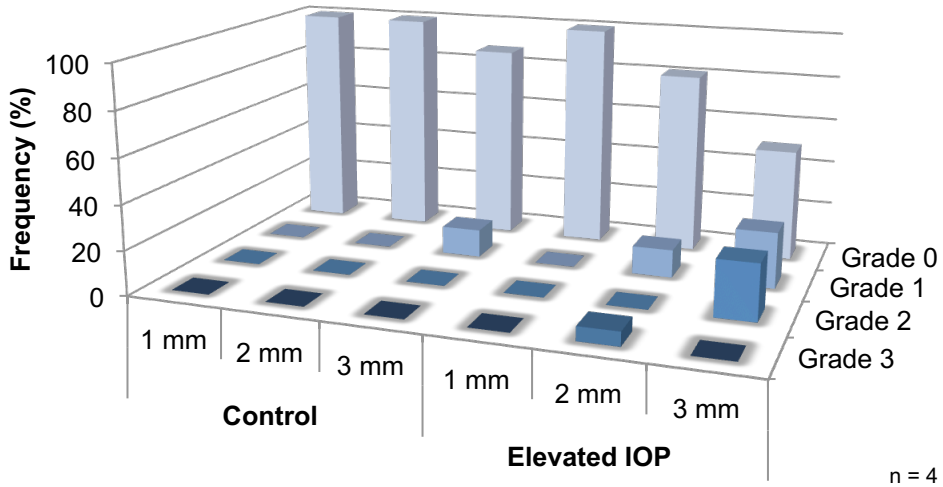

B) 6 Hours Recovery

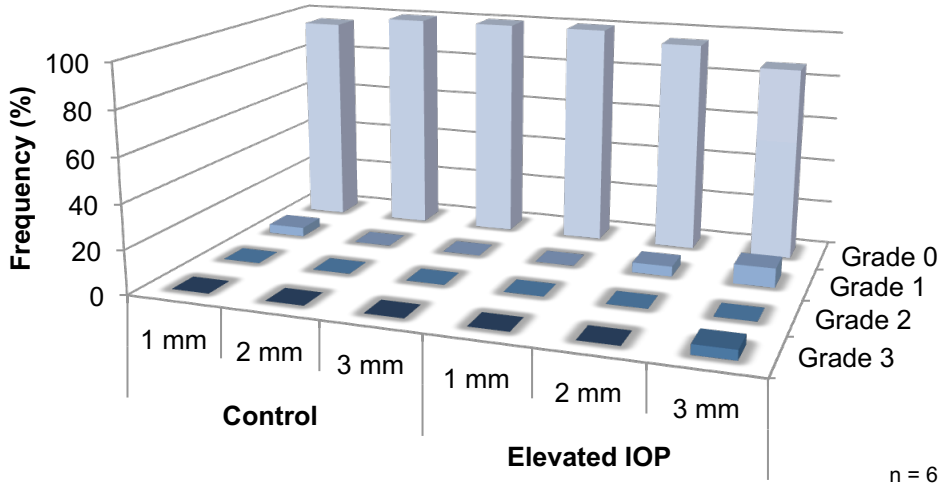

C) 24 Hours Recovery

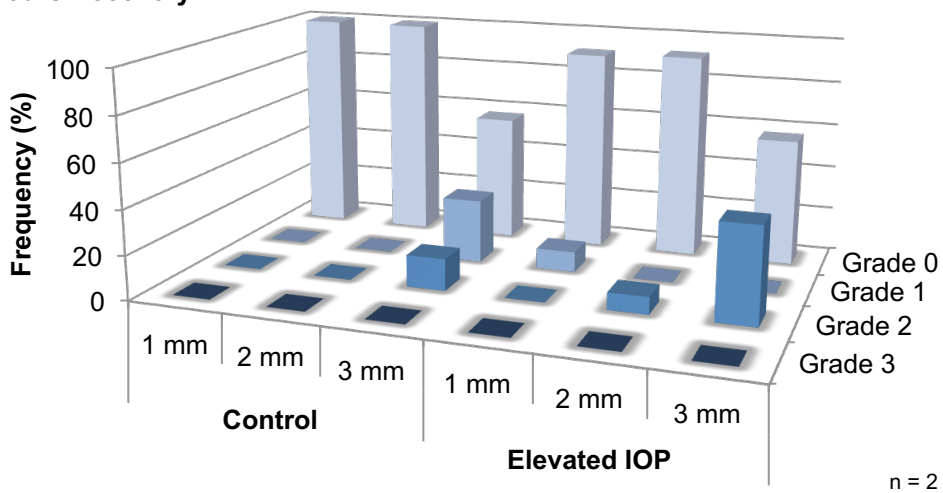

Figure 6.3 Somal pNF Grading in Retinal Whole Mounts Following 90 Minutes of Elevated IOP. Grading of somal pNF labelling at 3 hours **(A)**, 6 hours **(B)**, and 24 hours **(C)** following elevated IOP is shown. Ninety minutes of elevated IOP had marked effects on somal pNF grading. Increases in grade, correlating to increased retinal area exhibiting somal pNF labelling, were associated with elevated IOP damage and were more pronounced as retinal eccentricity increased.

A) 3 Hours Recovery

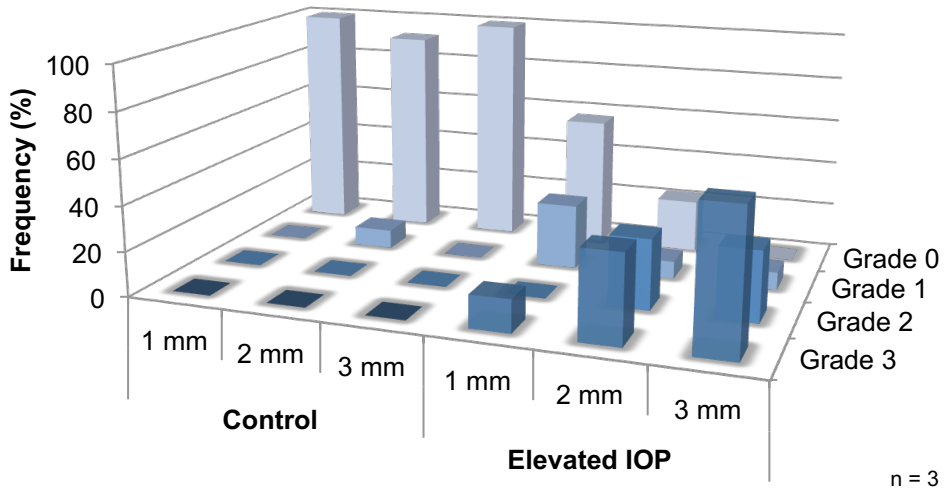

B) 6 Hours Recovery

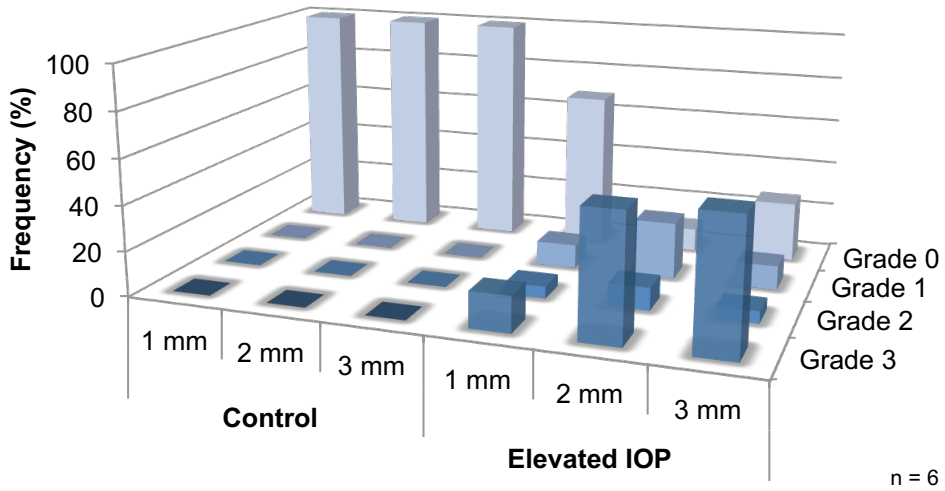

C) 24 Hours Recovery

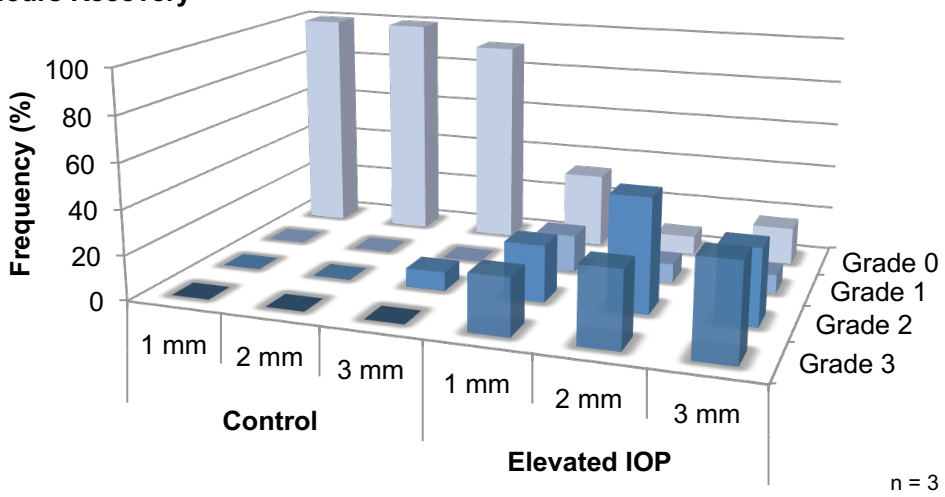

6.3.3 pNF and nonpNF Expression in the ONH Following Elevated IOP

pNF and nonpNF expression was examined in serial longitudinal sections obtained from each ONH, and intensity measurements in all ONH regions were normalized to the pre-LC values. Examples of pNF and nonpNF labelling in a control ONH are shown in Figure 6.4.

6.3.3.1 Description of nonpNF Labelling Within Control and Experimental ONHs

6.3.3.1.1 Thirty-Minute IOP Elevation

The intensity of nonpNF labelling in the 30-minute group varied significantly across ONH regions (ANOVA, $p < 0.01$) at all recovery times and for both control and experimental ONHs. Labelling intensity in control ONHs, relative to the pre-LC region, peaked in the post-100 region for the 30min/3h group (+6%), the post-200 region in the 30min/6h group (+15%), and the LC2 region in the 30min/24h group (+47%), thereafter decreasing through more distal ONH regions (Figure 6.5 A, left panel). In experimental ONHs, labelling intensity peaked at the post-100 region for both the 30min/3h group (+33%) and the 30min/6h group (+39%), and in the LC2 region for the 30min/24h group (+50%; Figure 6.5 A, right panel).

6.3.3.1.2 Ninety-Minute IOP Elevation

The intensity of nonpNF labelling in the 90-minute group varied significantly across ONH regions (ANOVA, $p < 0.01$) at all recovery times for both control and experimental ONHs. Labelling intensity in control ONHs, relative to the pre-LC values, peaked in the LC1 region (+18%) for the 90min/6h group (Figure 6.5 B, left

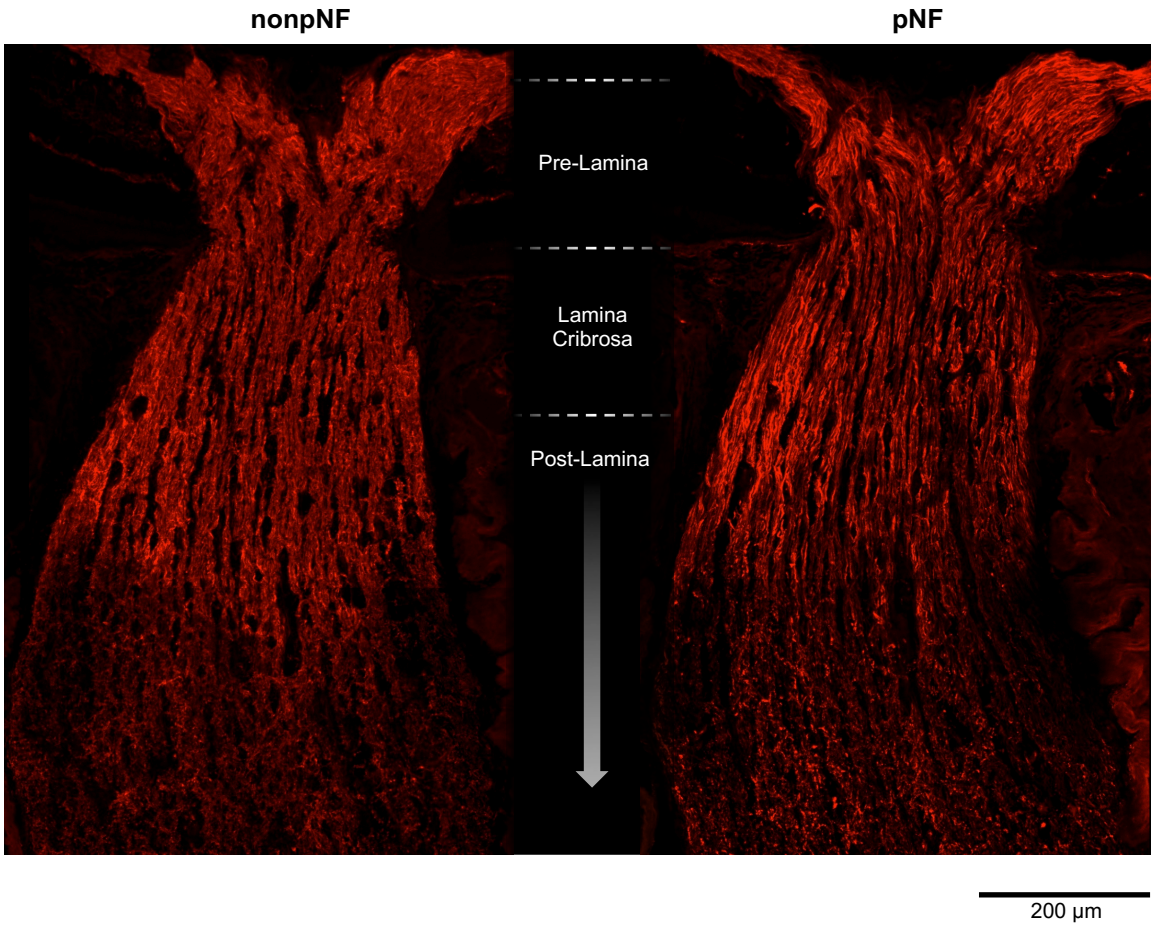

Figure 6.4 Example Images of nonpNF and pNF Labelling in Longitudinal Sections of a Control ONH. Images show the pattern of nonpNF and pNF labelling in the Pre-LC, LC and Post-LC regions of the ONH of an untreated eye.

Figure 6.5 Distribution of nonpNF Labelling in Control and Experimental ONHs at 3, 6, and 24 Hours Following 30 and 90 Minutes of Elevated IOP. A) Fluorescence intensity of nonpNF labelling in control and experimental ONHs at 3, 6, and 24 hours following 30 minutes of elevated IOP. **B)** Fluorescence intensity of nonpNF labelling in control and experimental ONHs at 3, 6, and 24 hours following 90 minutes of elevated IOP. All measurements were normalized to the pre-LC value. Greyed area indicates the LC region.

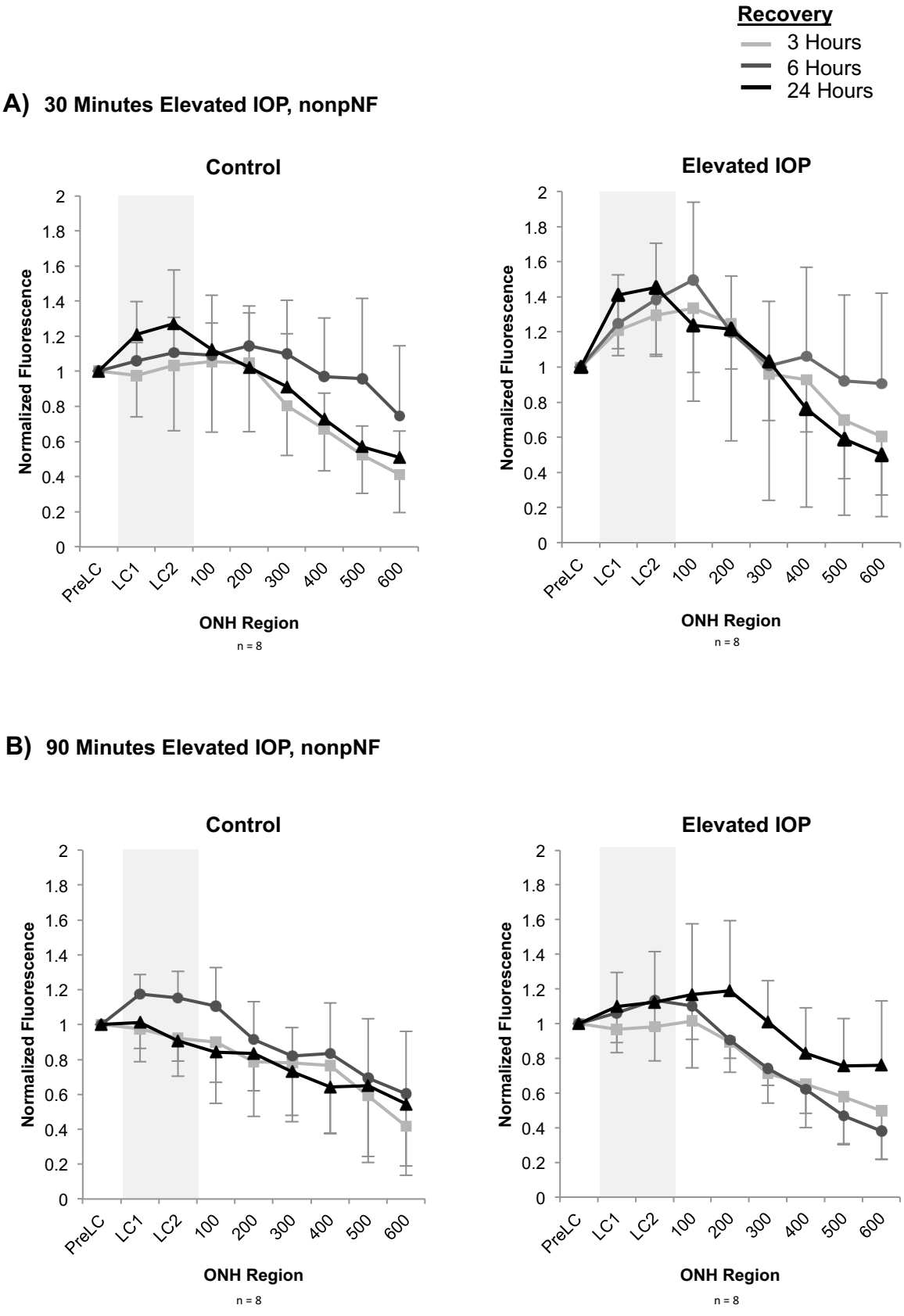
Recovery
3 Hours
6 Hours
24 Hours
A) 30 Minutes Elevated IOP, nonpNF
Control
Elevated IOP
Normalized Fluorescence
0
0.2
0.4
0.6
0.8
1
1.2
1.4
1.6
1.8
2
PreLC
LC1
LC2
100
200
300
400
500
600
ONH Region
n = 8
B) 90 Minutes Elevated IOP, nonpNF
Control
Elevated IOP
Normalized Fluorescence
ONH Region
n = 8

panel). Labelling intensity in control ONHs in 90min/3h and 90min/24h groups remained relatively stable between the pre-LC and LC1 regions (-2% and +1%, respectively), and steadily decreased thereafter. In experimental ONHs, labelling intensity following the pre-LC region was relatively stable in the 90min/3h group, with a small peak in the post-100 region (+1%; Figure 6.5 B, right panel). The experimental ONHs of the 90min/6h and 90min/24h groups showed peaks in labelling intensity in the LC2 (+14%) and post-200 (+19%) regions, respectively (Figure 6.5 B, right panel).

6.3.3.2 Comparison of nonpNF Labelling Between Control and Experimental ONHs

6.3.3.2.1 Thirty-Minute IOP Elevation

Neither elevated IOP (30 minutes) nor recovery time (3, 6, and 24 hours) had a significant overall effect on nonpNF labelling intensity ($p = 0.26$ and 0.74, respectively; ANOVA). Although not significant, labelling intensity was consistently increased in experimental ONHs across all regions compared to control in the 30min/3h group (Figure 6.6 A). Similarly, nonpNF intensity was higher in experimental ONHs from the LC1 to post-100 regions in the 30min/6h group, and from the LC1 to post-300 regions in the 30min/24h group (Figure 6.6 B and C). Percent differences in intensity between the LC region of control and experimental ONHs, calculated as an average of LC1 and 2 regions, were +25% in the 30min/3h group, +24% in the 30min/6h group, and +19% in the 30min/24h group.

Figure 6.6 Comparison of nonpNF Labelling Intensity Between Control and Experimental ONHs at 3, 6, and 24 Hours Following 30 Minutes of Elevated IOP. **A)** Intensity of nonpNF labelling in control (black) and experimental (red) ONHs at 3 hours of recovery. **B)** Intensity of nonpNF labelling control (black) and experimental (red) ONHs at 6 hours of recovery. **C)** Intensity of nonpNF labelling in control (black) and experimental (red) ONHs at 24 hours of recovery. All measurements were normalized to the pre-LC value. No significant differences were observed between experimental and control ONHs. Greyed area indicates the LC region.

30 Minutes Elevated IOP, nonpNF

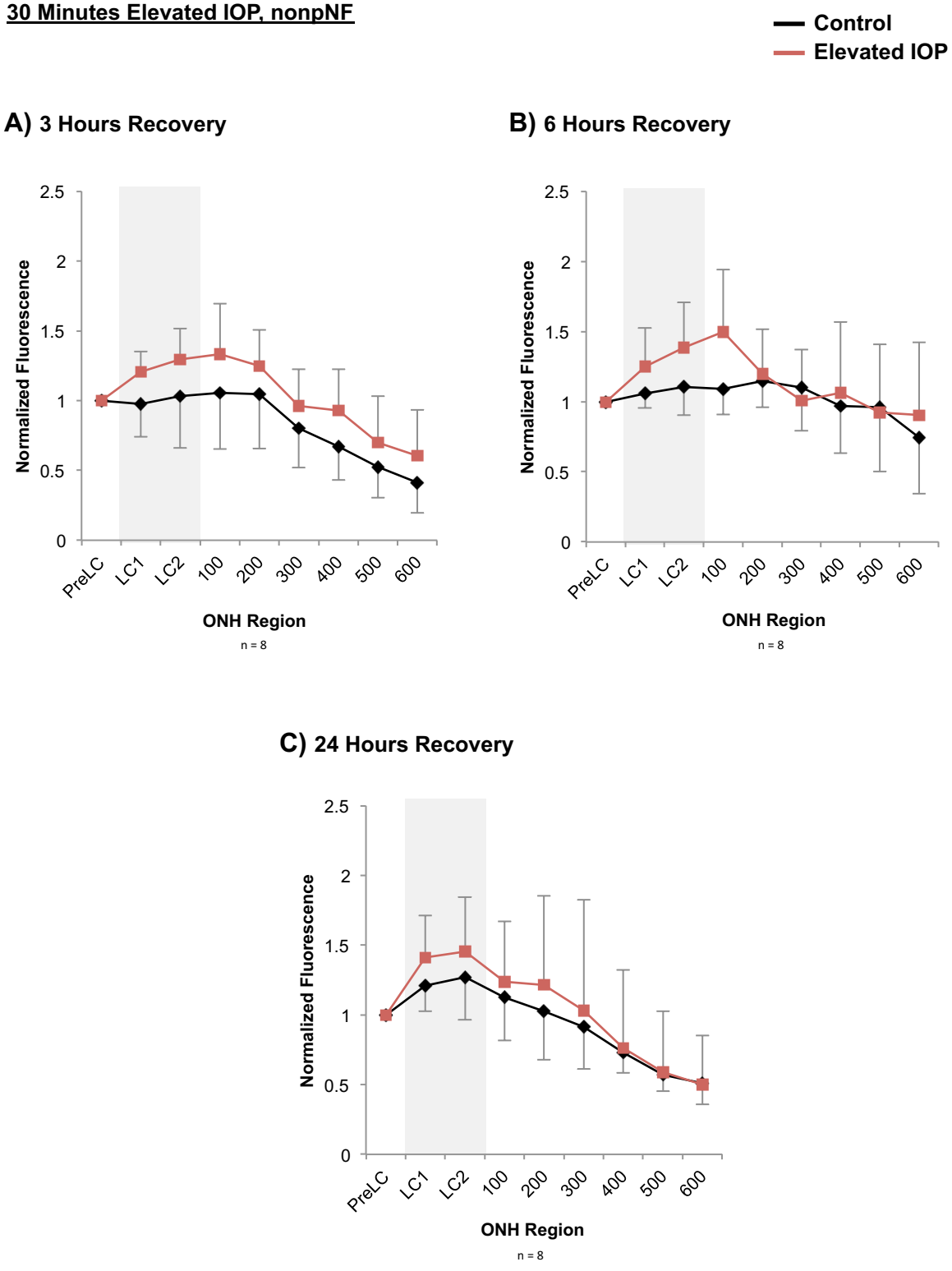

6.3.3.2.2 Ninety-Minute IOP Elevation

Neither elevated IOP (90 minutes) nor recovery time (3, 6, and 24 hours) had a significant overall effect on nonpNF labelling intensity ($p = 0.52$ and 0.69, respectively; ANOVA). Labelling intensity between control and experimental ONHs was comparable in the 90min/3h and 90min/6h groups (Figure 6.7 A and B), however, was consistently increased in experimental ONHs compared to control in the 90min/24h group from the LC1 to post-600 region (Figure 6.7 C). Percent differences in intensity between the entire LC region of control and experimental ONHs, calculated as an average of the LC1 and 2 regions, were +3% in the 90min/3h group, -7% in the 90min/6h group, and +15% in the 90min/24h group.

6.3.3.3 Description of pNF Labelling Intensity Within Control and Experimental ONHs

6.3.3.3.1 Thirty-Minute IOP Elevation

The intensity of pNF labelling in the 30-minute group varied significantly across ONH regions (ANOVA, $p < 0.01$) at all recovery times for both control and experimental ONHs. Labelling intensity in control ONHs peaked in the LC2 region for the 30min/3h group (+12% relative to pre-LC value), the LC2 region in the 30min/6h group (+5%), and the LC1 region in the 30min/24h group (+18%), and progressively decreased thereafter (Figure 6.8 A, left panel). Labelling intensity in experimental ONHs of the 30min/3h and 30min/24h groups was highest in the pre-LC region, and peaked in the post-100 region (+4%) for the 30min/6h group (Figure 6.8 A, right panel).

6.3.3.3.2 Ninety-Minute IOP Elevation

The intensity of pNF labelling in the 90-minute group varied significantly across ONH regions (ANOVA, $p < 0.01$) at all recovery times for both control and experimental ONHs. In control ONHs of both the 90min/3h and 90min/6h groups, labelling intensity progressively decreased from the pre-LC region through more distal ONH regions. In the 90min/24h group, labelling intensity dropped in the LC1 region (-14%), returned to the pre-LC value in the post-200 region (+2%), and progressively declined thereafter (Figure 6.8 B, left panel). In experimental ONHs, labelling intensity in all groups dropped in the LC1 region (90min/3h, -25%; 90min/6h, -23%; and 90min/24h, -17%), increased slightly in the LC2-post100 regions (90min/3h, -19%; 90min/6h, 14%; and 90min/24h, 7%), and progressively decreased thereafter (Figure 6.8 B, right panel).

6.3.3.4 Comparison of pNF Labelling Between Control and Experimental ONHs

6.3.3.4.1 Thirty-Minute IOP Elevation

Neither elevated IOP (30 minutes) nor recovery time (3, 6, and 24 hours) had a significant overall effect on pNF labelling intensity ($p = 0.86$ and 0.67, respectively; ANOVA). Although not significant, labelling intensity in experimental ONHs was consistently decreased between the LC1 and post-300 regions in the 30min/3h group (Figure 6.9 A), and similarly from LC1 to post-200 in the 30min/24h group (Figure 6.9 C). Differences between control and experimental labelling intensities were small and variable in the 30m/6h group, with the post-400 region being the only region to exceed a 10% difference between control and experimental values (-14%; Figure 6.9 B). Percent

Figure 6.7 Comparison of nonpNF Labelling Intensity Between Control and Experimental ONHs at 3, 6, and 24 Hours Following 90 Minutes of Elevated IOP. **A)** Intensity of nonpNF labelling in control (black) and experimental (red) ONHs at 3 hours of recovery. **B)** Intensity of nonpNF labelling control (black) and experimental (red) ONHs at 6 hours of recovery. **C)** Intensity of nonpNF labelling in control (black) and experimental (red) ONHs at 24 hours of recovery. All measurements were normalized to the pre-LC value. Greyed area indicates the LC region. * = $p < 0.05$.

90 Minutes Elevated IOP, nonpNF

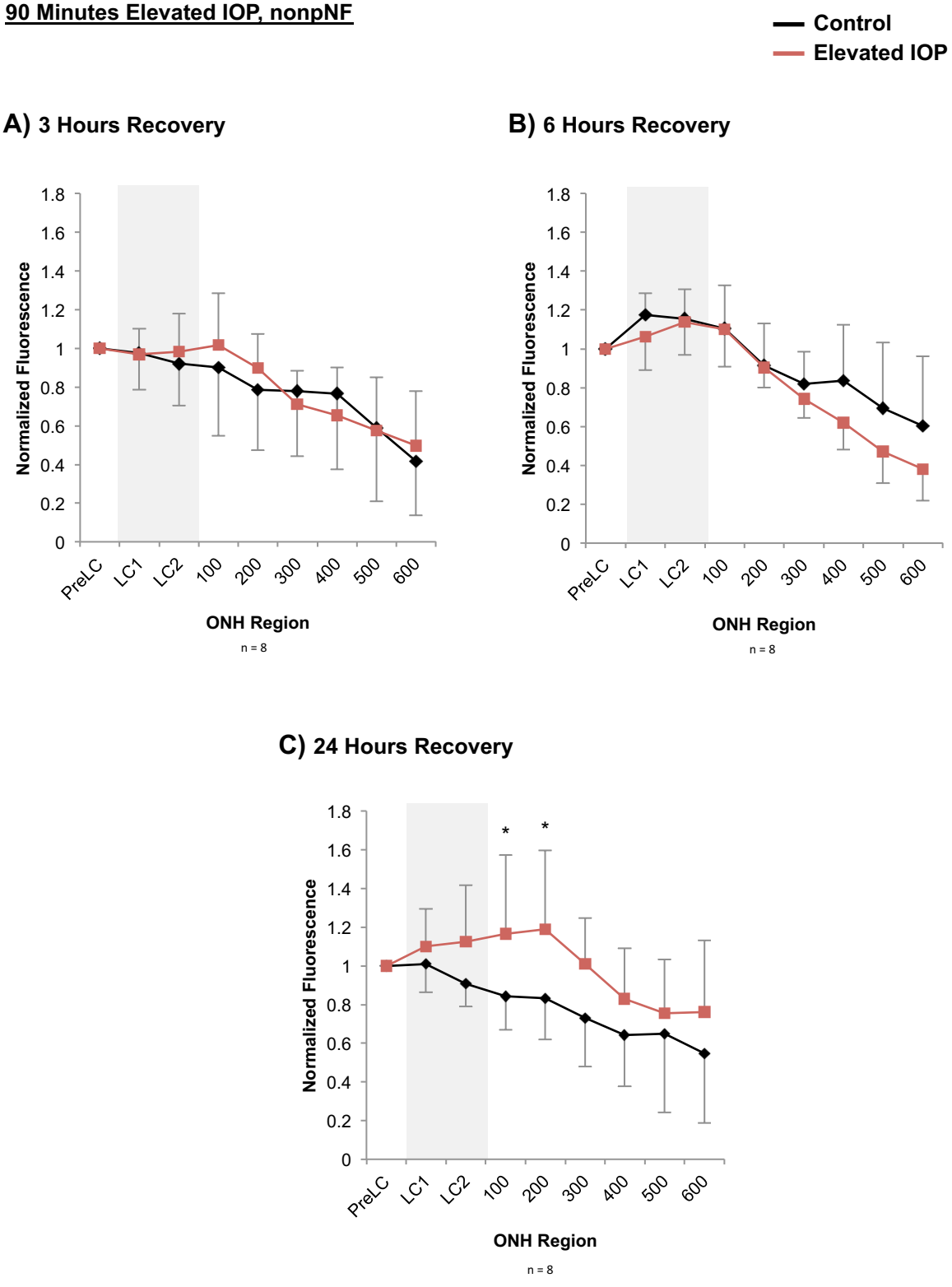

Figure 6.8 Distribution of pNF Labelling in Control and Experimental ONHs at 3, 6, and 24 Hours Following 30 and 90 Minutes of Elevated IOP. A) Fluorescence intensity of pNF labelling in control and experimental ONHs at 3, 6, and 24 hours following 30 minutes of elevated IOP. **B)** Fluorescence intensity of pNF labelling in control and experimental ONHs at 3, 6, and 24 hours following 90 minutes of elevated IOP. All measurements were normalized to the pre-LC value. Greyed area indicates the LC region.

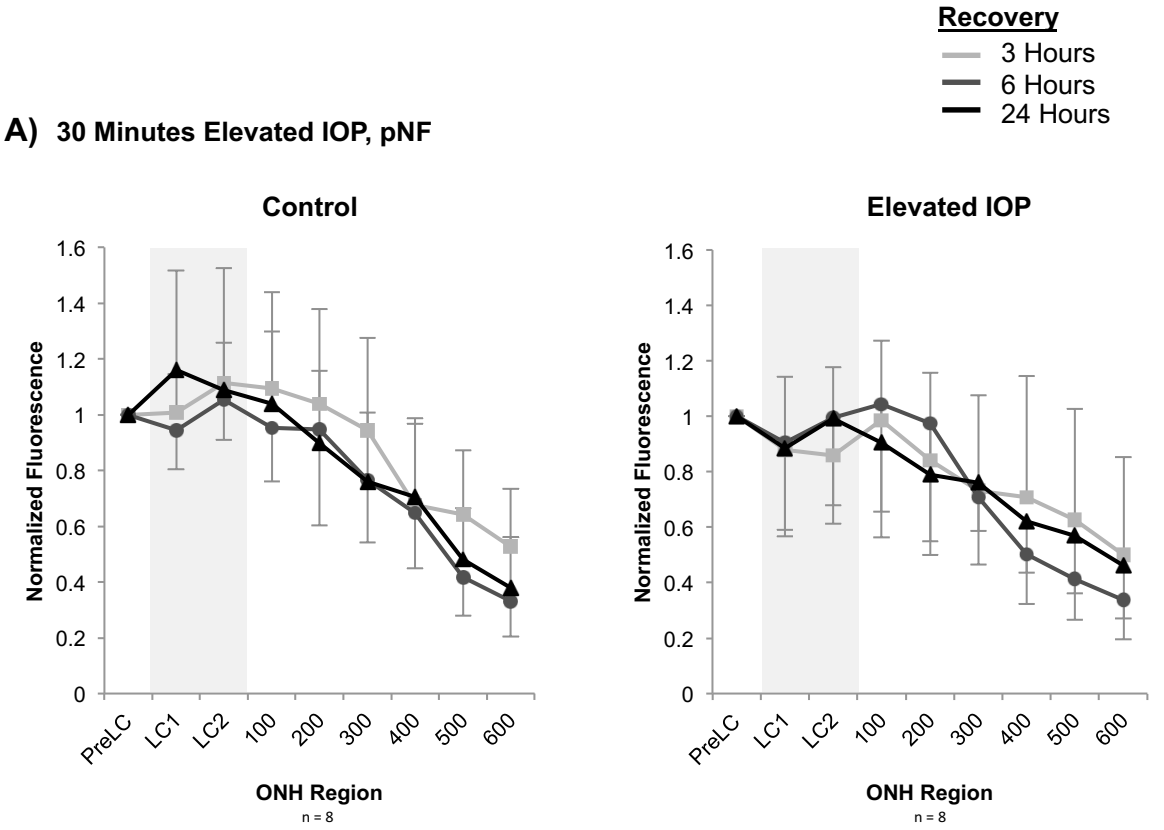
Recovery
3 Hours
6 Hours
24 Hours
A) 30 Minutes Elevated IOP, pNF
Control
Elevated IOP
Normalized Fluorescence
1.6
1.4
1.2
1
0.8
0.6
0.4
0.2
0
PreLC
LC1
LC2
100
200
300
400
500
600
ONH Region
n = 8
B) 90 Minutes Elevated IOP, pNF
Control
Elevated IOP
Normalized Fluorescence
ONH Region
n = 8

Figure 6.9 Comparison of pNF Labelling Intensity Between Control and Experimental ONHs at 3, 6, and 24 Hours Following 30 Minutes of Elevated IOP. **A)** Intensity of pNF labelling in control (black) and experimental (red) ONHs at 3 hours of recovery. **B)** Intensity of pNF labelling control (black) and experimental (red) ONHs at 6 hours of recovery. **C)** Intensity of pNF labelling in control (black) and experimental (red) ONHs at 24 hours of recovery. All measurements were normalized to the pre-LC value. Greyed area indicates the LC region.

30 Minutes Elevated IOP, pNF

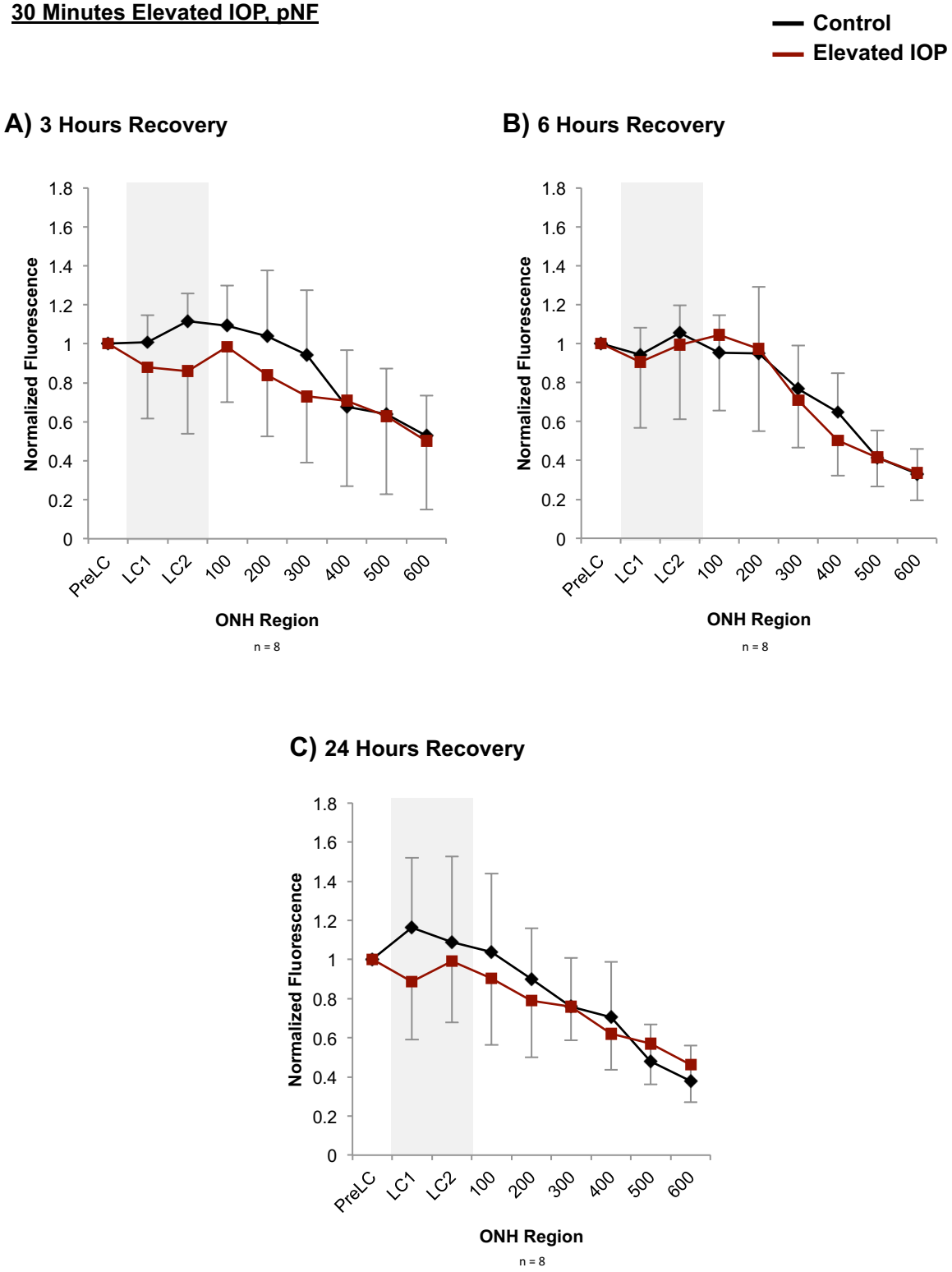

differences in intensity between the entire LC region of control and experimental ONHs, calculated as the average of LC1 and 2 regions, were -20% in the 30min/3h group, -5% in the 30min/6h group, and -19% in the 30min/24h group.

6.3.3.4.2 Ninety-Minute IOP Elevation

Neither elevated IOP (90 minutes) nor recovery time (3, 6, and 24 hours) had a significant overall effect on pNF labelling intensity ($p = 0.26$ and 0.74, respectively; ANOVA). Although not significant, labelling intensity in experimental ONHs was decreased compared to control values from the LC1 to post-500 regions in both the 90min/3h and 90min/6h groups (LC1 of 90min/3h: $p < 0.05$; Figure 6.10 A and B). In the 90min/24h group, labelling intensity in experimental ONHs was decreased compared to control in the post-100, -200 and -400 regions (Figure 6.10 C). Percent differences in intensity between the entire LC region of control and experimental ONHs, calculated as the average of LC1 and 2 regions, were -20% in the 90min/3h group, -13% in the 90min/6h group, and -2% in the 90min/24h group.

6.3.3.5 pNF and nonpNF Labelling in the ONH Following Sham Elevated IOP

pNF labelling intensity appeared increased in eyes that had undergone a 90-minute sham procedure, however, this difference was only significant in the post-400 region of the ONH ($p < 0.01$; Figure 6.11 A). There was no discernable difference in nonpNF labelling intensity between control and sham ONHs from the LC1 to the post-200 regions. NonpNF labelling intensity appeared decreased in the sham ONHs from the

Figure 6.10 Comparison of pNF Labelling Intensity Between Control and Experimental ONHs at 3, 6, and 24 Hours Following 90 Minutes of Elevated IOP. **A)** Intensity of pNF labelling in control (black) and experimental (red) ONHs at 3 hours of recovery. **B)** Intensity of pNF labelling control (black) and experimental (red) ONHs at 6 hours of recovery. **C)** Intensity of pNF labelling in control (black) and experimental (red) ONHs at 24 hours of recovery. All measurements were normalized to the pre-LC value. Greyed area indicates the LC region. * = $p < 0.05$.

90 Minutes Elevated IOP, pNF

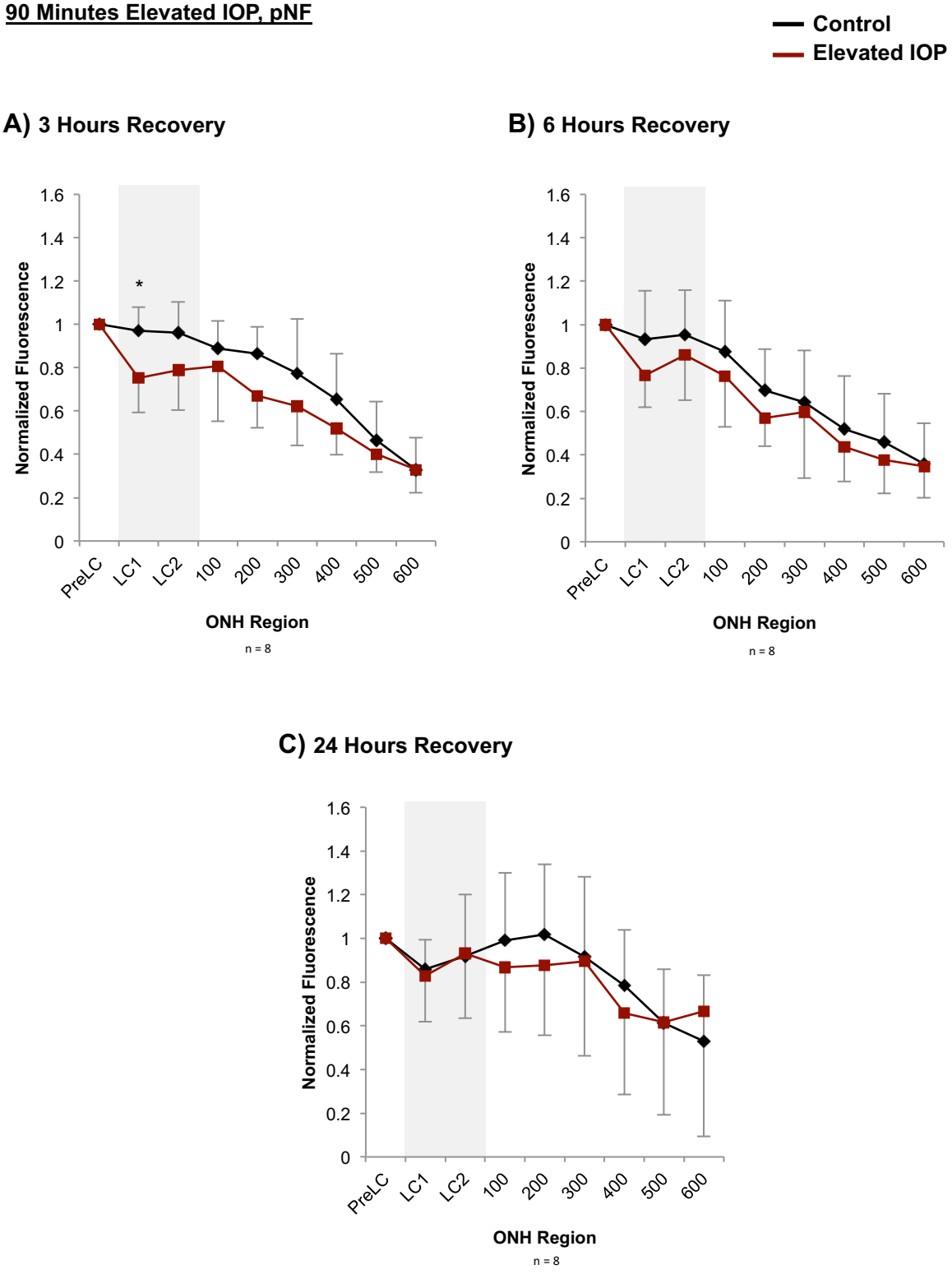

Sham 90 Minutes Elevated IOP, 24 Hours Recovery

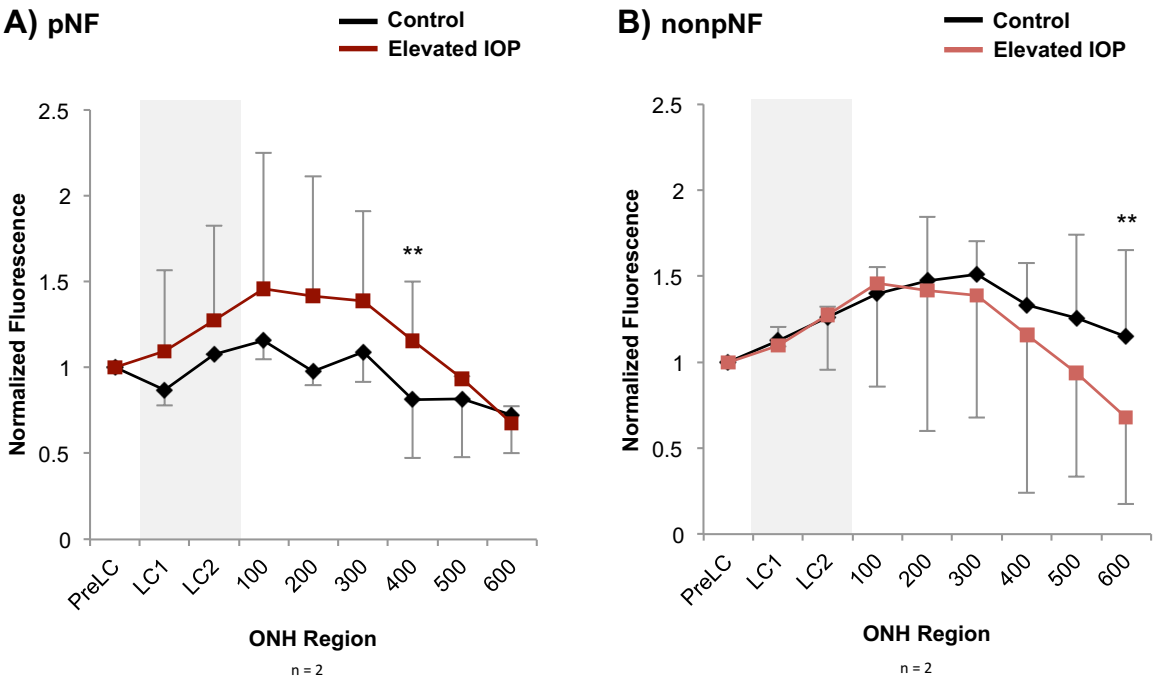

Figure 6.11 pNF and nonpNF Labelling Intensity in the ONH at 24 Hours Following Sham Elevated IOP. **A)** pNF labelling intensity through sequential ONH regions in control and sham eyes. **B)** pNF labelling intensity through sequential ONH regions in control and sham eyes. Greyed area indicates the LC region. ** = p <0.01.

post-300 to post-600 regions, a difference that was significant in the post-600 region ($p < 0.01$; Figure 6.11 B).

6.4 Summary and Key Findings

These experiments highlight the early effects of a transient elevation of IOP on the expression, phosphorylation, and distribution of NFs in RGCs within the retina and ONH.

Key findings include:

1) Ninety minutes of elevated IOP resulted in immediate damage to the RGC axon, as evidenced by the presence of pNF in RGC somas as early as 3 hours following elevated IOP, while this sign was absent following 30 minutes of elevated IOP.

2) Although effects on NF phosphorylation in the ONH did not, for the most part, attain significance, there was a trend favoring dephosphorylation – i.e. a decrease in pNF and increase in nonpNF labelling in experimental ONHs – following both mild (30 minute) and severe (90 minute) IOP-induced injuries, with little difference between the two durations.

Taken together, these findings suggest that alterations of NF proteins can reflect early axonal damage in RGCs. Further implications of these findings are discussed in sections 8.4, 8.5 and 8.6.

CHAPTER 7 – GLIAL ACTIVATION IN THE RETINA AND ONH FOLLOWING ELEVATED IOP

7.1 Rationale, Objective, and Hypotheses

As discussed in sections 1.4.4.3 and 1.4.5.4, RGC axonal health and function is directly modulated by the actions of surrounding glia in the retina and ON. From previous experiments examining anterograde AT function and NF phosphorylation in RGCs following elevated IOP (Chapters 5 and 6), it is evident that a transient elevation of IOP has rapid effects on both RGC axonal function and structure. Glial activation has been frequently associated with RGC damage and loss in acute and chronic models of elevated IOP [60, 241, 246, 248, 292, 294, 296, 314, 334]. Select studies have examined the time course of glial responses following a transient elevation of IOP [60, 241]; however, such studies are limited in number and scope. Furthermore, no studies have executed measurements of glial activation in synchrony with measurements of RGC survival, AT function, and axonal structure. This type of integrative approach can elucidate the time course of early glial responses following a transient insult to the retina and ONH, and how such responses relate to other cellular processes that may contribute to RGC death.

The objective of the following experiments was to investigate how glial activation is integrated in the temporal progression of early cellular responses in the retina and ONH following a transient elevated IOP. Two key glial markers – GFAP (expressed in astrocytes and activated Müller cells) and Iba1 (in microglia) – were examined for their responses at 3, 6, and 24 hours following a transient elevation of IOP for 30- or 90-minutes duration. Parts of this work were published in abstract form [332]

7.2 Experimental Design

Animals

Tissue for the following experiments was obtained from animals used in the anterograde AT study (Chapter 5).

GFAP and Iba1 Expression in the Retina Cross-Sections

GFAP and Iba1 protein expression in the retina following elevated IOP was examined with IHC (see section 2.8 for detailed procedures). Cross-sections of the peripapillary retina that were labeled with Iba1 and GFAP antibodies were qualitatively analysed for changes in number, morphology and distribution of labeled glia through the retinal layers (see section 2.10.3 for detailed procedures). Activated Müller glia were identified by the expression of GFAP in radial Müller cell processes, and signs of microglial activation included a morphological shift from ramified (quiescent) morphology to ameboid (activated) morphology (glial activation is described in greater detail in section 1.4.5.4).

Quantifying GFAP Protein in the Retina

WB was used to investigate GFAP expression in the retina, ONH, and the first 2 mm of the ON following elevated IOP. Animals underwent 90 minutes of elevated IOP followed by 24 hours of recovery. Samples from each animal were run in separate gels and GFAP levels in the experimental eye were ratiometrically compared to values from the contralateral control eye (detailed procedures in section 2.6).

GFAP and Iba1 Expression in the ONH

Both GFAP and Iba1 expression in the ONH were analysed by IHC in longitudinal ONH sections. Briefly, two serial ONH sections from each ONH underwent fluorescence IHC labelling for either GFAP or Iba1. For GFAP labelling, sections were imaged and fluorescence intensity was quantified in nine sequential 100 x 200 μm ONH regions from the Pre-LC region to 600 μm post- LC: Pre-LC, LC1, LC2, Post-100, -200, -300, -400, -500, and -600 (detailed procedures in sections 2.8, 2.9, and 2.11). For Iba1 labelling, the percent area of each ONH region that exhibited Iba1 labelling was calculated and compared between control and experimental ONHs.

Statistical Analysis

Main effects of elevated IOP, recovery time, and ONH region on GFAP labelling intensity and the percent Iba1+ area in the ONH were analyzed by two-way within-subject ANOVA with post-hoc testing. Data from 30- and 90-minute groups was included in separate models. Comparisons between control and experimental values in WB data and point-by-point differences within and between control and experimental ONHs were assessed by t-test.

Sample Sizes

Fifty-two animals were used in studies of retinal and ONH glia, which included tissue from the 50 animals in the anterograde AT study described in Chapter 5: 48 animals exposed to elevated IOP (six experimental groups, n = 8/group) as well as two sham animals. Additionally, two animals were used for the WBs of GFAP protein

expression in the retina at 24 hours of recovery following 90 minutes of elevated IOP. Qualitative analysis of Iba1 and GFAP labelling in the peripapillary retina was conducted in all experimental animals (n = 48). Quantitative analysis of GFAP and Iba1 labelling in the ONH was conducted in all experimental animals as well as the two sham animals.

7.3 Results

7.3.1 Qualitative Analysis of Iba1+ Microglia in the Retina Following Elevated IOP

Iba1+ microglia in the peripapillary region of control and experimental retinas were examined in cross-sections obtained at 3, 6, and 24 hours following elevated IOP. The distribution of Iba1+ microglia in control eyes extended from the NFL to the border between the IPL and the INL (Figure 7.1). Microglial somas were observed in the NFL, GCL and along the border between the IPL and INL. Microglial processes primarily extended into the IPL, but were present in all layers from the NFL to the INL. Individual microglia often extended processes into more than one layer. The morphology of microglia in control retinas was primarily ramified.

Thirty minutes of elevated IOP had little effect on the number or morphology of Iba1+ microglia in the peripapillary retina at 3 and 6 hours of recovery (Figure 7.2 A, top and middle panels). In the 30min/3h group, microglia were similar in morphology (ramified) and abundance between control and experimental retinas (Figure 7.2 A, top panel). Fifty percent of the animals in the 30min/6h group exhibited more prominent Iba1 labelling in the experimental retina (not shown), however, this was no longer observed in the 30min/24h group. Some animals in the 30min/6h group exhibited

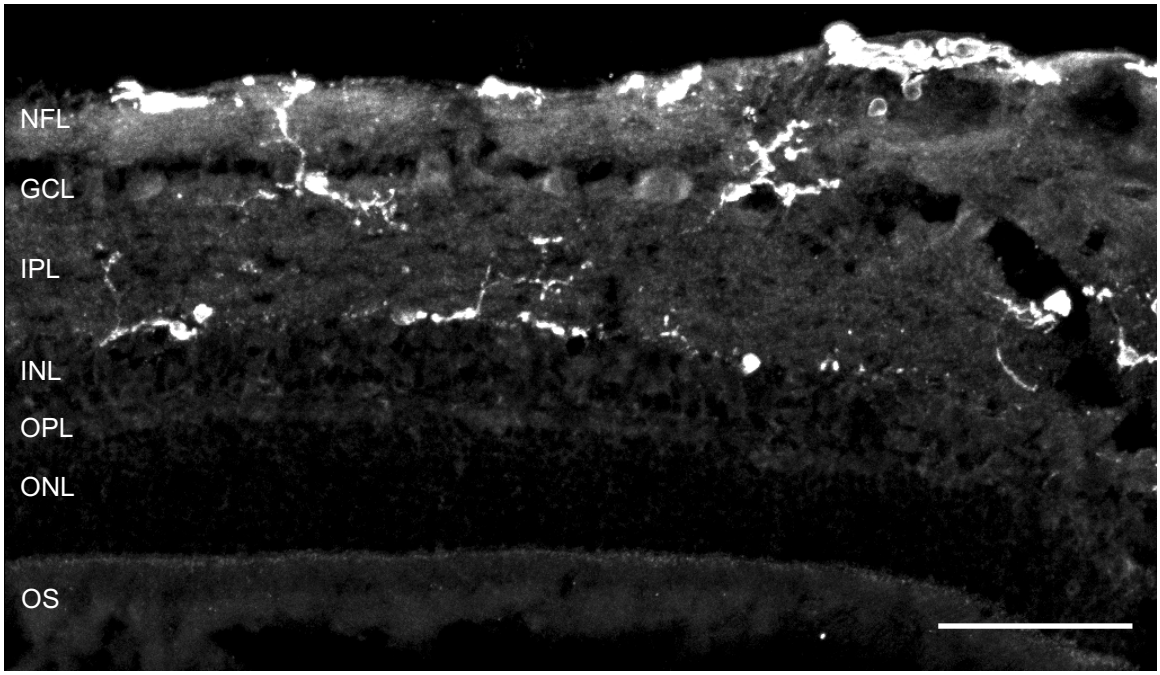

Figure 7.1 Example of Iba1 Labelling in a Cross-Section of the Peripapillary Retina. Iba1+ microglia in control ONHs exhibit a ramified morphology and are primarily isolated to the NFL, GCL, IPL, and the inner border of the INL. Scale 100 μm.

ameboid microglia in both control and experimental retinas (not shown). The presence of ameboid microglia was most prominent in the 30min/24h group, where all animals exhibited ameboid microglia in both control and experimental retinas (Figure 7.2 A, bottom panel). Ameboid microglia were primarily observed in the NFL, but were sometimes found throughout all layers from the NFL to the OPL.

Ninety minutes of elevated IOP had immediate effects on the distribution and morphology of Iba1+ microglia in the peripapillary retina (Figure 7.2 B). In the 90min/3h group, the majority of animals (71%) exhibited more Iba1+ processes extending into the IPL in the experimental eye (Figure 7.2 B, top panel), and this was also observed in the 90min/6h (57%) and 90min/24h groups (86%; Figure 7.2 B, middle and bottom panels). In the 90min/24h group, Iba1+ microglia in the experimental retina were markedly increased in number and nearly all microglia exhibited a more ameboid morphology - some microglia were completely spherical while others exhibited shorter, thicker, and less-branched processes (Figure 7.2 B, bottom panel). In the majority of animals in the 90min/3h and 90min/6h groups, the distribution of Iba1+ microglia in experimental retinas appeared altered, with a greater proportion of microglia observed in the IPL and fewer in the NFL and GCL (an example from the 90min/24h group is shown in Figure 7.2 C). Ameboid microglia were observed in both control and experimental retinas at all time points, however, were more prominent in experimental retinas at 6 and 24 hours (percent of animals exhibiting more ameboid microglia in the experimental retina compared to control: 90min/3h = 0%; 90min/6h = 71%; and 90min/24h = 86%). In the control retinas of the 90min/24h group, ameboid microglia were primarily isolated to the NFL (Figure 7.2 D, left panel, arrow), whereas ameboid microglia in experimental retinas were widely

Figure 7.2 Iba1 Labelling in Cross-Sections of the Peripapillary Retina at 3, 6, and 24 Hours Following 30 and 90 Minutes of Elevated IOP. **A)** Iba1 labelling in the peripapillary retina following 30 minutes of elevated IOP. Somas and processes of ramified Iba1+ microglia were observed in the NFL, GCL, IPL, and INL at 3 and 6 hours of recovery. At 24 hours of recovery, Iba1+ microglia were primarily ameboid in shape and isolated to the NFL in both control and experimental eyes. **B)** Iba1 labelling in the peripapillary retina following 90 minutes of elevated IOP. Iba1+ labelling in the IPL was markedly increased in experimental eyes compared to control eyes at all recovery times. Iba1+ microglia became more ameboid in shape at 6 and 24 hours of recovery and were primarily distributed in the NFL, GCL, and IPL. **C** and **D**: Patterns of Iba1+ labelling observed after 90 minutes of elevated IOP. Iba1+ microglia became more isolated to the IPL in experimental eyes conpaed to control eyes in approximately 50% of animals examined at 3 and 6 hours of recovery (**C**). Many ameboid Iba1+ microglia were observed in the ILM and NFL of control eyes (arrow) and throughout all retinal layers from the NFL to the ONL (arrow) in 43% of animals examined at 24 hours of recovery following 90 minutes of elevated IOP (**D**). All scales are 100 μm.

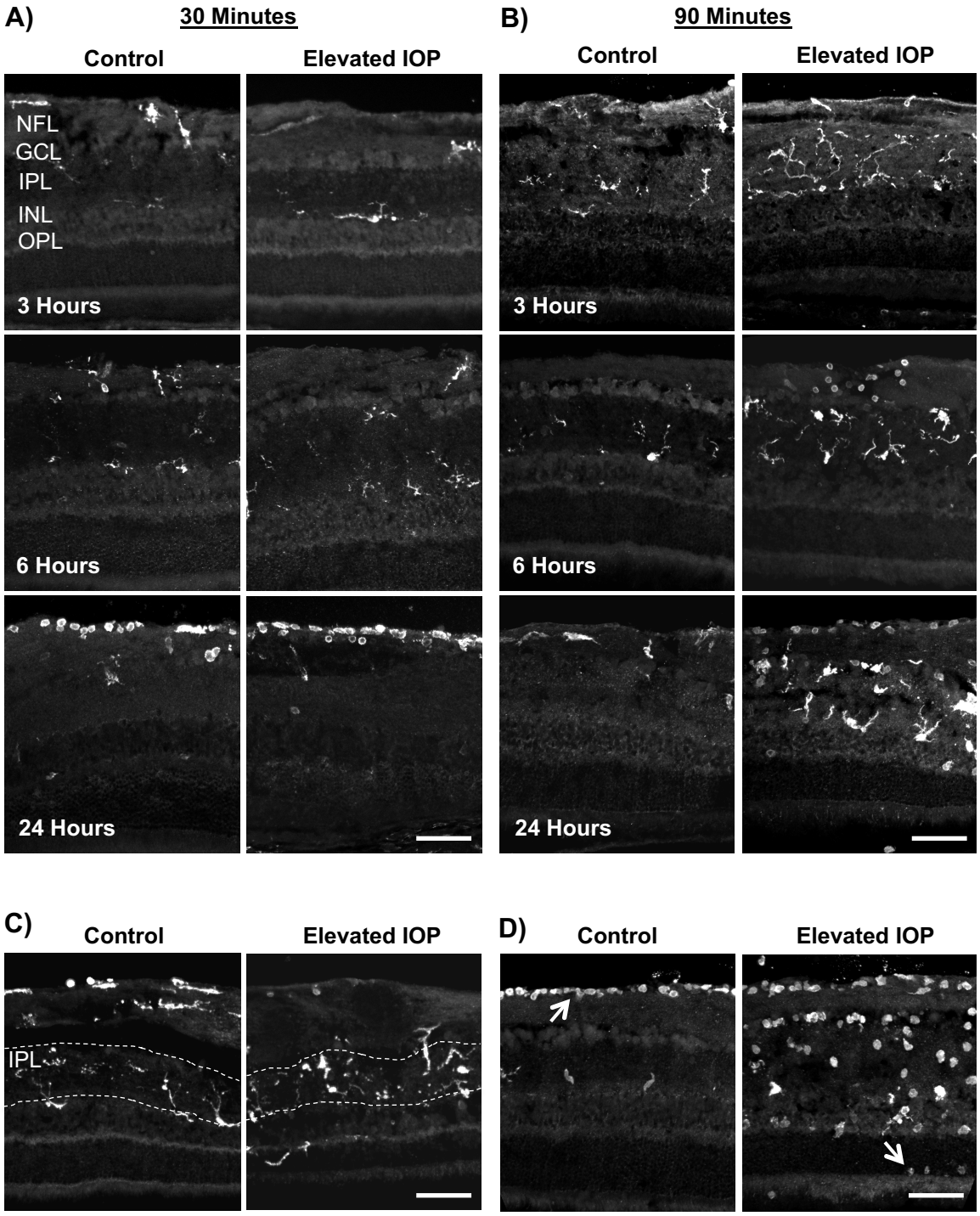
A)
30 Minutes
Control
Elevated IOP
NFL
GCL
IPL
INL
OPL
3 Hours
6 Hours
24 Hours
B)
90 Minutes
Control
Elevated IOP
3 Hours
6 Hours
24 Hours
C)
Control
Elevated IOP
IPL
D)
Control
Elevated IOP

distributed, extending from the NFL to the OPL, and sometimes as deep as the OS layer (Figure 7.2 D, right panel, arrow).

7.3.2 Qualitative Analysis of GFAP Expression in the Retina Following Elevated IOP

GFAP expression in the peripapillary retina, which is typically isolated to the NFL, was primarily unchanged between the control and experimental retinas in the 30min/3h, 30min/6h, and 30min/24h groups (Figure 7.3 A). One animal in the 30min/24h group exhibited GFAP+ fibres spanning the thickness of the experimental retina (Figure 7.3 C).

Similarly, GFAP expression was primarily unchanged in both control and experimental retinas of 90min/3h and 90min/6h groups (Figure 7.3 B). GFAP expression remained primarily unchanged in the experimental retinas of the 90m/24h group, however, approximately 57% of animals examined exhibited faint GFAP+ fibres spanning the control retina (for examples, see Figure 7.3 B, bottom panels, and D).

7.3.3 Quantitative Analysis of GFAP Expression in the Retina Following Elevated IOP

WB for GFAP in the retina, ONH and ON at 24 hours following 90 minutes of elevated IOP revealed a greater than 7-fold increase (mean ± 2SEM = 7.42 ± 1.91) in GFAP expression in the retina, which was significantly different from control levels ($p < 0.05$; Figure 7.4 A and B). GFAP expression in the ONH - tissue isolated from the

Figure 7.3 GFAP Labelling in the Peripapillary Retina at 3, 6, and 24 Hours Following 30 and 90 Minutes of Elevated IOP. A) GFAP IHC in cross-sections of the peripapillary retina from control and experimental eyes at 3, 6, and 24 hours of recovery following 30 minutes of elevated IOP. GFAP labelling at 3 and 6 hours of recovery was isolated to the inner surface of the retina in both control and experimental eyes. In some animals, a marked increase in GFAP labelling extending through all retinal layers was observed in both control and experimental eyes. **B)** GFAP IHC in cross-sections of the peripapillary retina from control and experimental eyes at 3, 6, and 24 hours of recovery following 90 minutes of elevated IOP. GFAP labelling was primarily isolated to the ILM and NFL in both control and experimental eyes at 3 and 6 hours of recovery. **C)** Example of GFAP+ fibres observed in the experimental retina of one animal in the 30min/24h group. **D)** Example of faint GFAP+ fibres observed in some control retinas of the 90min/24h group. Scales 100 μm.

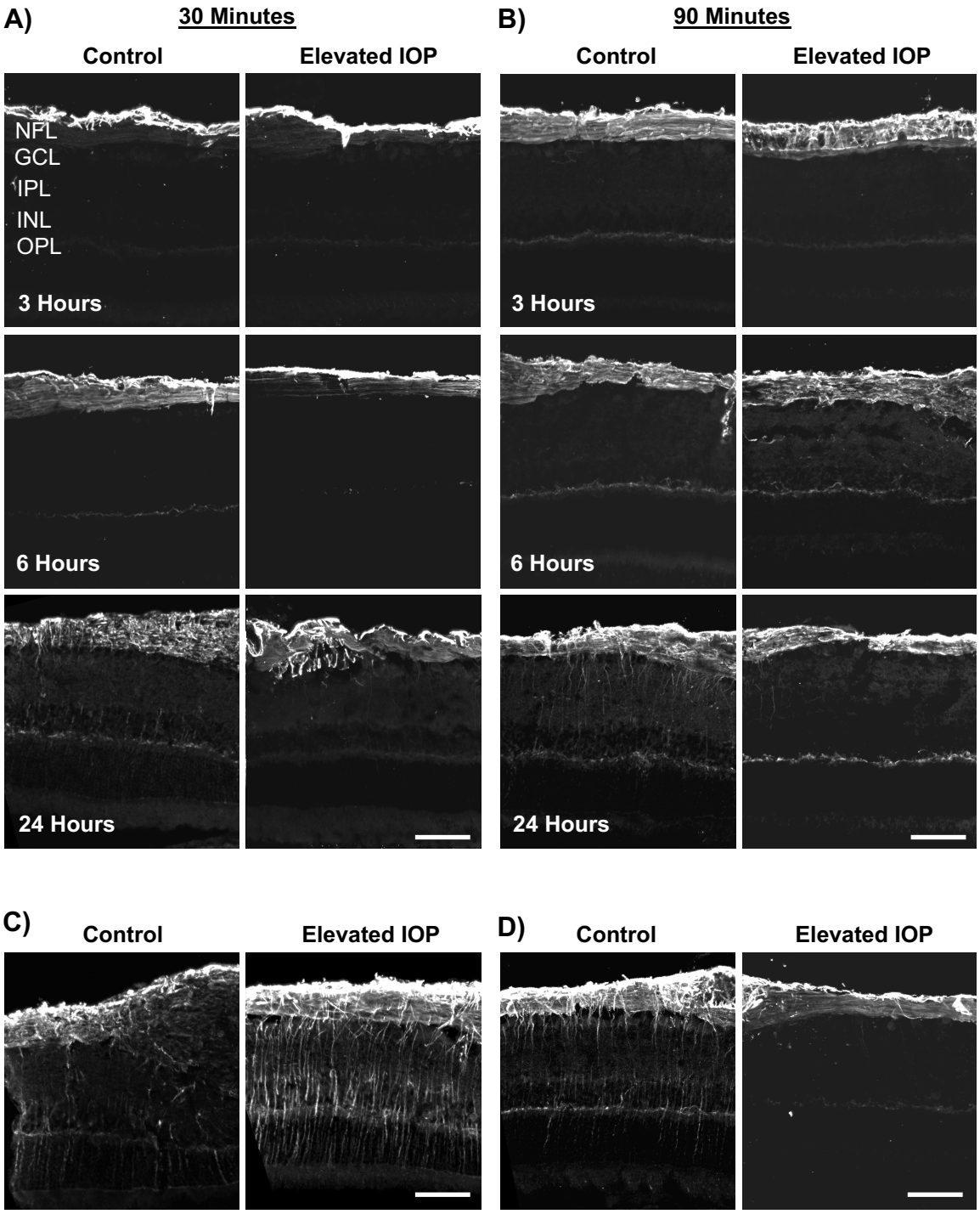
A)
30 Minutes
Control
Elevated IOP
NFL
GCL
IPL
INL
OPL
3 Hours
6 Hours
24 Hours
B)
90 Minutes
Control
Elevated IOP
3 Hours
6 Hours
24 Hours
C)
Control
Elevated IOP
D)
Control
Elevated IOP

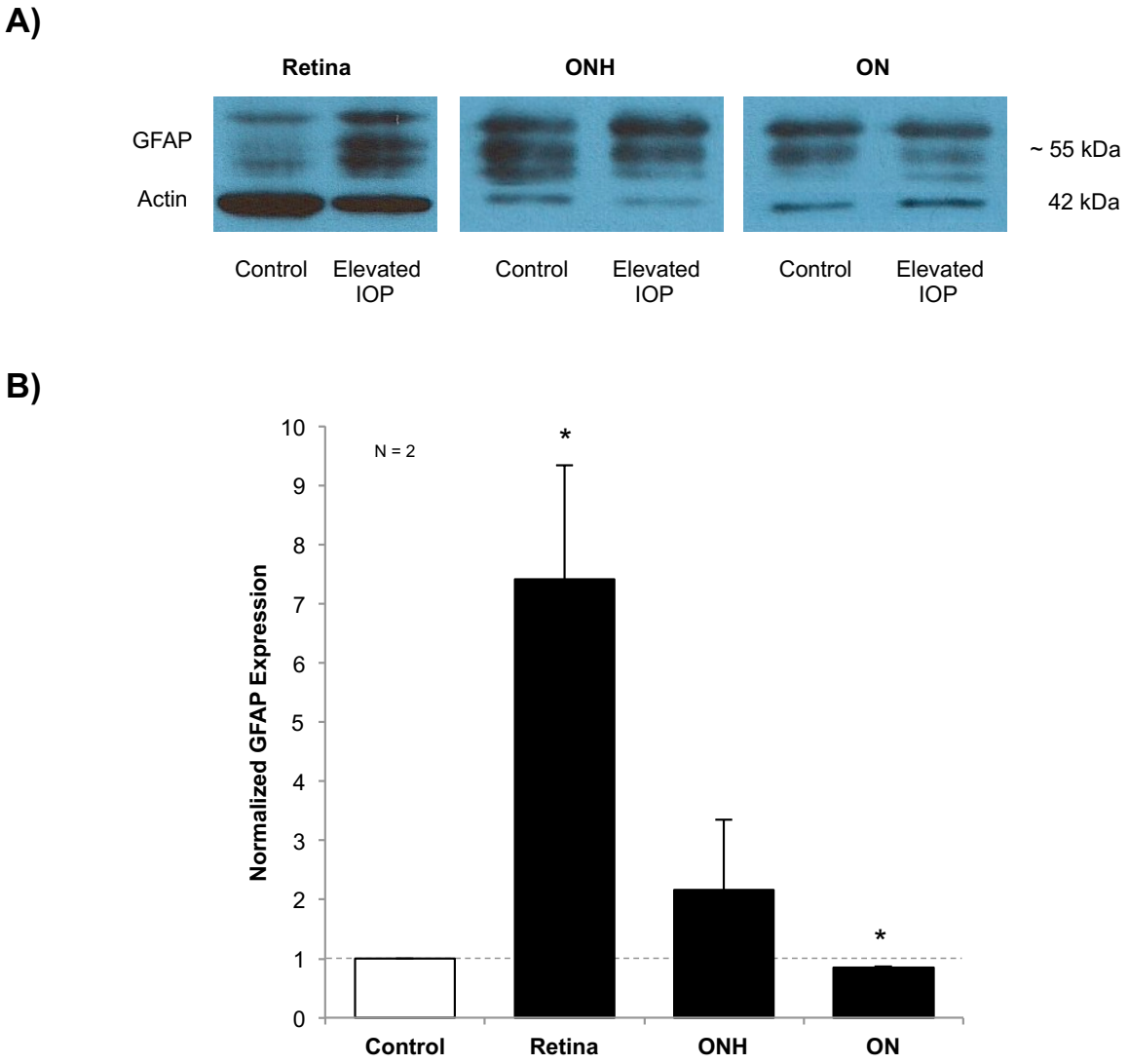

Figure 7.4 Retinal GFAP Quantification Using WB at 24 Hours Following 90 Minutes of Elevated IOP. **A)** GFAP protein was noticeably increased in the retina of experimental eyes compared to controls, while changes in the ONH and ON were less pronounced. **B)** Quantification of WB gels revealed a greater than 7-fold increase in GFAP in experimental retinas, an approximately 2-fold increase in GFAP in experimental ONHs and an approximate 15% decrease in GFAP in the remaining ON of experimental eyes. * = $p < 0.05$.

unmyelinated anterior 0.5 mm of the ON – exhibited an approximate 2-fold increase (2.16 ± 1.19), while GFAP in the following 2 mm of ON exhibited a small (15%) but significant decrease in expression (0.85 ± 0.01; $p < 0.05$; Figure 7.4 A and B).

7.3.4 Quantitative Analysis of Iba1 and GFAP Expression in the ONH Following Elevated IOP

Iba1 and GFAP labelling in the ONH (example of labelling in Figure 7.5) was quantified through sequential regions of the ONH, extending from the pre-LC region to 600 μm beyond the LC.

7.3.4.1 Description of Iba1 Labelling Within Control and Experimental ONHs

7.3.4.1.1 Thirty-Minute IOP Elevation

In the 30-minute group, the percent Iba1+ area varied significantly across ONH regions (ANOVA, $p < 0.01$) and recovery times (ANOVA, $p < 0.01$), in both control and experimental ONHs (Figure 7.6 A). Post-hoc testing revealed significant differences in the profile of Iba1+ area through the ONH between the 30min/6h and 30min/24h groups ($p < 0.01$) and the 30min/3h and 30min/24h groups ($p < 0.01$), while 30min/3h and 30min/6h groups were not significantly different ($p = 0.64$; Figure 7.6 A).

Further examination of the distribution of Iba1 labelling through the ONH revealed that, in control ONHs, the percent Iba1+ area in the pre-LC region of 30min/6h and 30min/24h groups was significantly elevated compared to the 30min/3h group (both $p < 0.05$; Figure 7.6 A, left panel). Iba1+ area was unchanged in the LC1 and LC2 regions

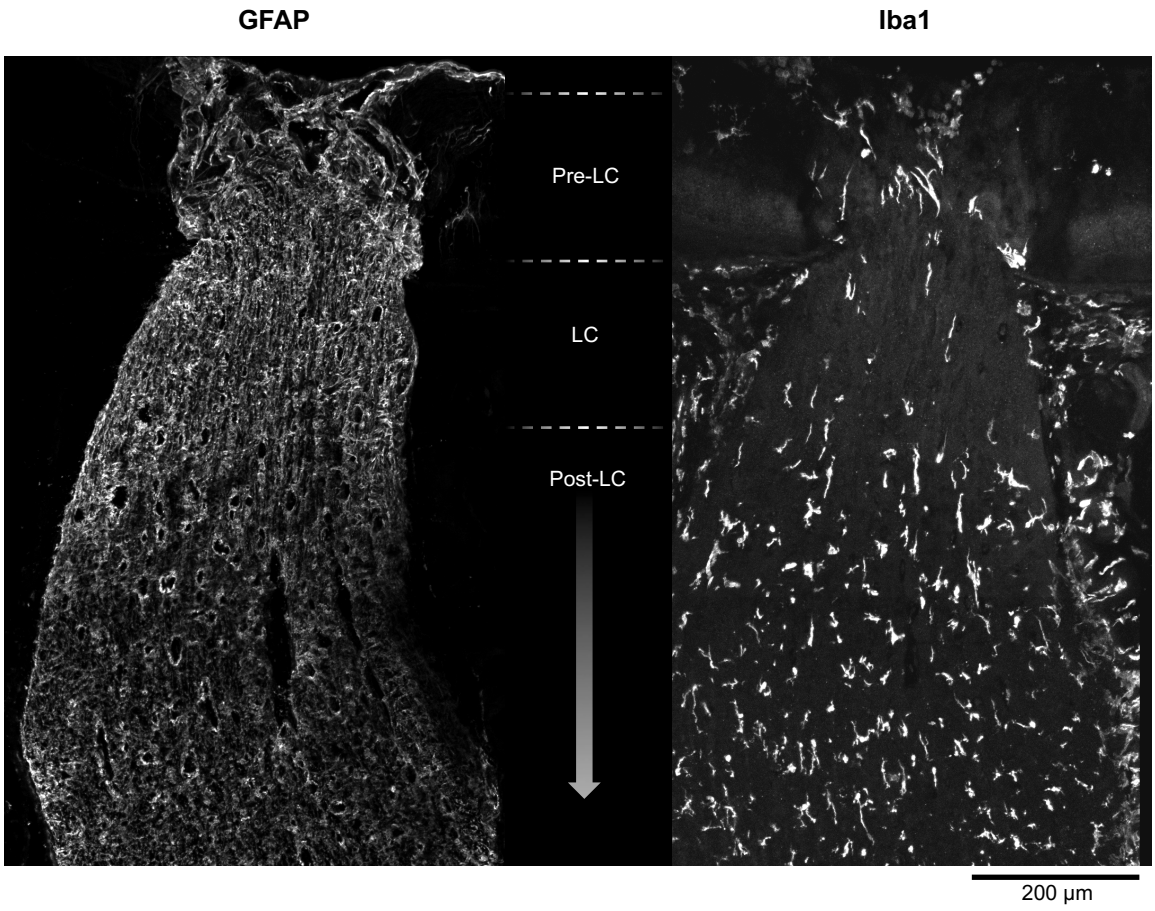

<u>Figure 7.5</u> Example Images of GFAP and Iba1 Labelling in Longitudinal Sections of Control ONHs. GFAP and Iba1 IHC, shown here in a longitudinal section of a control ONH, was used to investigate changes in ONH astrocytes and microglia, respectively, following acute elevated IOP. The intensity of GFAP labelling and the percent Iba1+ area were measured in sequential ONH sections from the pre-LC region to 600 µm beyond the LC.

over time, however, the post-200 to post-600 regions exhibited significantly more Iba1+ area in the 30min/3h and 30min/6h groups compared to the 30min/24h group (both p <0.05; Figure 7.6 A, left panel). Iba1+ area in experimental ONHs demonstrated a similar pattern of change over time, with the 30min/3h and 30min/6h groups exhibiting significantly more Iba1+ area than the 30min/24h group in the post-100 to post-600 regions (all $p < 0.03$; Figure 7.6 A, right). However, unlike the Iba1 labelling in control ONHs, the amount of Iba1+ area in LC1 and LC2 region of experimental ONHs was significantly greater in the 30min/3h group compared to 30min/6h and 30min/24h groups (both $p < 0.05$; Figure 7.6 A, right).

7.3.4.1.2 Ninety-Minute IOP Elevation

In the 90-minute elevated IOP group, the percent of Iba1+ area varied significantly across ONH regions (ANOVA, $p < 0.01$) and recovery times (ANOVA, $p < 0.01$) within both control and experimental ONHs (Figure 7.6 B). Post-hoc testing revealed significant differences in the profile of Iba1+ area through the ONH between the 90min/3h and 90min/6h groups ($p < 0.01$) and the 90min/3h and 90min/24h groups ($p < 0.01$), while the difference between 90min/6h and 90min/24h groups was not significant ($p = 0.94$).

Further examination of the distribution of Iba1 Labelling through the ONH revealed that, in control ONHs, the percent Iba1+ area from the pre-LC to post-100 regions did not change significantly over the time points examined (Figure 7.6 B, left panel). However, Iba1+ area from the post-200 to post-400 regions was significantly elevated in the 90min/6h and 90min/24h groups compared to the 90min/3h group ($p <$

0.05; Figure 7.6 B, left panel). Similarly, Iba1+ area in experimental ONHs from the LC1 to post-100 regions did not change significantly over time (Figure 7.6 B, right panel), however, was significantly elevated in the pre-LC and post-300 to post-600 regions of the 90min/6h group, and in the pre-LC and post-300 regions of the 90min/24h, compared to values from corresponding ONH regions in the 90min/3h group (all $p \leq 0.01$; Figure 7.6 B, right panel).

7.3.4.2 Comparison of Iba1 Labelling Between Control and Experimental ONHs

7.3.4.2.1 Thirty-Minute IOP Elevation

Thirty minutes of elevated IOP had no significant main effect on Iba1 labelling in the ONH (ANOVA, $p = 0.23$). However, although not significant, Iba1+ area was elevated compared to control in nearly all ONH regions (pre-LC to post-500; Figure 7.7 A). In the 30min/6h group, the percent Iba1+ area was comparable between control and experimental ONHs (Figure 7.7 B). In the 30min/24h group, the percent Iba1+ area of the LC2 region in the experimental ONH was significantly reduced compared to control ($p < 0.05$; Figure 7.7 C). Notably, Iba1+ area in the pre-LC region of both control and experimental ONHs became progressively increased relative to the LC regions over the time points examined.

7.3.4.2.2 Ninety-Minute IOP Elevation

Ninety minutes of elevated IOP had a significant main effect on Iba1 labelling in the ONH (ANOVA; $p = 0.01$). Similar to the 30-minute elevated IOP group, Iba1+ area in the pre-LC region following 90 minutes of elevated IOP increased over time in both

Figure 7.6 Change in the Percent of Iba1+ Area in the ONH Over 3, 6, and 24 Hours of Recovery Following 30 or 90 Minutes of Elevated IOP. A) Quantification of the percent Iba1+ area in sequential ONH regions over time following 30 minutes of elevated IOP. **B)** Quantification of the percent Iba1+ area in sequential ONH regions over time following 90 minutes of elevated IOP. Greyed area indicates the LC region.

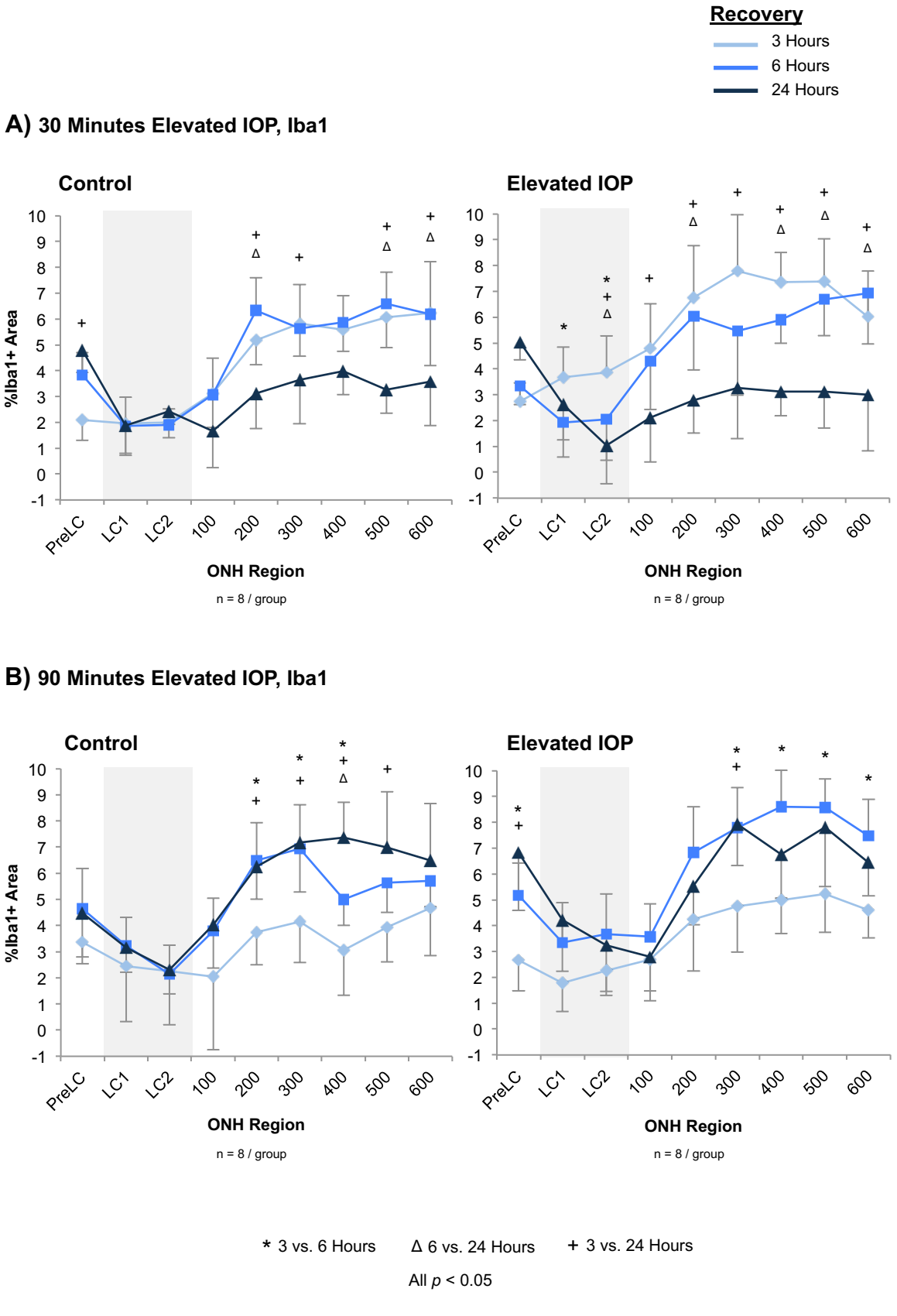
Recovery
3 Hours
6 Hours
24 Hours
A) 30 Minutes Elevated IOP, Iba1
Control
Elevated IOP
%Iba1+ Area
PreLC
LC1
LC2
100
200
300
400
500
600
ONH Region
n = 8 / group
B) 90 Minutes Elevated IOP, Iba1
Control
Elevated IOP
%Iba1+ Area
ONH Region
n = 8 / group
* 3 vs. 6 Hours
Δ 6 vs. 24 Hours
+ 3 vs. 24 Hours
All p < 0.05

Figure 7.7 Comparison of the Percent of Iba1+ Area in the ONH Between Control and Experimental ONHs at 3, 6, and 24 Hours Following 30 Minutes of Elevated IOP. A) Percent Iba1+ area in control and experimental ONHs at 3 hours of recovery. **B)** Percent Iba1+ area in control and experimental ONHs at 6 hours of recovery. **C)** Percent Iba1+ area in control and experimental ONHs at 24 hours of recovery. Greyed area indicates the LC region; * = $p < 0.05$.

30 Minutes Elevated IOP, Iba1

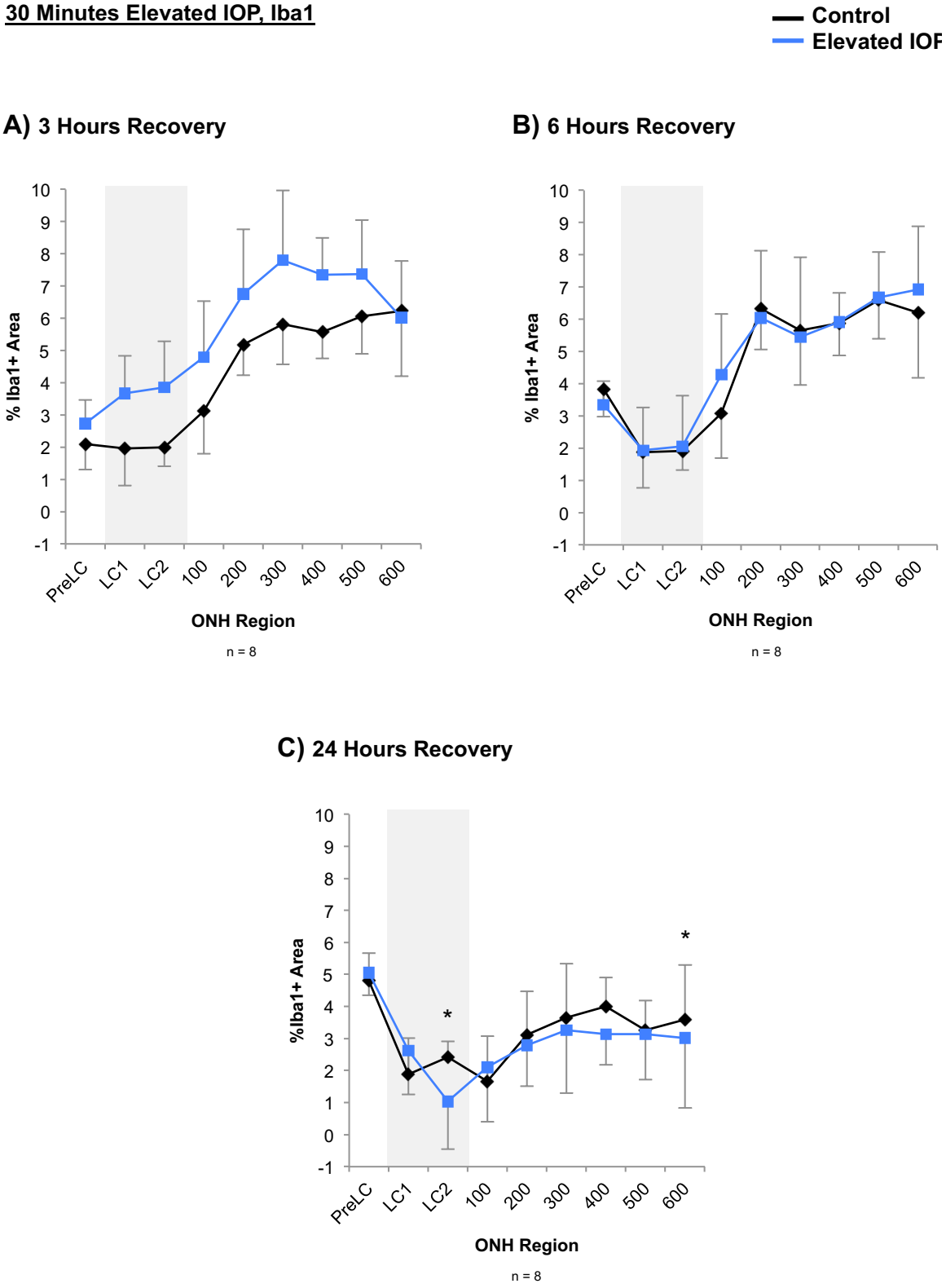

control and experimental ONHs, however this effect was more prominent in the experimental ONH (Figure 7.8 A, B and C). Iba1+ area in the 90min/3h and 90min/24h groups was not significantly different between control and experimental ONHs across any of the ONH regions (Figure 7.8 A and C). Iba1+ area in the post-400 and post-500 regions of experimental ONHs in the 90min/6h group was significantly increased compared to control levels (both $p < 0.01$; Figure 7.8 B).

7.3.4.3 Description of GFAP Labelling Within Control and Experimental ONHs

7.3.4.3.1 Thirty-Minute IOP Elevation

The intensity of GFAP labelling in the 30-minute group varied significantly across ONH regions (ANOVA, $p < 0.01$) at all recovery times and for both control and experimental ONHs (Figure 7.9 A). Labelling intensity in control ONHs increased relative to the pre-LC region, peaking in the LC1 region for all groups (30m/3h group = +10%, 30m/6h = +18%, 30m/24h = +7%) and progressively decreased through more distal ONH regions (Figure 7.9 A, left panel). In experimental ONHs, labelling intensity peaked in the LC1 region for both the 30m/3h group (+33%) and the 30m/24h group (+23%), but was highest in the pre-LC region in the 30m/6h group (Figure 7.9 A, right panel). Although the difference was not significant, GFAP intensity in the 30m/3h group was elevated across all experimental ONH regions compared to experimental ONHs of 30m/6h and 30m/24h groups (Figure 7.9 A, right panel).

Figure 7.8 Comparison of the Percent of Iba1+ Area in the ONH Between Control and Experimental ONHs at 3, 6, and 24 Hours Following 90 Minutes of Elevated IOP. A) Percent Iba1+ area in control and experimental ONHs at 3 hours of recovery. **B)** Percent Iba1+ area in control and experimental ONHs at 6 hours of recovery. **C)** Percent Iba1+ area in control and experimental ONHs at 24 hours of recovery. Greyed area indicates the LC region; ** = $p < 0.01$.

90 Minutes Elevated IOP, Iba1

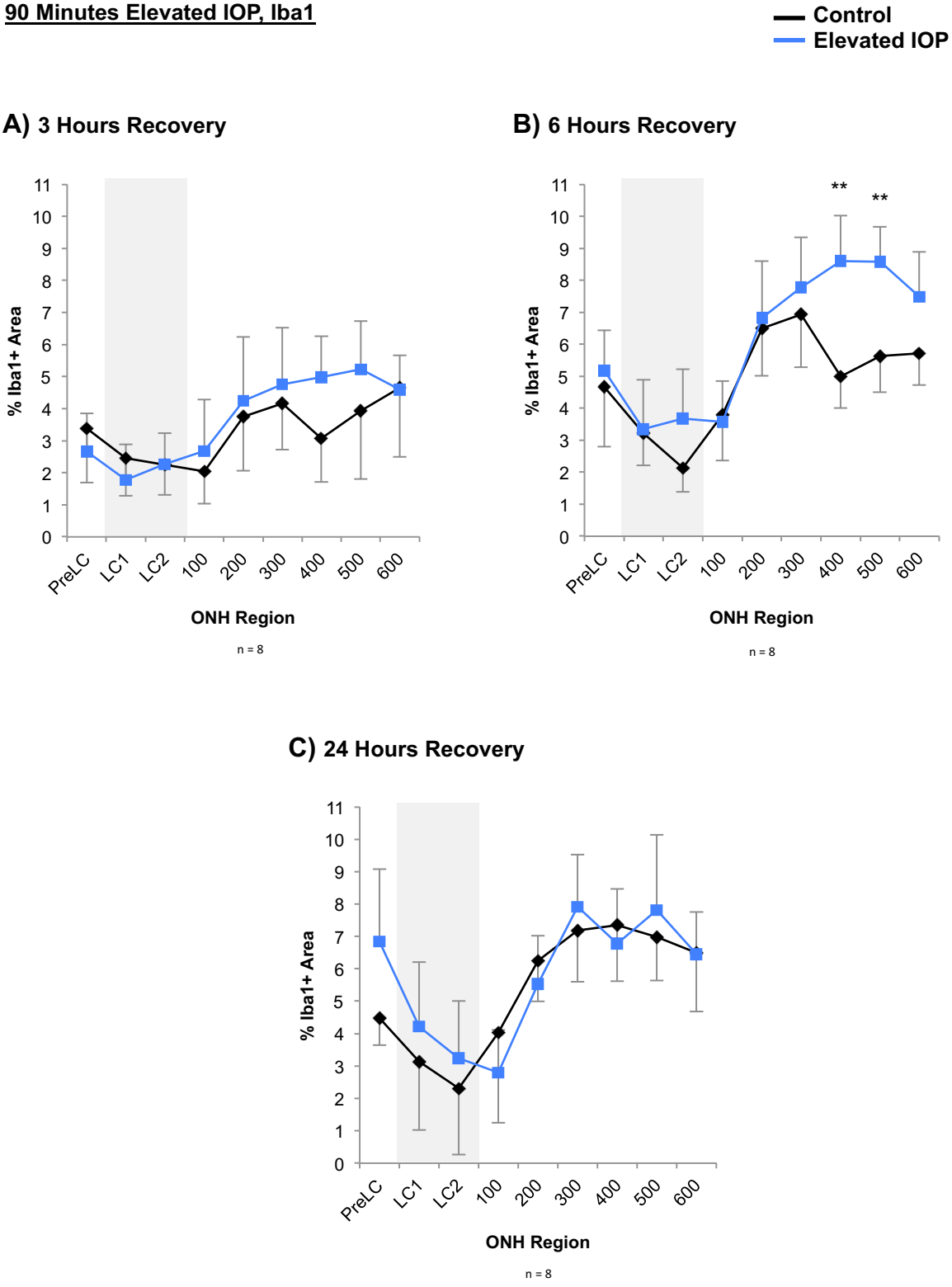

Figure 7.9 Change in GFAP Labelling in the ONH Over 3, 6, and 24 Hours of Recovery Following 30 or 90 Minutes of Elevated IOP. A) Quantification of GFAP labelling intensity in sequential ONH regions over time following 30 minutes of elevated IOP. **B)** Quantification of the GFAP labelling intensity in sequential ONH regions over time following 90 minutes of elevated IOP. Greyed area indicates the LC region; all values normalized to the pre-LC value.

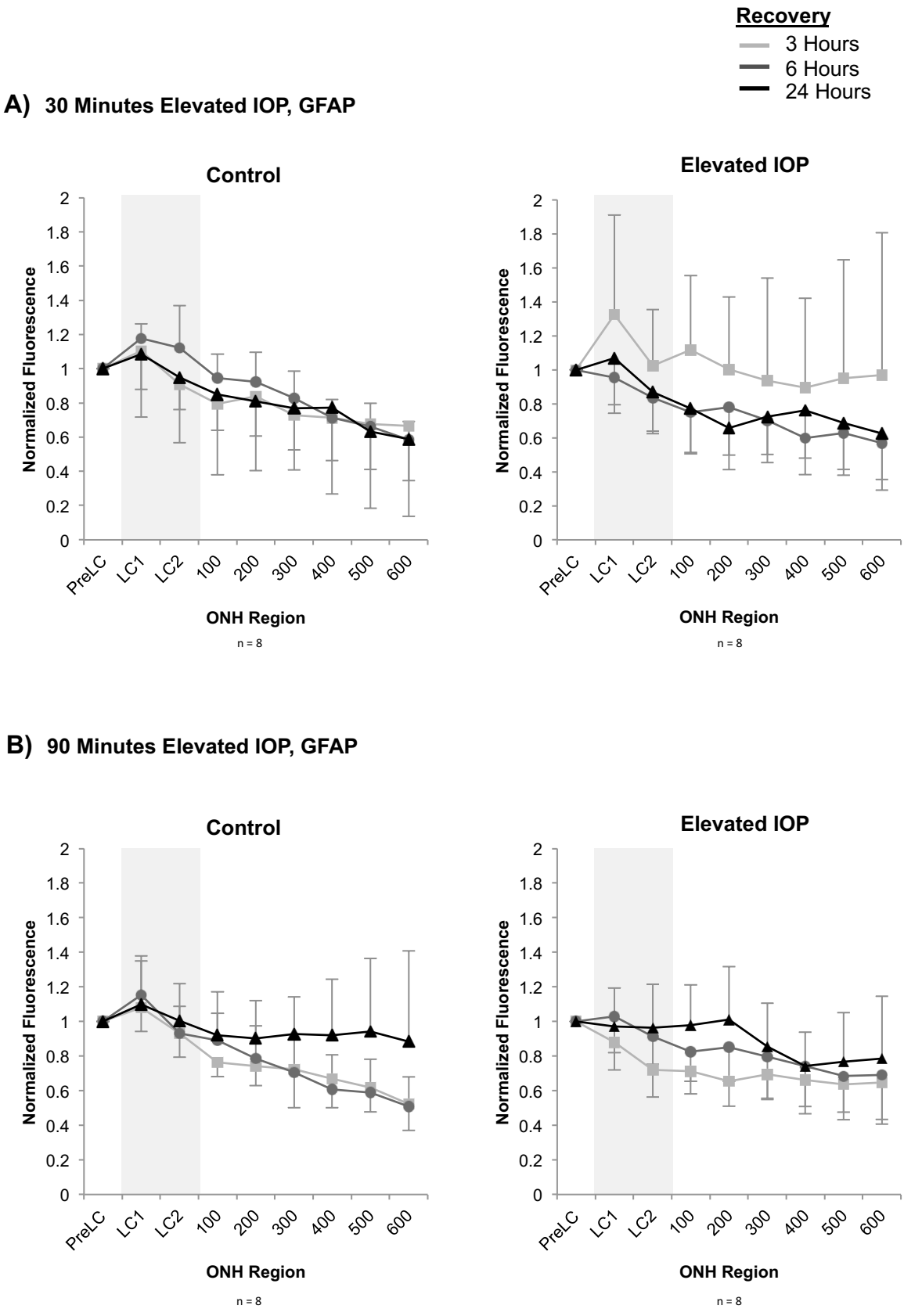
Recovery
3 Hours
6 Hours
24 Hours
A) 30 Minutes Elevated IOP, GFAP
Control
Elevated IOP
Normalized Fluorescence
0
0.2
0.4
0.6
0.8
1
1.2
1.4
1.6
1.8
2
PreLC
LC1
LC2
100
200
300
400
500
600
ONH Region
n = 8
B) 90 Minutes Elevated IOP, GFAP
Control
Elevated IOP
Normalized Fluorescence
ONH Region
n = 8

7.3.4.3.2 Ninety-Minute IOP Elevation

The intensity of GFAP labelling in the 90-minute group varied significantly across ONH regions (ANOVA, $p < 0.01$) at all recovery times and for both control and experimental ONHs (Figure 7.9 B). Labelling intensity in control ONHs increased relative to the pre-LC region, peaking in the LC1 region for all groups (90m/3h group = +8%, 90m/6h = +15%, 90m/24h = +10%) and progressively decreased through more distal ONH regions (Figure 7.9 B, left panel). In experimental ONHs, labelling intensity peaked in the LC1 region only in the 90m/6h group (+3%), while GFAP intensity was greatest in the pre-LC region for the 90m/3h group, and in the post-200 region for the 90m/24h group (+1%) (Figure 7.9 B, right panel).

7.3.4.4 Comparison of GFAP Labelling Between Control and Experimental ONHs

7.3.4.4.1 Thirty-Minute IOP Elevation

There was no significant main effect of 30 minutes of elevated IOP (ANOVA, $p = 0.23$) and no significant interaction between recovery time and elevated IOP (ANOVA, $p = 0.20$) on GFAP labelling intensity. Although the differences were not significant, GFAP labelling intensity was elevated in all experimental ONH regions compared to control in the 30m/3h group (Figure 7.10 A). Contrary to this, GFAP intensity was decreased from the LC1 to post-500 regions in the 30m/6h group (Figure 7.10 B). There was little difference between control and experimental intensity values in all ONH regions of the 30m/24h group (Figure 7.10 C).

Figure 7.10 Comparison of GFAP Labelling Between Control and Experimental ONHs at 3, 6, and 24 Hours Following 30 Minutes of Elevated IOP. A) GFAP labelling intensity in control and experimental ONHs at 3 hours of recovery. **B)** GFAP labelling intensity in control and experimental ONHs at 6 hours of recovery. **C)** GFAP labelling intensity in control and experimental ONHs at 24 hours of recovery. Greyed area indicates the LC region; all values normalized to the pre-LC value.

30 Minutes Elevated IOP, GFAP

Control
Elevated IOP

A) 3 Hours Recovery

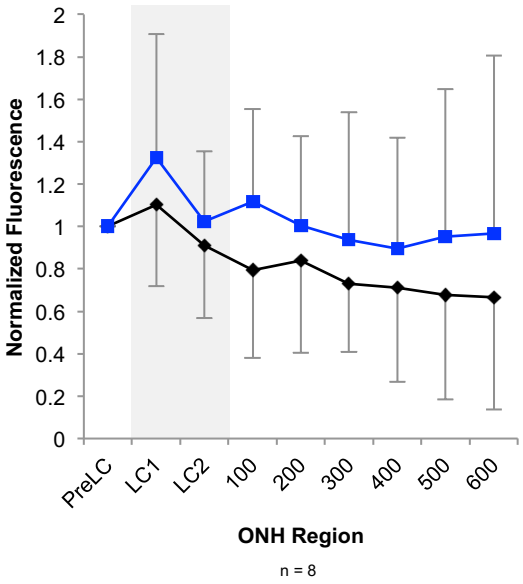

n = 8

B) 6 Hours Recovery

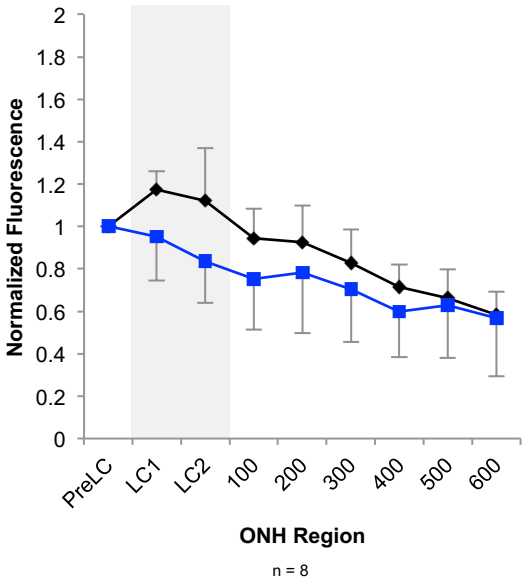

n = 8

C) 24 Hours Recovery

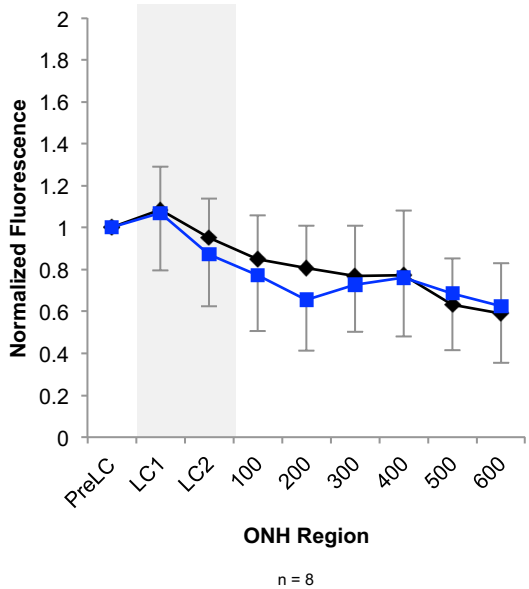

n = 8

7.3.4.4.2 Ninety-Minute IOP Elevation

There was no significant main effect of 90 minutes of elevated IOP (ANOVA, p = 0.62) and no significant interaction of recovery time and elevated IOP (ANOVA, p = 0.67) on GFAP labelling intensity. However, GFAP intensity was significantly reduced in the LC1 and LC2 region in 90m/3h group (both $p < 0.05$; Figure 7.11 A). No significant differences or notable trends between control and experimental intensity values were observed in the 90m/6h and 90m/24h groups (Figure 7.11 B and C).

7.3.5 Iba1 and GFAP Labelling in the ONH Following Sham Elevated IOP

The percent Iba1+ area in sham-injured ONHs was not significantly different from the percent Iba1+ area measured in control ONHs at any of the ONH regions examined (Figure 7.12 A). While GFAP labelling intensity in sham ONHs was not significantly different from control values in the LC1 and LC2 regions, GFAP intensity in the experimental ONH appeared reduced from the post-200 to the post-600 region (post-200: $p < 0.01$; Figure 7.12 B).

Figure 7.11 Comparison of GFAP Labelling Between Control and Experimental ONHs at 3, 6, and 24 Hours Following 90 Minutes of Elevated IOP. A) GFAP labelling intensity in control and experimental ONHs at 3 hours of recovery. **B)** GFAP labelling intensity in control and experimental ONHs at 6 hours of recovery. **C)** GFAP labelling intensity in control and experimental ONHs at 24 hours of recovery. Greyed area indicates the LC region; all values normalized to the pre-LC value; * = $p < 0.05$.

90 Minutes Elevated IOP, GFAP

Control
Elevated IOP

A) 3 Hours Recovery

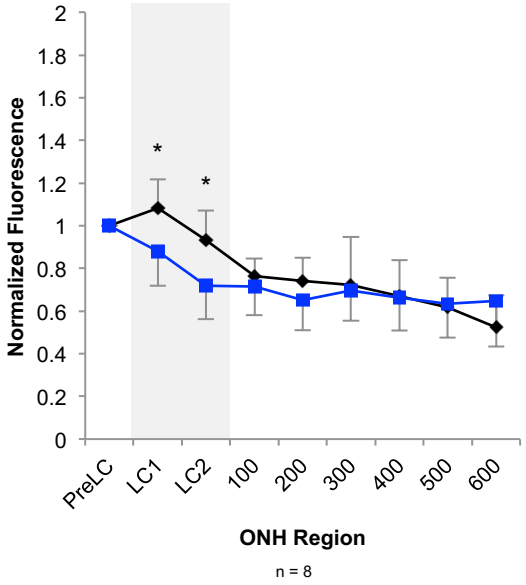

B) 6 Hours Recovery

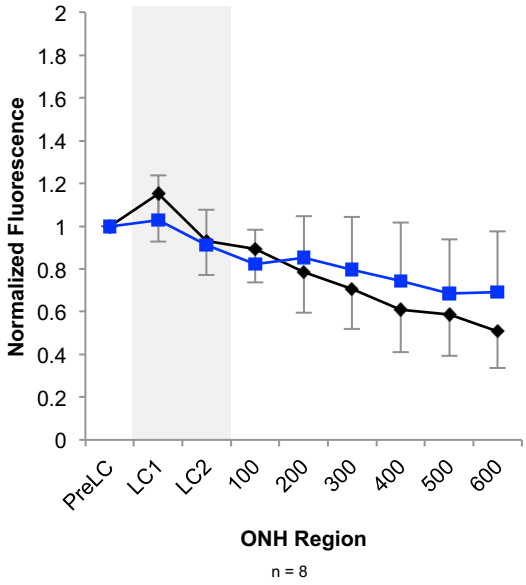

C) 24 Hours Recovery

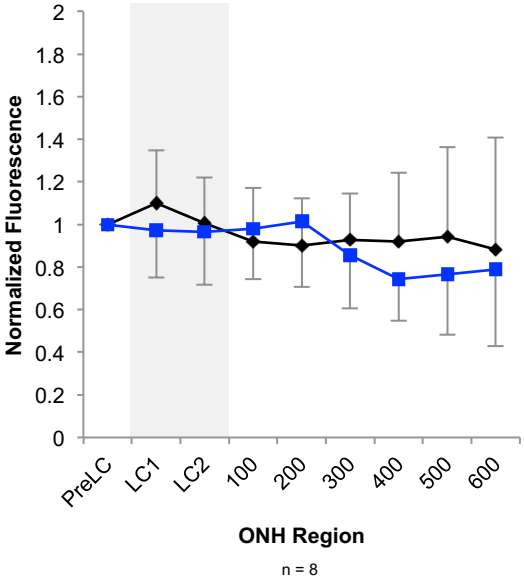

Sham 90 Minutes Elevated IOP, 24 Hours Recovery

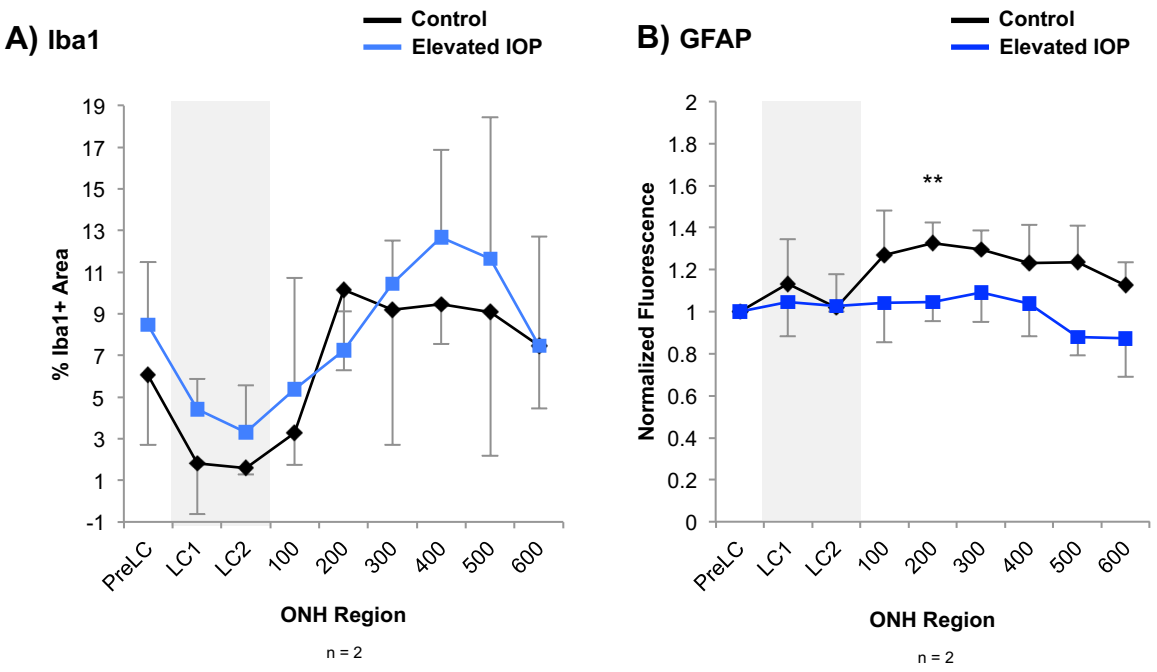

Figure 7.12 Comparison of Iba1 and GFAP Labelling Between Control and Sham ONHs at 24 Hours Following 90 Minutes of Elevated IOP. A) Percent Iba1+ area in control and sham ONHs. **B)** GFAP labelling intensity in control and sham ONHs. Greyed area indicates the LC region; GFAP values normalized to the pre-LC value; ** = $p <$ 0.01.

7.4 Summary and Key Findings

These experiments highlight the time course of some of the early responses of retinal and ON glia in response to a transient elevated IOP.

Key findings include:

1) Thirty minutes of elevated IOP had only mild effects on retinal microglia, while 90 minutes of elevated IOP caused an immediate microglial response that progressed over time.
2) Apart from an increase in retinal GFAP protein at 24 hours following 90 minutes of elevated IOP, responses of Müller cells and/or astrocytes were either not pronounced, or not readily distinguishable using the methods and time points of the present experiments.
3) Microglia of contralateral retinas and ONHs showed similar, albeit blunted, responses to both 30- and 90-minute insults.
4) The glial response in the retina following transient elevated IOP is different from that observed in the ONH.

Together, these findings demonstrate that microglial activation is an early indicator of damage to the retina and ONH; however, there is considerable variability in the responses of glia in the retina and ONH to a transient elevation of IOP. Further implications of these findings are discussed in Chapter 8.7.

CHAPTER 8 – DISCUSSION

8.1 Overview

This thesis has provided novel insight into the pathophysiological mechanisms underlying RGC loss following acute elevated IOP, and has also advanced current knowledge of experimental techniques for evaluating AT function in the rat visual system. While many previous studies have examined functional and structural changes in RGCs during prolonged periods of elevated IOP, few have examined their progression over a period of recovery following a transient IOP elevation. The current experiments examined functional and structural changes in RGCs and surrounding glia following two different durations of IOP elevation, i.e., 30 and 90 minutes, which represent either a sub-critical or critical insults, respectively. The purpose of this comparison was to examine cellular responses over time in the retina, ONH, and ON that are associated with either RGC survival or death following elevated IOP.

Both RITC and fluorescently conjugated CTB have been previously applied to trace AT in the rat visual system. While RITC is visualized in RGC axonal profiles in the ON following anterograde application [157, 195, 198, 225, 335, 336], description of retrogradely-transported RITC has been primarily isolated to the intra-retinal compartments of RGCs [195, 198, 337, 338]. Qualitative description of retrograde CTB AT in RGCs is similarly limited. The experiments described in Chapter 3 ("Characterization of RITC and CTB for Tracking AT in RGCs") are likely to represent the first qualitative description of the spatiotemporal labelling qualities of retrogradely transported RITC and CTB in the ON. These experiments, as well as those described for anterograde AT of CTB in Chapter 5 ("Anterograde AT in RGCs Following Elevated

IOP"), have also provided updated estimations of the transport rates of both RITC and CTB. CTB was selected as the ideal tracer for subsequent investigation of AT function (Chapters 4 and 5). Key findings from the tracer characterization studies are discussed in section 8.2.

The experiments described in Chapter 4 ("Retrograde AT in RGCs at 3, 7, and 14 Days Following Elevated IOP") provide important information regarding the onset and progression of AT dysfunction in RGCs following exposure to acute elevated IOP. It was demonstrated that retrograde AT disruption in RGCs following 90 minutes of elevated IOP can manifest in more than one intracellular location – in addition to AT blockade at the ONH, a finding that is strongly supported in previous literature [129, 131], CTB transport was significantly reduced throughout the ON of the experimental eye, indicating a source of AT dysfunction in the distal RGC axon. AT disruption in the distal axon was also evident following 30 minutes of elevated IOP, although to a lesser extent, while there was no evidence of retrograde AT blockade at the ONH. Retrograde AT disruption progressed over time following 90 minutes of elevated IOP, however, neither progressed nor recovered following 30 minutes of elevated IOP. These findings provide clues regarding the onset and progression of AT dysfunction in RGCs in response to elevated IOP, and the nature of RGC vulnerability and death in general – topics that are discussed further in sections 8.4 and 8.8, respectively.

The experiments described in Chapter 5 ("Anterograde AT in RGCs at 3, 6, and 24 Hours Following Elevated IOP") elaborated upon those in Chapter 4 ("Retrograde AT in RGCs at 3, 7, and 14 Days Following Elevated IOP") by examining AT function at earlier time points following transient IOP elevation. Since no transient blockade of

retrograde AT was observed from 3 to 14 days following 30 minutes of elevated IOP, it was hypothesized that a transient blockade in AT function may occur closer in time to IOP elevation (i.e. within 24 hours). Unexpectedly, the effects of elevated IOP of anterograde AT at early time points were similar to those of retrograde AT at later time points: 30 minutes of elevated IOP caused a mild disruption of AT that did not progress over time, whereas 90 minutes of elevated IOP caused a more pronounced disruption that worsened over 24 hours. Furthermore, these experiments elucidated the spatiotemporal patterns of RGC loss within the first 24 hours following elevated IOP. The implications of these findings are discussed in sections 8.4, 8.7 and 8.8.

Finally, the progression of both AT and cytoskeletal changes in RGCs, as well as local changes in retinal and ONH glia, have never been simultaneously investigated over time following elevated IOP. The experiments in Chapters 6 ("NF Regulation in the Retina and ONH Following Elevated IOP") and 7 ("Glial Activation in the Retina and ONH Following Elevated IOP) were designed to study the progression of RGC and glial pathologies, as well as their capacity for recovery, over a 24-hour period following elevated IOP. Thirty minutes of elevated IOP was found to have little effect on retinal NFs and glia. On the contrary, 90 minutes of elevated IOP resulted in the rapid development of NF pathology and microglial activation in the retina. NFs in the ONH displayed a trend towards dephosphorylation following both durations of elevated IOP. Additionally, microglial area in the ONH changed over time following 30- and 90-minutes of elevated IOP, although the spatiotemporal pattern of microglial changes differed between insult duration. Interestingly, both durations of elevated IOP induced changes in microglia in both contralateral and experimental ONHs. The results from the

studies of NFs and glia are discussed in sections 8.5 and 8.6, respectively. The spatiotemporal integration of findings from the AT, NF, and glia studies is discussed in section 8.7.

8.2 RITC and CTB as Tracers of AT in the Rat Visual System

Fluorescent tracers have been, and continue to be, useful agents for examining AT function in neurons, and their application has advanced current knowledge regarding the pathophysiological effects of elevated IOP on RGCs. The tracer characterization experiments described in Chapter 3 have provided novel information regarding the uptake dynamics, transport rates and labelling qualities of RITC and CTB. The impact of these findings, as well as the value of these tracers in the context of their use in the rat visual system, is discussed in the following sections.

8.2.1 Factors Affecting the Speed and Uniformity of RITC and CTB Uptake and Transport in RGCs

Following application at the SC, the fluorescence intensity of both RITC and CTB in the ON, ONH and retina increased gradually over time, eventually reaching a peak, and either plateauing or declining thereafter. Similarly, intensity of anterogradely transported CTB in the ON continued to increase until 3 days following application. Two factors likely affecting the speed with which tracers are taken up and transported to RGC somas are: 1) the method of surgical application (injection, gelfoam pledget, etc.); and 2) the rate and range of diffusion over, or into, the target tissue following application. Contributing

to the uptake dynamics following application at the SC are the quality of surgical dissection (when using gelfoam tracer application); the number, speed and angle of injections; and the concentration, composition and volume of tracer solution, among others factors. The location, angle, and depth of needle entry and speed of ejection likely also play a role in tracer uptake following intravitreal injections, in addition to the volume and composition of the tracer solution. In an effort to reduce intra- and inter-animal variability in the present study, care was taken to optimize and maintain consistency of these factors. As such, the gradual increase in fluorescence observed in the ON, ONH and retina likely reflects the time taken for the tracer to passively diffuse across the application site. Indeed, a previous study in rats reported a similar lag time between the application of CTB at the retina and its detection in the ON [206].

Some degree of non-uniformity (i.e. certain RGCs filling with tracer before others) was seen at early time points in both the RITC and CTB retrograde time course experiments; however, CTB labelling, but not RITC labelling, remained non-uniform in the retina even at later time points, suggesting that injection of tracer into the SC, as opposed to placing a tracer-soaked gelfoam on its surface, may result in less homogeneous uptake across the RGC population. Indeed, Abbott and colleagues [206] found good agreement between the degree of CTB diffusion from injection sites in the SC, and the amount and uniformity of RGC labelling in the retina. To remedy this, it may be feasible to apply CTB to the SC by way of gelfoam pledget; however, a much larger volume of tracer would be needed and, given the relatively high cost of CTB fluorescent conjugates, would be a considerably less economical approach than stereotaxic injection. Other ways to promote homogeneous labelling of the RGC population with CTB could

include increasing the number of injections, or adding an organic solvent, such as dimethyl sulfoxide (DMSO), to the tracer solution to facilitate diffusion from the injection site(s). Full field images of the surface of the SC [206] may provide a good measure of diffusion and ensure that an absence of tracer in the RGC axon or soma is not due to lack of diffusion at the application site. Following anterograde application, dispersion of CTB across the retina from the site of intravitreal injection remained incomplete up to 6 hours following application. Certain adjustments, such as increasing needle gauge [339] or changing the type of needle [340] for intravitreal injection may improve dispersion of CTB through the vitreous and increase the area of retina exposed to the tracer.

Finally, beyond the aforementioned technical variables impacting tracer uptake and transport in RGCs, it may also be possible that RGCs are inherently heterogeneous in their uptake efficiency and rate of AT. Greater surface area of the RGC plasma membrane – either at their somas and axons in the eye, or at their terminals in the SC – might increase the rate and volume of tracer uptake. Furthermore, greater numbers of microtubules (associated with larger axons [341, 342]) may lead to a higher rate of AT. There is indeed variation in the size of RGC somas, dendrites, axons, and terminals. For instance, alpha RGCs have larger diameter somas, dendrites and axons than beta RGCs [15]. Additionally, while RGC axons in the ON are, on average, 0.7 μm in diameter, regardless of species, some subtypes can exceed 3.5 μm [343]. Akin to their adjoining axons, RGC terminal arbours in the SC are also proposed exhibit a range of sizes [343].

8.2.2 Rates of RITC and CTB Transport in RGC Axons

In the present study, retrograde AT of RITC was found to progress at a rate of approximately 60 mm/day. The only other report of the rate of retrograde AT of RITC in the ON is in chicken and approximately 5 mm/day [198]), considerably slower than the present estimate. Given that rates of AT within a species can vary significantly with age [344], it is likely that such differences also exist between species. Differences in the rate of AT also appear to be tracer specific, as the rate of retrograde AT of CTB from the present experiments was much greater than that of RITC, potentially exceeding 200 mm/day. Interestingly, the latter estimate is comparable to a previous estimate of retrograde CTB AT rate, also in rat, of 136-191 mm/day [206]). Finally, the estimation of the CTB anterograde AT rate in RGCs obtained in the present study (64-88 mm/day) was also comparable to a previous study in rat (80-90 mm/day; Abbott et al., 2013). Updated retrograde and anterograde AT rates for RITC and CTB are summarized in Table 8.1.

The origins of tracer-specific differences in AT rates are unknown; however, they could result from differing methods of application (as described above) or differences in their tissue permeability and method of uptake. CTB fluorescent conjugates are water soluble and applied to tissue as an aqueous solution, while RITC is hydrophobic and requires use of a water-miscible organic solvent (e.g. DMSO) to dissolve into solution. Such differing solubility is likely to affect penetration into, and diffusion though, the target tissue to reach sites of absorption on the RGC membrane. Furthermore, while both CTB and RITC are known to enter neurons via endocytosis, their specific endocytotic mechanisms are different [345]. A combination of the method of tracer application, permeability and uptake mechanism likely contributes to the differences in AT rate

Table 8.1 Updated Estimations of RITC and CTB AT Rates in the Rat Visual Pathway

	Anterograde	**Retrograde**
RITC	10 mm/day (source: Thanos and colleagues [195])	60 mm/day (source: A.Nuschke, 2016)
CTB	64-90 mm/day (source: A.Nuschke, 2016; Abbott and colleagues [206])	136-200 mm/day (source: A.Nuschke, 2016; Abbott and colleagues [206])

observed between CTB and RITC, and between many other tracers previously described for use in the visual system [194, 206, 285, 346].

8.2.3 Advantages and Disadvantages of RITC and CTB Tracers

Compared to RITC, CTB consistently provided brighter and more complete labelling in the soma, dendrites, axon and terminals of RGCs. Following retrograde application, RITC was not easily visible in axons within the ON, and while it did fill somas and dendrites, the labelling was often incomplete – many soma profiles were only partially visible, and only primary dendrites were labeled. Contrary to this, CTB was easily visualized in the axon, soma and dendrites, and appeared to fill all compartments completely, allowing superior morphologic characterization and a more inclusive report of AT function throughout the RGC. These results are consistent with previous studies describing the quality of axonal tracing with RITC and CTB [195, 201]. Anterograde labelling of axons in the ONH and ON with CTB was discernable in a matter of hours following intravitreal injection and became brighter over time, allowing evaluation of anterograde AT function in RGC axons from the ONH to the chiasm.

Retrograde application of both RITC and CTB offers the added advantage of labelling intact RGC somas that can then be quantified in studies of RGC damage, with little to no leaking of the tracer from the tissue post-mortem [198]. Indeed, CTB does fill the cytosol of RGC somas and dendrites brightly and completely. Bright axonal CTB labelling could interfere with quantification of RGC somas in the central retina, however this can be circumvented through the use of optical sectioning below the level of the NFL when imaging [197]. Retrograde identification of RGCs with RITC, on the other hand,

often requires co-localization with a nuclear marker for quantification, as filling of the cytosol is often incomplete, making it difficult to distinguish some cells from background or debris [197]. Unfortunately, application of CTB via intravitreal injection to characterize anterograde AT produced intense and non-specific labelling in the retina that interfered with visualization of RGC somas and intra-retinal axon structure. Hence, when CTB is applied intravitreally, alternative methods to identify RGCs would be required.

8.2.4 Summary of RITC and CTB Tracer Characterization

The characterization studies in this thesis have added support to the value of RITC and CTB as fluorescent tracers of AT in the rat visual pathway, and have also highlighted some variables that should be considered in their use. Specifically, it is not only the rate of AT of individual tracers that dictates the timing of their progression through the axon, but also their uptake dynamics at the site of application. Because tracers are not immediately taken up and transported by the entire RGC population, the time to peak fluorescence in the ON following either retrograde or anterograde application can take several hours or days. This lag-time should be considered in AT studies when examining early time points, although the internal validity of the results should not be affected as long as proper time-matched or paired controls are included for comparison. Methods to optimize tracer dispersion at the application site could improve the timing and uniformity of transport throughout the RGC population. The present time course studies have also provided updated estimations of RITC and CTB AT rates in rat RGCs, and represent the first qualitative assessment of retrogradely transported RITC and CTB in the ON. Finally, while visibility of RITC+ RGC axons in the ON is poor following retrograde

application, fluorescently conjugated CTB provided bright and easily visualized labelling in RGC axons, regardless of transport direction. For that reason, CTB was determined to be the superior tracer for examining AT function in later studies of elevated IOP.

8.3 Considerations Regarding Variation in Animal Models of Elevated IOP

Considerable knowledge of the mechanisms of pressure-induced RGC death has been gained over the past few decades in experimental animal models. These models, introduced in section 1.4.2, induce either acute or chronic elevations of IOP. Numerous methods of induction have been developed, each exhibiting variation from multiple sources that can impact study outcomes. Sources of variation include, but are not limited to: the species, strain and age of the animal; the experimental method for IOP elevation; and the duration and magnitude of IOP elevation. This variation across models can be considered advantageous as it allows investigators to study a range of RGC responses to elevated IOP, as well as the degree to which individual factors contribute to RGC survival. Integrating findings across studies enriches the global understanding of the RGC response to elevated IOP; however, investigators should be mindful of inter-study variation and censor their interpretations accordingly. Relevant inter-study differences are addressed throughout this thesis, where appropriate. The purpose of this section is to highlight pertinent sources of variation between studies of elevated IOP, and to provide a perspective on the spectrum of models and techniques that exist in this field, and that are referred to frequently in subsequent discussions.

8.3.1 Species Used in Studies of Elevated IOP

Initial studies of experimentally elevated IOP were conducted in non-human primates [330, 347, 348]. It is well established that primates exhibit a high degree of genetic homology to humans, and that the study of primate models yields information that is highly relevant to human disease [50]. However, primate models also present significant challenges – namely high cost and lack of availability [50]. Models of experimentally elevated IOP have since been developed in numerous other species, including rabbit [349, 350], pig [157, 225, 351], ferret [352], rat [146, 150, 153, 259, 353, 354] and mouse [146, 148, 355-358]. Each species exhibits unique retinal and ON anatomy and physiology that undoubtedly influences how their RGCs are affected by elevated IOP [359]. Furthermore, strain differences within species can also be a source of significant variation [149, 360].

8.3.2 Species- and Strain-Specific Variation in Retinal Blood Supply and ONH Structure

Because ischemia and mechanical stress are crucial contributors to RGC damage secondary to elevated IOP, species- and strain-specific differences in vascular anatomy and structure of the retina and ONH are likely to impact the susceptibility RGCs.

Differences in the position of retinal vessels in the ON as they pass through the scleral canal opening – in the centre of the ON in primates, and near the inferior pole in rodents – may result in differing topological patterns of RGC loss [359, 361]. Indeed, the presence of retinal vessels in the inferior ON, positioned between RGC axons and the ON

sheath, was postulated to be the reason for sectorial RGC loss (greater in the superior quadrant) in both mouse [361] and rat [259] models of elevated IOP, either by shielding axons in the inferior ON from the biomechanical strain of the adjacent sclera, or by providing greater local metabolic support [361]. Primates, on the other hand, have been shown to exhibit the greatest loss of RGC axons in both the superior and inferior poles of the ON [362]. The diversity of the retinal and ONH blood supply between species and strains is substantial [359, 363] and should be considered in studies where elevated IOP affects retinal and ONH perfusion.

The structure of the ONH also varies across species and strains. Humans and non-human primates exhibit a collagenous and substantially fibrous LC, while the LC structure of mice is purely glial. The rat LC is primarily glial, but can contain varying levels of structural fibres, depending on strain [359]. Due to the supportive function of the structural LC on passing axon bundles, it is likely that species and strains exhibiting different LC structure may be differentially susceptible to mechanical insult at the ONH [215, 355, 364]. Finally, the position where RGC axons become myelinated in the ON varies with species – in human and non-human primates, RGC axons become myelinated immediately posterior to the LC, while those of rats remain unmyelinated for and additional 0.5-1 mm [63, 353] posterior. The onset of myelination in the ON is an important anatomical consideration in studies examining AT function in response to elevated IOP, as AT blockades have been reported to spatially coincide with the unmyelinated zone [63, 130]. Indeed, such an observation was made in the present thesis, and is discussed in section 8.4.1.

8.3.3 RGC Susceptibility to Damage Varies with Species, Strain, and Age

Some studies have explicitly investigated the relative susceptibility of RGCs to elevated IOP between animals of different species, strains and ages. Tan and colleagues [290] used anterior chamber cannulation to demonstrate that rats aged 2 months did not exhibit cell loss in the GCL until IOP was increased to 90 mmHg, whereas rats aged 18 months showed significant loss at an IOP of 45 mmHg. Another study found that mice of different strains and ages differed in the amount of ocular elongation and RGC damage they exhibited in response to elevated IOP [149]. Finally, species- and strain-specific differences in the expression of melanin, a pigment molecule produced by melanocytes, has been associated with different degrees of damage following retinal insult – specifically, pigmented animals appear more resilient to retinal damage [365-368], potentially due to melanin's antioxidant activity [369]. It is clear from these studies that the choice of species, strain, and age of animal models can have tangible consequences on the susceptibility of RGCs to experimentally elevated IOP.

8.3.4 Variation in Techniques to Elevate IOP

Experimental techniques to induce elevated IOP vary widely (previously introduced in section 1.4.2), and can be grossly categorized into either chronic or acute in duration.

Briefly, techniques used to elevate IOP in chronic models include sclerosis of the episcleral veins with hypertonic saline [259, 370], laser photocoagulation of the trabecular meshwork [260], laser photocoagulation or cauterization of limbal and/or

episcleral veins [274, 371, 372], and injection of polystyrene [146] or magnetic [150] microbeads into the anterior chamber to block aqueous outflow. These models produce a range (from 5-50 mmHg) and duration (from 3 days to several months) of IOP elevation, and exhibit significant variability, even between studies employing the same technique [355]. Furthermore, different strains of mice have been shown to exhibit differing aqueous outflow facility [373], indicating that any given IOP-elevating technique may produce different effects in different mouse strains.

Contrary to chronic models, acute IOP elevation by anterior chamber cannulation is reproducible and comparable between studies. Although the severity of the insult, and the resulting damage, is often not considered to be physiological in reference to human disease, the titratable control offered by this model allows comprehensive investigation of the relationship between the degree and duration of IOP elevation and important aspects of RGC physiology, such as retinal and ONH perfusion [183], ONH biomechanical strain [165, 374, 375], RGC function [154, 312, 376-378], and the degree of RGC loss itself [264]. The application of this model in the present study allowed for controlled examination of the cascade of events following two distinct, previously characterized, severities of IOP-induced injury in RGCs, and to examine these events on a condensed, and less variable time line.

8.3.5 Variation in Techniques to Measure IOP

IOP measurement is a challenge in laboratory animals - many techniques require anaesthesia, and many are not suited to smaller eyes. The most accurate current approach to measuring IOP is to sample it directly via a pressure transducer that is connected to a

needle placed in the anterior chamber. However, this approach is invasive and requires anaesthesia. Anaesthetics generally reduce IOP [379, 380], and different combinations of anaesthetics can have different influences on IOP [381]. Depending on species and strain, applanation tonometry (usually with the Tonopen® tonometer), can be performed in conscious animals [382], however, the technique usually requires sedation or general anesthesia. Although some studies have reported reliable measurements in rodents with applanation tonometry, the high curvature of the cornea can make it technically challenging to obtain reliable readings in smaller animals [355, 382]. Contrary to the Tonopen®, the TonoLab® uses rebound tonometry, and has been designed specifically for rodents [382]. The TonoLab® achieves accurate and reproducible measurements in conscious or lightly sedated rats and mice [355]; however, readings can be influenced by corneal thickness [355] and may also be less reliable when IOPs exceed 80 mmHg, as observed by Morrison and colleagues [383] and during calibration experiments in the present thesis. In the present thesis, the cannula in the anterior chamber was connected to both the pressure column and a pressure transducer, serving a dual purpose of modulating hydrostatic pressure and measuring IOP accurately throughout the duration of the experiment.

Because it can be assessed non-invasively, IOP, and its magnitude and duration, is often the only reported measure of insult severity in studies of IOP-induced RGC dysfunction. More accurately, however, it is the difference between IOP and MAP (i.e. ocular perfusion pressure) and IOP and retrolaminar tissue/ cerebrospinal fluid pressure (i.e. the translaminar pressure gradient) that determine ocular perfusion (ischemia) and ONH mechanical displacement, respectively [156, 180, 384-386]. Measurement of

pressure gradients is necessary to understand the true impact of IOP, especially in mild to moderate IOP elevations where small changes in pressure can have significant effects on retinal and ONH perfusion [156, 183]. Indeed, the translaminar pressure gradient has been suggested to have direct consequences on AT function in the ONH (discussed further in section 8.4.3). Some studies have experimentally manipulated ocular perfusion and/or translaminar pressure gradients [305, 320, 330, 387], rather than IOP alone, however these studies are the exception. Without knowing the magnitude of these pressure gradients, it can be difficult to reliably compare studies on the basis of IOP alone. Notably, this caveat has less bearing on the results of studies employing acute elevated IOP above MAP, such as in the present thesis, as the level of IOP greatly outweighs the opposing forces of MAP and the cerebrospinal fluid. Consequently, comparison between studies of acute elevated IOP is more straightforward than between studies of chronic elevated IOP.

8.3.6 Variation in Techniques to Assess RGC Loss

Several techniques for quantifying RGCs are currently available and used in studies of elevated IOP. These techniques range from invasive labelling procedures, such as retrograde labelling with a tracer or dye, to *in vitro* assessments of healthy axon profiles or IHC-labeled RGC somas [197]. Each method presents unique advantages and limitations [197]; consequently, the choice of technique is likely to influence the interpretation of RGC loss in studies of elevated IOP. Description of all available methods of RGC quantification is beyond the scope of this discussion, however a review

from our group [197] can be consulted for a comprehensive description of current techniques.

Comparing RGC quantification between Brn3a IHC and retrograde labelling methods demonstrates how varying measurements of RGC loss may be obtained depending on the method of quantification. The present study demonstrated around 42% loss of RGCs as early as 3 hours following 90 minutes of elevated IOP, as measured with Brn3a IHC. Assuming that Brn3a+ cell density is a reflection of RGC survival, this cell loss is far more rapid than other accounts of RGC loss in response to acute elevated IOP [264], and more than double the decrease in Brn3a+ cell density observed in the GCL at 2 days following ON transection in rats [318]. The reason for the rapid RGC loss in the present study compared to other studies is not obvious, however, differences between methods of RGC quantification may play a role. In retinal or ON injury, retrograde labelling of RGCs requires phagocytic breakdown of the somal membrane for the fluorescence signal to be lost, whereas Brn3a protein, a pro-survival transcription factor [388], is likely down regulated in damaged RGCs prior to physical loss of the RGC soma – a change that is immediately reflected in IHC labelling. In this way, expression of Brn3a may be a more sensitive indicator of viable RGCs than other methods, such as retrograde labelling. The same phenomenon was observed by Nadal-Nicolas and colleagues [318], where loss of Brn3a+ cells occurred at a faster rate than Fluorogold labeled RGCs following ON transection and crush in rats.

8.3.7 Summary of Variation in Animal Models of Elevated IOP

Integration of findings between studies is vital towards understanding of the effects of elevated IOP on RGCs. However, meaningful inter-study comparison can be impaired by variation in the models and techniques employed. The susceptibility of RGCs to elevated IOP can be affected by the species, strain and age of the animal; by differences in the vascular and structural anatomy of the retina and ONH; and by the technique used to elevate IOP. Furthermore, quantification of the severity of elevated IOP insult can be affected by the methods used to quantify IOP exposure. Such variations are of particular concern when comparing studies of chronic IOP elevation, whereas the effects of acute elevated IOP tend to be more reproducible and translatable between studies.

8.4 AT Dysfunction in Response to Elevated IOP

RGCs have long axons that possess limited protein transcription capability, rendering them particularly reliant on AT for the maintenance of cellular functions. As was introduced in section 1.4.4.3, AT disruption has been observed in numerous experimental models of elevated IOP. Experiments in this thesis have demonstrated important aspects of the manifestation and progression of anterograde and retrograde AT disruption following elevated IOP; particularly, that unique patterns and magnitudes of AT disruption can arise depending on the duration of IOP elevation. Furthermore, it was shown that disruption of AT function does not recover over time following acute elevated IOP, regardless of the transport direction or duration of IOP insult. The following

sections discuss the spatiotemporal manifestation and progression of AT disruption following 30-and 90-minute elevations of IOP, the relationship between AT function and RGC survival, and proposed mechanisms underlying AT disruption in elevated IOP.

8.4.1 Spatiotemporal Progression of AT Disruption Following Elevated IOP

The spatiotemporal manifestation of AT disruption in RGC axons in response to elevated IOP depends on the magnitude and duration of the insult - lower and more chronic IOP elevations give rise to mild AT disruption with protracted periods of progression, whereas acute and large IOP elevations tend to cause severe AT pathology that worsens rapidly over time. Key differences in the location, degree, and progression of AT disruption were found between the two durations of elevated IOP.

8.4.1.1 AT Disruption Following 30 Minutes of Elevated IOP

Thirty minutes of elevated IOP was hypothesized to cause an early disruption, and subsequent recovery, of anterograde AT in the early hours following IOP elevation; however, anterograde AT was not significantly impaired in the ONH or ON at any time point examined. These results are in contrast with a previous study in primates, where 30 minutes of IOP-induced ocular ischemia caused a transient disruption of anterograde AT function at the ONH that recovered over 24 hours [305]. Another study using a 30-minute duration of acute elevated IOP in mice did not find any effects on anterograde AT [389]; however, the lower magnitude of IOP (50 mmHg, versus 120 mmHg in the present study) and longer duration of recovery (7 days, versus 3, 6 and 24 hours in the present study) make comparison to the present study difficult. The reason for variable effects on

AT following 30 minutes of elevated IOP is not obvious. It is possible that AT in the present study was impaired during IOP elevation, but recovered prior to the 3-hour time point, or that AT responds differently in different species to elevated IOP. However, inter-animal variability likely also plays a role; indeed, while 90 minutes of elevated IOP consistently reduced CTB in the experimental ON, 30 minutes of elevated IOP reduced, had no effect, or even increased CTB in the experimental ON. It is possible that 30 minutes of elevated IOP approaches a critical point of insult in RGCs, where slight variations between animals can sway the outcome one way or another. Together, these findings highlight that 30 minutes of elevated IOP can have variable consequences on AT function in RGCs.

Retrograde AT, examined at 3, 7, and 14 days, was also not visibly impaired at the ONH following 30 minutes of elevated IOP; however, there was a small, but significant, reduction in CTB transport throughout the experimental ON. This reduction did not appear to progress over time, although significant variation in the data made interpretation difficult. However, it is possible that select axons were critically affected by 30 minutes of elevated IOP, causing AT disruption in a small population of RGCs. Indeed, Quigley and colleagues [331] suggested that AT in RGCs fails on an axon-by-axon basis in response to acute elevated IOP, as opposed to all axons exhibiting the same degree of partial AT disruption, with the proportion of axons affected being dependent upon the severity of IOP-induced injury. Selective expression IOP-induced AT disruption between adjacent axons has been confirmed in other studies in primates and mice [305, 390]. Presumably, longer durations of elevated IOP would cause AT failure in a greater proportion of axons, which is consistent with findings of the present experiments

(discussed in the following section). The concept of critical injury and selective vulnerability in RGCs is discussed further in section 8.8.

8.4.1.2 AT Disruption Following 90 Minutes of Elevated IOP

Increasing the duration of elevated IOP to 90 minutes had profound effects on AT. Anterograde AT of CTB was significantly impaired in both the ONH and ON. There were no signs of localized AT disruption at any point along the ON; however, a significant accumulation of CTB in the pre-LC region was observed at 6 hours of recovery. These results suggest that disruption of anterograde AT function in the first 24 hours following 90 minutes of acute elevated IOP likely originates at or before the anterior (nearer the retina) border of the ONH. A similar finding was reported in a previous study in primates, where a rapid build up of transported material was observed at the anterior border of the LC only 2 hours following acute elevation of IOP [283]. Disruption of CTB uptake at the retina could also result in a reduction in CTB intensity in the ONH and ON; however, a difference in the intensity of CTB labelling between control and experimental retinas was not observed. These findings demonstrate that anterograde AT in RGCs is blocked at the level of the anterior LC following 90 minutes of elevated IOP, and that this blockade persists, and likely progresses, over time.

Similar to the anterograde AT findings, the intensity of retrogradely transported CTB was uniformly reduced in the ON following 90 minutes of elevated IOP, and an accumulation of CTB in the ONH was also observed. The disruption of retrograde AT in the ON appeared to progress over time, while progression of AT disruption at the ONH was overshadowed by the significant tissue degeneration at that level. These results

highlight a significant structural component to AT disruption at these time points, and indicate that retrograde AT disruption can arise both at the ONH and at a site distal to the chiasm, perhaps in the optic tract or at RGC terminals in the SC (discussed further in section 8.4.1.3).

8.4.1.3 Retrograde AT Disruption Manifests at Two Intracellular Locations

As a region where densely packed axons are directly exposed to mechanical and vascular stress, the ONH is a logical site of AT disruption in response to acute elevated IOP. This is evident in studies of AT function in acute IOP elevation or experimental glaucoma, where the ONH has been frequently described as a primary site of anterograde and retrograde AT blockade [129-131, 157, 225, 285, 320, 330, 331, 391]. Interestingly, the accumulation of retrogradely transported CTB at the ONH in the present experiments had a distinct anterior border that, like the site of anterograde AT blockade, corresponded to where axons exit the retina and enter the scleral canal opening. This anterior limit was highly reproducible (observed in all 90-minute animals). A similar spatial pattern of AT blockade has been previously described after prolonged IOP elevation in monkeys [285], and may be due to increased metabolic demand and biomechanical stress caused by the large pressure gradient at that location [215]. Posteriorly, the limit of CTB accumulation was less defined, however CTB fluorescence did appear to decrease as the ON widened, likely coinciding with the onset of myelination (approximately 1-2 mm behind the sclera in rats and immediately posterior to the LC in monkeys and humans; [63]). Indeed, other studies have described a similar inverse relationship between AT accumulation and the amount of myelination in the ON [130]. Therefore, it appears that retrograde AT

disruption in the ONH following elevated IOP manifests as an accumulation of transported material that is topographically limited based on the mechanical and physiological constraints of the surrounding tissue.

Uniform reductions in intensity of retrogradely transported CTB in the ON, observed following both 90- and 30-minute elevations of IOP, indicate that a transient mechanical and ischemic insult to RGC somas and axons in the retina and ONH can result in disruption of AT function in the distal axon or terminal. The mechanism by which this occurs is not well known, however, it is possible that injury of the soma or proximal axon initiates an anterograde stress signal that affects distal axonal function, or that early disruption of anterograde AT near the eye causes the distal axon to be deprived of vital nutrients and organelles. Indeed, RGCs are shown to increase intracellular Ca^{2+} in response to acute IOP elevation [178, 392] and axonal Ca^{2+} waves are implicated as rapid injury signals between the axon and soma following neuronal injury [393]. Moreover, early disruption of anterograde AT has been implicated in distal axonopathy in a mouse model of elevated IOP [321, 394]. These findings suggest that elevated IOP may trigger an anterior signal in RGCs that initiates degenerative processes in the distal axon.

8.4.2 AT Function and RGC Loss in Response to Elevated IOP

Anterograde and retrograde AT perform vital molecular functions in neurons (previously discussed in section 1.3). Impaired AT has been associated with neuronal loss in many human neurodegenerative diseases – a finding reinforced by experimental models of CNS injury and disease, including those of elevated IOP [63, 217, 323, 325, 362, 395].

It is well known that elevations of IOP above MAP lead to AT disruption and RGC death; however, shorter durations – 30 minutes or less – appear to have no significant effects on RGC survival [264, 396]. RGC loss in the present study was not significant following 30 minutes of IOP elevation at any of the time points examined (3, 6, and 24 hours, 7 and 14 days). Interestingly, many studies have observed significant RGC loss and AT disruption following an only slightly longer duration of elevated IOP (45 minutes) [264, 396]. These findings associate intact AT function with RGC survival, and suggest that RGCs are resilient to mechanical and ischemic insult up to a critical point, a concept that is discussed further in section 8.8.

While disruption of anterograde AT appeared to progress over the first 24 hours following 90 minutes of elevated IOP, RGC loss did not. Despite the lack of progressive RGC loss at early time points, Brn3a+ cells were almost completely lost by 7 days following 90 minutes of elevated IOP. This temporal pattern of RGC loss - an initial, acute loss of RGCs followed by a pause and then a secondary wave of loss later on – has been reported in other studies of elevated IOP [263, 397] and ON trauma [398, 399], and is linked to AT function [397], as well as other forms of accumulated stress [326, 400]. It is likely that the RGC loss observed within the first 24 hours in the present study represents a primary, traumatic loss of RGCs, while a secondary wave of RGC loss is initiated sometime between 24 hours and 7 days following elevated IOP. WoldeMussie and colleagues [401] observed that 36% of RGCs were lost within the first 3 weeks after the onset of elevated IOP, and a secondary, slower form of loss was observed months later. Considering that the method they used to elevate IOP – laser photocoagulation of the trabecular meshwork – was chronic in nature [401], rather than acute and severe, it is

possible that the same phenomenon occurred in the present study, but on a more condensed timeline.

The role of AT in secondary RGC loss is not entirely clear. While some studies have suggested that failure of AT promotes RGC loss [348], another study has demonstrated that it is rather the temporary return of AT function that is damaging [326]. It is conceivable that both types of AT dysfunction may be present in RGCs in response to elevated IOP, but that their temporal onset and respective influence on RGC survival varies with the degree and duration of IOP elevation. Further research is warranted to determine the contribution of AT function, or dysfunction, towards the onset and progression of secondary RGC loss following elevated IOP.

Although AT disruption frequently coincides with RGC loss, as observed in this study and others, there are many pathophysiologic mechanisms that may contribute to RGC loss in IOP-induced injury. This is particularly true when an insult involves multiple modes of physiological stress, such as the ischemia and mechanical stress that occurs during elevated IOP. Consequently, determining a causal relationship between AT dysfunction and RGC loss can be problematic. However, certain findings – improving RGC survival through application of exogenous or virally expressed BDNF protein [402], and the observation that functional impairment of AT often precedes structural degeneration of the axon or soma [217] – strongly suggest that changes in AT function do contribute to RGC loss in response to elevated IOP.

8.4.3 Mechanisms Underlying AT Disruption in Response to Elevated IOP

AT is a complex process that relies on the function and homeostasis of many intracellular processes. Several mechanisms by which mechanical and ischemic stresses in the retina, ONH, and ON translate to AT disruption following experimentally elevated IOP have been proposed, including traumatic injury to axons, disruption of the axonal cytoskeleton, axonal ion imbalance, and ATP deprivation.

In primates, stress and strain in the LC in experimentally elevated IOP has been proposed to cause local compression of axons, resulting in their structural collapse and a physical blockade of AT [403-405]. Indeed, acute axonal stretching, similar to what may occur in the retina and ONH during large increases of IOP [165, 374], has been shown to physically rupture microtubules [406], disturbing the cytoskeletal scaffold needed for anterograde and retrograde AT. Signs of RGC structural degeneration in the present study, i.e., pNF+ somas, and axonal varicosities and retraction bulbs, were visible in the retina as early as 3 hours following 90 minutes of elevated IOP, suggesting a traumatic mechanism of AT disruption (see section 8.5 for further discussion of IOP-induced NF pathology).

It should be noted that LC structure in rats is fundamentally different from that of primates (primarily glial and lacking structural proteins) and likely exhibits different biomechanics. While mechanical stress may play a role in IOP-induced AT disruption, it is probable that factors other than the LC are contributing to AT disruption in this region in rats. In agreement with this theory, APP accumulation in the ONH of rats exposed to elevated IOP has been shown to be inversely related to the expression of myelin basic protein, a marker for oligodendrocytes [130]. The distribution of retrogradely

accumulated CTB in the present study was very similar. The unmyelinated portion of the ON may be particularly susceptible to the accumulation of transported organelles and vesicles during elevated IOP, however, the underlying reasons remain to be confirmed. Possibilities include: 1) that the lack of myelin allows for physical distension of the axolemma, affording greater axonal volume and encouraging buildup of AT cargo; 2) the energy deficit associated with reduced perfusion has a proportionally greater effect on the energetically-expensive unmyelinated ON, or 3) other unique characteristics of the unmyelinated ON bestow greater vulnerability.

Both AT disruption and structural degeneration in the retina and ONH continued to worsen up to 7 days following 90 minutes of elevated IOP, suggesting that, beyond traumatic structural damage, degenerative intracellular cascades likely contribute to the progression of AT dysfunction in IOP-induced RGC injury. As mentioned in section 1.4.3, both mechanical and ischemic insult to RGC axons can contribute to an increase in intracellular Ca^{2+}. Activation of Ca^{2+}-dependent proteases and phosphatases have been shown to contribute to cytoskeletal breakdown in RGCs in response to elevated IOP [108, 228, 407, 408], and their activity is associated with impaired AT in a mouse model of traumatic axonal injury in the ON [409]. Mechanisms of IOP-induced axonal degeneration are discussed further in section 8.5.

In primates, an increase in the translaminar pressure gradient has been suggested to create an anterograde flow of axoplasm that interferes with AT function. One hypothesis is that the intra-axonal flow of axoplasm overcomes the driving force of AT [405, 410]. Alternatively, Band and colleagues hypothesized that, rather than physically opposing the force of transport [405], pressure-induced intra-axonal flow effectively

sweeps away ATP, thereby starving axons of the energy required to fuel AT [411]. However, because of the technical difficulty of measuring such a pressure gradient, the presence of axoplasmic flow in response to elevated IOP has yet to be confirmed.

The ONH exhibits a high density of mitochondria to fuel the significant local energy demands associated with maintaining signal propagation in unmyelinated axons [412]. Although the involvement of the translaminar pressure gradient is uncertain, other causes of localized ATP depletion at the ONH are possible. Both mechanical and ischemic insults can induce release of ATP through pannexin channels on the RGC membrane [160, 173], depleting intracellular ATP. Furthermore, ischemia can lead to mitochondrial dysfunction in RGCs, reducing their ATP production [413]. Notably, IOP-induced elevation in intracellular Ca^{2+} can impair mitochondrial mobility directly by interfering with the association between mitochondria and their AT adaptor proteins, thereby preventing mitochondria from associating with kinesin [414]. As observed by Lu et al. [413], this creates a paradox where AT is reliant on ATP from mitochondria, but mitochondria require intact AT to be distributed to areas of high metabolic demand (such as the ONH). With many ATP-depleting mechanisms that are relevant to the types of cellular stress observed in the ONH during elevated IOP, it is likely that alterations in ATP availability contribute to AT disruption in this injury.

8.4.5 Summary of AT Following Elevated IOP

The present studies of retrograde and anterograde AT have revealed important characteristics of AT function and dysfunction in RGCs following a transient elevation of IOP that imposed mechanical and ischemic stress on RGC somas and axons. While 90

minutes of elevated IOP consistently impaired anterograde and retrograde AT in the ON, 30 minutes of elevated IOP had relatively minor effects – a small, but consistent reduction in retrograde AT. It was hypothesized that this decrease in retrograde AT represented the loss or impairment of a subset of selectively vulnerable RGCs that had reached a critical level of injury. The proximity of the 30-minute duration of elevated IOP to a critical insult in RGCs was further supported by the inter-animal variability observed in the 30-minute group. Interestingly, while anterograde AT disruption following 90 minutes of elevated IOP was initially similar in magnitude to RGC loss, it did not follow the same pattern of progression over time. However, prolonged AT blockade, as evidenced by the degree and progression of retrograde AT disruption at later time points, was associated with severe RGC loss. In support of previous literature, the location of AT blockade at the ONH was delineated anteriorly by the border of the LC nearest the scleral canal opening, and posteriorly by the onset of myelination. However, retrograde AT has the potential to be impaired at two intracellular locations, as accumulation of CTB in the ONH occurred in tandem with a uniform decrease in CTB in the ON. Distal disruption of retrograde AT may arise due to an anterograde stress signal originating at the primary site of injury – the retina and ONH – or due to a deprivation in anterogradely-transported essential materials. Finally, while AT disruption in the present study may have a functional component, significant degenerative histopathology was evident from the earliest time point onwards, indicating that structural blockade is likely the primary cause of AT dysfunction in this model.

8.5 Alterations of NFs in the RGC Soma and Axon Following Elevated IOP

A pivotal event in neuronal injury is the translation from functional impairment to permanent and progressive structural degeneration. As the most abundant structural filament in the axonal cytoskeleton [415], changes in NF protein have long been used to study the severity and progression of structural pathology in neuropathies [86, 276, 416-418] and acute neural injury [268, 409, 419, 420], and have been used for similar purposes in studies of RGC injury and loss [3, 110, 147, 157, 221, 222, 225, 235, 245, 274, 275, 333, 394, 409, 421]. In the present study, NF phosphorylation was altered in the ONH and pNF accumulated in RGC somas following elevated IOP. The following sections discuss these results and their meaning, as well as possible mechanisms underlying NF modulation and the potential of NFs as markers of neural injury.

8.5.1 IOP-Induced Somal Accumulation of pNF and Axonal Degeneration in the Retina

Abberrant accumulation of pNF in neuronal somas is associated with neurons that have lost connections their targets. This is evident from numerous studies where pNF+ somas were observed following nerve transection [220], and in studies of RGC damage, where pNF+ somas remain unlabeled following retrograde labelling from the SC [275, 333]. In the present study, pNF accumulation was evident in RGC somas as early as 3 hours following 90 minutes of elevated IOP. The number and distribution of pNF+ somas was relatively consistent over the first 24 hours. At later time points, severe degeneration of the GCL was apparent: the density of RGC somas was visibly reduced,

and the majority of remaining RGCs exhibited beaded, swollen and retracting axons. In contrast, few pNF+ somas were visible following 30 minutes of elevated IOP. These findings were consistent across all time points, and suggest that elevated IOP for 90 minutes is an acute traumatic injury to the retina that causes rapid structural damage to RGC axons, whereas axonal integrity is primarily unaffected by 30 minutes of elevated IOP.

The results from these experiments indicate that the insult associated with acute elevated IOP does not appear to affect all RGCs equally. Somal accumulation of pNF has been postulated to be subtype-dependent in other models of RGC injury [222, 422, 423]. In the present study, RGCs exhibiting pNF+ somas in the retina were detectable soon after 90 minutes of elevated IOP, and their proportion remained relatively constant over the first 24 hours. The density of Brn3a+ cells was also relatively constant over the same time period. Assuming that Brn3a+ cell density reflects the number of surviving RGCs, this finding suggests that IOP-induced pNF accumulation is exhibited by a subpopulation of RGCs that do not die within the first 24 hours following acute elevated IOP. The resilience of RGCs with pNF+ somas was also reported in a study of optic nerve crush [222], where the same proportion of pNF+ RGCs was observed at both 2 and 4 weeks following injury, whilst the majority of the RGC population was lost a much faster rate. Furthermore, the radial distribution of pNF+ RGC somas in the retina also suggests a subtype-specific pathology. In the present study, pNF+ somas became increasingly prevalent at greater eccentricities from the optic disc. It is well documented that alpha RGCs are found in greater proportion in the peripheral retina [7]. In line with these observations, Silveira and colleagues [423] demonstrated that alpha RGCs were relatively

resilient to ON transection, whereas beta RGCs, which are more prevalent in the central retina, exhibited pyktonic nuclei that degenerated rapidly. Intrinsically photosensitive RGCs (ipRGCs) are also found in greater proportion in the peripheral retina [424] and demonstrate exceptional resilience to ON transection [425]. These findings suggest that the pNF+ somas observed in the present study represent a subtype of RGCs – possibly alpha or ipRGCs – that, despite disconnection from their target, are comparatively resistant to degeneration, at least as measured in the present studies.

8.5.2 NF Phosphorylation in the ONH Following Elevated IOP

Detection of abnormal NF expression is a widely used measure of structural damage in studies of neuronal degeneration [3, 222, 423]. Thirty minutes of elevated IOP had no significant effects on NF phosphorylation in the ONH, and very few effects were observed following 90 minutes of elevated IOP. However, following both 30-minute and 90-minute insults there was a general trend of more non-pNF and less pNF in experimental ONHs. This observation is in agreement with a previous study in primates, where NF dephosphorylation occurred in proportion with RGC damage in response to elevated IOP [221]. Furthermore, non-pNF accumulates in axonal swellings following acute stretch injury to the ON [409] and pNF decreases in association with RGC axonal degeneration in a transgenic mouse model of glaucoma [333]. Therefore, it is possible that NFs in the RGC axon become dephosphorylated in response to elevated IOP. In the case of the 30-minute duration of elevated IOP, this effect may reverse over time – such a pattern was not observed in the present data, however, a large variability in the observations was noted.

8.5.3 Mechanisms Underlying Alteration of NFs in Elevated IOP

The physiological significance of somal pNF in RGCs is not clear; however, the phenomenon of aberrant phosphorylation suggests activation of local protein kinases. CDK5 has been known to become deregulated in mouse models of Alzheimer's disease [418] and amyotrophic lateral sclerosis (ALS; [105]), as well as in human Alzheimer tissue [418], leading to hyperphosphorylation of tau and NF. Hyperphosphorylation of NF increases NF-NF associations and reduces interaction between NF and kinesin, thus impairing NF transport into the axon [113] and promoting somal accumulation. Pathological activation of CDK5 has also been reported in studies of RGC axonal transection [426], and acute and chronic elevated IOP [232, 233]. Whether this activation promotes neuronal survival or death is controversial [427]. For example, while some studies have associated CDK5 activity with RGC death [232, 233, 426], CDK5 has also been linked to anti-apoptotic pathways [427], and greater numbers of somal pNF inclusions were associated with improved longevity in a mouse model of ALS [105]. Nguyen and colleagues [105] postulated that NF in the soma acted as a phosphorylation sink for CDK5, sequestering the ability of the enzyme to hyperphosphorylate other important cytoskeletal proteins, such as tau. Therefore, although pNF+ RGCs are associated with early axonal injury, the presence of pNF in RGC somas may, in fact, be indicative of neuroprotective processes. Indeed, pNF+ RGCs have been known to persist for months following ON transection, despite the loss of trophic support from their target tissue. It is unclear what role somal pNF plays in RGC injury following 90 minutes of elevated IOP; however, it is conceivable that the accumulation of pNF in RGC somas

observed in the present experiments represents an action of self-preservation by select RGCs.

Pathological phosphorylation of NF in RGC somas appears to be accompanied by a complimentary decrease in phosphorylation in the axon [221, 333]. Notably, dephosphorylation of NFs increases their vulnerability to proteolysis by calpain [93, 94, 420]. A likely suspect in the enzymatic dephosphorylation of NFs in the RGC axon is the Ca^{2+}/calmodulin-dependent protein phosphatase calcineurin. Indeed, calcineurin is cleaved and activated in response to elevated IOP, and inhibition of calcineurin promotes RGC survival by preventing dephosphorylation, and consequent activation, of pro-apoptotic intermediates [234]. Furthermore, calpain activity is markedly increased in the retina at 4 hours following acute IOP elevation to 110 mmHg for 40 minutes [295]. It is possible that a pathophysiological influx of Ca^{2+} into RGCs in response to the insult associated with acute elevated IOP in the present study leads to local activation of calpain and calcineurin in the axon, imposing a two-faceted attack on NF structure, where activated calcineurin dephosphorylates NFs, following which they become proteolysed by calpain.

Finally, an interesting proposal by Kang and Yu [428] regarding the mechanism of axonal degeneration in glaucoma postulates that, in healthy axons, pNF may act as a metabolic stockpile for phosphate bonds. At times of metabolic stress in the axon, phosphate molecules on NFs can be harvested to fuel local ATP generation and mitochondrial respiration [413]; however, during states of NF dephosphorylation in glaucoma, this backup supply of phosphate is compromised and axons become more vulnerable to degeneration [428].

8.5.4 NF Expression and Phosphorylation as an Early Marker of Neuronal Injury

Changes in NF expression and phosphorylation occur within hours of axonal injury in RGCs, and pathological accumulations of pNF in neuronal somas have been used as markers of neurodegeneration. These qualities of NF dynamics in trauma and disease suggest the utility of NF as an early indicator of neuronal injury. Assays to detect serum levels of NF phosphoforms are being developed as a measure to detect neural injury in many degenerative conditions, including traumatic brain injury [429], stroke [430], multiple sclerosis [431, 432], and ALS [432]. Ghonemi and colleagues [429] demonstrated that the serum level of pNF was useful both as a diagnostic and prognostic measure in traumatic brain injury – increasing levels of serum pNF were negatively correlated with level of consciousness, and a threshold level of pNF was able to predict death and disability with a high degree of sensitivity and specificity. Interestingly, measures of serum pNF in individuals with Leber's hereditary optic neuropathy [433], a mitochondrial disease that is characterized by the degeneration of the GCL and the ON [434], were found to reflect the degree of axonal neurodegeneration in the retina and ON, and may be useful to detect subclinical ON degeneration in other forms of optic neuropathy [433]. Finally, pNF levels measured directly from the vitreous are elevated in patients exhibiting retinal detachment [435]. These findings support the use of serum and vitreal pNF concentrations to diagnose and predict degeneration in various forms of RGC injury. However, body fluid concentrations of pNF would provide no information regarding the location or morphology of degenerating RGCs. Development of *in vivo* markers of retinal NFs could allow for longitudinal evaluation of RGC degeneration in

experimental models of ON injury and glaucoma, and, in future, could be a method of tracking RGC damage and loss in human optic neuropathies.

8.5.4 Summary of IOP-Induced NF Alterations

Modulation of the cytoskeleton is an important event in RGC injury, the degree of which may determine the fate of the RGC – recovery, or progressive degeneration and death. The experiments in this thesis have demonstrated that changes in somal and axonal NFs are acute reactions to RGC trauma induced by elevated IOP. NF pathology was found to be much more severe following the duration of elevated IOP that culminates in massive RGC loss (90 minutes), while NF modulation following the recoverable duration of elevated IOP (30 minutes) was comparatively mild. Indeed, the trend of NF dephosphorylation in the ONH following 30 minutes of elevated IOP is fundamentally a reversible process, as phosphorylation and dephosphorylation of NFs in the axon is a typical regulatory process in healthy neurons [113]. However, pNF+ accumulation in the neuronal soma, such as that observed following 90 minutes of elevated IOP in the present study, is strongly associated with states of neurodegeneration. Somal accumulation of pNF following 90 minutes of elevated IOP appeared to be isolated to a subset of RGCs that were acutely injured, but which did not die within the first 24 hours. The resilience and radial distribution of these cells suggests that they may be alpha- or ip-RGCs. Measurement of NF phosphoforms in both the blood and vitreous may be a promising diagnostic tool for detecting axonal damage in optic neuropathies and acute retinal and ON trauma. Development of a technique to label NFs *in vivo* may be useful in longitudinal tracking of disease progression.

8.6 Modulation of Glia in the Retina and ONH Following Elevated IOP

Retinal and ON glia closely interact with RGCs to modulate signaling activity, provide direct metabolic and structural support, and manage the homeostasis of the extracellular environment. Glia in the retina and ONH are known to respond to mechanical and ischemic insult that occurs with elevated IOP, and their responses are intimately linked to RGC health. Furthermore, and relevant to the present study, glial responses to pathological insult exist on a continuum, depending on the severity of insult – in initial stages of activation, glia exhibit responses that are primarily beneficial to RGC survival, whereas more severe activation can initiate damaging molecular cascades [58]. In the experiments described in Chapter 7, markers of glial activation (e.g., GFAP, which is known to be upregulated in both astrocytes and Müller cells upon their activation, and Iba1, which reveals morphologic changes in activated microglia) were studied in the retina and ONH over the first 24 hours following either 30 or 90 minutes of elevated IOP. The following sections discuss the spatiotemporal progression of glial activation in the retina and ONH following mild and severe IOP-induced injuries, the mechanisms underlying glial activation, and the relationship between glial activation and RGC survival.

8.6.1 Changes in Retinal Glia Following Elevated IOP

8.6.1.1 Microglia

As with AT function and NF expression/ phosphorylation, retinal glia exhibited very few changes at early time points following 30 minutes of elevated IOP. There were

no signs of microglial activation in the peripapillary retina at either 3 or 6 hours following elevated IOP, and the effects observed at 24 hours of recovery were mild, consisting of an accumulation of activated microglia on the inner surface of the retina. Given the lack of impact of this insult on RGC survival [264], these findings were not entirely unexpected. Increasing the duration of IOP elevation to 90 minutes, however, caused a rapid increase in Iba1+ microglial processes in the IPL, visible as early as 3 hours following the insult, which persisted at 6 and 24 hours. Liu and colleagues [436], using *in vivo* imaging of transgenic mice that express GFP in their microglia, tracked the density of microglia in the inner retina following IOP elevations similar to those in the present study: 110 mmHg for either 30 or 60 minutes. At 3 days following IOP elevation, microglial density increased by approximately 20% and 45% for the 30- and 60-minute elevations, respectively. These findings demonstrate a relationship between insult duration and microglial response, similar to what was observed in the present study. Notably, Liu and colleagues [436] demonstrated the largest increase in microglial density at 7 days following both insult durations (35% after 30 minutes and 103% after 60 minutes). It is possible that a more remarkable microglial reaction following the 30-minute IOP elevation might have been observed in the present study had the temporal analysis been extended to 7 days. Finally, Liu and colleagues also observed that microglial density was significantly correlated with the number of surviving RGCs [436]. These findings demonstrate that a sub-critical duration of elevated IOP likely causes a mild reaction in microglia, whereas a critical duration, which culminates in significant RGC loss, induces a prominent microglial response throughout multiple retinal layers. It is possible that tracking microglial density and morphology holds potential as an experimental, and

possibly clinical, tool to follow RGC damage and loss in degenerative retinal and ON diseases.

While microglia initially retained a ramified morphology following elevated IOP in the present study, they became more ameboid over 24 hours, exhibiting visibly shorter and blunter processes, and were observed in deeper retinal layers. These findings are consistent with the spatiotemporal progression of retinal degeneration following IOP-induced ischemia. Specifically, RGCs are the first retinal cell type to succumb to IOP-induced injury in the retina [154, 376]. The increase in microglia in the IPL is likely a phagocytic response to the dying back of local RGC processes. Over time degenerative processes continue, evidenced by the pan-retinal degeneration observed in the present study, attracting phagocytic microglia into deeper anatomical layers.

The accumulation of ameboid microglia on the inner surface of the retina in the present study was accompanied by a similar, although less pronounced, response in the contralateral control eye. The significance of contralateral glial activation is unknown; however, this phenomenon has been demonstrated in many recent studies of chronic IOP elevation [245, 251, 288, 291, 437]. Interestingly, ameboid microglia in the contralateral normal eye have been shown to be morphologically and phenotypically different from the experimental eye with chronic elevated IOP [251]. For example, activated microglia in experimental eyes strongly express CD68, a protein in the scavenger-receptor family that is a marker of phagocytic microglia and macrophages [438], while microglia in contralateral normal eyes demonstrate only weak CD68 labelling [251]. It is likely that microglia in experimental eyes exhibit a primarily phagocytic function, while those in contralateral normal eyes serve a different purpose. These findings suggest that microglia

in the retina are capable of responding to mechanical and ischemic stress in the fellow eye. Further discussion regarding potential mechanisms of contralateral glial activation is included in section 8.6.3.

8.6.1.2 Astrocytes and Müller Cells

Although both astrocytes and Müller cells have been shown to respond to ischemic and mechanical stress in the retina [160, 162], the responses of peripapillary macroglia in the present study, as demonstrated by GFAP IHC, were primarily unremarkable following both insult durations. There was no remarkable increase in GFAP fluorescence in the NFL – the anatomical location of retinal astrocytes – at any point following either insult duration. Some increases in GFAP+ radial processes were observed at the 24-hour time point, however these were inconsistent. For example, at 24 hours following 30 minutes of elevated IOP, one animal exhibited intensely labeled GFAP+ processes that spanned all retinal layers in the experimental eye. This was accompanied by similar, but weaker, labelling in the contralateral retina. Also, at 24 hours following 90 minutes of elevated IOP, GFAP+ radial processes were observed in 57% of the control retinas. The lack of GFAP upregulation in Müller cells of the injured eye is interesting, as many other studies have reported GFAP+ Müller cells in response to elevated IOP [60, 159, 241, 263, 290]. However, it is likely that the time frame of investigation in the present study may have been too narrow; indeed, the earliest documented observation of GFAP+ Müller cell processes following an acute elevation of IOP is at 24 hours [60], with many studies citing a peak in GFAP expression at 3 days or later [60, 159, 241, 290], and persisting to 3 and 4 weeks following the insult [60, 263].

Contrary to the IHC observations at the same time point, the level of GFAP protein, as assessed by WB, was markedly increased (up to 7-fold) in the experimental retina 24 hours following 90 minutes of elevated IOP. The reason for different findings between IHC and WB analysis of GFAP are unknown, however they could be related to differences in the scope of the sampling area – IHC investigation was isolated to the peripapillary retina, whereas WB analysis was a measure of GFAP protein in whole retina lysate. Furthermore, an increase of GFAP in astrocytes, may not have been noticeable in radial sections of the retina. Differences in the reactivity of the GFAP antibodies used and the small sample sizes in each study may have also played a role.

8.6.2 Changes in ONH Glia Following Elevated IOP

8.6.2.1 Microglia

Interestingly, in spite of highly contrasting effects on RGC survival, both durations of elevated IOP in the present study induced changes in Iba1+ area throughout the ONH. The pattern of change over time was unique following each insult. After 30 minutes of elevated IOP, Iba1+ area, measured as the percent area in each ONH region that was covered by Iba1 labelling, throughout most of the ONH (LC to 600 μm posterior the LC) was initially highest at 3 hours and significantly decreased over 24 hours. Ninety minutes of elevated IOP caused the opposite trend, where Iba1+ area from 100 to 600 μm posterior the LC was lowest at 3 hours, and significantly increased over 24 hours. Notably, the progression of Iba1+ area in the pre-LC region was the same for both durations of elevated IOP, with Iba1+ area being lowest at 3 hours and highest at 24 hours. This effect was markedly more pronounced following 90 minutes of elevated IOP.

These findings suggest that the spatiotemporal progression of microglial activation following elevated IOP is dependent upon both the duration of the insult and the location in the tissue. Furthermore, given the respective effects of 30- and 90-minute IOP elevations on RGC survival observed in the present study, it is likely that 30 minutes of elevated IOP induces a rapid, but transient activation of ONH microglia, whereas 90 minutes of elevated IOP results in a delayed, yet sustained, microglial activation. Indeed, following an IOP elevation to 160 mmHg for 60 minutes in rats, significant RGC loss was accompanied by an increase in OX-42+ microglia in the ONH that was sustained from 2 days to 1 week [241].

An alternate explanation for the different temporal patterns of microglial activation in the ONH between the two durations of insult in the present study is a different latency to reperfusion upon cessation of elevated IOP. Following 30 minutes of elevated IOP, reperfusion was fast and seemingly uninhibited, as evidenced by the visible return of blood flow to the retina, while following 90 minutes of elevated IOP, the eye often exhibited significant edema and structural enlargement. It is possible that retinal vasculature was damaged and that complete reperfusion was slower following 90 minutes of elevated IOP. This is significant, as microglia are suggested to enter into a static state during acute ischemia, only beginning their transformation to an activated phenotype after reperfusion is complete [439]. If reperfusion following the 90-minute IOP elevation was delayed, it is conceivable that the onset of microglial activation would also be, as was observed in the present results.

Surprisingly, the contralateral ONHs for both durations of insult also showed significant changes in Iba1+ area, the spatiotemporal pattern of which was strikingly

similar to the posterior ONH regions in the experimental ONHs: microglial area decreased over time following 30 minutes of elevated IOP, and increased over time following 90 minutes of elevated IOP. However, there were no signs of microglial change in the LC region of control eyes following either duration of elevation. These findings suggest that damage to the experimental eye may induce a signal of injury that is capable of activating microglia in the contralateral tissue (discussed further in section 8.6.3). Finally, the relatively greater change in Iba1+ area in the posterior regions of the ONH compared to the LC – the site of primary dysfunction and degeneration following elevated IOP, as supported by the AT results in the present study, and others [130] – is puzzling. Interestingly, another study has documented a similar pattern of microglial proliferation throughout the regions of the ONH following sclerosis of the episcleral veins via hypertonic saline [61]. Compared to the unmyelinated LC region of the ONH, Ebneter and colleagues [61] observed greater microglial activity beginning at the transition zone of the retrobulbar ON, where RGC axons become myelinated. This was regionally correlated with greater degenerative axonal pathology, as shown through NF labelling. The reason for these regional differences is not obvious, however, it is possible that traumatic damage to axons at the LC region during elevated IOP would result in anterograde degeneration of the distal axon segment, and the consequential recruitment of phagocytic microglia.

8.6.2.2 Astrocytes

Astrocyte activation in the ONH, as observed with GFAP IHC, was not remarkably increased after both durations of elevated IOP. Furthermore, although WB

analysis revealed a 2-fold increase in overall GFAP protein in the ONH of the experimental eye at 24 hours following 90 minutes of elevated IOP, this effect was not statistically significant. There is a high degree of discrepancy in the literature regarding GFAP expression in ONH astrocytes following elevated IOP, with some studies reporting upregulation of GFAP [243], and others a downregulation [292, 440, 441] or no change [248]. It is possible that astrocytes are highly sensitive to small differences in the method, duration and magnitude of IOP elevation, and that their responses vary in time depending on such details, leading to different observations amongst studies.

8.6.3 Mechanisms of IOP-Induced Glial Activation and its Influence on RGC Survival

The mechanisms by which retinal glia become activated in response to elevated IOP are complex [4], and a full review on this topic is beyond the scope of this thesis. This section highlights some relevant mechanisms of glial activation and glial influence on RGC survival.

The pathological release of ATP from retinal neurons and glia in response to mechanical and ischemic stress has significant implications for RGC survival. However, in addition to purinergic modulation of RGCs, retinal glia also express purinergic receptors, and their activation can have significant effects on microglial behavior following traumatic injury. Haynes and colleagues [442] showed that microglia in the hippocampus extended their processes and moved towards a source of ATP. This motility was found to be dependent on the purinergic metabotropic receptor $P2Y_{12}$, as microglia lacking this receptor did not translocate towards the source of ATP.

Furthermore, as activated microglia became more ameboid in shape, their expression of $P2Y_{12}$ was attenuated. Notably, P2Y receptors are expressed in the retina [443, 444]. These findings highlight ATP as a crucial signaling pathway in pathological microglial responses, both inducing microglial activation and acting as a chemoattractant to draw distant microglia to sites of tissue damage. ATP has also been shown to activate retinal macroglia in response to optic nerve injury [445], leading to significant dysfunction in their maintenance of extracellular homeostasis.

An unexpected result in the present study was the activation of glia in the contralateral retina and ONH following unilateral elevation of IOP. There was a rapid increase in retinal microglia over 24 hours on the inner surface of the retina, and the spatiotemporal changes in ONH microglia were similar in both the experimental and contralateral normal eyes. Furthermore, GFAP+ Müller cell processes were observed in the contralateral retinas of some animals, more frequently so following the 90 minutes of elevated IOP, at the 24-hour time point. This phenomenon has been observed in studies of unilateral optic nerve injury [446] and chronic elevated IOP [245, 251, 288, 291, 437, 447]. Comparatively fewer studies have demonstrated changes in contralateral glia following IOP-induced ischemia. Kerr and colleagues [289] demonstrated hypertrophy and increased GFAP labelling in astrocytes and Müller cells of the contralateral retina following IOP elevation to 120 mmHg for 60 minutes, which was accompanied by an increase in the expression of the gap junction channel protein connexin 43, as early as 4 hours following the insult. The mechanism by which glia in the contralateral eye respond to injury in the fellow eye is not well understood; however, both systemic and trans-synaptic influences have been suggested. It is conceivable that an injury-induced

elevation in diffusible inflammatory factors may stimulate glia in the contralateral eye through the circulation; indeed, Kanamori and colleagues [288] suggested that immunological alterations caused by retinal or ON injury may increase production of serum autoantibodies. Glial activation as a side effect of trans-synaptic degenerative signaling has also been proposed as a mechanism in the contralateral normal eye in response to unilateral IOP elevation in the experimental eye [448]. In support of this, results from a recent study by Sapienza and colleagues [291] demonstrated that contralateral glial activation was related to the interconnectivity between the left and right SC. Such trans-synaptic conveyance of degenerative signals between fellow eyes may also occur through a subset of RGCs that extend retino-retinal projections [449, 450]. Finally, while glial activation following damage to the retina and ON is often associated with damaging molecular signaling events, glial activation in the contralateral eye may represent an attempt at neuroprotection [451]. Indeed, glial activation in the contralateral normal eye has been shown to exhibit features unique from the glial activation observed in the ipsilateral experimental eye [245, 447].

Activated retinal and ON glia can influence RGC function and survival through a variety of signaling pathways. A well-studied example is the upregulated production and release of pro-inflammatory substances such as IL-6, TNF-α, and nitric oxide (NO) [162, 185, 186, 452, 453]. While IL-6 release from microglial cells in response to intraocular pressure has been shown to have protective effects on RGCs [451], TNF-α released from astrocytes and microglia induces RGC apoptosis via caspase activation [453]. In a study by Tezel and Wax [453], retinal glial cells that were co-cultured with RGCs were found to secrete TNF-α and NO in response to simulated ischemia, and disruption of TNF-α and

NO signaling reduced RGC loss by 66% and 55%, respectively. Furthermore, upregulation of NO synthetase has been observed in glaucomatous ONHs [454]. Finally, astrocytes in the retina and ON are highly interconnected by gap junctions, allowing them to spatially buffer neurotoxic substances, neurotransmitters and metabolites, thereby protecting RGCs from damage and supporting their function [455]. In response to IOP-induced ischemia, activated astrocytes upregulate their expression of connexin 43 [289], likely influencing the permeability and interconnectivity of the astrocyte syncytium; however, whether such changes are beneficial [456] or detrimental [457] to RGC survival remains to be determined [240]. These findings indicate that glial physiology in the retina and ONH is affected by elevated IOP, and that activated glia participate in numerous signaling pathways to affect RGC survival. In the present study, it is possible that these changes in glial physiology and signaling behaviour may have played a role in the progression of RGC axonal dysfunction and structural degeneration, and eventually loss of RGCs.

8.6.5 Summary of Glial Responses to Elevated IOP

Studies of molecular markers of glial activation in the present study have demonstrated the spatiotemporal progression of glial responses in the retina and ONH following two severities of acute elevated IOP. Thirty minutes of elevated IOP, which had no significant effect on RGC survival, was shown to have no effect on retinal microglia at 3 and 6 hours, but resulted in a mild increase in the number of microglia on the surface of the retina at 24 hours of recovery. Conversely, 90 minutes of elevated IOP, which caused catastrophic RGC loss, resulted in a massive and immediate upregulation in

microglial processes in the IPL, and subsequently the significant presence of ameboid microglia in all retinal layers. These findings demonstrated that the degree of microglial activation in the retina approximates the amount of RGC damage during injury, a quality that supports the application of microglial tracking as a method to evaluate progressive RGC degeneration in injury and disease. The responses of ONH microglia appear to also be specific to the severity of injury, as Iba1+ area was initially high after 30 minutes of elevated IOP and decreased over time, while showing the opposite pattern of progression following 90 minutes of elevated IOP. However, due to similar observations in the contralateral ONHs, further experiments with additional naïve controls are needed to allow for further interpretation of these findings (see section 8.9 for further discussion). There was no remarkable activation in retinal or ONH astrocytes in the first 24 hours following either insult, however some limitations of the present experiments warrants further study into this topic. In addition to the contralateral microglial responses observed in the ONH, Müller cells in the contralateral retina were also activated in some animals following acute elevated IOP. Contralateral glial activation, reported in previous studies, may arise through long distance signaling of diffusible inflammatory factors, or via trans-synaptic stress signaling during neurodegeneration. Future experiments comparing the active molecular pathways between contralateral and ipsilateral glial activation may help to differentiate between pro-survival and pro-apoptotic glial signaling in elevated IOP.

8.7 Time Course of Retinal, ONH, and ON Pathology Following Elevated IOP

Understanding the etiology of elevated IOP-induced RGC dysfunction and loss requires identification of the underlying cellular events and determination of their sequence in time. This section integrates the findings from current experiments with relevant findings from the literature to compose theoretical timelines of functional and structural events associated with RGC loss following sub-critical (RGCs recover from transient dysfunction) and critical (RGC damage is severe and loss is progressive) acute elevations of IOP. The variability between injury models in studies of elevated IOP is substantial, making it difficult to arrive at a universal definition of what constitutes either a recoverable or severe and permanent insult. For example, while a moderate elevation of IOP to 50 mmHg for 2 hours has been shown to be a recoverable injury [306], increasing the magnitude of IOP to a level above MAP for the same duration results in the loss of approximately 75% of RGCs by 5 days following the insult [264]. For IOP elevations above MAP in rats, the longest duration of insult that does not result in significant RGC loss is between 30 and 45 minutes, as 30-minute IOP elevations are consistently reported to not cause RGC loss [264, 396], whereas the results of 45-minute IOP elevations are mixed [264, 296, 396]. Using these guidelines, and assessments of RGC survival within each study, the findings included in this integrative analysis were grouped into either the sub-critical or critical injury categories.

8.7.1 Early Events During IOP Elevation

Regardless of the ultimate duration of acute elevated IOP, the initial physiologic responses to IOP-induced mechanical and metabolic stress are presumably universal. Indeed, when IOP is raised above MAP, retinal function, as measured by the electroretinogram (ERG), is extinguished within 10 minutes [154]. This is accompanied by the initiation of multiple signalling pathways, a large number of which converge on the product of elevated cytosolic Ca^{2+} in RGCs (described in section 1.4.3). Presumably, as elevated IOP is prolonged, homeostatic mechanisms for regulating intracellular Ca^{2+} will fail to compensate for the large influx of Ca^{2+} [458]. When intracellular Ca^{2+} exceeds a critical concentration for a threshold amount time, RGC death occurs ([160]; critical threshold discussed further in section 8.8). However, return of IOP to baseline levels prior to this threshold allows for a full functional recovery [154, 281, 459].

From the present experiments, it is apparent that return of IOP to baseline after only 30 minutes of elevated IOP avoids both severe axonal trauma and the initiation of potentially critical signaling pathways in the majority of RGCs, as evidenced by the lack of significant structural damage and RGC loss assessed over multiple time points following elevated IOP. In contrast, extending the duration of IOP elevation to 90 minutes results in activation of kinases and phosphatases, as suggested by changes in NF phosphorylation, AT disruption, and severe progressive structural degeneration of RGC axons. The following sections discuss the timeline of molecular events following recoverable or severe and permanent acute IOP-induced injury.

8.7.2 Progression of Events Following a Sub-Critical IOP-Induced Injury to RGCs

During acute elevated IOP, RGC axons exhibit mild to moderate dysfunction – impaired AT leads to accumulation of transported organelles in RGC axons [281, 305], and signs of early degenerative changes, such as swollen axons and mitochondria [305] are evident in the ONH. Depending on the magnitude of IOP elevation, axonal pathology is accompanied by the loss of RGC-specific, or all, components of the ERG [154]. Should the magnitude and duration of IOP elevation remain relatively mild, these changes begin to recover immediately following return of IOP to baseline.

Components of the ERG that had been depressed during IOP elevation have been shown to recover within minutes upon return to baseline IOP, and nearly complete functional recovery has been observed following 1 hour [154]. Return of AT has been shown to occur on a similar timeline [305]. Radius and Anderson [305] demonstrated that accumulated organelles visible in the LC of monkeys following 30 minutes of IOP elevation had dissipated by 1 hour. The results of the present experiments support this timeline, as there were no significant signs of anterograde AT disruption at 3 hours following IOP elevation.

As early as 3 hours following elevated IOP, there was a shift from phosphorylated to dephosphorylated NF in the RGC axon (see Section 6.3.3), particularly in the region of the LC, a primary site of axonal stress in this injury model [130, 285, 331]. Although the effects of elevated IOP on expression of NF phosphoforms did not attain statistical significance, it is possible that sub-critical elevations of IOP initiate localized and transient activation of NF regulatory phosphatases. Changes in NF expression and phosphorylation have been shown to occur prior to AT disruption following 3 hours of

continuous elevated IOP at 45 mmHg in pigs [157]. However, a longer duration of the same IOP elevation in rats was shown to have no lasting effects on AT [158]. Given these findings, it is feasible that, like AT, early changes in NF expression and phosphorylation that manifest within the first few hours following elevated IOP may be reversed over time. The present study did not reveal any significant progression of NF dephosphorylation at the examined time points, however, it is possible that other combinations of IOP elevation and duration could demonstrate reversibility.

Beginning as early as 24 hours following the insult, retinal microglia exhibit a delayed response to sub-critical IOP elevation. In the present study, the number of microglia in the NFL and adjacent the inner limiting membrane was visibly increased at 24 hours following 30 minutes of elevated IOP. Liu and colleagues [436] made a similar observation, where the density of microglia in the inner retina of mice, as measured by *in vivo* confocal imaging, was increased by 35% from baseline, and microglial morphology had become predominantly ameboid, by 1 week following 30 minutes of elevated IOP above MAP. By 4 weeks of recovery, microglial density had been reduced to only 15% above baseline, and microglial morphology had returned to a ramified form. It is possible that a transient pattern of microglial activation would have been observed in the present study had examinations been extended to later time points. The purpose of transiently activated microglia is unknown. It is possible that microglia were initially recruited to, or induced to proliferate in, the retina in response to IOP-induced ATP release and other molecular stress signals [460], but the lack of structural degeneration did not encourage a pro-inflammatory phenotype or necessitate further microglial action. Indeed, following focal cerebral ischemia in mice, local microglia and infiltrating macrophages initially

assume a “healthy” neuroprotective phenotype, characterized by reduced expression of pro-inflammatory cytokines and identified by the markers arginase-1 and CD206, but can transition to a detrimental pro-inflammatory phenotype in response to ischemic and degenerating neurons [461, 462]. Further research is warranted to identify the functional phenotypes of activated microglia in the retina and ONH following sub-critical IOP-induced injury.

There are few signs of IOP-induced damage or dysfunction beyond 1-2 weeks of recovery following sub-critical IOP elevations. Abbott and colleagues [158] demonstrated no impairment of anterograde or retrograde AT at either 1 or 2 weeks following an IOP elevation of 50 mmHg for 8 hours in rats, nor was there any increase in microglial density. The present studies demonstrated a significant disruption in retrograde AT between 3 and 14 days following elevated IOP, however, the effect was small and did not change over time. As discussed in section 8.4, it is possible that retrograde AT function was reduced or lost in a population of selectively vulnerable RGCs (see section 8.8 for further discussion). The concomitant lack of detectable anterograde AT disruption at early time points following 30 minutes of elevated IOP in the current study suggests that dysfunction of retrograde AT was driven by a mechanism other than anterograde deprivation. Notably, retrograde AT has been shown to be more vulnerable than anterograde AT, with AT dysfunction progressing distally-to-proximally in two models of chronic elevated IOP [463]. Finally, Li and colleagues performed an *in vivo* longitudinal assessment of RGC dendrite morphology over time following various durations of acute elevated IOP and found no morphologic changes in RGC dendrites at any time point from 1 day, to as long as 2 months following elevated IOP [266].

Taken together, these findings demonstrate that changes in RGC AT function and axonal and dendritic structure are relatively mild following sub-critical elevations of IOP, predominantly reversed within hours following return to baseline IOP, and rarely observed beyond 2 weeks of recovery. Furthermore, delayed reactions of nearby microglia beginning between 24 hours and 1 week following elevated IOP appear to be transient, and are not associated with further RGC damage.

8.7.3 Progression of Events Following a Critical IOP-Induced Injury to RGCs

Significant RGC loss was observed as early as 3 hours following 90 minutes of elevated IOP in the current study, reflecting either a traumatic and immediate loss of RGCs (i.e. significant structural damage), or a rapid down-regulation of Brn3a expression in RGCs under stress. This finding compliments the pattern of ERG recovery upon reperfusion, where functional recovery, especially of RGC-specific components, is delayed and incomplete following IOP elevations severe enough to cause RGC loss [228, 377]. Together, these findings demonstrate that an acute elevation of IOP that exceeds a critical threshold of injury can result in rapid cell loss and functional impairment in the retina (Figure 8.1 A).

Figure 8.1 Time Course of Degenerative Pathology in the Visual Pathway Following 90 Minutes of Elevated IOP to 120 mmHg. Mechanical and ischemic stress due to elevated IOP leads to rapid and progressive functional and structural pathology in the retinal, ONH and ON. **A)** Within 24 hours of elevated IOP, acute trauma to the retina results in damage and loss of RGCs, activation of microglia, and the initiation of an anterograde stress signal. At the ONH, AT becomes impaired at the anterior LC, local microglia increase in number and enzymatic processes begin to alter the cytoskeleton. **B)** In the following 1-3 days, Müller cells in the retina are activated and their glutamate regulation is impaired, while astrocytes become activated in the SC. Structural degeneration progresses at all levels of the visual pathway and a both anterograde and retrograde AT continues to be impaired. **C)** At 7 days and beyond, all retinal layers have significantly degenerated. Severe degeneration of RGC axons leads to a reduction in ON volume.

A) Recovery Time < 24 Hours

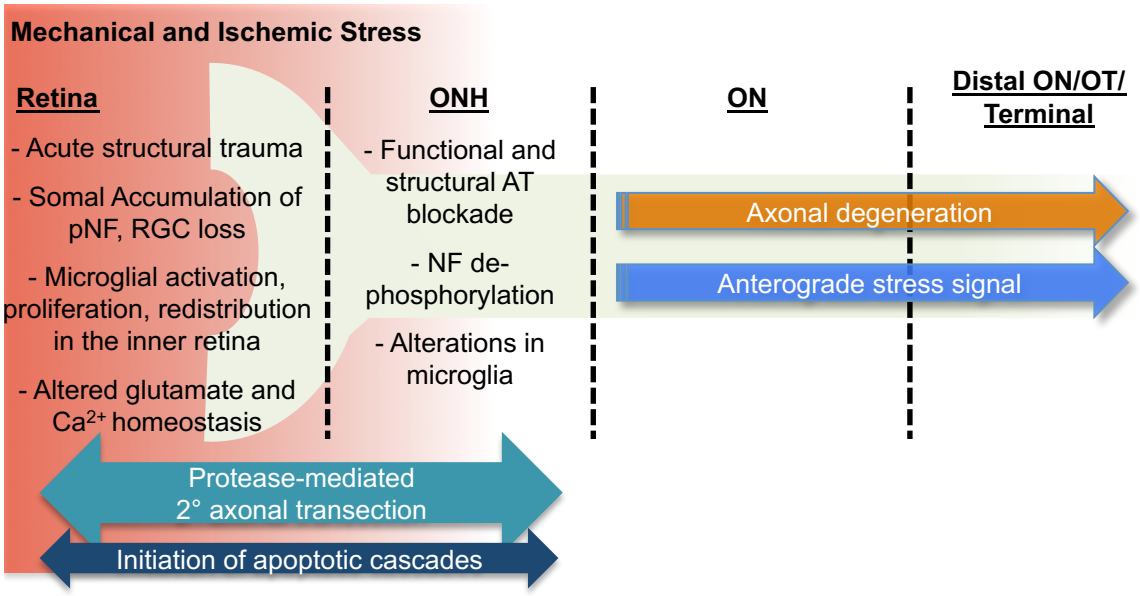

B) Recovery Time 1-3 Days

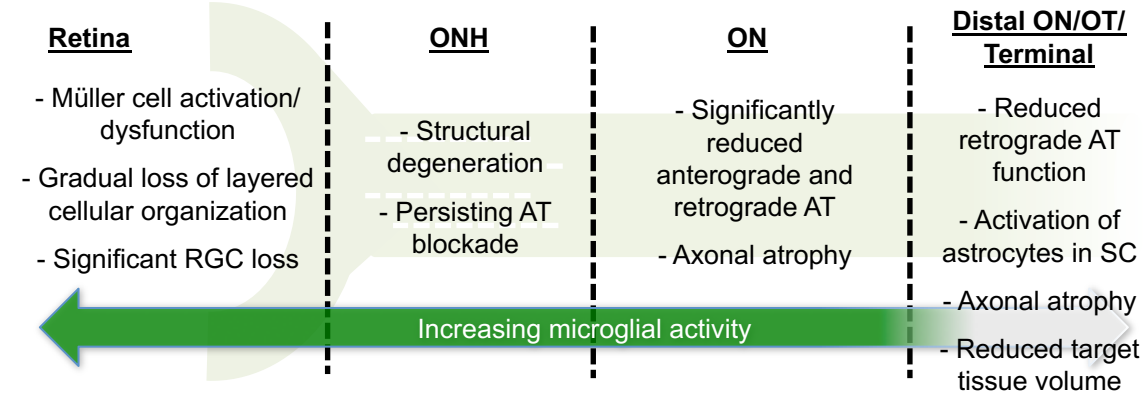

C) Recovery Time 7+ Days

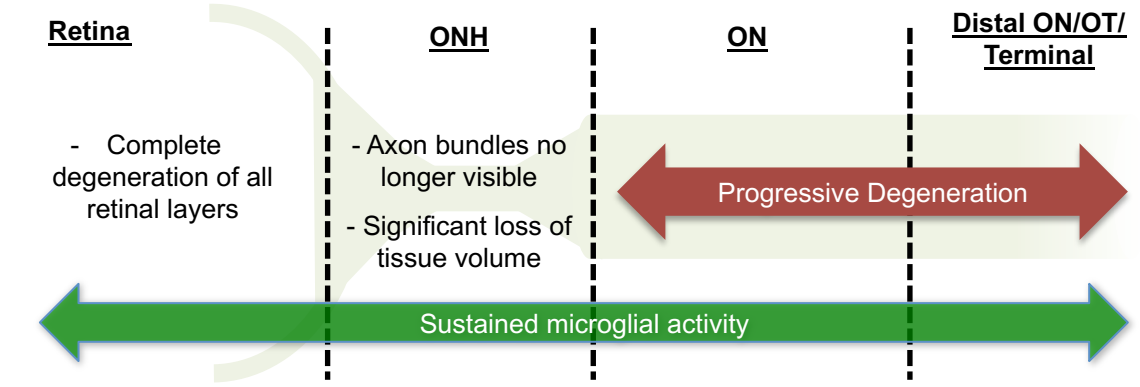

Signs of RGC axonal trauma are also evident immediately following severe elevated IOP (Figure 8.1 A). In the current study, RGCs exhibited somal accumulation of pNF beginning at 3 hours following elevated IOP, suggesting rapid traumatic and/or enzymatic axonal transection. Both calpain activity and total retinal Ca^{2+} has been shown to be significantly elevated as early as 4 hours following acute elevated IOP [228]. Over-activation of NMDA channels in response to a peak in retinal glutamate, demonstrated to occur 1-2 hours following transient elevated IOP above MAP [151, 464] may contribute to these early changes in retinal Ca^{2+}. Early calpain activity in the retina and ONH may lead to proteolysis of the RGC axonal cytoskeleton, effectively transecting axons, thereby initiating aberrant accumulation of pNF in the soma. Calpain-dependent proteolysis may be facilitated by simultaneous IOP-induced phosphatase activation, leading to dephosphorylation of axonal NFs, although a comprehensive timeline of phosphatase activity following acute elevated IOP remains to be established. Finally, aberrant phosphorylation of NF in the soma is executed through the activity of local protein kinases, such as CDK5. In agreement with the presence of pNF+ somas at the 3-hour time point in the present study, conversion of the CDK5 regulator p35 to its deregulated version p25, which is associated with prolonged activation and mislocation of CDK5, was markedly apparent at 4 hours following 60 minutes of acute elevated IOP above MAP in another study [228]. Therefore, in addition to rapid RGC loss and functional decline, mechanical trauma and Ca^{2+}-dependent enzymatic degradation lead to significant RGC axonal damage within hours following a critical elevation of IOP (Figure 8.1 A).

Given the early structural pathology observed in RGC axons in this model, it is not surprising that AT is rapidly affected by acute elevated IOP. AT disruption is

observed in the ONH during the actual period of IOP elevation [131, 157, 225, 305, 391], and, while it appears to recover upon return to baseline IOP after sub-critical IOP elevation [158, 305], AT disruption following sufficiently high IOP for a longer time period that exceeds a critical threshold does not appear to exhibit any recovery. It is likely that both the structural axonal damage and degeneration, as well as early Ca^{2+} deregulation [228, 465] and ATP deprivation [174, 177-179] during and following elevated IOP contributes to early, and persisting, AT disruption (Figure 8.1 A and B).

While retrograde AT function in the proximal RGC axon, e.g. in the retina and ONH, has been shown to be rapidly impaired by acute elevated IOP [285], it is likely that AT dysfunction in the distal axon, as observed at later time points in the current study, is a product of insult and dysfunction in the proximal axon, and therefore occurs subsequent to proximal dysfunction. In addition to failure of anterograde AT, early initiation of an anterograde, Ca^{2+}- mediated stress signal may cause critical stress to the distal axon, leading to subsequent failure, or alteration of retrograde AT (Figure 8.1 A, B). Indeed, the current study demonstrated a significant disruption of retrograde AT as early as 3 days following elevated IOP.

Many studies have demonstrated glial activation in the visual pathway in response to acute elevated IOP at 24 hours of recovery and later following return of IOP to baseline [60, 241, 248]. Although upregulation of GFAP in Müller cell radial processes in response to elevated IOP was not consistently observed in the present study, other studies have demonstrated an upregulation of Müller cell GFAP expression beginning between 24 hours and 3 days following acute elevated IOP in rats (Figure 8.1 B; [60, 241, 466]). Müller cell activation at 3 days following acute elevated IOP has been associated with

impaired buffering of K+ [466]. Impaired buffering of K+ and other retinal substances by Müller cells [238] may in turn alter the homeostatic balance of the extracellular environment, furthering damage and degeneration of RGCs and other retinal neurons following acute elevated IOP. Astrocyte activation in the ONH, as indicated by increased GFAP expression, has been observed beginning at 2 days following elevated IOP [241], and in distal RGC targets, i.e. the LGN and SC, beginning at 3 days ([60]; Figure 8.1 B). However, the effect of elevated IOP on ONH astrocytes is unclear. On the other hand, studies of microglial activation following critical IOP-induced injury demonstrate increased microglial density and a transition to predominantly ameboid morphology in the inner retina of rats and mice beginning between 3 and 7 days following acute elevated IOP ([290, 467]; Figure 8.1 B and C). Increased microglial processes in the inner retina were observed as early as 3 hours following 90 minutes of elevated IOP in the current study, demonstrating that microglia can be activated very shortly following IOP elevation (Figure 8.1 A). Investigation of microglial activation at time points within the first 24 hours following elevated IOP in the literature is lacking; however, microglial activation in response to focal cerebral ischemia exhibits a similar time of onset (3.5 hours) [468]. Activated retinal microglia in the current study were primarily ameboid in morphology by 24 hours of recovery. The proportion of Iba1+ area in ONH regions increased from 3 to 6 hours of recovery, and remained elevated at 24 hours (Figure 8.1 A). Due to the significant degeneration in the retina, ONH, and ON observed following a critical elevation of IOP (Figure 8.1 A, B and C), it is likely that microglia assume a pro-inflammatory and phagocytic phenotype. Furthermore, given their importance in clearing cellular debris, activated microglia likely remain present in the retina, ONH and ON

throughout the duration of the degenerative process (Figure 8.1 C). Indeed, an increase in activated Iba1+/ED1+ microglia was correlated with RGC axonal degeneration in the retina, ONH, ON, and optic tract over 6 weeks following induction of elevated IOP in the rat [61].

In the current study, RGC loss following elevated IOP for 90 minutes remained relatively constant over 3, 6, and 24 hours of recovery (between 30 and 40%); however, there was a significant drop in RGC survival by 7 days (98% loss) of recovery. RGC loss in the first 6 hours following IOP-induced retinal ischemia has been shown to be primarily necrotic [469], whereas apoptotic cascades are activated between 4 and 24 hours following reperfusion [469-472], and apoptotic RGC loss can continue for weeks to months [264, 471, 473]. This pattern of primary and secondary RGC loss is also present in other models of retinal ischemia [395].

As the injury progresses, degeneration in all retinal layers, the RGC projection (ON and optic tract), and RGC target tissues becomes more prominent (Figure 8.1 B and C). In the current study the layered cellular appearance of the retina was lost by as early as 3 days following elevated IOP, and the majority of the cellular volume was lost between 7 and 14 days. Individual axon bundle morphology was no longer visible in the ONH by 7 days, and the width of ONHs was visibly reduced by 14 days. The brightness of accumulated CTB at the ONH was reduced over 7 and 14 days, which, due to the apparent structural degeneration, is likely due to a loss of tissue, accompanied by microglial phagocytosis, rather than a dissipation of the accumulated label. These findings are in agreement with previous studies, where atrophy of the optic tract was apparent by 3 days following elevated IOP, demonstrating a reduction in cross-sectional

area by approximately 10%, progressing to 50% by 14 days [60]. Neurons in RGC target structures, such as the LGN and SC, exhibit reduced soma size and increased density beginning approximately 3 days to 1 week following elevated IOP [60]. Degeneration of the RGC soma, axon, and dendrites continues for months following cessation of elevated IOP [266].

8.7.3 Summary of Time Course of IOP-Induced Pathology

Integrating findings from the current study with those of previous research helps to elucidate a time course of many crucial events in the progression of retinal and ONH injury following both sub-critical and critical degrees of elevated IOP. Furthermore, a comparison of changes in retinal, ONH, and ON structure and function between sub-critical and critical IOP-induced injuries highlights processes and pathways that are unique to each injury severity, and in turn provides a greater understanding of pro-survival and pro-degenerative events following transient elevation of IOP. Table 8.2 compares key events following sub-critical and critical elevations of IOP.

Elevated IOP rapidly initiates a multitude of pathological pathways, many of which culminate in elevated intracellular Ca^{2+} in RGCs. Retinal function is also acutely inhibited. However, when IOP elevation does not exceed a critical level of insult, these dysfunctions and imbalances can be regulated and potentially reversed. While some RGC axons exhibit long lasting AT dysfunction following even mild IOP insult, accumulation of transported organelles at the ONH and functional inhibition of the retina are predominantly resolved shortly after return of IOP to baseline. Other transient responses, including delayed activation and recruitment and/or proliferation of retinal

Table 8.2 Comparison of Sub-Critical and Critical Elevated IOP-Induced Injury

Sub-Critical/ Recoverable Injury	Critical/ Permanent Injury
• Complete recovery from transient inhibition of retinal function during IOP elevation • No significant RGC loss • Recovery of mild AT blockade and structural degeneration at the ONH upon return of IOP to baseline • NF dephosphorylation at the ONH • No significant structural degeneration over time in the retina or ONH • Retrograde AT dysfunction in the distal axon of some RGCs • Transient activation of microglia	• Recovery of retinal function is incomplete or absent • Primary RGC loss by necrosis, secondary loss by apoptosis • Acute traumatic axonal transection in the retina and ONH, secondary axonal transection and degeneration from over activation of phosphatases and proteases • NF dephosphorylation at the ONH • Wallerian-like/ anterograde degeneration from the ONH • Anterograde and Retrograde AT dysfunction – anterograde AT blocked at the ONH, retrograde AT at the ONH and in the distal axon. • Aberrant expression of pNF in somas of transected, but persisting RGCs • No structural or functional recovery • Progressive atrophy throughout the ON, optic tract and target structures • Sustained activation of microglia

microglia, appear to be resolved by 4 weeks after elevated IOP, and no significant RGC loss is observed.

Alternately, increased IOP exposure, either through a greater magnitude or longer duration of IOP elevation, can lead to increased trauma and prolonged homeostatic imbalance and metabolic deficiency that can exceed a critical threshold of insult, resulting in permanent and progressive RGC dysfunction, degeneration, and loss. A marked increase in RGC membrane Ca^{2+} permeability through both direct and indirect mechanisms likely contribute to the rapid, and likely necrotic, initial loss of RGCs that occurs within hours of a critical IOP elevation. It is possible that the RGCs that are initially lost represent a subgroup that exhibits greater susceptibility to elevated IOP insult. Subsequent activation of apoptotic cascades and Ca^{2+}-dependent protein phosphatases, kinases and proteases leads to progressive degeneration and aberrant expression of cytoskeletal proteins throughout the RGC soma, dendrites, and axon. This is accompanied by sustained activation of microglia.

8.8 Factors Underlying the Vulnerability of RGCs to Injury

Selective loss of neuronal subsets is observed throughout many forms of neurodegeneration [474]. The factors and pathways that influence whether a neuron survives or dies in response to stress are complex and not fully understood. RGCs show resilience and recovery following relatively mild insults, suggesting a critical threshold of damage. Variability of the critical threshold throughout neuronal populations generates selective vulnerability. Many findings of the current research are likely a reflection of selective vulnerability to acute elevated IOP within the RGC population, including rapid

loss of Brn3a expression in a proportion of RGCs; expression of pNF in a proportion of RGC somas, which was more prevalent in the peripheral retina; and an incomplete blockade of anterograde and retrograde AT. The following sections discuss the concept of a critical threshold and what events might underlie a 'tipping point' in neuronal injury, as well as examples and mechanisms of vulnerability within the RGC population.

8.8.1 Critical Threshold

The critical threshold of damage in RGCs can be defined as the point at which the amount of cellular dysfunction in response to cumulative stress is no longer compatible with survival [303]. In modeling the transition from reversible dysfunction to irreversible degeneration, Porciatti and Ventura [303] proposed that single RGCs initially employ auto-regulatory mechanisms, to maintain normal function while exposed to sub-critical stress. However, with continued stress, auto-regulation fails, and the cell switches to survival mechanisms. Without relief, survival mechanisms become progressively less effective at maintaining function until a point of critical dysfunction is reached, after which apoptosis is initiated and irreversible degeneration proceeds. Notably, the critical threshold for irreversible damage, sometimes referred to as the 'point of no return' [475], has been shown to vary across the RGC population [476-478]. Such studies of selective vulnerability and critical thresholds are invaluable, as they provide clues regarding the origin of differential responses to injury, potentially enabling more accurate prognosis and treatment of degeneration due to injury or disease.

The precipitating event(s) that mark the transition of RGC injury from a state of reversibility to permanence are not fully understood. It is possible that the onset of AT

failure could mark a degenerative turn in RGC pathophysiology. However, the earliest documented onset of AT failure in response to acute elevated IOP is 30 minutes following onset [305] – a duration of IOP-induced ischemia that is not associated with significant RGC loss [264, 305]. Furthermore, the observation that AT blockade can be reversed in some cases [281, 285, 305, 306] demonstrates a quality of impermanence that does not support AT failure as an ultimate predictor of RGC death; however, the associated pathology of AT failure, such as the loss of neurotrophic supply, has been suggested to stimulate a series of signaling events that leads towards apoptosis [479]. Nickells [475] has suggested that activation of BAX protein on mitochondria and the subsequent release of cytochrome C, an initiator of the intrinsic pathway of apoptosis [480], marks the point of no return in IOP-induced RGC death. Similarly, Boehning et al. (2003) suggested that release of cytochrome C may be the precipitating factor that pushes a cell into a state of Ca^{2+} dysregulation and subsequent demise, as cytochrome C has been shown to bind to the inositol triphosphate (IP3) receptor on the sarcoplasmic reticulum and block autoregulation of Ca^{2+}-induced Ca^{2+} release. It should be noted that the aforementioned critical events are relevant to RGC death by apoptosis, whereas IOP elevations above MAP are likely to be accompanied by some degree of axonal trauma, after which necrosis is also likely to occur.

Saxena and Caroni [474] proposed that vulnerable neurons enter a state of mounting dysfunction, where hyperexcitability leads to Ca^{2+} dysfunction and accumulation of misfolded proteins, causing further stress and perpetuating the cycle of damage. RGCs exhibit a spectrum of vulnerability to elevated IOP, the range of which shifts with the severity of the insult. Figure 8.2 illustrates the relationship between

Figure 8.2 Latency to Reach a Critical Threshold of Injury in RGCs During Different Severities of IOP Elevation. RGCs accumulate IOP-related damage at different rates, depending on the severity of elevated IOP. When an RGC has met its injury threshold, damage is permanent and fatal. In acute elevated IOP above MAP, a combination of mechanical and ischemic stress causes RGCs to rapidly approach their critical injury threshold. RGCs exposed to acute elevated IOP below MAP approach their critical threshold at a slower rate, spending more time in the critical zone where reversible IOP-induced alterations of RGC physiology are at risk of becoming permanent. RGCs exposed to chronic, low-level elevations of IOP accrue damage at a markedly slower rate, possibly never reaching their threshold of critical injury.

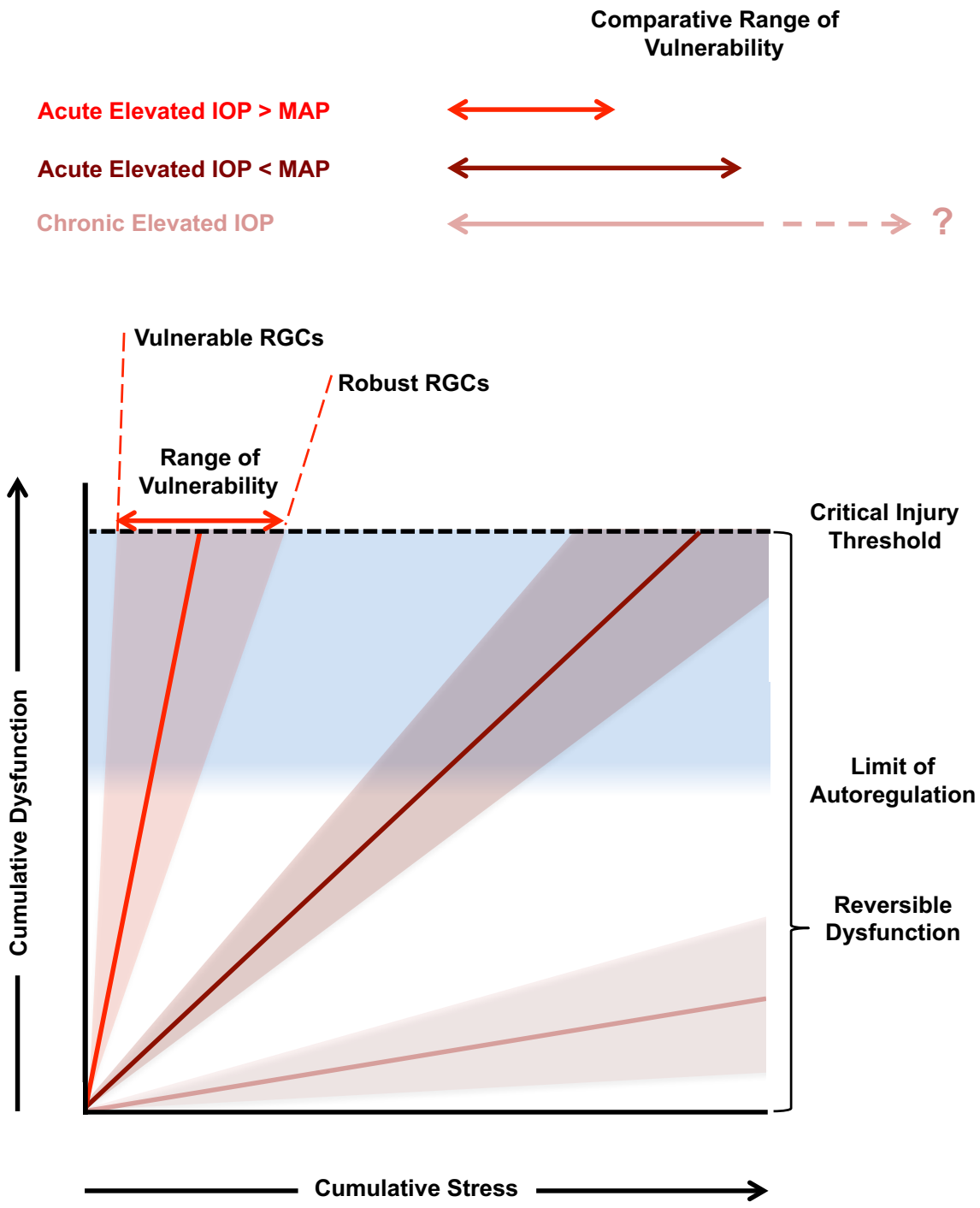
Comparative Range of Vulnerability
Acute Elevated IOP > MAP
Acute Elevated IOP < MAP
Chronic Elevated IOP
?
Vulnerable RGCs
Robust RGCs
Range of Vulnerability
Critical Injury Threshold
Limit of Autoregulation
Reversible Dysfunction
Cumulative Dysfunction
Cumulative Stress

accumulating stress and dysfunction in RGC populations during varying severities of elevated IOP. RGCs in each injury model reach their critical threshold for dysfunction over a range of time (cumulative stress). During early stages of injury, when autoregulation is intact and normal function is maintained, the impact of variation in vulnerability is not significant. As stress accumulates, variations in intrinsic responses will become more significant, causing the most vulnerable RGCs to reach the critical threshold for dysfunction at a faster rate than more resistant RGCs. The range between vulnerable and resistant RGCs will theoretically expand with more mild injuries, as the time to critical dysfunction is increased. With mild stress, some RGCs may never reach the critical threshold. Should therapeutic interventions be employed prior to the point of critical dysfunction, recovery is possible. While the linear relationships between stress and dysfunction illustrated in this model are an oversimplification, they are useful in demonstrating the dynamic range of RGC susceptibility to differing severity of insults. This spectrum of vulnerability is something that should be considered in studies of disease and injury progression, and is also relatable to other forms of neurodegeneration.

8.8.2 Variations in Vulnerability Within the RGC Population

Selective loss of subsets of neurons is a hallmark of many neurodegenerative diseases [474]. Evidence for selective vulnerability of RGC subtypes first arose in the late 1980's in studies of experimental and human glaucoma [481, 482] and continues to be a common topic of investigation in studies of RGC dysfunction and loss [275, 278, 423, 476-478, 483-485]. The relative susceptibility of RGCs to stress is likely a product of heterogeneity in both extrinsic and intrinsic influences (see Table 8.3).

Table 8.3 Extrinsic and Intrinsic Influences on RGC Selective Vulnerability

Extrinsic Factors	Intrinsic Factors
• Proximity to compromised vascular supply [163, 486] • Position in the ON (peripheral vs. central) [163] • Position in axon bundles [163] • Presence or absence of glial support [216, 278]	• Ca^{2+} dynamics in response to injury [485, 487, 488] • Ca^{2+} buffering capacity [478, 489-492] • Expression of excitatory and inhibitory receptors [477] • Metabolic expense of the neuron [484] • Expression of anti-apoptotic genes [493] • NF content of the neuron [478, 483]

Differential susceptibility of RGCs to elevated IOP was first acknowledged in studies of experimental glaucoma in non-human primates, where large RGCs were shown to exhibit greater vulnerability than small RGCs [476, 481, 482]. Quigley and colleagues [481] attributed this finding to both the position of large axon fibres in the ON – a higher density of large fibres in areas where greatest damage was observed – as well as an inherent susceptibility to chronically elevated IOP. However, although other investigators have reproduced this finding [477, 494], there is no consensus on size-related vulnerability to elevated IOP in RGCs, as other studies have shown equal loss of small and large RGCs [495] and even greater susceptibility of small RGCs [484, 496]. Interestingly, small and large RGCs appear to be genetically distinct in many pathways important for survival, such as cell adhesion, synaptic transmission, and ion transport, among others [497]. Further research is needed to determine the impact of genetic variability on the susceptibility of RGCs to stress.

Despite the uncertainty of size-related vulnerability, selective dysfunction and loss of RGCs is a consistent phenomenon in IOP-induced insults. AT function in RGCs appears to drop off on an axon-by-axon basis in response to elevated IOP [283, 331, 362, 498]. Quigley and Anderson [283] observed an incomplete block of anterograde AT in owl monkeys in response to acute elevated IOP. Concurrent EM analysis revealed that, rather than an incomplete block in all axons, there were some axons that exhibited accumulation of transported organelles, while adjacent axons appeared normal. Selective AT blockade has since been observed in other studies of elevated IOP in non-human primates [330, 331, 362], mice [274], and rats [217]. In the present study, retrograde and anterograde AT blockade in response to elevated IOP was incomplete. It is possible that

AT function was lost in selectively vulnerable RGCs, whereas more resistant RGCs maintained AT function, accounting for the reduction, but not elimination, of CTB AT.

An obvious extrinsic influence on RGC survival during elevated IOP is the topographical heterogeneity in exposure to vascular and biomechanical insult in the retina and ONH. As noted in section 8.3.2, species-specific variation in vascular anatomy at the ONH is associated with different topographical patterns of RGC. Similarly, RGC axons in the periphery of the ON have been suggested to experience proportionally more biomechanical strain than those in the middle of the ON [217, 481]. Position-dependent vulnerability was further demonstrated by Quigley and colleagues [163] as axons in the centre of individual axon bundles were proposed to experience greater vascular insufficiency, whereas those in the periphery experienced greater biomechanical strain. Specifically, greater AT blockade and structural deformities were observed in peripheral axons in 47% of bundles, while the remaining bundles exhibited a uniform distribution of pathology [163]. Notably, acute elevation of IOP above MAP provides a considerably different insult to RGCs than chronic, low levels of elevated IOP, and this is reflected in the differing patterns of topographical RGC loss in the retina: chronic elevated IOP often causes progressive RGC loss beginning in the periphery [141, 478, 481], while acute elevated IOP, as observed in the present experiments, does not [499]. Finally, survival of RGC axons in the ONH is tightly linked with the functions of local astrocytes [237]. It is possible that, should ONH astrocytes experience localized IOP-induced stress, they could in turn exhibit localized dysfunction, causing further stress to neighbouring axons.

Intracellular Ca^{2+} dynamics appear to have a determining influence on whether neurons survive or die in response to acute stress. Spinal neurons that recover normal

cytosolic Ca^{2+} levels within 1 to 2 hours following a mechanical injury-induced Ca^{2+} spike have been shown to be protected from later degeneration, and this critical window of reversal likely extends beyond 4 hours following injury [487]. A similar phenomenon is observed in cultured RGCs, where a transient exposure to glutamate can induce a recoverable spike in intracellular Ca^{2+} in some RGCs, where as others exhibit a prolonged loss of Ca^{2+} homeostasis, termed 'delayed Ca^{2+} deregulation', even after glutamate washout [485]. RGCs exhibiting Ca^{2+} deregulation died, while those that recovered baseline Ca^{2+} concentrations were spared [485]. As glutamate dysregulation has been implicated in retinal pathology following acute elevated IOP above MAP [151], it is plausible that differential Ca^{2+} dynamics had a role in the selective functional and structural pathology observed in the present experiments.

Interestingly, the NF content of RGCs appears to impact their vulnerability to elevated IOP. Vickers and colleagues [478] described proportionally greater loss of RGCs in the monkey retina that had exhibited strong non-phosphorylated NF expression in their somas. Further analysis revealed a dichotomous pattern of NF expression that appeared subtype-specific – large RGCs in the periphery were more likely to exhibit strong NF labelling and were more susceptible to damage, whereas a population of smaller RGCs in the central retina exhibited weaker NF expression and were less susceptible to damage [478]. In agreement with those findings, somal expression of non-phosphorylated NF has been associated with greater dendritic atrophy in a mouse model of chronic elevated IOP [483]. Furthermore, NF expression has been closely linked to RGC survival following elevated IOP in other studies of elevated IOP [274, 275] and RGC axonal injury [423]. In the present experiments, somal accumulation of pNF

appeared to occur in a subset of resistant RGCs, however, only after injury. From these findings it is clear that NF expression is associated in some way with the survival of RGCs in response to stress, however, the mechanism(s) and meaning behind this phenomenon remain to be elucidated.

Numerous studies have demonstrated that, in comparison to other RGC subtypes, melanopsin-expressing RGCs are more resilient to various retinal and optic nerve insults in rodents [425, 500-504], and in different forms of optic neuropathy in humans [41, 43, 505, 506]. Interestingly, Rovere and colleagues [502] demonstrated that melanopsin expression in ipRGCs is rapidly downregulated in response to stress but returns over time in surviving ipRGCs, suggesting that melanopsin expression alone may not always be an accurate reflection of ipRGC viability. The mechanism underlying the robustness of ipRGCs remains to be defined, but may be related to the selective expression of phospho-Akt [507] and/or pituitary adenylate cyclase-activating polypeptide [508], which have both been shown to promote the neuronal survival [507-509].

In addition to structural phenotype-associated vulnerability in RGCs, there is also evidence that physiological subtypes of RGCs exhibit differential susceptibility to IOP-induced damage. Physiologically identified Y-cells in the cat retina, which are morphologically large RGCs, have been shown to be less functionally susceptible to acute elevated IOP than X-cells [510, 511], contradicting initial reports of the relative vulnerability of large RGCs [476, 481, 511]. ON-RGCs have been reported to be more susceptible to elevated IOP-induced dendritic shrinkage[483, 510] and functional changes [478]; however, OFF-transient RGCs were fastest to exhibit structural and functional decline in a similar study [261]. The mechanisms behind differential vulnerability of

RGC physiological subtypes remain to be described. It is possible that differential effects of elevated IOP on retinal neurons upstream of RGCs in the ON and OFF pathways may play a role [510].

Finally, differential expression of excitatory and inhibitory receptors in RGC subtypes may predispose vulnerability to some insults [512]. Acute elevated IOP has been shown to disrupt homeostatic maintenance of extracellular ions [151, 294], creating an altered retinal environment and impacting RGC physiology. Osborne and colleagues [133] suggested that differing susceptibility to IOP-induced insult in RGCs may be a reflection of their receptor profile, i.e. an RGC expressing a given number of excitatory receptors may be more susceptible to an excitotoxic environment than an RGC expressing the same excitatory receptors in addition to inhibitory receptors. Some studies have indeed reported cell-type variation in the expression of excitatory and inhibitory receptors in RGCs [513, 514]. Moreover, the temporal progression of RGC loss in response to chronic elevated IOP in rats varies depending on the type of glutamate receptor expressed [477], and large RGCs have exhibited greater susceptibility to kainate than to NMDA, while the opposite was observed in smaller RGCs [515].

8.9 Limitations

8.9.1 Sample Size

The most notable limitation in the present studies, and one that is common to many in animal research, was that of a small sample size. The greatest factor influencing sample size was the complexity of the experimental design. A two-by-three factorial

design (two insult severities and three recovery time points) was used in both retrograde and anterograde AT studies. Time course experiments such as these are valuable for elucidating the progression of pathological responses; however, they are also time-consuming and labour intensive, making the inclusion of many animals in each group difficult. As variation was a persistent issue in the present data, larger samples sizes would likely have been beneficial.

8.9.2 Tracer Uptake Dynamics

The time course of tracer uptake should be considered when examining AT function. AT function along the ON was analyzed by calculating the difference between control and experimental CTB intensity. Consequently, an increasing difference in CTB intensity between control and experimental ONs may have reflected either a true, progressive impairment of AT, or that CTB intensity in the control nerve was increasing, while AT disruption in the experimental nerve remained constant. Indeed, the amount of CTB in the control ONH and ON appeared to be increasing over 3, 6, and 24 hours following elevated IOP. Therefore, although it is clear that AT was disrupted following elevated IOP, the rate of progression of AT disruption over the first 24 hours after elevated IOP may have been impacted by the compressed time scale. Similarly, it is possible that the AT disruption inferred from the measured difference in intensity between experimental and control ONs may be a persistent underestimation.

8.9.3 Sources of Error in Fluorescence Quantification

IHC was used to examine changes in RGC function, structure, and survival, as well as glial activation in the retina and ONH following elevated IOP. Brn3a+ and Iba1+ cells, which were automatically traced in ImageJ, were quantified by number and area, respectively; consequently, Brn3a and Iba1 analyses were not dependent on the intensity IHC labelling. The same was true for manually identified pNF+ somas in whole-mounted retinas. However, GFAP, pNF, and nonpNF labelling in the ONH was quantified based on fluorescence intensity. Both IHC and quantitative fluorescence are vulnerable to sources of error. Numerous variables can affect IHC labelling, including antibody specificity; variations in concentration, blocking procedure, and incubation time; and other factors which influence antibody exposure and tissue permeability. Furthermore, quantitative fluorescence can be affected by variations in imaging conditions. For these reasons, significant measures were taken to ensure minimal procedural variability between experiments, appropriate controls were included when necessary, and control and experimental ONHs and ONs were imaged under identical conditions. Additionally, GFAP, pNF and nonpNF labelling intensity was normalized to the pre-LC value within each section to eliminate artifactual variation in labelling intensity between control and experimental tissue. However, while internal normalization preserved the relative changes in labelling distribution within each ONH section, the relative differences between control and experimental intensity may have been altered by the assumption that the pre-LC intensity values were equal. CTB fluorescence was not subject to the limitations of IHC and therefore did not require the same internal normalization, however

control and experimental ONs were imaged in the same image frame, and all CTB ONHs were imaged under the same excitation parameters.

8.9.4 Phospho-Specific Antibodies

NF phosphorylation in the ONH was examined by comparing labelling intensity between pNF and nonpNF. In immunological investigation of phosphorylation, it is valuable to test antibodies for their phosphoform specificity. Pre-treatment of tissue with alkaline phosphatase causes global protein dephosphorylation, which should abolish labelling from antibodies specific to phosphorylated epitopes and may increase labelling from antibodies specific to dephosphorylated epitopes. The absence of these tests was a weakness in the present experiments; however, the specificity of 2F11 (for pNF) and SMI-32 (for nonpNF) antibodies has been previously confirmed [416, 516, 517]. The presence of pNF+ RGC somas in severely injured retinas, and not in healthy retinas, was also supportive of its efficacy at detecting NF in its phosphorylated form.

8.9.5 CTB and Inflammation

CTB was injected either intravitreally or into the SC in all animals in the AT experiments, however the effect of CTB itself on retinal and ON physiology was not evaluated. It is possible that the contralateral increase in microglia observed in the anterograde AT experiments was an inflammatory reaction to the CTB tracer, rather than a contralateral effect of elevated IOP. Information regarding the immune tolerance of CTB in rats is lacking, however, some studies have noted potent immunomodulary effects

of CTB in cell culture [518-520]. In future studies using CTB, including a control group where one eye receives CTB application and the other remains naïve may be beneficial.

8.10 Conclusions and Future Directions

This work has provided insight into the sub-cellular responses of RGCs and surrounding glia to acute IOP-induced stress, and how such responses relate spatiotemporally following sub-critical (30-minute) and critical (90-minute) durations of elevated IOP. Additionally, tracer characterization experiments provided new knowledge regarding the use of RITC and fluorescently conjugated CTB in the rat visual pathways. RGCs were shown not to exhibit transient dysfunction following 30 minutes of elevated IOP, while dysfunction and degeneration following 90 minutes of elevated IOP was progressive and permanent. These findings implied that RGCs rapidly attain a level of critical injury in response to elevated IOP above MAP, with a preceding window of dysfunction being either short or absent. The response of retinal microglia was commensurate with the severity of IOP insult and degree of RGC damage, and was spatially related to regions of significant RGC degeneration (e.g. the IPL), prompting the suggestion that microglial activation might be a useful indicator of the degree of RGC damage in future studies of RGC pathology. Furthermore, microglial activation in ONH regions posterior to the LC showed contrasting patterns of spatiotemporal progression, depending on the duration of elevated IOP. Retinal and ONH GFAP expression was primarily unaffected by elevated IOP. Reference to previous studies [60] indicated that this was likely an issue of timing, as most reports of GFAP elevation have occurred beyond 24 hours following elevated IOP insult. Integration of the present findings with

those of previous studies suggested that RGC dysfunction and structural damage is recovered in hours and transient microglial activation is resolved in weeks following a subcritical elevation of IOP. Conversely, a critical elevation of IOP causes rapid (within 24 hours) degenerative cascades in the proximal axon and soma of RGCs, involving AT dysfunction, cytoskeletal degeneration, and microglial activation. This is followed by dysfunction and degeneration in the distal axon, as well as changes in Müller cells and astrocytes throughout the RGC projection between 1 and 3 days following the insult, and severe RGC loss and axonal atrophy by 7 days. Selective loss of some RGCs immediately following the critical insult, as well as somal pNF expression in some RGCs and not others, suggested heterogeneity of vulnerability to acute elevated IOP across the RGC population that may be sub-type specific. Finally, contralateral activation of retinal and ONH microglia suggests that elevated IOP in one eye can cause pathological responses in the fellow eye, which has been supported in previous studies [245, 251]. Further details and ideas for future studies are presented in the following paragraphs.

The characterization studies of CTB and RITC in this thesis have improved practical knowledge regarding their utility in rat RGCs, as well as other AT-dependent neurons. The time course studies provided updated estimations of CTB and RITC transport rates that will enable the accuracy of their use in future studies of AT. Qualitative assessments of CTB in the retina, ONH, and ON confirmed CTB tracing as a suitable method of assessing anterograde and retrograde AT function in RGCs, with advantages over RITC, and a reliable method of obtaining bright and complete labelling throughout all RGC compartments in morphological studies.

The ONH was confirmed as a major site of AT blockade following elevated IOP. In primate studies of elevated IOP, AT blockade has been hypothesized to coincide with the structural LC [283, 362, 521]. However, as discussed above, accumulation of transported material in rats is more closely associated with the unmyelinated region of the retrobulbar ON [130]. This suggests a unique vulnerability of this region to AT disruption, and warrants further investigation into the causative mechanisms. Few studies have focused on the unique physiology and pathophysiology of the unmyelinated ONH; however, Fu and Sretavan [522] have demonstrated that glutamatergic presynaptic machinery accumulates specifically in the unmyelinated region of the ONH in mice exposed to elevated IOP, and that this is accompanied by localized glutamate release, which could in turn exacerbate regional dysfunction. Further characterization of the mechanisms underlying the vulnerability of the unmyelinated ONH is indicated, and may facilitate the development of treatments to fortify this region and protect RGC axons during or following acute or chronic IOP elevations. Experiments examining AT function and blockade in various conditions of myelination may also be useful.

The present findings also suggest that AT function in the distal RGC axon can be concurrently affected by acute IOP-induced stress to the proximal axon and soma. This raises the possibility that acute elevated IOP initiates an anterograde damage signal that is capable of rapidly disrupting retrograde AT function in the distal axon. Such a signal could represent either the propagation of a wave of ion disruption, such as a Na^{+} or Ca^{2+}[393], or a change in, or disruption of, anterograde AT that negatively impacts the initiation of retrograde AT [321, 463]. Anterograde stress signalling may also play a role in the response of the contralateral eye to elevated IOP, as microglia in the contralateral

eye and ONH showed signs of activation by 24 hours following elevated IOP in the fellow eye. It is possible that IOP-induced stress signals may be conveyed trans-synaptically at target structures [60], or via the retino-retinal projection [449, 450]. Experimentally interfering with anterograde communication at different locations in the RGC projection, and at different times, during or following elevated IOP – perhaps by inhibition of Na^+ influx, and therefore consequent Ca^{2+} waves, with tetrodotoxin [523], by inhibiting the reversal of the Na^+/Ca^{2+} exchanger [524, 525], by blocking IP3-gated Ca^{2+} channels [393], or by localized application of lidocaine to interfere with transport [526] – may help to clarify the origin of the contralateral response.

The primary goal of the this thesis was to examine how RGCs and surrounding glia in the retina, ONH, and ON respond over time *following* a transient elevation of IOP, with the hypothesis that there would be some initial, acute dysfunction, followed by a pattern of recovery over time. However, there was little evidence of any reversible AT disruption, neurofilament changes, or glial activation following the 30-minute insult, despite its proximity to a critical duration of injury (e.g. 45 minutes [396]). In fact, AT, NF, and glial pathologies were primarily absent following the 30-minute insult, while all were present as early as 3 hours following the 90-minute insult. These findings suggest that RGCs rapidly transition from a functional state to permanent dysfunction and degeneration over a narrow time window once the duration of elevated IOP becomes critical. Notably, reversible changes in AT function and axonal structure have been primarily reported following elevations of IOP that do not cause global ischemia [285, 305, 306], suggesting that the involvement of reduced or blocked perfusion in elevated IOP may shorten or eliminate the critical window of dysfunction that has been

hypothesized to precede irreversible structural degeneration in IOP-induced RGC death [303]. Further investigation is needed to identify the spatiotemporal onset of critical events that are associated with the determination of death in RGCs. Such studies may benefit from employing a magnitude of IOP elevation just below the MAP to allow pathological events to expand temporally, facilitating the determination of their respective temporal onsets with more accuracy. Once a critical point, or window, is characterized, focused comparative studies of gene and protein expression, as well as signalling pathways before, during, and after the critical point could help to reveal cellular events essential to the transition from reversible dysfunction to structural degeneration.

Expression of NF and microglial markers in the present studies appeared to be associated with the degree of structural degeneration in the tissue. It was suggested that these markers could be used as *in vivo* indicators of RGC damage in experimental studies, with possible translatability for tracking human diseases of RGC death. Indeed, *in vivo* imaging of GFP-labelled microglia in mouse retina has demonstrated that the degree of microgliosis is negatively correlated with the density of surviving RGCs following optic nerve crush and acute elevated IOP [436]. Although *in vivo* labels of NFs remain to be developed, serum pNF shows promise as a non-invasive indicator of retinal and ON damage [433]. It will be interesting to determine whether serum levels of pNF can accurately predict the degree of RGC damage in various models of elevated IOP, and if it also holds prognostic value in glaucomatous disease.

The time span over which a given population of RGCs succumbs to IOP-induced stress depends on both the severity IOP insult, measured by the duration and magnitude of elevated IOP, as well as the range of vulnerability throughout the RGC population.

Selective vulnerability of RGCs was apparent in the current study, indicated by the rapid loss of select RGCs, and aberrant expression of pNF in the somas of others. Further investigation of selectively vulnerable RGC populations will help to identify unique features that are associated with either vulnerability or robustness, and may help in the development of new neuroprotective strategies, as well as our understanding of RGC-related disease progression. Recent publications have begun to address this [477, 527, 528].

Overall, this thesis has demonstrated how RGCs recover following a transient elevation of IOP above MAP, and how the responses of RGCs and glia are different depending on the duration of IOP elevation. Comparing the observations of RGC function and structure between the 30-minute and 90-minute insults, two conclusions can be drawn regarding the resiliency of RGCs to acute elevated IOP: 1) that RGCs exhibit impressive resiliency to sub-critical elevated IOP, and 2) that once a critical duration of elevated IOP is reached, RGC dysfunction and degeneration is rapid and inherently irreversible. These findings highlight the importance of identifying critical events in RGC injury, and the cumulative stresses that lead to them, for the purpose of developing methods of preventing or reversing RGC damage in injury and disease.

REFERENCES

1. Thurston, M., A. Thurston, and J. McLeod, *Socio-emotional effects of the transition from sight to blindness.* British Journal of Visual Impairment, 2010. **28**(2): p. 90-112.
2. Quigley, H.A., *Glaucoma.* Lancet, 2011. **377**(9774): p. 1367-77.
3. Vickers, J.C., *The cellular mechanism underlying neuronal degeneration in glaucoma: parallels with Alzheimer's disease.* Aust N Z J Ophthalmol, 1997. **25**(2): p. 105-9.
4. Almasieh, M., et al., *The molecular basis of retinal ganglion cell death in glaucoma.* Prog Retin Eye Res, 2012. **31**(2): p. 152-81.
5. Quigley, H.A., et al., *Optic nerve damage in human glaucoma. II. The site of injury and susceptibility to damage.* Arch Ophthalmol, 1981. **99**(4): p. 635-49.
6. Levin, L.A. and P.L. Kaufman, *Adler's physiology of the eye : clinical application*. 11th ed. 2011, Edinburgh ; New York: Saunders/Elsevier. xii, 795 p.
7. Kolb, H., et al., *Cellular organization of the vertebrate retina.* Prog Brain Res, 2001. **131**: p. 3-26.
8. Lee, B.B., P.R. Martin, and U. Grunert, *Retinal connectivity and primate vision.* Prog Retin Eye Res, 2010. **29**(6): p. 622-39.
9. Field, G.D. and E.J. Chichilnisky, *Information processing in the primate retina: circuitry and coding.* Annu Rev Neurosci, 2007. **30**: p. 1-30.
10. Amthor, F.R., C.W. Oyster, and E.S. Takahashi, *Morphology of on-off direction-selective ganglion cells in the rabbit retina.* Brain Res, 1984. **298**(1): p. 187-90.
11. Chen, Y. and J. Naito, *A quantitative analysis of cells in the ganglion cell layer of the chick retina.* Brain Behav Evol, 1999. **53**(2): p. 75-86.
12. Jeon, C.J., E. Strettoi, and R.H. Masland, *The major cell populations of the mouse retina.* J Neurosci, 1998. **18**(21): p. 8936-46.
13. Curcio, C.A. and K.A. Allen, *Topography of ganglion cells in human retina.* J Comp Neurol, 1990. **300**(1): p. 5-25.
14. Nadal-Nicolas, F.M., et al., *Long-Term Effect of Optic Nerve Axotomy on the Retinal Ganglion Cell Layer.* Invest Ophthalmol Vis Sci, 2015. **56**(10): p. 6095-112.
15. Kolb, H., *Morphology and Circuitry of Ganglion Cells*, in *Webvision: The Organization of the Retina and Visual System*, H. Kolb, E. Fernandez, and R. Nelson, Editors. 1995, University of Utah Health Sciences Center: Salt Lake City (UT).
16. Hartline, H.K., *The response of single optic nerve fibers of the vertebrate eye to illumination of the retina.* American Journal of Physiology Legacy, 1938. **121**: p. 400-416.

17. Volgyi, B., S. Chheda, and S.A. Bloomfield, *Tracer coupling patterns of the ganglion cell subtypes in the mouse retina.* J Comp Neurol, 2009. **512**(5): p. 664-87.

18. Kolb, H., R. Nelson, and A. Mariani, *Amacrine cells, bipolar cells and ganglion cells of the cat retina: a Golgi study.* Vision Res, 1981. **21**(7): p. 1081-1114.

19. Berson, D.M., *1.25 - Retinal Ganglion Cell Types and Their Central Projections*, in *The Senses: A Comprehensive Reference*, R.H. Gardner, et al., Editors. 2008, Academic Press: New York. p. 491-519.

20. Boycott, B.B. and H. Wassle, *The morphological types of ganglion cells of the domestic cat's retina.* J Physiol, 1974. **240**(2): p. 397-419.

21. Hebel, R. and H. Hollander, *Size and distribution of ganglion cells in the human retina.* Anat Embryol (Berl), 1983. **168**(1): p. 125-36.

22. Perry, V.H., R. Oehler, and A. Cowey, *Retinal ganglion cells that project to the dorsal lateral geniculate nucleus in the macaque monkey.* Neuroscience, 1984. **12**(4): p. 1101-23.

23. Perry, V.H. and A. Cowey, *Retinal ganglion cells that project to the superior colliculus and pretectum in the macaque monkey.* Neuroscience, 1984. **12**(4): p. 1125-37.

24. Fukuda, Y., et al., *Nasotemporal overlap of crossed and uncrossed retinal ganglion cell projections in the Japanese monkey (Macaca fuscata).* J Neurosci, 1989. **9**(7): p. 2353-73.

25. Ghosh, K.K., et al., *Morphology of retinal ganglion cells in a new world monkey, the marmoset Callithrix jacchus.* J Comp Neurol, 1996. **366**(1): p. 76-92.

26. Stein, J.J. and D.M. Berson, *On the distribution of gamma cells in the cat retina.* Vis Neurosci, 1995. **12**(4): p. 687-700.

27. Isayama, T., et al., *Morphology of retinal ganglion cells in the ferret (Mustela putorius furo).* J Comp Neurol, 2009. **517**(4): p. 459-80.

28. Hofbauer, A. and U.C. Drager, *Depth segregation of retinal ganglion cells projecting to mouse superior colliculus.* J Comp Neurol, 1985. **234**(4): p. 465-74.

29. Perry, V.H., *The ganglion cell layer of the retina of the rat: a Golgi study.* Proc R Soc Lond B Biol Sci, 1979. **204**(1156): p. 363-75.

30. Dreher, B., et al., *The morphology, number, distribution and central projections of Class I retinal ganglion cells in albino and hooded rats.* Brain Behav Evol, 1985. **26**(1): p. 10-48.

31. Fukuda, Y., et al., *Morphological correlates of physiologically identified Y-, X-, and W-cells in cat retina.* J Neurophysiol, 1984. **52**(6): p. 999-1013.

32. Wassle, H. and B.B. Boycott, *Functional architecture of the mammalian retina.* Physiol Rev, 1991. **71**(2): p. 447-80.

33. Kandel, E.R., J.H. Schwartz, and T.M. Jessell, *Principles of neural science*. 4th ed. 2000, New York: McGraw-Hill, Health Professions Division. xli, 1414 p.

34. Masland, R.H., *The fundamental plan of the retina.* Nat Neurosci, 2001. **4**(9): p. 877-86.

35. Williams, R.W. and L.M. Chalupa, *An analysis of axon caliber within the optic nerve of the cat: evidence of size groupings and regional organization.* J Neurosci, 1983. **3**(8): p. 1554-64.

36. Ryan, S.J., *Retina*. 4th ed. 2006, Philadelphia: Elsevier/Mosby.

37. Watanabe, M., H. Sawai, and Y. Fukuda, *Number, distribution, and morphology of retinal ganglion cells with axons regenerated into peripheral nerve graft in adult cats.* J Neurosci, 1993. **13**(5): p. 2105-17.

38. Peichl, L., *Morphological types of ganglion cells in the dog and wolf retina.* J Comp Neurol, 1992. **324**(4): p. 590-602.

39. Hannibal, J., et al., *Central projections of intrinsically photosensitive retinal ganglion cells in the macaque monkey.* J Comp Neurol, 2014. **522**(10): p. 2231-48.

40. Graham, D.M. and K.Y. Wong, *Melanopsin-expressing, Intrinsically Photosensitive Retinal Ganglion Cells (ipRGCs)*, in *Webvision: The Organization of the Retina and Visual System*, H. Kolb, E. Fernandez, and R. Nelson, Editors. 1995: Salt Lake City (UT).

41. Cui, Q., et al., *The injury resistant ability of melanopsin-expressing intrinsically photosensitive retinal ganglion cells.* Neuroscience, 2015. **284**: p. 845-53.

42. Nadal-Nicolas, F.M., et al., *Displaced retinal ganglion cells in albino and pigmented rats.* Front Neuroanat, 2014. **8**: p. 99.

43. Obara, E.A., et al., *Loss of Melanopsin-Expressing Retinal Ganglion Cells in Severely Staged Glaucoma Patients.* Invest Ophthalmol Vis Sci, 2016. **57**(11): p. 4661-7.

44. Gregg, R.G., M.A. McCall, and S.C. Massey, *Chapter 15 - Function and Anatomy of the Mammalian Retina*, in *Retina (Fifth Edition)*, S.J. Schachat, et al., Editors. 2013, W.B. Saunders: London. p. 360-400.

45. Anderson, D.R., *Ultrastructure of human and monkey lamina cribrosa and optic nerve head.* Arch Ophthalmol, 1969. **82**(6): p. 800-14.

46. Sun, D., et al., *The morphology and spatial arrangement of astrocytes in the optic nerve head of the mouse.* J Comp Neurol, 2009. **516**(1): p. 1-19.

47. Levy, N.S., E.E. Crapps, and R.C. Bonney, *Displacement of the optic nerve head. Response to acute intraocular pressure elevation in primate eyes.* Arch Ophthalmol, 1981. **99**(12): p. 2166-74.

48. Radius, R.L. and D.R. Anderson, *The course of axons through the retina and optic nerve head.* Arch Ophthalmol, 1979. **97**(6): p. 1154-8.

49. Squire, L.R., *Fundamental neuroscience*. 4th ed. 2013, Amsterdam ; Boston: Elsevier/Academic Press. xxiv, 1127 p.

50. Levkovitch-Verbin, H., *Animal models of optic nerve diseases.* Eye (Lond), 2004. **18**(11): p. 1066-74.

51. Lund, R.D., P.W. Land, and J. Boles, *Normal and abnormal uncrossed retinotectal pathways in rats: an HRP study in adults.* J Comp Neurol, 1980. **189**(4): p. 711-20.

52. Lee, B.B., *Visual pathways and psychophysical channels in the primate.* J Physiol, 2011. **589**(Pt 1): p. 41-7.

53. Forrester, J. and A. Peters, *Nerve fibres in optic nerve of rat.* Nature, 1967. **214**(5085): p. 245-7.

54. Hattar, S., et al., *Central projections of melanopsin-expressing retinal ganglion cells in the mouse.* J Comp Neurol, 2006. **497**(3): p. 326-49.

55. Fleming, M.D., R.M. Benca, and M. Behan, *Retinal projections to the subcortical visual system in congenic albino and pigmented rats.* Neuroscience, 2006. **143**(3): p. 895-904.

56. May, P.J., *The mammalian superior colliculus: laminar structure and connections.* Prog Brain Res, 2006. **151**: p. 321-78.

57. Elkington, A.R., et al., *The structure of the lamina cribrosa of the human eye: an immunocytochemical and electron microscopical study.* Eye (Lond), 1990. **4 (Pt 1)**: p. 42-57.

58. Vecino, E., et al., *Glia-neuron interactions in the mammalian retina.* Prog Retin Eye Res, 2016. **51**: p. 1-40.

59. Newman, E. and A. Reichenbach, *The Muller cell: a functional element of the retina.* Trends Neurosci, 1996. **19**(8): p. 307-12.

60. Zhang, S., et al., *Detection of early neuron degeneration and accompanying glial responses in the visual pathway in a rat model of acute intraocular hypertension.* Brain Res, 2009. **1303**: p. 131-43.

61. Ebneter, A., et al., *Microglial activation in the visual pathway in experimental glaucoma: spatiotemporal characterization and correlation with axonal injury.* Invest Ophthalmol Vis Sci, 2010. **51**(12): p. 6448-60.

62. Morrison, J.C., et al., *Understanding mechanisms of pressure-induced optic nerve damage.* Prog Retin Eye Res, 2005. **24**(2): p. 217-40.

63. Quigley, H.A., et al., *Retrograde axonal transport of BDNF in retinal ganglion cells is blocked by acute IOP elevation in rats.* Invest Ophthalmol Vis Sci, 2000. **41**(11): p. 3460-6.

64. Butt, A.M., et al., *Functions of optic nerve glia: axoglial signalling in physiology and pathology.* Eye (Lond), 2004. **18**(11): p. 1110-21.

65. Nixon, R.A., *Dynamic behavior and organization of cytoskeletal proteins in neurons: reconciling old and new findings.* Bioessays, 1998. **20**(10): p. 798-807.

66. Portier, M.M., *[Neuronal cytoskeleton: structural, functional and dynamic aspects].* Rev Neurol (Paris), 1992. **148**(1): p. 1-19.

67. Woolf, N.J., A. Priel, and J.A. Tuszynski, *Nanoneuroscience : structural and functional roles of the neuronal cytoskeleton in health and disease*. Biological and medical physics, biomedical engineering,. 2009, Heidelberg: Springer. xii, 279 p.

68. Schek, H.T., 3rd, et al., *Microtubule assembly dynamics at the nanoscale.* Curr Biol, 2007. **17**(17): p. 1445-55.

69. Fletcher, D.A. and R.D. Mullins, *Cell mechanics and the cytoskeleton.* Nature, 2010. **463**(7280): p. 485-92.

70. Cheeseman, I.M. and A. Desai, *Molecular architecture of the kinetochore-microtubule interface.* Nat Rev Mol Cell Biol, 2008. **9**(1): p. 33-46.

71. Allen, C. and G.G. Borisy, *Structural polarity and directional growth of microtubules of Chlamydomonas flagella.* J Mol Biol, 1974. **90**(2): p. 381-402.

72. Baas, P.W., et al., *Polarity orientation of microtubules in hippocampal neurons: uniformity in the axon and nonuniformity in the dendrite.* Proc Natl Acad Sci U S A, 1988. **85**(21): p. 8335-9.

73. Chen, J., et al., *Projection domains of MAP2 and tau determine spacings between microtubules in dendrites and axons.* Nature, 1992. **360**(6405): p. 674-7.

74. Chen, H., B.W. Bernstein, and J.R. Bamburg, *Regulating actin-filament dynamics in vivo.* Trends Biochem Sci, 2000. **25**(1): p. 19-23.

75. Sekino, Y., N. Kojima, and T. Shirao, *Role of actin cytoskeleton in dendritic spine morphogenesis.* Neurochem Int, 2007. **51**(2-4): p. 92-104.

76. Kalil, K. and E.W. Dent, *Touch and go: guidance cues signal to the growth cone cytoskeleton.* Curr Opin Neurobiol, 2005. **15**(5): p. 521-6.

77. Barry, D.M., et al., *New movements in neurofilament transport, turnover and disease.* Exp Cell Res, 2007. **313**(10): p. 2110-20.

78. Sihag, R.K. and R.A. Nixon, *In vivo phosphorylation of distinct domains of the 70-kilodalton neurofilament subunit involves different protein kinases.* J Biol Chem, 1989. **264**(1): p. 457-64.

79. Liem, R.K. and S.B. Hutchison, *Purification of individual components of the neurofilament triplet: filament assembly from the 70 000-dalton subunit.* Biochemistry, 1982. **21**(13): p. 3221-6.

80. Petzold, A., *Neurofilament phosphoforms: surrogate markers for axonal injury, degeneration and loss.* J Neurol Sci, 2005. **233**(1-2): p. 183-98.

81. Yuan, A., et al., *Peripherin is a subunit of peripheral nerve neurofilaments: implications for differential vulnerability of CNS and peripheral nervous system axons.* J Neurosci, 2012. **32**(25): p. 8501-8.

82. Yuan, A., et al., *Alpha-internexin is structurally and functionally associated with the neurofilament triplet proteins in the mature CNS.* J Neurosci, 2006. **26**(39): p. 10006-19.

83. Nixon, R.A. and A. Yuan, *Cytoskeleton of the nervous system*. Advances in neurobiology,. 2011, New York: Springer. xv, 774 p.

84. Hirokawa, N., M.A. Glicksman, and M.B. Willard, *Organization of mammalian neurofilament polypeptides within the neuronal cytoskeleton.* J Cell Biol, 1984. **98**(4): p. 1523-36.

85. Guillery, R.W., *Some Electron Microscopical Observations of Degenerative Changes in Central Nervous Synapses.* Prog Brain Res, 1965. **14**: p. 57-76.

86. Lariviere, R.C. and J.P. Julien, *Functions of intermediate filaments in neuronal development and disease.* J Neurobiol, 2004. **58**(1): p. 131-48.

87. Zhang, Z., et al., *Normal dendritic arborization in spinal motoneurons requires neurofilament subunit L.* J Comp Neurol, 2002. **450**(2): p. 144-52.

88. Benitez-King, G., et al., *Phosphorylation-dephosphorylation imbalance of cytoskeletal associated proteins in neurodegenerative diseases.* Recent Pat CNS Drug Discov, 2006. **1**(2): p. 219-30.

89. Siegel, G.J., *Basic neurochemistry : molecular, cellular, and medical aspects*. 7th ed. 2006, Amsterdam ; Boston: Elsevier. xxiv, 992 p.

90. Humphrey, S.J., D.E. James, and M. Mann, *Protein Phosphorylation: A Major Switch Mechanism for Metabolic Regulation.* Trends Endocrinol Metab, 2015. **26**(12): p. 676-87.

91. Shenolikar, S., *Reversible protein phosphorylation. Preface.* Prog Mol Biol Transl Sci, 2012. **106**: p. xv-xvii.

92. Lee, S., H.C. Pant, and T.B. Shea, *Divergent and convergent roles for kinases and phosphatases in neurofilament dynamics.* J Cell Sci, 2014. **127**(Pt 18): p. 4064-77.

93. Pant, H.C., *Dephosphorylation of neurofilament proteins enhances their susceptibility to degradation by calpain.* Biochem J, 1988. **256**(2): p. 665-8.

94. Goldstein, M.E., N.H. Sternberger, and L.A. Sternberger, *Phosphorylation protects neurofilaments against proteolysis.* J Neuroimmunol, 1987. **14**(2): p. 149-60.

95. Yabe, J.T., et al., *Phospho-dependent association of neurofilament proteins with kinesin in situ.* Cell Motil Cytoskeleton, 2000. **45**(4): p. 249-62.

96. Jung, C., J.T. Yabe, and T.B. Shea, *C-terminal phosphorylation of the high molecular weight neurofilament subunit correlates with decreased neurofilament axonal transport velocity.* Brain Res, 2000. **856**(1-2): p. 12-9.

97. Shea, T.B. and L.A. Flanagan, *Kinesin, dynein and neurofilament transport.* Trends Neurosci, 2001. **24**(11): p. 644-8.

98. Omary, M.B., et al., *"Heads and tails" of intermediate filament phosphorylation: multiple sites and functional insights.* Trends Biochem Sci, 2006. **31**(7): p. 383-94.

99. Matus, A., *Microtubule-associated proteins and the determination of neuronal form.* J Physiol (Paris), 1990. **84**(1): p. 134-7.

100. Drewes, G., A. Ebneth, and E.M. Mandelkow, *MAPs, MARKs and microtubule dynamics.* Trends Biochem Sci, 1998. **23**(8): p. 307-11.

101. Taniguchi, T., et al., *Phosphorylation of tau is regulated by PKN.* J Biol Chem, 2001. **276**(13): p. 10025-31.

102. Aizawa, H., et al., *Phosphorylation of cofilin by LIM-kinase is necessary for semaphorin 3A-induced growth cone collapse.* Nat Neurosci, 2001. **4**(4): p. 367-73.

103. Guan, R.J., B.S. Khatra, and J.A. Cohlberg, *Phosphorylation of bovine neurofilament proteins by protein kinase FA (glycogen synthase kinase 3).* J Biol Chem, 1991. **266**(13): p. 8262-7.

104. Roder, H.M. and V.M. Ingram, *Two novel kinases phosphorylate tau and the KSP site of heavy neurofilament subunits in high stoichiometric ratios.* J Neurosci, 1991. **11**(11): p. 3325-43.

105. Nguyen, M.D., R.C. Lariviere, and J.P. Julien, *Deregulation of Cdk5 in a mouse model of ALS: toxicity alleviated by perikaryal neurofilament inclusions.* Neuron, 2001. **30**(1): p. 135-47.

106. Sihag, R.K. and R.A. Nixon, *Identification of Ser-55 as a major protein kinase A phosphorylation site on the 70-kDa subunit of neurofilaments. Early turnover during axonal transport.* J Biol Chem, 1991. **266**(28): p. 18861-7.

107. Yuan, A., et al., *Neurofilaments at a glance.* J Cell Sci, 2012. **125**(Pt 14): p. 3257-63.

108. Huang, W., et al., *Calpain activation in experimental glaucoma.* Invest Ophthalmol Vis Sci, 2010. **51**(6): p. 3049-54.

109. McKernan, D.P., et al., *A key role for calpains in retinal ganglion cell death.* Invest Ophthalmol Vis Sci, 2007. **48**(12): p. 5420-30.

110. Ryu, M., et al., *Critical role of calpain in axonal damage-induced retinal ganglion cell death.* J Neurosci Res, 2012. **90**(4): p. 802-15.

111. Yokoyama, Y., et al., *The role of calpain in an in vivo model of oxidative stress-induced retinal ganglion cell damage.* Biochem Biophys Res Commun, 2014. **451**(4): p. 510-5.

112. Mata, M., P. Honegger, and D.J. Fink, *Modulation of phosphorylation of neuronal cytoskeletal proteins by neuronal depolarization.* Cell Mol Neurobiol, 1997. **17**(1): p. 129-40.

113. Shea, T.B. and W.K. Chan, *Regulation of neurofilament dynamics by phosphorylation.* Eur J Neurosci, 2008. **27**(8): p. 1893-901.

114. Kroemer, K.H.E., H.J. Kroemer, and K.E. Kroemer-Elbert, *Engineering physiology : bases of human factors engineering/ergonomics*. 4th ed. 2010, Berlin: Springer. xxiii, 338 p.

115. Setou, M., T. Hayasaka, and I. Yao, *Axonal transport versus dendritic transport.* J Neurobiol, 2004. **58**(2): p. 201-6.

116. Grafstein, B. and D.S. Forman, *Intracellular transport in neurons.* Physiol Rev, 1980. **60**(4): p. 1167-283.

117. Miki, H., et al., *All kinesin superfamily protein, KIF, genes in mouse and human.* Proc Natl Acad Sci U S A, 2001. **98**(13): p. 7004-11.

118. Svoboda, K., et al., *Direct observation of kinesin stepping by optical trapping interferometry.* Nature, 1993. **365**(6448): p. 721-7.

119. Carter, N.J. and R.A. Cross, *Mechanics of the kinesin step.* Nature, 2005. **435**(7040): p. 308-12.

120. Hirokawa, N. and R. Takemura, *Molecular motors and mechanisms of directional transport in neurons.* Nat Rev Neurosci, 2005. **6**(3): p. 201-14.

121. Hirokawa, N., *Kinesin and dynein superfamily proteins and the mechanism of organelle transport.* Science, 1998. **279**(5350): p. 519-26.

122. Karki, S. and E.L. Holzbaur, *Cytoplasmic dynein and dynactin in cell division and intracellular transport.* Curr Opin Cell Biol, 1999. **11**(1): p. 45-53.

123. Hook, P. and R.B. Vallee, *The dynein family at a glance.* J Cell Sci, 2006. **119**(Pt 21): p. 4369-71.

124. Bridgman, P.C., *Myosin-dependent transport in neurons.* J Neurobiol, 2004. **58**(2): p. 164-74.

125. Ross, J.L., M.Y. Ali, and D.M. Warshaw, *Cargo transport: molecular motors navigate a complex cytoskeleton.* Curr Opin Cell Biol, 2008. **20**(1): p. 41-7.

126. Gross, S.P., M. Vershinin, and G.T. Shubeita, *Cargo transport: two motors are sometimes better than one.* Curr Biol, 2007. **17**(12): p. R478-86.

127. Wang, L., et al., *Rapid movement of axonal neurofilaments interrupted by prolonged pauses.* Nat Cell Biol, 2000. **2**(3): p. 137-41.

128. Wang, L. and A. Brown, *Rapid movement of microtubules in axons.* Curr Biol, 2002. **12**(17): p. 1496-1501.

129. Martin, K.R., et al., *Optic nerve dynein motor protein distribution changes with intraocular pressure elevation in a rat model of glaucoma.* Exp Eye Res, 2006. **83**(2): p. 255-62.

130. Chidlow, G., et al., *The optic nerve head is the site of axonal transport disruption, axonal cytoskeleton damage and putative axonal regeneration failure in a rat model of glaucoma.* Acta Neuropathol, 2011. **121**(6): p. 737-51.

131. Pease, M.E., et al., *Obstructed axonal transport of BDNF and its receptor TrkB in experimental glaucoma.* Invest Ophthalmol Vis Sci, 2000. **41**(3): p. 764-74.

132. Brown, A., *Slow axonal transport: stop and go traffic in the axon.* Nat Rev Mol Cell Biol, 2000. **1**(2): p. 153-6.

133. Osborne, N.N., et al., *A hypothesis to explain ganglion cell death caused by vascular insults at the optic nerve head: possible implication for the treatment of glaucoma.* Br J Ophthalmol, 2001. **85**(10): p. 1252-9.

134. Zhang, L., et al., *Retrograde axonal transport impairment of large- and medium-sized retinal ganglion cells in diabetic rat.* Curr Eye Res, 2000. **20**(2): p. 131-6.

135. Casson, R.J., et al., *Definition of glaucoma: clinical and experimental concepts.* Clin Experiment Ophthalmol, 2012. **40**(4): p. 341-9.

136. Weinreb, R.N., T. Aung, and F.A. Medeiros, *The pathophysiology and treatment of glaucoma: a review.* JAMA, 2014. **311**(18): p. 1901-11.

137. Tham, Y.C., et al., *Global prevalence of glaucoma and projections of glaucoma burden through 2040: a systematic review and meta-analysis.* Ophthalmology, 2014. **121**(11): p. 2081-90.

138. Johnson, T.V. and S.I. Tomarev, *Rodent models of glaucoma.* Brain Res Bull, 2010. **81**(2-3): p. 349-58.

139. Bouhenni, R.A., et al., *Animal models of glaucoma.* J Biomed Biotechnol, 2012. **2012**: p. 692609.

140. Langham, M., *The Morphology and Hydrodynamics of the Chamber Angle Draining the Aqueous Humor*, in *Ischemia and Loss of Vascular Autoregulation in Ocular and Cerebral Diseases*. 2009, Springer New York. p. 41-43.

141. Holcombe, D.J., et al., *Selective inner retinal dysfunction precedes ganglion cell loss in a mouse glaucoma model.* Br J Ophthalmol, 2008. **92**(5): p. 683-8.

142. Grozdanic, S.D., et al., *Functional evaluation of retina and optic nerve in the rat model of chronic ocular hypertension.* Exp Eye Res, 2004. **79**(1): p. 75-83.

143. Cuenca, N., et al., *Changes in the inner and outer retinal layers after acute increase of the intraocular pressure in adult albino Swiss mice.* Exp Eye Res, 2010. **91**(2): p. 273-85.

144. Goel, M., et al., *Aqueous humor dynamics: a review.* Open Ophthalmol J, 2010. **4**: p. 52-9.

145. Khan, A.K., et al., *Prolonged elevation of intraocular pressure results in retinal ganglion cell loss and abnormal retinal function in mice.* Exp Eye Res, 2015. **130**: p. 29-37.

146. Sappington, R.M., et al., *The microbead occlusion model: a paradigm for induced ocular hypertension in rats and mice.* Invest Ophthalmol Vis Sci, 2010. **51**(1): p. 207-16.

147. Matsumoto, Y., et al., *Rat chronic glaucoma model induced by intracameral injection of microbeads suspended in sodium sulfate-sodium hyaluronate.* Jpn J Ophthalmol, 2014. **58**(3): p. 290-7.

148. Bunker, S., et al., *Experimental glaucoma induced by ocular injection of magnetic microspheres.* J Vis Exp, 2015(96).

149. Cone, F.E., et al., *Differential susceptibility to experimental glaucoma among 3 mouse strains using bead and viscoelastic injection.* Exp Eye Res, 2010. **91**(3): p. 415-24.

150. Samsel, P.A., et al., *A novel method for the induction of experimental glaucoma using magnetic microspheres.* Invest Ophthalmol Vis Sci, 2011. **52**(3): p. 1671-5.

151. Nucci, C., et al., *Neurochemical evidence to implicate elevated glutamate in the mechanisms of high intraocular pressure (IOP)-induced retinal ganglion cell death in rat.* Neurotoxicology, 2005. **26**(5): p. 935-41.

152. Smith, G.G. and C.D. Baird, *Survival time of retinal cells when deprived of their blood supply by increased intraocular pressure.* Am J Ophthalmol, 1952. **35**(5:2): p. 133-6.

153. Büchi, E.R., I. Suivaizdis, and J. Fu, *Pressure-Induced Retinal Ischemia in Rats: An Experimental Model for Quantitative Study.* Ophthalmologica, 1991. **203**(3): p. 138-147.

154. Bui, B.V., et al., *Using the electroretinogram to understand how intraocular pressure elevation affects the rat retina.* J Ophthalmol, 2013. **2013**: p. 262467.

155. Rosenbaum, D.M., et al., *Functional and morphologic comparison of two methods to produce transient retinal ischemia in the rat.* J Neuroophthalmol, 2001. **21**(1): p. 62-8.

156. He, Z., et al., *Blood pressure modifies retinal susceptibility to intraocular pressure elevation.* PLoS One, 2012. **7**(2): p. e31104.

157. Balaratnasingam, C., et al., *Time-dependent effects of elevated intraocular pressure on optic nerve head axonal transport and cytoskeleton proteins.* Invest Ophthalmol Vis Sci, 2008. **49**(3): p. 986-99.

158. Abbott, C.J., et al., *Evaluation of retinal nerve fiber layer thickness and axonal transport 1 and 2 weeks after 8 hours of acute intraocular pressure elevation in rats.* Invest Ophthalmol Vis Sci, 2014. **55**(2): p. 674-87.

159. Crowston, J.G., et al., *An acute intraocular pressure challenge to assess retinal ganglion cell injury and recovery in the mouse.* Exp Eye Res, 2015.

160. Osborne, N.N., et al., *Retinal ischemia: mechanisms of damage and potential therapeutic strategies.* Prog Retin Eye Res, 2004. **23**(1): p. 91-147.

161. Goldblum, D. and T. Mittag, *Prospects for relevant glaucoma models with retinal ganglion cell damage in the rodent eye.* Vision Res, 2002. **42**(4): p. 471-8.

162. Krizaj, D., et al., *From mechanosensitivity to inflammatory responses: new players in the pathology of glaucoma.* Curr Eye Res, 2014. **39**(2): p. 105-19.

163. Quigley, H.A., et al., *The mechanism of optic nerve damage in experimental acute intraocular pressure elevation.* Invest Ophthalmol Vis Sci, 1980. **19**(5): p. 505-17.

164. Yan, D.B., et al., *Deformation of the lamina cribrosa by elevated intraocular pressure.* Br J Ophthalmol, 1994. **78**(8): p. 643-8.

165. Fortune, B., et al., *Deformation of the rodent optic nerve head and peripapillary structures during acute intraocular pressure elevation.* Invest Ophthalmol Vis Sci, 2011. **52**(9): p. 6651-61.

166. Yang, H., et al., *Deformation of the normal monkey optic nerve head connective tissue after acute IOP elevation within 3-D histomorphometric reconstructions.* Invest Ophthalmol Vis Sci, 2009. **50**(12): p. 5785-99.

167. Levy, N.S. and E.E. Crapps, *Displacement of optic nerve head in response to short-term intraocular pressure elevation in human eyes.* Arch Ophthalmol, 1984. **102**(5): p. 782-6.

168. Sappington, R.M. and D.J. Calkins, *Contribution of TRPV1 to microglia-derived IL-6 and NFkappaB translocation with elevated hydrostatic pressure.* Invest Ophthalmol Vis Sci, 2008. **49**(7): p. 3004-17.

169. Kurtenbach, S., S. Kurtenbach, and G. Zoidl, *Emerging functions of pannexin 1 in the eye.* Frontiers in Cellular Neuroscience, 2014. **8**: p. 263.

170. Beckel, J.M., et al., *Mechanosensitive release of adenosine 5'-triphosphate through pannexin channels and mechanosensitive upregulation of pannexin channels in optic nerve head astrocytes: a mechanism for purinergic involvement in chronic strain.* Glia, 2014. **62**(9): p. 1486-501.

171. Newman, E.A., *Glial cell inhibition of neurons by release of ATP.* J Neurosci, 2003. **23**(5): p. 1659-66.

172. Bao, L., S. Locovei, and G. Dahl, *Pannexin membrane channels are mechanosensitive conduits for ATP.* FEBS Lett, 2004. **572**(1-3): p. 65-8.

173. Xia, J., et al., *Neurons respond directly to mechanical deformation with pannexin-mediated ATP release and autostimulation of P2X7 receptors.* J Physiol, 2012. **590**(Pt 10): p. 2285-304.

174. Sugiyama, T., et al., *P2X(7) receptor activation may be involved in neuronal loss in the retinal ganglion cell layer after acute elevation of intraocular pressure in rats.* Mol Vis, 2013. **19**: p. 2080-91.

175. Sun, X., S. Barnes, and W.H. Baldridge, *Adenosine inhibits calcium channel currents via A1 receptors on salamander retinal ganglion cells in a mini-slice preparation.* J Neurochem, 2002. **81**(3): p. 550-6.

176. Casson, R.J., *Possible role of excitotoxicity in the pathogenesis of glaucoma.* Clin Experiment Ophthalmol, 2006. **34**(1): p. 54-63.

177. Reigada, D., et al., *Elevated pressure triggers a physiological release of ATP from the retina: Possible role for pannexin hemichannels.* Neuroscience, 2008. **157**(2): p. 396-404.

178. Resta, V., et al., *Acute retinal ganglion cell injury caused by intraocular pressure spikes is mediated by endogenous extracellular ATP.* Eur J Neurosci, 2007. **25**(9): p. 2741-54.

179. Zhang, X., et al., *Acute increase of intraocular pressure releases ATP into the anterior chamber.* Exp Eye Res, 2007. **85**(5): p. 637-43.

180. He, Z., et al., *The role of blood pressure in glaucoma.* Clin Exp Optom, 2011. **94**(2): p. 133-49.

181. Ryskamp, D.A., et al., *The polymodal ion channel transient receptor potential vanilloid 4 modulates calcium flux, spiking rate, and apoptosis of mouse retinal ganglion cells.* J Neurosci, 2011. **31**(19): p. 7089-101.

182. Kiel, J.W. and W.A. van Heuven, *Ocular perfusion pressure and choroidal blood flow in the rabbit.* Invest Ophthalmol Vis Sci, 1995. **36**(3): p. 579-85.

183. Zhi, Z., et al., *Impact of intraocular pressure on changes of blood flow in the retina, choroid, and optic nerve head in rats investigated by optical microangiography.* Biomed Opt Express, 2012. **3**(9): p. 2220-33.

184. Bargiotas, P., et al., *Pannexins in ischemia-induced neurodegeneration.* Proceedings of the National Academy of Sciences, 2011. **108**(51): p. 20772-20777.

185. Osborne, N.N., *Pathogenesis of ganglion "cell death" in glaucoma and neuroprotection: focus on ganglion cell axonal mitochondria.* Prog Brain Res, 2008. **173**: p. 339-52.

186. Tezel, G. *The role of glia, mitochondria, and the immune system in glaucoma.* Invest Ophthalmol Vis Sci, 2009. **50**(3): p. 1001-12

187. Li, S.Y., Z.J. Fu, and A.C. Lo, *Hypoxia-induced oxidative stress in ischemic retinopathy.* Oxid Med Cell Longev, 2012. **2012**: p. 426769.

188. Agudo-Barriuso, M., et al., *Anatomical and functional damage in experimental glaucoma.* Curr Opin Pharmacol, 2013. **13**(1): p. 5-11.

189. Mikkelsen, J.D., *Visualization of efferent retinal projections by immunohistochemical identification of cholera toxin subunit B.* Brain Research Bulletin, 1992. **28**(4): p. 619-623.

190. Matteau, I., D. Boire, and M. Ptito, *Retinal projections in the cat: a cholera toxin B subunit study.* Vis Neurosci, 2003. **20**(5): p. 481-93.

191. Wakakura, M. and S. Uga, *Distribution and orthograde axonal transport of HRP in feline eyes following intravitreal injection: an ultrastructural study.* Exp Eye Res, 1987. **45**(2): p. 305-15.

192. Minckler, D.S., *The organization of nerve fiber bundles in the primate optic nerve head.* Arch Ophthalmol, 1980. **98**(9): p. 1630-6.

193. Zhang, H.Y. and K.P. Hoffmann, *Retinal projections to the pretectum, accessory optic system and superior colliculus in pigmented and albino ferrets.* Eur J Neurosci, 1993. **5**(5): p. 486-500.

194. Vidal-Sanz, M., et al., *Persistent retrograde labeling of adult rat retinal ganglion cells with the carbocyanine dye diI.* Exp Neurol, 1988. **102**(1): p. 92-101.

195. Thanos, S., M. Vidal-Sanz, and A.J. Aguayo, *The use of rhodamine-B-isothiocyanate (RITC) as an anterograde and retrograde tracer in the adult rat visual system.* Brain Res, 1987. **406**(1-2): p. 317-21.

196. LaVail, J.H. and M.M. LaVail, *Retrograde axonal transport in the central nervous system.* Science, 1972. **176**(4042): p. 1416-7.

197. Nuschke, A.C., et al., *Assessment of retinal ganglion cell damage in glaucomatous optic neuropathy: Axon transport, injury and soma loss.* Exp Eye Res, 2015. **141**: p.111-24.

198. Thanos, S. and F. Bonhoeffer, *Investigations on the development and topographic order of retinotectal axons: anterograde and retrograde staining of axons and perikarya with rhodamine in vivo.* J Comp Neurol, 1983. **219**(4): p. 420-30.

199. Heyningen, S.V., *Cholera toxin: interaction of subunits with ganglioside GM1.* Science, 1974. **183**(4125): p. 656-7.

200. Fishman, P.H., *Role of membrane gangliosides in the binding and action of bacterial toxins.* J Membr Biol, 1982. **69**(2): p. 85-97.

201. Angelucci, A., F. Clasca, and M. Sur, *Anterograde axonal tracing with the subunit B of cholera toxin: a highly sensitive immunohistochemical protocol for revealing fine axonal morphology in adult and neonatal brains.* J Neurosci Methods, 1996. **65**(1): p. 101-12.

202. Flink, R. and J. Westman, *Different neuron populations in the feline lateral cervical nucleus: a light and electron microscopic study with the retrograde axonal transport technique.* J Comp Neurol, 1986. **250**(3): p. 265-81.

203. Formichella, C.R., et al., *Astrocyte Reactivity: A Biomarker for Retinal Ganglion Cell Health in Retinal Neurodegeneration.* J Clin Cell Immunol, 2014. **5**(1).

204. Luppi, P.H., P. Fort, and M. Jouvet, *Iontophoretic application of unconjugated cholera toxin B subunit (CTb) combined with immunohistochemistry of neurochemical substances: a method for transmitter identification of retrogradely labeled neurons.* Brain Res, 1990. **534**(1-2): p. 209-24.

205. Dederen, P.J., A.A. Gribnau, and M.H. Curfs, *Retrograde neuronal tracing with cholera toxin B subunit: comparison of three different visualization methods.* Histochem J, 1994. **26**(11): p. 856-62.

206. Abbott, C.J., et al., *Imaging axonal transport in the rat visual pathway.* Biomed Opt Express, 2013. **4**(2): p. 364-86.

207. Wu, C.C., R.M. Russell, and H.J. Karten, *The transport rate of cholera toxin B subunit in the retinofugal pathways of the chick.* Neuroscience, 1999. **92**(2): p. 665-76.

208. Morin, P.J., et al., *Amyloid precursor protein is synthesized by retinal ganglion cells, rapidly transported to the optic nerve plasma membrane and nerve terminals, and metabolized.* J Neurochem, 1993. **61**(2): p. 464-73.

209. O'Brien, R.J. and P.C. Wong, *Amyloid precursor protein processing and Alzheimer's disease.* Annu Rev Neurosci, 2011. **34**: p. 185-204.

210. Muresan, V. and Z. Ladescu Muresan, *Amyloid-beta precursor protein: Multiple fragments, numerous transport routes and mechanisms.* Exp Cell Res, 2015. **334**(1): p. 45-53.

211. Kamal, A., et al., *Kinesin-mediated axonal transport of a membrane compartment containing beta-secretase and presenilin-1 requires APP.* Nature, 2001. **414**(6864): p. 643-8.

212. Kamal, A., et al., *Axonal transport of amyloid precursor protein is mediated by direct binding to the kinesin light chain subunit of kinesin-I.* Neuron, 2000. **28**(2): p. 449-59.

213. Weber, A.J., C.D. Harman, and S. Viswanathan, *Effects of optic nerve injury, glaucoma, and neuroprotection on the survival, structure, and function of ganglion cells in the mammalian retina.* J Physiol, 2008. **586**(Pt 18): p. 4393-400.

214. Ma, Y.T., et al., *BDNF injected into the superior colliculus reduces developmental retinal ganglion cell death.* J Neurosci, 1998. **18**(6): p. 2097-107.

215. Burgoyne, C.F., *A biomechanical paradigm for axonal insult within the optic nerve head in aging and glaucoma.* Exp Eye Res, 2011. **93**(2): p. 120-32.

216. Morrison, J.C., W.O. Cepurna Ying Guo, and E.C. Johnson, *Pathophysiology of human glaucomatous optic nerve damage: insights from rodent models of glaucoma.* Exp Eye Res, 2011. **93**(2): p. 156-64.

217. Salinas-Navarro, M., et al., *Ocular hypertension impairs optic nerve axonal transport leading to progressive retinal ganglion cell degeneration.* Exp Eye Res, 2010. **90**(1): p. 168-83.

218. Godement, P., et al., *A study in developing visual systems with a new method of staining neurones and their processes in fixed tissue.* Development, 1987. **101**(4): p. 697-713.

219. Anderson, D.R. and A. Hendrickson, *Effect of intraocular pressure on rapid axoplasmic transport in monkey optic nerve.* Invest Ophthalmol, 1974. **13**(10): p. 771-83.

220. Mansour, H., et al., *Neurofilament phosphorylation in neuronal perikarya following axotomy: a study of rat spinal cord with ventral and dorsal root transection.* J Comp Neurol, 1989. **283**(4): p. 481-5.

221. Kashiwagi, K., et al., *Increase in dephosphorylation of the heavy neurofilament subunit in the monkey chronic glaucoma model.* Invest Ophthalmol Vis Sci, 2003. **44**(1): p. 154-9.

222. Dieterich, D.C., et al., *Partial regeneration and long-term survival of rat retinal ganglion cells after optic nerve crush is accompanied by altered expression, phosphorylation and distribution of cytoskeletal proteins.* Eur J Neurosci, 2002. **15**(9): p. 1433-43.

223. Vecino, E., L. Ulloa, and J. Avila, *The phosphorylated isoform of microtubule associated protein 1B (MAP1B) is expressed in the visual system of the tench (Tinca tinca, L) during optic nerve regeneration.* Neurosci Lett, 1998. **245**(2): p. 93-6.

224. Vecino, E. and J. Avila, *Distribution of the phosphorylated form of microtubule associated protein 1B in the fish visual system during optic nerve regeneration.* Brain Res Bull, 2001. **56**(2): p. 131-7.

225. Balaratnasingam, C., et al., *Axonal transport and cytoskeletal changes in the laminar regions after elevated intraocular pressure.* Invest Ophthalmol Vis Sci, 2007. **48**(8): p. 3632-44.

226. Espina, V., et al., *A portrait of tissue phosphoprotein stability in the clinical tissue procurement process.* Mol Cell Proteomics, 2008. **7**(10): p. 1998-2018.

227. Kanshin, E., M. Tyers, and P. Thibault, *Sample Collection Method Bias Effects in Quantitative Phosphoproteomics.* J Proteome Res, 2015. **14**(7): p. 2998-3004.

228. Oka, T., et al., *Presence of calpain-induced proteolysis in retinal degeneration and dysfunction in a rat model of acute ocular hypertension.* J Neurosci Res, 2006. **83**(7): p. 1342-51.

229. Oka, T., et al., *Amelioration of retinal degeneration and proteolysis in acute ocular hypertensive rats by calpain inhibitor ((1S)-1-((((1S)-1-benzyl-3-cyclopropylamino-2,3-di-oxopropyl)amino)carbonyl)-3-me thylbutyl)carbamic acid 5-methoxy-3-oxapentyl ester.* Neuroscience, 2006. **141**(4): p. 2139-45.

230. Campello, L., et al., *The ubiquitin-proteasome system in retinal health and disease.* Mol Neurobiol, 2013. **47**(2): p. 790-810.

231. Korhonen, L. and D. Lindholm, *The ubiquitin proteasome system in synaptic and axonal degeneration: a new twist to an old cycle.* J Cell Biol, 2004. **165**(1): p. 27-30.

232. Chen, J., et al., *Elevation of p-NR2A(S1232) by Cdk5/p35 contributes to retinal ganglion cell apoptosis in a rat experimental glaucoma model.* Neurobiol Dis, 2011. **43**(2): p. 455-64.

233. Sakamoto, K., et al., *Small molecule cyclin-dependent kinase inhibitors protect against neuronal cell death in the ischemic-reperfused rat retina.* J Ocul Pharmacol Ther, 2011. **27**(5): p. 419-25.

234. Huang, W., et al., *Calcineurin cleavage is triggered by elevated intraocular pressure, and calcineurin inhibition blocks retinal ganglion cell death in experimental glaucoma.* Proc Natl Acad Sci U S A, 2005. **102**(34): p. 12242-7.

235. Qu, J., et al., *Calcineurin activation causes retinal ganglion cell degeneration.* Mol Vis, 2012. **18**: p. 2828-38.

236. Ma, M., et al., *Calpains mediate axonal cytoskeleton disintegration during Wallerian degeneration.* Neurobiol Dis, 2013. **56**: p. 34-46.

237. Hernandez, M.R., H. Miao, and T. Lukas, *Astrocytes in glaucomatous optic neuropathy.* Prog Brain Res, 2008. **173**: p. 353-73.

238. Bringmann, A., et al., *Muller cells in the healthy and diseased retina.* Prog Retin Eye Res, 2006. **25**(4): p. 397-424.

239. Vilhardt, F., *Microglia: phagocyte and glia cell.* Int J Biochem Cell Biol, 2005. **37**(1): p. 17-21.

240. Pekny, M. and M. Nilsson, *Astrocyte activation and reactive gliosis.* Glia, 2005. **50**(4): p. 427-34.

241. Cho, K.J., et al., *Glial cell response and iNOS expression in the optic nerve head and retina of the rat following acute high IOP ischemia-reperfusion.* Brain Res, 2011. **1403**: p. 67-77.

242. Ju, K.R., et al., *Retinal glial cell responses and Fas/FasL activation in rats with chronic ocular hypertension.* Brain Res, 2006. **1122**(1): p. 209-21.

243. Sun, D., J. Qu, and T.C. Jakobs, *Reversible reactivity by optic nerve astrocytes.* Glia, 2013. **61**(8): p. 1218-35.

244. Li, L., N. Eter, and P. Heiduschka, *The microglia in healthy and diseased retina.* Exp Eye Res, 2015. **136**: p. 116-30.

245. Gallego, B.I., et al., *IOP induces upregulation of GFAP and MHC-II and microglia reactivity in mice retina contralateral to experimental glaucoma.* J Neuroinflammation, 2012. **9**: p. 92.

246. Woldemussie, E., M. Wijono, and G. Ruiz, *Muller cell response to laser-induced increase in intraocular pressure in rats.* Glia, 2004. **47**(2): p. 109-19.

247. Guo, Y., et al., *Early gene expression changes in the retinal ganglion cell layer of a rat glaucoma model.* Invest Ophthalmol Vis Sci, 2011. **52**(3): p. 1460-73.

248. Lam, T.T., J.M. Kwong, and M.O. Tso, *Early glial responses after acute elevated intraocular pressure in rats.* Invest Ophthalmol Vis Sci, 2003. **44**(2): p. 638-45.

249. Hovens, I., C. Nyakas, and R. Schoemaker, *A novel method for evaluating microglial activation using ionized calcium-binding adaptor protein-1 staining: cell body to cell size ratio.* Neuroimmunology and Neuroinflammation, 2014. **1**(2): p. 82-88.

250. Das Sarma, S., et al., *Cytomorphological and Cytochemical Identification of Microglia.* ISRN Immunology, 2013. **2013**: p. 10.

251. Rojas, B., et al., *Microglia in mouse retina contralateral to experimental glaucoma exhibit multiple signs of activation in all retinal layers.* J Neuroinflammation, 2014. **11**: p. 133.

252. Chen, L., P. Yang, and A. Kijlstra, *Distribution, markers, and functions of retinal microglia.* Ocul Immunol Inflamm, 2002. **10**(1): p. 27-39.

253. Aartsen, W.M., et al., *GFAP-driven GFP expression in activated mouse Muller glial cells aligning retinal blood vessels following intravitreal injection of AAV2/6 vectors.* PLoS One, 2010. **5**(8): p. e12387.

254. Kuzmanovic, M., V.J. Dudley, and V.P. Sarthy, *GFAP promoter drives Muller cell-specific expression in transgenic mice.* Invest Ophthalmol Vis Sci, 2003. **44**(8): p. 3606-13.

255. Vazquez-Chona, F.R., A.M. Clark, and E.M. Levine, *Rlbp1 promoter drives robust Muller glial GFP expression in transgenic mice.* Invest Ophthalmol Vis Sci, 2009. **50**(8): p. 3996-4003.

256. Brenner, M., et al., *GFAP promoter directs astrocyte-specific expression in transgenic mice.* J Neurosci, 1994. **14**(3 Pt 1): p. 1030-7.

257. Nolte, C., et al., *GFAP promoter-controlled EGFP-expressing transgenic mice: a tool to visualize astrocytes and astrogliosis in living brain tissue.* Glia, 2001. **33**(1): p. 72-86.

258. Lee, J.E., et al., *Ex vivo dynamic imaging of retinal microglia using time-lapse confocal microscopy.* Invest Ophthalmol Vis Sci, 2008. **49**(9): p. 4169-76.

259. Morrison, J.C., et al., *A rat model of chronic pressure-induced optic nerve damage.* Exp Eye Res, 1997. **64**(1): p. 85-96.

260. Levkovitch-Verbin, H., et al., *Translimbal laser photocoagulation to the trabecular meshwork as a model of glaucoma in rats.* Invest Ophthalmol Vis Sci, 2002. **43**(2): p. 402-10.

261. Della Santina, L., et al., *Differential progression of structural and functional alterations in distinct retinal ganglion cell types in a mouse model of glaucoma.* J Neurosci, 2013. **33**(44): p. 17444-57.

262. Guo, L., et al., *Retinal ganglion cell apoptosis in glaucoma is related to intraocular pressure and IOP-induced effects on extracellular matrix.* Invest Ophthalmol Vis Sci, 2005. **46**(1): p. 175-82.

263. Schmid, H., et al., *Loss of inner retinal neurons after retinal ischemia in rats.* Invest Ophthalmol Vis Sci, 2014. **55**(4): p. 2777-87.

264. Selles-Navarro, I., et al., *Retinal ganglion cell death after different transient periods of pressure-induced ischemia and survival intervals. A quantitative in vivo study.* Invest Ophthalmol Vis Sci, 1996. **37**(10): p. 2002-14.

265. Vidal-Sanz, M., et al., *Retinal ganglion cell death induced by retinal ischemia. neuroprotective effects of two alpha-2 agonists.* Surv Ophthalmol, 2001. **45 Suppl 3**: p. S261-7; discussion S273-6.

266. Li, Z.W., et al., *Tracking dendritic shrinkage of retinal ganglion cells after acute elevation of intraocular pressure.* Invest Ophthalmol Vis Sci, 2011. **52**(10): p. 7205-12.

267. Klosen, P., et al., *Perikaryal neurofilament phosphorylation in axotomized and 6-OH-dopamine-lesioned CNS neurons.* Brain Res, 1990. **526**(2): p. 259-69.

268. DiLeonardi, A.M., J.W. Huh, and R. Raghupathi, *Impaired axonal transport and neurofilament compaction occur in separate populations of injured axons following diffuse brain injury in the immature rat.* Brain Res, 2009. **1263**: p. 174-82.

269. Piri, N., et al., *Gene expression changes in the retina following optic nerve transection.* Mol Vis, 2006. **12**: p. 1660-73.

270. Buki, A. and J.T. Povlishock, *All roads lead to disconnection?--Traumatic axonal injury revisited.* Acta Neurochir (Wien), 2006. **148**(2): p. 181-93; discussion 193-4.

271. Huang, W., et al., *Transcriptional up-regulation and activation of initiating caspases in experimental glaucoma.* Am J Pathol, 2005. **167**(3): p. 673-81.

272. Das, A., et al., *Calpeptin provides functional neuroprotection to rat retinal ganglion cells following Ca2+ influx.* Brain Res, 2006. **1084**(1): p. 146-57.

273. Ma, M., F.S. Shofer, and R.W. Neumar, *Calpastatin overexpression protects axonal transport in an in vivo model of traumatic axonal injury.* J Neurotrauma, 2012. **29**(16): p. 2555-63.

274. Salinas-Navarro, M., et al., *Functional and morphological effects of laser-induced ocular hypertension in retinas of adult albino Swiss mice.* Mol Vis, 2009. **15**: p. 2578-98.

275. Soto, I., et al., *Retinal ganglion cell loss in a rat ocular hypertension model is sectorial and involves early optic nerve axon loss.* Invest Ophthalmol Vis Sci, 2011. **52**(1): p. 434-41.

276. Miller, C.C., et al., *Axonal transport of neurofilaments in normal and disease states.* Cell Mol Life Sci, 2002. **59**(2): p. 323-30.

277. Weber, A.J. and C.D. Harman, *Structure-function relations of parasol cells in the normal and glaucomatous primate retina.* Invest Ophthalmol Vis Sci, 2005. **46**(9): p. 3197-207.

278. Jakobs, T.C., et al., *Retinal ganglion cell degeneration is topological but not cell type specific in DBA/2J mice.* J Cell Biol, 2005. **171**(2): p. 313-25.

279. Kisiswa, L., et al., *Retinal ganglion cell death postponed: giving apoptosis a break?* Ophthalmic Res, 2010. **43**(2): p. 61-78.

280. McKerracher, L., et al., *Selective impairment of slow axonal transport after optic nerve injury in adult rats.* J Neurosci, 1990. **10**(8): p. 2834-41.

281. Johansson, J.O., *Retrograde axoplasmic transport in rat optic nerve in vivo. What causes blockage at increased intraocular pressure?* Exp Eye Res, 1986. **43**(4): p. 653-60.

282. Sossi, N. and D.R. Anderson, *Blockage of axonal transport in optic nerve induced by elevation of intraocular pressure. Effect of arterial hypertension induced by angiotensin I.* Arch Ophthalmol, 1983. **101**(1): p. 94-7.

283. Quigley, H. and D.R. Anderson, *The dynamics and location of axonal transport blockade by acute intraocular pressure elevation in primate optic nerve.* Invest Ophthalmol, 1976. **15**(8): p. 606-16.

284. Osborne, N.N., *Mitochondria: Their role in ganglion cell death and survival in primary open angle glaucoma.* Exp Eye Res, 2010. **90**(6): p. 750-7.

285. Minckler, D.S., A.H. Bunt, and G.W. Johanson, *Orthograde and retrograde axoplasmic transport during acute ocular hypertension in the monkey.* Invest Ophthalmol Vis Sci, 1977. **16**(5): p. 426-41.

286. Morfini, G., et al., *Glycogen synthase kinase 3 phosphorylates kinesin light chains and negatively regulates kinesin-based motility.* EMBO J, 2002. **21**(3): p. 281-93.

287. Neufeld, A.H. and B. Liu, *Glaucomatous optic neuropathy: when glia misbehave.* Neuroscientist, 2003. **9**(6): p. 485-95.

288. Kanamori, A., et al., *Long-term glial reactivity in rat retinas ipsilateral and contralateral to experimental glaucoma.* Exp Eye Res, 2005. **81**(1): p. 48-56.

289. Kerr, N.M., et al., *High pressure-induced retinal ischaemia reperfusion causes upregulation of gap junction protein connexin43 prior to retinal ganglion cell loss.* Exp Neurol, 2012. **234**(1): p. 144-52.

290. Tan, C., et al., *Age of rats seriously affects the degree of retinal damage induced by acute high intraocular pressure.* Curr Eye Res, 2015. **40**(3): p. 300-6.

291. Sapienza, A., et al., *Bilateral neuroinflammatory processes in visual pathways induced by unilateral ocular hypertension in the rat.* J Neuroinflammation, 2016. **13**(1): p. 44.

292. Balaratnasingam, C., et al., *Elevated pressure induced astrocyte damage in the optic nerve.* Brain Res, 2008. **1244**: p. 142-54.

293. Piras, A., et al., *Activation of autophagy in a rat model of retinal ischemia following high intraocular pressure.* PLoS One, 2011. **6**(7): p. e22514.

294. Holcombe, D.J., et al., *The effects of acute intraocular pressure elevation on rat retinal glutamate transport.* Acta Ophthalmol, 2008. **86**(4): p. 408-14.

295. Suzuki, R., et al., *Degeneration and dysfunction of retinal neurons in acute ocular hypertensive rats: involvement of calpains.* J Ocul Pharmacol Ther, 2014. **30**(5): p. 419-28.

296. Osborne, N.N. and A.K. Larsen, *Antigens associated with specific retinal cells are affected by ischaemia caused by raised intraocular pressure: effect of glutamate antagonists.* Neurochem Int, 1996. **29**(3): p. 263-70.

297. Uckermann, O., et al., *Ischemia-reperfusion causes exudative detachment of the rabbit retina.* Invest Ophthalmol Vis Sci, 2005. **46**(7): p. 2592-600.

298. Morrison, J.C., Choe, T. E., O Cepurna, W., Johnson, E., *Optic nerve head (ONH) gene expression responses to elevated intraocular pressure (IOP), anesthesia and anterior chamber cannulation in the CEI (controlled elevation of IOP) model of IOP-induced optic nerve injury.* Invest Ophthalmol Vis Sci, 2011. **55**: p. 2402.

299. Trost, A., et al., *Time-dependent retinal ganglion cell loss, microglial activation and blood-retina-barrier tightness in an acute model of ocular hypertension.* Exp Eye Res, 2015. **136**: p. 59-71.

300. Bosco, A., et al., *Early reduction of microglia activation by irradiation in a model of chronic glaucoma.* PLoS One, 2012. **7**(8): p. e43602.

301. Bosco, A., et al., *Reduced retina microglial activation and improved optic nerve integrity with minocycline treatment in the DBA/2J mouse model of glaucoma.* Invest Ophthalmol Vis Sci, 2008. **49**(4): p. 1437-46.

302. Dibas, A., et al., *Changes in ocular aquaporin-4 (AQP4) expression following retinal injury.* Mol Vis, 2008. **14**: p. 1770-83.

303. Porciatti, V. and L.M. Ventura, *Retinal ganglion cell functional plasticity and optic neuropathy: a comprehensive model.* J Neuroophthalmol, 2012. **32**(4): p. 354-8.

304. Fortune, B., et al., *Selective ganglion cell functional loss in rats with experimental glaucoma.* Invest Ophthalmol Vis Sci, 2004. **45**(6): p. 1854-62.

305. Radius, R.L. and D.R. Anderson, *Reversibility of optic nerve damage in primate eyes subjected to intraocular pressure above systolic blood pressure.* Br J Ophthalmol, 1981. **65**(10): p. 661-72.

306. Johansson, J.O., *Inhibition and recovery of retrograde axoplasmic transport in rat optic nerve during and after elevated IOP in vivo.* Exp Eye Res, 1988. **46**(2): p. 223-7.

307. Sehi, M., et al., *Reversal of retinal ganglion cell dysfunction after surgical reduction of intraocular pressure.* Ophthalmology, 2010. **117**(12): p. 2329-36.

308. Salgarello, T., et al., *Morpho-functional follow-up of the optic nerve in treated ocular hypertension: disc morphometry and steady-state pattern electroretinogram.* Curr Eye Res, 2008. **33**(8): p. 709-21.

309. Ventura, L.M. and V. Porciatti, *Restoration of retinal ganglion cell function in early glaucoma after intraocular pressure reduction: a pilot study.* Ophthalmology, 2005. **112**(1): p. 20-7.

310. Ventura, L.M., W.J. Feuer, and V. Porciatti, *Progressive loss of retinal ganglion cell function is hindered with IOP-lowering treatment in early glaucoma.* Invest Ophthalmol Vis Sci, 2012. **53**(2): p. 659-63.

311. Nagaraju, M., M. Saleh, and V. Porciatti, *IOP-dependent retinal ganglion cell dysfunction in glaucomatous DBA/2J mice.* Invest Ophthalmol Vis Sci, 2007. **48**(10): p. 4573-9.

312. Kong, Y.X., et al., *Functional changes in the retina during and after acute intraocular pressure elevation in mice.* Invest Ophthalmol Vis Sci, 2009. **50**(12): p. 5732-40.

313. Chidlow, G., et al., *Spatiotemporal characterization of optic nerve degeneration after chronic hypoperfusion in the rat.* Invest Ophthalmol Vis Sci, 2010. **51**(3): p. 1483-97.

314. Johnson, E.C., et al., *Cell proliferation and interleukin-6-type cytokine signaling are implicated by gene expression responses in early optic nerve head injury in rat glaucoma.* Invest Ophthalmol Vis Sci, 2011. **52**(1): p. 504-18.

315. Harris, A., et al., *Chapter 5 - Retinal and Choroidal Blood Flow in Health and Disease*, in *Retina (Fourth Edition)*, Wilkinson, S. et al., Editors. 2006, Mosby: Edinburgh. p. 83-102.

316. Mikula, S., et al., *Internet-enabled high-resolution brain mapping and virtual microscopy.* Neuroimage, 2007. **35**(1): p. 9-15.

317. He, Z., et al., *Coupling blood flow and neural function in the retina: a model for homeostatic responses to ocular perfusion pressure challenge.* Physiol Rep, 2013. **1**(3): p. e00055.

318. Nadal-Nicolas, F.M., et al., *Brn3a as a marker of retinal ganglion cells: qualitative and quantitative time course studies in naive and optic nerve-injured retinas.* Invest Ophthalmol Vis Sci, 2009. **50**(8): p. 3860-8.

319. Bull, N.D., et al., *Reduced axonal transport and increased excitotoxic retinal ganglion cell degeneration in mice transgenic for human mutant P301S tau.* PLoS One, 2012. **7**(4): p. e34724.

320. Zhang, Z., et al., *Axonal Transport in the Rat Optic Nerve Following Short-Term Reduction in Cerebrospinal Fluid Pressure or Elevation in Intraocular Pressure.* Invest Ophthalmol Vis Sci, 2015. **56**(8): p. 4257-66.

321. Dengler-Crish, C.M., et al., *Anterograde transport blockade precedes deficits in retrograde transport in the visual projection of the DBA/2J mouse model of glaucoma.* Front Neurosci, 2014. **8**: p. 290.

322. Crish, S.D., et al., *Failure of axonal transport induces a spatially coincident increase in astrocyte BDNF prior to synapse loss in a central target.* Neuroscience, 2013. **229**: p. 55-70.

323. Knox, D.L., R.C. Eagle, Jr., and W.R. Green, *Optic nerve hydropic axonal degeneration and blocked retrograde axoplasmic transport: histopathologic features in human high-pressure secondary glaucoma.* Arch Ophthalmol, 2007. **125**(3): p. 347-53.

324. Iwabe, S., et al., *Retrograde axonal transport obstruction of brain-derived neurotrophic factor (BDNF) and its TrkB receptor in the retina and optic nerve of American Cocker Spaniel dogs with spontaneous glaucoma.* Vet Ophthalmol, 2007. **10 Suppl 1**: p. 12-9.

325. Kim, D.H., et al., *Ganglion cell death in rat retina by persistent intraocular pressure elevation.* Korean J Ophthalmol, 2004. **18**(1): p. 15-22.

326. Prilloff, S., P. Henrich-Noack, and B.A. Sabel, *Recovery of axonal transport after partial optic nerve damage is associated with secondary retinal ganglion cell death in vivo.* Invest Ophthalmol Vis Sci, 2012. **53**(3): p. 1460-6.

327. Wang, X., W.H. Baldridge, and B.C. Chauhan, *Acute endothelin-1 application induces reversible fast axonal transport blockade in adult rat optic nerve.* Invest Ophthalmol Vis Sci, 2008. **49**(3): p. 961-7.

328. Nuschke, A., et al., *Axonal Transport Disruption in Retinal Ganglion Cells Following Transient Increase in Intraocular Pressure.* Investigative Ophthalmology & Visual Science, 2013. **54**(15): p. 5097-5097.

329. Windisch, B.K., et al., *Induction of heat shock proteins 27 and 72 in retinal ganglion cells after acute pressure-induced ischaemia.* Clin Experiment Ophthalmol, 2009. **37**(3): p. 299-307.

330. Quigley, H.A. and D.R. Anderson, *Distribution of axonal transport blockade by acute intraocular pressure elevation in the primate optic nerve head.* Invest Ophthalmol Vis Sci, 1977. **16**(7): p. 640-4.

331. Quigley, H.A., J. Guy, and D.R. Anderson, *Blockade of rapid axonal transport. Effect of intraocular pressure elevation in primate optic nerve.* Arch Ophthalmol, 1979. **97**(3): p. 525-31.

332. Nuschke, A., Wang, X., Smith, C., Danthurebandara, V., O'Leary, N., Chauhan, B., *Axonal transport disruption and cytoskeletal restructuring in retinal ganglion cells following elevated intraocular pressure.* Neuroscience Meeting Planner, 2014. **Program No. 797.11/Q6**(Washington, DC: Society for Neuroscience, 2014.).

333. Soto, I., et al., *Retinal ganglion cells downregulate gene expression and lose their axons within the optic nerve head in a mouse glaucoma model.* J Neurosci, 2008. **28**(2): p. 548-61.

334. Naskar, R., M. Wissing, and S. Thanos, *Detection of early neuron degeneration and accompanying microglial responses in the retina of a rat model of glaucoma.* Invest Ophthalmol Vis Sci, 2002. **43**(9): p. 2962-8.

335. Weidner, C., et al., *An anatomical study of ipsilateral retinal projections in the quail using radioautographic, horseradish peroxidase, fluorescence and degeneration techniques.* Brain Res, 1985. **340**(1): p. 99-108.

336. Sievers, J., et al., *Regeneration in the optic nerve of adult rats: influences of cultured astrocytes and optic nerve grafts of different ontogenetic stages.* J Neurocytol, 1995. **24**(10): p. 783-93.

337. Thanos, S., *Bidirectional fluorescent labelling techniques for the developing and regenerating visual system.* Acta Histochem Suppl, 1990. **38**: p. 259-67.

338. Hong, Y.M. and S. Thanos, *A quantitative approach to identify and isolate pure populations of fluorescently labeled adult retinal ganglion cells using a pressure-driven microaspiration technique.* Neurosci Lett, 1996. **214**(2-3): p. 111-4.

339. Montero, J.A., et al., *Intravitreal drug dispersion and needle gauge.* Acta Ophthalmol, 2013. **91**(8): p. e646-7.

340. Asami, T., et al., *A novel quadraport needle with improved intravitreal drug dispersion.* Retina, 2012. **32**(6): p. 1222-5.

341. Hsu, A., et al., *Functional architecture of primate cone and rod axons.* Vision Res, 1998. **38**(17): p. 2539-49.

342. Peters, A. and J.E. Vaughn, *Microtubules and filaments in the axons and astrocytes of early postnatal rat optic nerves.* J Cell Biol, 1967. **32**(1): p. 113-9.

343. Perge, J.A., et al., *How the optic nerve allocates space, energy capacity, and information.* J Neurosci, 2009. **29**(24): p. 7917-28.

344. Viancour, T.A. and N.A. Kreiter, *Vesicular fast axonal transport rates in young and old rat axons.* Brain Res, 1993. **628**(1-2): p. 209-17.

345. Doherty, G.J. and H.T. McMahon, *Mechanisms of endocytosis.* Annu Rev Biochem, 2009. **78**: p. 857-902.

346. Weidner, C., D. Miceli, and J. Reperant, *Orthograde axonal and transcellular transport of different fluorescent tracers in the primary visual system of the rat.* Brain Res, 1983. **272**(1): p. 129-36.

347. Gaasterland, D. and C. Kupfer, *Experimental glaucoma in the rhesus monkey.* Invest Ophthalmol, 1974. **13**(6): p. 455-7.

348. Quigley, H.A. and E.M. Addicks, *Chronic experimental glaucoma in primates. I. Production of elevated intraocular pressure by anterior chamber injection of autologous ghost red blood cells.* Invest Ophthalmol Vis Sci, 1980. **19**(2): p. 126-36.

349. Luntz, M.H., *Experimental glaucoma in the rabbit.* Am J Ophthalmol, 1966. **61**(4): p. 665-80.

350. ElGohary, A.A. and L.H. Elshazly, *Photopic negative response in diagnosis of glaucoma: an experimental study in glaucomatous rabbit model.* Int J Ophthalmol, 2015. **8**(3): p. 459-64.

351. Ruiz-Ederra, J., et al., *[Comparison of three methods of inducing chronic elevation of intraocular pressure in the pig (experimental glaucoma)].* Arch Soc Esp Oftalmol, 2005. **80**(10): p. 571-9.

352. Fujishiro, T., et al., *Establishment of an experimental ferret ocular hypertension model for the analysis of central visual pathway damage.* Sci Rep, 2014. **4**: p. 6501.

353. Morrison, J.C., *Elevated intraocular pressure and optic nerve injury models in the rat.* J Glaucoma, 2005. **14**(4): p. 315-7.

354. Ueda, J., et al., *Experimental glaucoma model in the rat induced by laser trabecular photocoagulation after an intracameral injection of India ink.* Jpn J Ophthalmol, 1998. **42**(5): p. 337-44.

355. Pang, I.H. and A.F. Clark, *Rodent models for glaucoma retinopathy and optic neuropathy.* J Glaucoma, 2007. **16**(5): p. 483-505.

356. McKinnon, S.J., C.L. Schlamp, and R.W. Nickells, *Mouse models of retinal ganglion cell death and glaucoma.* Exp Eye Res, 2009. **88**(4): p. 816-24.

357. Yun, H., et al., *A laser-induced mouse model with long-term intraocular pressure elevation.* PLoS One, 2014. **9**(9): p. e107446.

358. Ji, J., et al., *Effects of elevated intraocular pressure on mouse retinal ganglion cells.* Vision Res, 2005. **45**(2): p. 169-79.

359. Albrecht May, C., *Comparative anatomy of the optic nerve head and inner retina in non-primate animal models used for glaucoma research.* Open Ophthalmol J, 2008. **2**: p. 94-101.

360. Reid, W.M., et al., *Strain-related differences after experimental traumatic brain injury in rats.* J Neurotrauma, 2010. **27**(7): p. 1243-53.

361. Mabuchi, F., et al., *Regional optic nerve damage in experimental mouse glaucoma.* Invest Ophthalmol Vis Sci, 2004. **45**(12): p. 4352-8.

362. Quigley, H.A. and E.M. Addicks, *Chronic experimental glaucoma in primates. II. Effect of extended intraocular pressure elevation on optic nerve head and axonal transport.* Invest Ophthalmol Vis Sci, 1980. **19**(2): p. 137-52.

363. Rodriguez-Ramos Fernandez, J. and R.R. Dubielzig, *Ocular comparative anatomy of the family Rodentia.* Vet Ophthalmol, 2013. **16 Suppl 1**: p. 94-9.

364. Nguyen, C., et al., *Studies of scleral biomechanical behavior related to susceptibility for retinal ganglion cell loss in experimental mouse glaucoma.* Invest Ophthalmol Vis Sci, 2013. **54**(3): p. 1767-80.

365. Safa, R. and N.N. Osborne, *Retinas from albino rats are more susceptible to ischaemic damage than age-matched pigmented animals.* Brain Res, 2000. **862**(1-2): p. 36-42.

366. Muller, A., et al., *Differential effect of ischemia/reperfusion on pigmented and albino rabbit retina.* J Ocul Pharmacol Ther, 1996. **12**(3): p. 337-42.

367. Humpel, C., et al., *Effects of bright artificial light on monoamines and neuropeptides in eight different brain regions compared in a pigmented and nonpigmented rat strain.* J Neurosci Res, 1992. **32**(4): p. 605-12.

368. Zemel, E., et al., *Ocular pigmentation protects the rabbit retina from gentamicin-induced toxicity.* Invest Ophthalmol Vis Sci, 1995. **36**(9): p. 1875-84.

369. Wang, Z., J. Dillon, and E.R. Gaillard, *Antioxidant properties of melanin in retinal pigment epithelial cells.* Photochem Photobiol, 2006. **82**(2): p. 474-9.

370. Morrison, J.C., W.O. Cepurna, and E.C. Johnson, *Modeling glaucoma in rats by sclerosing aqueous outflow pathways to elevate intraocular pressure.* Exp Eye Res, 2015.

371. Danias, J., et al., *Characterization of retinal damage in the episcleral vein cauterization rat glaucoma model.* Exp Eye Res, 2006. **82**(2): p. 219-28.

372. Garcia-Valenzuela, E., et al., *Programmed cell death of retinal ganglion cells during experimental glaucoma.* Exp Eye Res, 1995. **61**(1): p. 33-44.

373. Boussommier-Calleja, A. and D.R. Overby, *The influence of genetic background on conventional outflow facility in mice.* Invest Ophthalmol Vis Sci, 2013. **54**(13): p. 8251-8.

374. Fatehee, N., et al., *The impact of acutely elevated intraocular pressure on the porcine optic nerve head.* Invest Ophthalmol Vis Sci, 2011. **52**(9): p. 6192-8.

375. Sigal, I.A., et al., *Eye-specific IOP-induced displacements and deformations of human lamina cribrosa.* Invest Ophthalmol Vis Sci, 2014. **55**(1): p. 1-15.

376. Bui, B.V., et al., *The gradient of retinal functional changes during acute intraocular pressure elevation.* Invest Ophthalmol Vis Sci, 2005. **46**(1): p. 202-13.

377. He, Z., B.V. Bui, and A.J. Vingrys, *The rate of functional recovery from acute IOP elevation.* Invest Ophthalmol Vis Sci, 2006. **47**(11): p. 4872-80.

378. Tsai, T.I., B.V. Bui, and A.J. Vingrys, *Effect of acute intraocular pressure challenge on rat retinal and cortical function.* Invest Ophthalmol Vis Sci, 2014. **55**(2): p. 1067-77.

379. Jia, L., et al., *Patterns of intraocular pressure elevation after aqueous humor outflow obstruction in rats.* Invest Ophthalmol Vis Sci, 2000. **41**(6): p. 1380-5.

380. Wang, W.H., et al., *Noninvasive measurement of rodent intraocular pressure with a rebound tonometer.* Invest Ophthalmol Vis Sci, 2005. **46**(12): p. 4617-21.

381. Danias, J., et al., *Method for the noninvasive measurement of intraocular pressure in mice.* Invest Ophthalmol Vis Sci, 2003. **44**(3): p. 1138-41.

382. Millar, J.C. and I.H. Pang, *Non-continuous measurement of intraocular pressure in laboratory animals.* Exp Eye Res, 2015. **141**: p. 74-90.

383. Morrison, J.C., et al., *Reliability and sensitivity of the TonoLab rebound tonometer in awake Brown Norway rats.* Invest Ophthalmol Vis Sci, 2009. **50**(6): p. 2802-8.

384. Cherecheanu, A.P., et al., *Ocular perfusion pressure and ocular blood flow in glaucoma.* Curr Opin Pharmacol, 2013. **13**(1): p. 36-42.

385. Lee, D.S., et al., *Influence of translaminar pressure dynamics on the position of the anterior lamina cribrosa surface.* Invest Ophthalmol Vis Sci, 2015. **56**(5): p. 2833-41.

386. Morgan, W.H., et al., *Optic disc movement with variations in intraocular and cerebrospinal fluid pressure.* Invest Ophthalmol Vis Sci, 2002. **43**(10): p. 3236-42.

387. Hayreh, S.S., W. March, and D.R. Anderson, *Pathogenesis of block of rapid orthograde axonal transport by elevated intraocular pressure.* Exp Eye Res, 1979. **28**(5): p. 515-23.

388. Farooqui-Kabir, S.R., et al., *Regulation of Hsp27 expression and cell survival by the POU transcription factor Brn3a.* Cell Death Differ, 2004. **11**(11): p. 1242-4.

389. Fahy, E.T., et al., *Axonal transport along retinal ganglion cells is intact during reduced function post-injury.* Exp Eye Res, 2016.

390. Fu, C.T. and D. Sretavan, *Laser-induced ocular hypertension in albino CD-1 mice.* Invest Ophthalmol Vis Sci, 2010. **51**(2): p. 980-90.

391. Radius, R.L. and D.R. Anderson, *Rapid axonal transport in primate optic nerve. Distribution of pressure-induced interruption.* Arch Ophthalmol, 1981. **99**(4): p. 650-4.

392. Niittykoski, M., et al., *Altered calcium signaling in an experimental model of glaucoma.* Invest Ophthalmol Vis Sci, 2010. **51**(12): p. 6387-93.

393. Rishal, I. and M. Fainzilber, *Axon-soma communication in neuronal injury.* Nat Rev Neurosci, 2014. **15**(1): p. 32-42.

394. Buckingham, B.P., et al., *Progressive ganglion cell degeneration precedes neuronal loss in a mouse model of glaucoma.* J Neurosci, 2008. **28**(11): p. 2735-44.

395. Lafuente Lopez-Herrera, M.P., et al., *Transient ischemia of the retina results in altered retrograde axoplasmic transport: neuroprotection with brimonidine.* Exp Neurol, 2002. **178**(2): p. 243-58.

396. Jehle, T., et al., *Quantification of ischemic damage in the rat retina: a comparative study using evoked potentials, electroretinography, and histology.* Invest Ophthalmol Vis Sci, 2008. **49**(3): p. 1056-64.

397. Bautista, R.D., *Glaucomatous neurodegeneration and the concept of neuroprotection.* Int Ophthalmol Clin, 1999. **39**(3): p. 57-70.

398. Staal, J.A., et al., *Initial calcium release from intracellular stores followed by calcium dysregulation is linked to secondary axotomy following transient axonal stretch injury.* J Neurochem, 2010. **112**(5): p. 1147-55.

399. Levkovitch-Verbin, H., et al., *Optic nerve transection in monkeys may result in secondary degeneration of retinal ganglion cells.* Invest Ophthalmol Vis Sci, 2001. **42**(5): p. 975-82.

400. Munemasa, Y. and Y. Kitaoka, *Molecular mechanisms of retinal ganglion cell degeneration in glaucoma and future prospects for cell body and axonal protection.* Front Cell Neurosci, 2012. **6**: p. 60.

401. WoldeMussie, E., et al., *Neuroprotection of retinal ganglion cells by brimonidine in rats with laser-induced chronic ocular hypertension.* Invest Ophthalmol Vis Sci, 2001. **42**(12): p. 2849-55.

402. Ren, R., et al., *Long-term rescue of rat retinal ganglion cells and visual function by AAV-mediated BDNF expression after acute elevation of intraocular pressure.* Invest Ophthalmol Vis Sci, 2012. **53**(2): p. 1003-11.

403. Krieglstein, G.K. and International Congress of Ophthalmology. Glaucoma Society., *Glaucoma update III*. 1987, Berlin ; New York: Springer-Verlag. xv, 270 p.

404. Grytz, R., G. Meschke, and J.B. Jonas, *The collagen fibril architecture in the lamina cribrosa and peripapillary sclera predicted by a computational remodeling approach.* Biomech Model Mechanobiol, 2011. **10**(3): p. 371-82.

405. Yablonski, M.E. and A. Asamoto, *Hypothesis concerning the pathophysiology of optic nerve damage in open angle glaucoma.* J Glaucoma, 1993. **2**(2): p. 119-27.

406. Tang-Schomer, M.D., et al., *Partial interruption of axonal transport due to microtubule breakage accounts for the formation of periodic varicosities after traumatic axonal injury.* Exp Neurol, 2012. **233**(1): p. 364-72.

407. Nakajima, E., et al., *Calpain-specific proteolysis in primate retina: Contribution of calpains in cell death.* Invest Ophthalmol Vis Sci, 2006. **47**(12): p. 5469-75.

408. Russo, R., et al., *Calpain-mediated cleavage of Beclin-1 and autophagy deregulation following retinal ischemic injury in vivo.* Cell Death Dis, 2011. **2**: p. e144.

409. Saatman, K.E., et al., *Traumatic axonal injury results in biphasic calpain activation and retrograde transport impairment in mice.* J Cereb Blood Flow Metab, 2003. **23**(1): p. 34-42.

410. Hahnenberger, R.W., *Effects of pressure on fast axoplasmic flow. An in vitro study in the vagus nerve of rabbits.* Acta Physiol Scand, 1978. **104**(3): p. 299-308.

411. Band, L.R., et al., *Intracellular flow in optic nerve axons: a mechanism for cell death in glaucoma.* Invest Ophthalmol Vis Sci, 2009. **50**(8): p. 3750-8.

412. Morgan, J.E., *Circulation and axonal transport in the optic nerve.* Eye (Lond), 2004. **18**(11): p. 1089-95.

413. Yu, D.Y., et al., *Retinal ganglion cells: Energetics, compartmentation, axonal transport, cytoskeletons and vulnerability.* Prog Retin Eye Res, 2013. **36**: p. 217-46.

414. Cai, Q., M.L. Davis, and Z.H. Sheng, *Regulation of axonal mitochondrial transport and its impact on synaptic transmission.* Neurosci Res, 2011. **70**(1): p. 9-15.

415. Lee, M.K. and D.W. Cleveland, *Neuronal intermediate filaments.* Annu Rev Neurosci, 1996. **19**: p. 187-217.

416. Wang, J., et al., *Hyperphosphorylation and accumulation of neurofilament proteins in Alzheimer disease brain and in okadaic acid-treated SY5Y cells.* FEBS Lett, 2001. **507**(1): p. 81-7.

417. Perrot, R. and J. Eyer, *Neuronal intermediate filaments and neurodegenerative disorders.* Brain Res Bull, 2009. **80**(4-5): p. 282-95.

418. Shukla, V., S. Skuntz, and H.C. Pant, *Deregulated Cdk5 activity is involved in inducing Alzheimer's disease.* Arch Med Res, 2012. **43**(8): p. 655-62.

419. Creed, J.A., et al., *Concussive brain trauma in the mouse results in acute cognitive deficits and sustained impairment of axonal function.* J Neurotrauma, 2011. **28**(4): p. 547-63.

420. Schumacher, P.A., J.H. Eubanks, and M.G. Fehlings, *Increased calpain I-mediated proteolysis, and preferential loss of dephosphorylated NF200, following traumatic spinal cord injury.* Neuroscience, 1999. **91**(2): p. 733-44.

421. Balaratnasingam, C., et al., *Time-dependent effects of focal retinal ischemia on axonal cytoskeleton proteins.* Invest Ophthalmol Vis Sci, 2010. **51**(6): p. 3019-28.

422. Drager, U.C. and A. Hofbauer, *Antibodies to heavy neurofilament subunit detect a subpopulation of damaged ganglion cells in retina.* Nature, 1984. **309**(5969): p. 624-6.

423. Silveira, L.C., M. Russelakis-Carneiro, and V.H. Perry, *The ganglion cell response to optic nerve injury in the cat: differential responses revealed by neurofibrillar staining.* J Neurocytol, 1994. **23**(2): p. 75-86.

424. Galindo-Romero, C., et al., *Number and spatial distribution of intrinsically photosensitive retinal ganglion cells in the adult albino rat.* Exp Eye Res, 2013. **108**: p. 84-93.

425. Perez de Sevilla Muller, L., et al., *Melanopsin ganglion cells are the most resistant retinal ganglion cell type to axonal injury in the rat retina.* PLoS One, 2014. **9**(3): p. e93274.

426. Lefevre, K., et al., *Involvement of cyclin-dependent kinases in axotomy-induced retinal ganglion cell death.* J Comp Neurol, 2002. **447**(1): p. 72-81.

427. Cheung, Z.H., K. Gong, and N.Y. Ip, *Cyclin-dependent kinase 5 supports neuronal survival through phosphorylation of Bcl-2.* J Neurosci, 2008. **28**(19): p. 4872-7.

428. Kang, M.H. and D.Y. Yu, *Distribution pattern of axonal cytoskeleton proteins in the human optic nerve head.* Neural Regen Res, 2015. **10**(8): p. 1198-200.

429. Ghonemi, M.O., et al., *Role of Phosphorylated Neurofilament H as a diagnostic and prognostic marker in traumatic brain injury.* The Egyptian Journal of Critical Care Medicine, 2013. **1**(3): p. 139-144.

430. Radwan, W.M., et al., *A new marker for ischemic cerebrovascular stroke: Phosphorylated Neurofilament H.* The Egyptian Journal of Critical Care Medicine, 2013. **1**(2): p. 105-108.

431. Gresle, M.M., H. Butzkueven, and G. Shaw, *Neurofilament proteins as body fluid biomarkers of neurodegeneration in multiple sclerosis.* Mult Scler Int, 2011. **2011**: p. 315406.

432. Vorobyeva, A.A., et al., *Phosphorylated neurofilament heavy subunits as a marker of neurodegeneration in demyelinating diseases of the CNS.* Neurochemical Journal, 2014. **8**(3): p. 221-225.

433. Guy, J., et al., *Phosphorylated neurofilament heavy chain is a marker of neurodegeneration in Leber hereditary optic neuropathy (LHON).* Mol Vis, 2008. **14**: p. 2443-50.

434. Man, P.Y., D.M. Turnbull, and P.F. Chinnery, *Leber hereditary optic neuropathy.* J Med Genet, 2002. **39**(3): p. 162-9.

435. Petzold, A., et al., *A novel biomarker for retinal degeneration: vitreous body neurofilament proteins.* J Neural Transm, 2009. **116**(12): p. 1601-6.

436. Liu, S., et al., *Tracking retinal microgliosis in models of retinal ganglion cell damage.* Invest Ophthalmol Vis Sci, 2012. **53**(10): p. 6254-62.

437. Ramirez, A.I., et al., *Quantification of the effect of different levels of IOP in the astroglia of the rat retina ipsilateral and contralateral to experimental glaucoma.* Invest Ophthalmol Vis Sci, 2010. **51**(11): p. 5690-6.

438. Perego, C., S. Fumagalli, and M.G. De Simoni, *Temporal pattern of expression and colocalization of microglia/macrophage phenotype markers following brain ischemic injury in mice.* J Neuroinflammation, 2011. **8**: p. 174.

439. Fumagalli, S., et al., *The ischemic environment drives microglia and macrophage function.* Front Neurol, 2015. **6**: p. 81.

440. Johnson, E.C., et al., *Chronology of optic nerve head and retinal responses to elevated intraocular pressure.* Invest Ophthalmol Vis Sci, 2000. **41**(2): p. 431-42.

441. Morrison, J.C., et al., *Optic Nerve Head (ONH) Gene Expression Responses to Elevated Intraocular Pressure (IOP), Anesthesia and Anterior Chamber Cannulation in the CEI (Controlled Elevation of IOP) Model of IOP-induced Optic Nerve Injury.* Investigative Ophthalmology & Visual Science, 2014. **55**(13): p. 2402-2402.

442. Haynes, S.E., et al., *The P2Y12 receptor regulates microglial activation by extracellular nucleotides.* Nat Neurosci, 2006. **9**(12): p. 1512-9.

443. James, G. and A.M. Butt, *P2X and P2Y purinoreceptors mediate ATP-evoked calcium signalling in optic nerve glia in situ.* Cell Calcium, 2001. **30**(4): p. 251-9.

444. Fries, J.E., et al., *Distribution of metabotropic P2Y receptors in the rat retina: a single-cell RT-PCR study.* Brain Res Mol Brain Res, 2004. **130**(1-2): p. 1-6.

445. Mac Nair, C., C. Schlamp, and R. Nickells, *Adenosine triphosphate (ATP) Signaling Pathways Trigger Glial Activation in the Mouse Retina.* Investigative Ophthalmology & Visual Science, 2013. **54**(15): p. 286-286.

446. Bodeutsch, N., et al., *Unilateral injury to the adult rat optic nerve causes multiple cellular responses in the contralateral site.* J Neurobiol, 1999. **38**(1): p. 116-28.

447. de Hoz, R., et al., *Rod-like microglia are restricted to eyes with laser-induced ocular hypertension but absent from the microglial changes in the contralateral untreated eye.* PLoS One, 2013. **8**(12): p. e83733.

448. Burgoyne, C.F., *The non-human primate experimental glaucoma model.* Exp Eye Res, 2015. **141**: p. 57-73.

449. Nadal-Nicolas, F.M., et al., *Retino-retinal projection in juvenile and young adult rats and mice.* Exp Eye Res, 2015. **134**: p. 47-52.

450. Avellaneda-Chevrier, V.K., et al., *The retino-retinal projection: Tracing retinal ganglion cells projecting to the contralateral retina.* Neurosci Lett, 2015. **591**: p. 105-9.

451. Madeira, M.H., et al., *Contribution of microglia-mediated neuroinflammation to retinal degenerative diseases.* Mediators Inflamm, 2015. **2015**: p. 673090.

452. Tezel, G., *TNF-alpha signaling in glaucomatous neurodegeneration.* Prog Brain Res, 2008. **173**: p. 409-21.

453. Tezel, G. and M.B. Wax, *Increased production of tumor necrosis factor-alpha by glial cells exposed to simulated ischemia or elevated hydrostatic pressure induces apoptosis in cocultured retinal ganglion cells.* J Neurosci, 2000. **20**(23): p. 8693-700.

454. Neufeld, A.H., M.R. Hernandez, and M. Gonzalez, *Nitric oxide synthase in the human glaucomatous optic nerve head.* Arch Ophthalmol, 1997. **115**(4): p. 497-503.

455. Li, Y., et al., *An energy theory of glaucoma.* Glia, 2015. **63**(9): p. 1537-52.

456. Nakase, T., S. Fushiki, and C.C. Naus, *Astrocytic gap junctions composed of connexin 43 reduce apoptotic neuronal damage in cerebral ischemia.* Stroke, 2003. **34**(8): p. 1987-93.

457. Chen, Y.S., et al., *Sustained intravitreal delivery of connexin43 mimetic peptide by poly(D,L-lactide-co-glycolide) acid micro- and nanoparticles--Closing the gap in retinal ischaemia.* Eur J Pharm Biopharm, 2015. **95**(Pt B): p. 378-86.

458. Marambaud, P., U. Dreses-Werringloer, and V. Vingtdeux, *Calcium signaling in neurodegeneration.* Mol Neurodegener, 2009. **4**: p. 20.

459. Gehlbach, P.L. and R.L. Purple, *A paired comparison of two models of experimental retinal ischemia.* Curr Eye Res, 1994. **13**(8): p. 597-602.

460. David, S. and A. Kroner, *Repertoire of microglial and macrophage responses after spinal cord injury.* Nat Rev Neurosci, 2011. **12**(7): p. 388-99.

461. Hu, X., et al., *Microglia/macrophage polarization dynamics reveal novel mechanism of injury expansion after focal cerebral ischemia.* Stroke, 2012. **43**(11): p. 3063-70.

462. Hu, X., et al., *Microglial and macrophage polarization-new prospects for brain repair.* Nat Rev Neurol, 2015. **11**(1): p. 56-64.

463. Crish, S.D., et al., *Distal axonopathy with structural persistence in glaucomatous neurodegeneration.* Proc Natl Acad Sci U S A, 2010. **107**(11): p. 5196-201.

464. Louzada-Junior, P., et al., *Glutamate release in experimental ischaemia of the retina: an approach using microdialysis.* J Neurochem, 1992. **59**(1): p. 358-63.

465. Knoferle, J., et al., *Mechanisms of acute axonal degeneration in the optic nerve in vivo.* Proc Natl Acad Sci U S A, 2010. **107**(13): p. 6064-9.

466. Wurm, A., et al., *Effects of ischemia-reperfusion on physiological properties of Muller glial cells in the porcine retina.* Invest Ophthalmol Vis Sci, 2011. **52**(6): p. 3360-7.

467. Kezic, J.M., et al., *Effect of anterior chamber cannulation and acute IOP elevation on retinal macrophages in the adult mouse.* Invest Ophthalmol Vis Sci, 2013. **54**(4): p. 3028-36.

468. Ito, D., et al., *Enhanced expression of Iba1, ionized calcium-binding adapter molecule 1, after transient focal cerebral ischemia in rat brain.* Stroke, 2001. **32**(5): p. 1208-15.

469. Joo, C.K., et al., *Necrosis and apoptosis after retinal ischemia: involvement of NMDA-mediated excitotoxicity and p53.* Invest Ophthalmol Vis Sci, 1999. **40**(3): p. 713-20.

470. Produit-Zengaffinen, N., C.J. Pournaras, and D.F. Schorderet, *Retinal ischemia-induced apoptosis is associated with alteration in Bax and Bcl-x(L) expression rather than modifications in Bak and Bcl-2.* Mol Vis, 2009. **15**: p. 2101-10.

471. Neufeld, A.H., et al., *Loss of retinal ganglion cells following retinal ischemia: the role of inducible nitric oxide synthase.* Exp Eye Res, 2002. **75**(5): p. 521-8.

472. Lam, T.T., A.S. Abler, and M.O. Tso, *Apoptosis and caspases after ischemia-reperfusion injury in rat retina.* Invest Ophthalmol Vis Sci, 1999. **40**(5): p. 967-75.

473. Rosenbaum, D.M., et al., *The role of the p53 protein in the selective vulnerability of the inner retina to transient ischemia.* Invest Ophthalmol Vis Sci, 1998. **39**(11): p. 2132-9.

474. Saxena, S. and P. Caroni, *Selective neuronal vulnerability in neurodegenerative diseases: from stressor thresholds to degeneration.* Neuron, 2011. **71**(1): p. 35-48.

475. Nickells, R.W., *The cell and molecular biology of glaucoma: mechanisms of retinal ganglion cell death.* Invest Ophthalmol Vis Sci, 2012. **53**(5): p. 2476-81.

476. Glovinsky, Y., H.A. Quigley, and G.R. Dunkelberger, *Retinal ganglion cell loss is size dependent in experimental glaucoma.* Invest Ophthalmol Vis Sci, 1991. **32**(3): p. 484-91.

477. Luo, X.G., et al., *The selective vulnerability of retinal ganglion cells in rat chronic ocular hypertension model at early phase.* Cell Mol Neurobiol, 2009. **29**(8): p. 1143-51.

478. Vickers, J.C., et al., *Differential vulnerability of neurochemically identified subpopulations of retinal neurons in a monkey model of glaucoma.* Brain Res, 1995. **680**(1-2): p. 23-35.

479. Nucci, C., et al., *Glaucoma an open window to neurodegeneration and neuroprotection*, in *Progress in brain research,*. Progress in Brain Res, 2008. **173**: p. iii.

480. Qu, J., D. Wang, and C.L. Grosskreutz, *Mechanisms of retinal ganglion cell injury and defense in glaucoma.* Exp Eye Res, 2010. **91**(1): p. 48-53.

481. Quigley, H.A., et al., *Chronic glaucoma selectively damages large optic nerve fibers.* Invest Ophthalmol Vis Sci, 1987. **28**(6): p. 913-20.

482. Quigley, H.A., G.R. Dunkelberger, and W.R. Green, *Chronic human glaucoma causing selectively greater loss of large optic nerve fibers.* Ophthalmology, 1988. **95**(3): p. 357-63.

483. Feng, L., et al., *Sustained ocular hypertension induces dendritic degeneration of mouse retinal ganglion cells that depends on cell type and location.* Invest Ophthalmol Vis Sci, 2013. **54**(2): p. 1106-17.

484. Baltan, S., et al., *Metabolic vulnerability disposes retinal ganglion cell axons to dysfunction in a model of glaucomatous degeneration.* J Neurosci, 2010. **30**(16): p. 5644-52.

485. Hartwick, A.T., et al., *Functional assessment of glutamate clearance mechanisms in a chronic rat glaucoma model using retinal ganglion cell calcium imaging.* J Neurochem, 2005. **94**(3): p. 794-807.

486. Rydevik, B., et al., *Blockage of axonal transport induced by acute, graded compression of the rabbit vagus nerve.* J Neurol Neurosurg Psychiatry, 1980. **43**(8): p. 690-8.

487. Williams, P.R., et al., *A recoverable state of axon injury persists for hours after spinal cord contusion in vivo.* Nat Commun, 2014. **5**: p. 5683.

488. Lee, J.K., S. Lu, and A. Madhukar, *Real-Time dynamics of Ca2+, caspase-3/7, and morphological changes in retinal ganglion cell apoptosis under elevated pressure.* PLoS One, 2010. **5**(10): p. e13437.

489. Calkins, D.J., *Critical pathogenic events underlying progression of neurodegeneration in glaucoma.* Prog Retin Eye Res, 2012. **31**(6): p. 702-19.

490. D'Orlando, C., et al., *Calretinin and calbindin D-28k delay the onset of cell death after excitotoxic stimulation in transfected P19 cells.* Brain Res, 2001. **909**(1-2): p. 145-58.

491. Wang, X., Y.K. Ng, and S.S. Tay, *Factors contributing to neuronal degeneration in retinas of experimental glaucomatous rats.* J Neurosci Res, 2005. **82**(5): p. 674-89.

492. Fan, Y., et al., *Pretreatment with PTD-calbindin D 28k alleviates rat brain injury induced by ischemia and reperfusion.* J Cereb Blood Flow Metab, 2007. **27**(4): p. 719-28.

493. Levkovitch-Verbin, H., et al., *Increase in retinal ganglion cells' susceptibility to elevated intraocular pressure and impairment of their endogenous neuroprotective mechanism by age.* Mol Vis, 2013. **19**: p. 2011-22.

494. Vickers, J.C., et al., *Intraperikaryal neurofilamentous accumulations in a subset of retinal ganglion cells in aged mice that express a human neurofilament gene.* Exp Neurol, 1995. **136**(2): p. 266-9.

495. Morgan, J.E., H. Uchida, and J. Caprioli, *Retinal ganglion cell death in experimental glaucoma.* Br J Ophthalmol, 2000. **84**(3): p. 303-10.

496. Grehn, F. and U.T. Eysel, *Patterns of Retinal Ganglion Cell Loss After Acute Elevation of Intraocular Pressure in the Cat.* Chibret International Journal of Ophthalmology, 1987. **5**(1): p. 17-26.

497. Ivanov, D., et al., *Differential gene expression profiling of large and small retinal ganglion cells.* J Neurosci Methods, 2008. **174**(1): p. 10-7.

498. Weiss, D.G. and A. Gorio, *Axoplasmic transport in physiology and pathology*. Proceedings in life sciences. 1982, Berlin ; New York: Springer-Verlag. ix, 192 p.

499. Fukuda, K., et al., *Neuroprotection against retinal ischemia-reperfusion injury by blocking the angiotensin II type 1 receptor.* Invest Ophthalmol Vis Sci, 2010. **51**(7): p. 3629-38.

500. Robinson, G.A. and R.D. Madison, *Axotomized mouse retinal ganglion cells containing melanopsin show enhanced survival, but not enhanced axon regrowth into a peripheral nerve graft.* Vision Res, 2004. **44**(23): p. 2667-74.

501. DeParis, S., C. Caprara, and C. Grimm, *Intrinsically photosensitive retinal ganglion cells are resistant to N-methyl-D-aspartic acid excitotoxicity.* Mol Vis, 2012. **18**: p. 2814-27.

502. Rovere, G., et al., *Melanopsin-Containing or Non-Melanopsin-Containing Retinal Ganglion Cells Response to Acute Ocular Hypertension With or Without Brain-Derived Neurotrophic Factor Neuroprotection.* Invest Ophthalmol Vis Sci, 2016. **57**(15): p. 6652-6661.

503. Nadal-Nicolas, F.M., et al., *Transient Downregulation of Melanopsin Expression After Retrograde Tracing or Optic Nerve Injury in Adult Rats.* Invest Ophthalmol Vis Sci, 2015. **56**(8): p. 4309-23.

504. Li, R.S., et al., *Melanopsin-expressing retinal ganglion cells are more injury-resistant in a chronic ocular hypertension model.* Invest Ophthalmol Vis Sci, 2006. **47**(7): p. 2951-8.

505. La Morgia, C., et al., *Melanopsin retinal ganglion cells are resistant to neurodegeneration in mitochondrial optic neuropathies.* Brain, 2010. **133**(Pt 8): p. 2426-38.

506. Bose, S., et al., *Relative post-mortem sparing of afferent pupil fibers in a patient with 3460 Leber's hereditary optic neuropathy.* Graefes Arch Clin Exp Ophthalmol, 2005. **243**(11): p. 1175-9.

507. Li, S.Y., et al., *Enhanced survival of melanopsin-expressing retinal ganglion cells after injury is associated with the PI3 K/Akt pathway.* Cell Mol Neurobiol, 2008. **28**(8): p. 1095-107.

508. Szabadfi, K., et al., *Mice deficient in pituitary adenylate cyclase activating polypeptide (PACAP) are more susceptible to retinal ischemic injury in vivo.* Neurotox Res, 2012. **21**(1): p. 41-8.

509. Reglodi, D., et al., *PACAP is an endogenous protective factor-insights from PACAP-deficient mice.* J Mol Neurosci, 2012. **48**(3): p. 482-92.

510. Zhou, Y., et al., *Receptive field properties of cat retinal ganglion cells during short-term IOP elevation.* Invest Ophthalmol Vis Sci, 1994. **35**(6): p. 2758-64.

511. Troy, J.B. and T. Shou, *The receptive fields of cat retinal ganglion cells in physiological and pathological states: where we are after half a century of research.* Prog Retin Eye Res, 2002. **21**(3): p. 263-302.

512. Osborne, N.N., et al., *Ganglion cell death in glaucoma: what do we really know?* Br J Ophthalmol, 1999. **83**(8): p. 980-6.

513. Macri, J., P.R. Martin, and U. Grunert, *Distribution of the alpha1 subunit of the GABA(A) receptor on midget and parasol ganglion cells in the retina of the common marmoset Callithrix jacchus.* Vis Neurosci, 2000. **17**(3): p. 437-48.

514. Chen, Y.P. and C.C. Chiao, *Spatial distribution of excitatory synapses on the dendrites of ganglion cells in the mouse retina.* PLoS One, 2014. **9**(1): p. e86159.

515. Vorwerk, C.K., et al., *Susceptibility of retinal ganglion cells to excitotoxicity depends on soma size and retinal eccentricity.* Curr Eye Res, 1999. **19**(1): p. 59-65.

516. O'Hanlon, G.M., et al., *Anti-GQ1b ganglioside antibodies mediate complement-dependent destruction of the motor nerve terminal.* Brain, 2001. **124**(Pt 5): p. 893-906.

517. Holzer, M., et al., *Alterations in content and phosphorylation state of cytoskeletal proteins in the sciatic nerve during ageing and in Alzheimer's disease.* J Neural Transm (Vienna), 1999. **106**(7-8): p. 743-55.

518. Burkart, V., et al., *Cholera toxin B pretreatment of macrophages and monocytes diminishes their proinflammatory responsiveness to lipopolysaccharide.* J Immunol, 2002. **168**(4): p. 1730-7.

519. Francis, M.L., et al., *Cyclic AMP-independent effects of cholera toxin on B cell activation. II. Binding of ganglioside GM1 induces B cell activation.* J Immunol, 1992. **148**(7): p. 1999-2005.

520. Burkart, V., et al., *Induction of tolerance in macrophages by cholera toxin B chain.* Pathobiology, 1999. **67**(5-6): p. 314-7.

521. Radius, R.L. and D.R. Anderson, *Morphology of axonal transport abnormalities in primate eyes.* Br J Ophthalmol, 1981. **65**(11): p. 767-77.

522. Fu, C.T. and D.W. Sretavan, *Ectopic vesicular glutamate release at the optic nerve head and axon loss in mouse experimental glaucoma.* J Neurosci, 2012. **32**(45): p. 15859-76.

523. Waxman, S.G., et al., *Anoxic injury of rat optic nerve: ultrastructural evidence for coupling between Na+ influx and Ca(2+)-mediated injury in myelinated CNS axons.* Brain Res, 1994. **644**(2): p. 197-204.

524. Iwamoto, T., T. Watano, and M. Shigekawa, *A novel isothiourea derivative selectively inhibits the reverse mode of Na+/Ca2+ exchange in cells expressing NCX1.* J Biol Chem, 1996. **271**(37): p. 22391-7.

525. Luo, X., et al., *Susceptibilities to and mechanisms of excitotoxic cell death of adult mouse inner retinal neurons in dissociated culture.* Invest Ophthalmol Vis Sci, 2004. **45**(12): p. 4576-82.

526. Fagiolini, M., et al., *Axonal transport blockade in the neonatal rat optic nerve induces limited retinal ganglion cell death.* J Neurosci, 1997. **17**(18): p. 7045-52.

527. Ou, Y., et al., *Selective Vulnerability of Specific Retinal Ganglion Cell Types and Synapses after Transient Ocular Hypertension.* J Neurosci, 2016. **36**(35): p. 9240-52.

528. Della Santina, L. and Y. Ou, *Who's lost first? Susceptibility of retinal ganglion cell types in experimental glaucoma.* Exp Eye Res, 2016.

APPENDIX 1: COPYRIGHT PERMISSIONS

ELSEVIER LICENSE
TERMS AND CONDITIONS

May 24, 2016

This is an Agreement between Andrea Nuschke ("You") and Elsevier ("Elsevier"). It consists of your order details, the terms and conditions provided by Elsevier, and the payment terms and conditions.

Supplier	Elsevier Limited The Boulevard,Langford Lane Kidlington,Oxford,OX5 1GB,UK
Registered Company Number	1982084
Customer name	Andrea Nuschke
Customer address	14 Burns Drive Halifax, NS B3P1V5
License number	3875450190632
License date	May 24, 2016
Licensed content publisher	Elsevier
Licensed content publication	Progress in Retinal and Eye Research
Licensed content title	Retinal connectivity and primate vision
Licensed content author	Barry B. Lee,Paul R. Martin,Ulrike Grünert
Licensed content date	November 2010
Licensed content volume number	29
Licensed content issue number	6
Number of pages	18
Start Page	622
End Page	639
Type of Use	reuse in a thesis/dissertation
Portion	figures/tables/illustrations
Number of figures/tables/illustrations	1
Format	both print and electronic
Are you the author of this Elsevier article?	No
Will you be translating?	No
Original figure numbers	Figure 1
Title of your	SPATIOTEMPORAL ASSESSMENT OF AXONAL TRANSPORT AND

thesis/dissertation	CYTOSKELETAL STRUCTURE IN RETINAL GANGLION CELLS FOLLOWING ACUTE ELEVATED INTRAOCULAR PRESSURE IN THE RAT
Expected completion date	Aug 2016
Estimated size (number of pages)	400

JOHN WILEY AND SONS LICENSE TERMS AND CONDITIONS

May 24, 2016

This Agreement between Andrea Nuschke ("You") and John Wiley and Sons ("John Wiley and Sons") consists of your license details and the terms and conditions provided by John Wiley and Sons and Copyright Clearance Center.

License Number	3875450524260
License date	May 24, 2016
Licensed Content Publisher	John Wiley and Sons
Licensed Content Publication	Journal of Comparative Neurology
Licensed Content Title	Morphology of retinal ganglion cells in a New World monkey, the marmoset Callithrix jacchus
Licensed Content Author	Krishna K. Ghosh,Ann K. Goodchild,Ann E. Sefton,Paul R. Martin
Licensed Content Date	Dec 6, 1998
Pages	17
Type of Use	Dissertation/Thesis
Requestor type	University/Academic
Format	Print and electronic
Portion	Figure/table
Number of figures/tables	1
Original Wiley figure/table number(s)	Figure 5
Will you be translating?	No
Title of your thesis / dissertation	SPATIOTEMPORAL ASSESSMENT OF AXONAL TRANSPORT AND CYTOSKELETAL STRUCTURE IN RETINAL GANGLION CELLS FOLLOWING ACUTE ELEVATED INTRAOCULAR PRESSURE IN THE RAT
Expected completion date	Aug 2016

Expected size (number of pages)	400

NATURE PUBLISHING GROUP LICENSE TERMS AND CONDITIONS

May 24, 2016

This is an Agreement between Andrea Nuschke ("You") and Nature Publishing Group ("Nature Publishing Group"). It consists of your order details, the terms and conditions provided by Nature Publishing Group, and the payment terms and conditions.

License Number	3875450905008
License date	May 24, 2016
Licensed Content Publisher	Nature Publishing Group
Licensed Content Publication	Eye
Licensed Content Title	The structure of the lamina cribrosa of the human eye: An immunocytochemical and electron microscopical study
Licensed Content Author	A R Elkington, C B E Inman, P V Steart and R O Weller
Licensed Content Date	Jan 1, 1990
Volume number	4
Issue number	1
Type of Use	reuse in a dissertation / thesis
Requestor type	academic/educational
Format	print and electronic
Portion	figures/tables/illustrations
Number of figures/tables/illustrations	3
Figures	Figures 2, 4, and 5
Author of this NPG article	no
Your reference number	None
Title of your thesis / dissertation	SPATIOTEMPORAL ASSESSMENT OF AXONAL TRANSPORT AND CYTOSKELETAL STRUCTURE IN RETINAL GANGLION CELLS FOLLOWING ACUTE ELEVATED INTRAOCULAR PRESSURE IN THE RAT
Expected completion date	Aug 2016
Estimated size (number of pages)	400

JOHN WILEY AND SONS LICENSE TERMS AND CONDITIONS

May 24, 2016

This Agreement between Andrea Nuschke ("You") and John Wiley and Sons ("John Wiley and Sons") consists of your license details and the terms and conditions provided by John Wiley and Sons and Copyright Clearance Center.

License Number	3875451068840
License date	May 24, 2016
Licensed Content Publisher	John Wiley and Sons
Licensed Content Publication	Journal of Comparative Neurology
Licensed Content Title	The morphology and spatial arrangement of astrocytes in the optic nerve head of the mouse
Licensed Content Author	Daniel Sun,Ming Lye-Barthel,Richard H. Masland,Tatjana C. Jakobs
Licensed Content Date	Mar 20, 2009
Pages	19
Type of Use	Dissertation/Thesis
Requestor type	University/Academic
Format	Print and electronic
Portion	Figure/table
Number of figures/tables	2
Original Wiley figure/table number(s)	Figures 1 and 2
Will you be translating?	No
Title of your thesis / dissertation	SPATIOTEMPORAL ASSESSMENT OF AXONAL TRANSPORT AND CYTOSKELETAL STRUCTURE IN RETINAL GANGLION CELLS FOLLOWING ACUTE ELEVATED INTRAOCULAR PRESSURE IN THE RAT
Expected completion date	Aug 2016
Expected size (number of pages)	400

NATURE PUBLISHING GROUP LICENSE TERMS AND CONDITIONS

May 24, 2016

This is an Agreement between Andrea Nuschke ("You") and Nature Publishing Group ("Nature Publishing

Group"). It consists of your order details, the terms and conditions provided by Nature Publishing Group, and the payment terms and conditions.

License Number	3875460142219
License date	May 24, 2016
Licensed Content Publisher	Nature Publishing Group
Licensed Content Publication	Nature
Licensed Content Title	Cell mechanics and the cytoskeleton
Licensed Content Author	Daniel A. Fletcher and R. Dyche Mullins
Licensed Content Date	Jan 27, 2010
Volume number	463
Issue number	7280
Type of Use	reuse in a dissertation / thesis
Requestor type	academic/educational
Format	print and electronic
Portion	figures/tables/illustrations
Number of figures/tables/illustrations	1
High-res required	no
Figures	Figure 1
Author of this NPG article	no
Your reference number	None
Title of your thesis / dissertation	SPATIOTEMPORAL ASSESSMENT OF AXONAL TRANSPORT AND CYTOSKELETAL STRUCTURE IN RETINAL GANGLION CELLS FOLLOWING ACUTE ELEVATED INTRAOCULAR PRESSURE IN THE RAT
Expected completion date	Aug 2016
Estimated size (number of pages)	400

NATURE PUBLISHING GROUP LICENSE TERMS AND CONDITIONS

May 24, 2016

This is an Agreement between Andrea Nuschke ("You") and Nature Publishing Group ("Nature Publishing Group"). It consists of your order details, the terms and conditions provided by Nature Publishing Group, and the payment terms and conditions.

License Number	3875460584865

License date	May 24, 2016
Licensed Content Publisher	Nature Publishing Group
Licensed Content Publication	Nature Reviews Molecular Cell Biology
Licensed Content Title	Molecular architecture of the kinetochore-microtubule interface
Licensed Content Author	Iain M. Cheeseman and Arshad Desai
Licensed Content Date	Jan 1, 2008
Volume number	9
Issue number	1
Type of Use	reuse in a dissertation / thesis
Requestor type	academic/educational
Format	print and electronic
Portion	figures/tables/illustrations
Number of figures/tables/illustrations	1
High-res required	no
Figures	Box 2
Author of this NPG article	no
Your reference number	None
Title of your thesis / dissertation	SPATIOTEMPORAL ASSESSMENT OF AXONAL TRANSPORT AND CYTOSKELETAL STRUCTURE IN RETINAL GANGLION CELLS FOLLOWING ACUTE ELEVATED INTRAOCULAR PRESSURE IN THE RAT
Expected completion date	Aug 2016
Estimated size (number of pages)	400

SPRINGER LICENSE TERMS AND CONDITIONS

May 24, 2016

This Agreement between Andrea Nuschke ("You") and Springer ("Springer") consists of your license details and the terms and conditions provided by Springer and Copyright Clearance Center.

License Number	3875470287147
License date	May 24, 2016
Licensed Content Publisher	Springer
Licensed Content Publication	Springer eBook
Licensed Content Title	The Morphology and Hydrodynamics of the Chamber Angle Draining the Aqueous

	Humor
Licensed Content Author	Maurice E. Langham
Licensed Content Date	Jan 1, 2009
Type of Use	Thesis/Dissertation
Portion	Figures/tables/illustrations
Number of figures/tables/illustrations	1
Author of this Springer article	No
Order reference number	None
Original figure numbers	Figure 8.1
Title of your thesis / dissertation	SPATIOTEMPORAL ASSESSMENT OF AXONAL TRANSPORT AND CYTOSKELETAL STRUCTURE IN RETINAL GANGLION CELLS FOLLOWING ACUTE ELEVATED INTRAOCULAR PRESSURE IN THE RAT
Expected completion date	Aug 2016
Estimated size(pages)	400

SPRINGER LICENSE
TERMS AND CONDITIONS

Dec 08, 2016

This Agreement between Andrea Nuschke ("You") and Springer ("Springer") consists of your license details and the terms and conditions provided by Springer and Copyright Clearance Center.

License Number	4004310067277
License date	Dec 08, 2016
Licensed Content Publisher	Elsevier
Licensed Content Publication	Experimental Eye Research
Licensed Content Title	Assessment of retinal ganglion cell damage in glaucomatous optic neuropathy: Axon transport, injury and soma loss
Licensed Content Author	Andrea C. Nuschke,Spring R. Farrell,Julie M. Levesque,Balwantray C. Chauhan
Licensed Content Date	December 2015
Licensed Content Volume	141
Licensed Content Issue	n/a
Licensed Content Pages	14
Start Page	111
End Page	124
Type of Use	reuse in a thesis/dissertation
Portion	figures/tables/illustrations

Number of figures/tables/illustrations	1
Format	both print and electronic
Are you the author of this Elsevier article?	Yes
Will you be translating?	No
Order reference number	
Original figure numbers	Figure 1
Title of your thesis/dissertation	SPATIOTEMPORAL ASSESSMENT OF AXONAL TRANSPORT AND CYTOSKELETAL STRUCTURE IN RETINAL GANGLION CELLS FOLLOWING ACUTE ELEVATED INTRAOCULAR PRESSURE IN THE RAT
Expected completion date	Aug 2016
Estimated size (number of pages)	400